ELECTROSPUN MEMBRANES FOR IMPLANTABLE GLUCOSE BIOSENSORS

A thesis submitted to Brunel University

for the degree of

Doctor of Philosophy

By

Ning Wang

Institute for Bioengineering, Brunel University, London

March 2012

Acknowledgements

Foremost, I would like to express my sincere gratitude to my supervisor, Dr. Wenhui Song. Her knowledge and logical thinking has been of an immense value to me. Through encouragement, sound advice, guidance, and providing access to the right resources and research collaborations, she helped me successfully complete this work, without which, I would have been lost.

I am also deeply grateful to my supervisor, Dr Krishna Burugapalli, who supported me with tremendous patience in answering my questions. He introduced me to the field of biocompatibility and *in vivo* functional efficacy testing. His meticulous guidance, especially with thesis writing, was indispensable to the completion of this work.

My warm thanks also go to Prof. Francis Moussy who gave me the opportunity to start my research and provided me a first glance of this interesting research. I must thank Dr Remco van den Heuvel, Tony Bunce, Roger Paton and Joost DeFolter for their valuable advice and help in constructing the electrospinning equipment.

I would like to thank Prof. Colin Clark, Prof. Derek Fisher, and Jenny Kume for their insightful comments, monitoring of research progress, and administrative support. The kind help and encouragement from Shavini Wijesuriya, Alessandra Borlotti and Mashid Yazdi Far in the lab is much appreciated.

I also wish to thank all my fellow PhD students – Gianpaolo Bruti, Yan Cai, Masoud Zoka Assadi, Xiao Liu, Yinhe Zhang, Ye Li, Yi Li, Chenchu Chen, Xiao Yan, Francesco Clavica, Nicolay Mikov and so on, for moral support during my study at BIB and for all the treasured memories during the time we spent together.

Last but not least, my deepest gratitude goes to my beloved parents, Mrs. Manling Shi and Mr. Hongqing Wang, for their endless love and encouragement. To them I dedicate this thesis.

Abstract

The goal for this thesis was to apply electrospun biomimetic coatings on implantable glucose biosensors and test their efficacy as mass-transport limiting and tissue engineering membranes, with special focus on achieving reliable and long sensing life-time for biosensors when implanted in the body. The 3D structure of electrospun membranes provides the unique combination of extensively interconnected pores, large pore volumes and mechanical strength, which are anticipated to improving sensor sensitivity. Their structure also mimics the 3D architecture of natural extracellular matrix (ECM), which is exploited to engineer tissue responses to implants.

A versatile vertical electrospinning setup was built in our workshop and used to electrospin single polymer - Selectophore™ polyurethane (PU) and two polymer (coaxial) – PU and gelatin (Ge) fibre membranes. Extensive studies involving optimization of electrospinning parameters (namely solvents, polymer solution concentration, applied electric potential, polymer solution feed flow rate, distance between spinneret and collector) were carried out to obtain electrospun membranes having tailorable fibre diameters, pore sizes and thickness. The morphology (scanning electron microscopy (SEM) and optical microscopy), fibre diameter (SEM), porosity (bubble point and gravimetry methods), hydrophilicity (contact angle), solute diffusion (biodialyzer) and uniaxial mechanical properties (tensile tester) were used to characterize certain shortlisted electrospun membranes. Static and dynamic collector configurations for electrospinning fibres directly on sensor surface were optimized of which the dynamic collections system helped achieve snugly fit membranes of uniform thickness on the entire surface of the sensor. The biocompatibility and the *in vivo* functional efficacy of electrospun membranes off and on glucose biosensors were evaluated in rat subcutaneous implantation model.

Linear increase in thickness of electrospun membranes with increasing electrospinning time was observed. Further, the smaller the fibre diameter, smaller was the pore size and higher was the fibre density (predicted), the hydrophilicity and the mechanical strength. Very thin membranes showed zero-order (Fickian diffusion exponent ‘n’ ~ 1) permeability for glucose transport. Increasing membrane thickness lowered ‘n’ value through non-Fickian towards Fickian (‘n’ = 0.5) diffusion. Thin electrospun PU membranes (~10 µm thick) did not affect, while thicknesses between 20 and 140 µm all decreased sensitivity of glucose biosensor by about 20%. PU core - Ge shell coaxial fibre membranes caused decrease in ex vivo sensitivity by up to 40%. The membranes with sub-micron to micron sized pore sizes functioned as mass-transport limiting membranes; but were not permeable to host cells when implanted in the body. However, PU-Ge coaxial

fibre membranes, having <2 µm pore sizes, were infiltrated with fibroblasts and deposition of collagen in their pores. Such tissue response prevented the formation of dense fibrous capsule around the implants, which helped improve the *in vivo* sensor sensitivity.

To conclude, this study demonstrated that electrospun membrane having tailorable fibre diameters, porosity and thickness, while having mechanical strength similar to the natural soft tissues can be spun directly on sensor surfaces. The membranes can function as mass-transport limiting membranes, while causing minimal or no effect on sensor sensitivity. With the added bioactive Ge surfaces, evidence from this study indicates that reliable long-term *in vivo* sensor function can be achieved.

Table of Contents

List of Figures

List of Tables

Abbreviations

A	Area of nanofibrous mat
AC	Alternating-current
ADA	American Diabetes Association
Ag/AgCl	Silver/silver chloride
ANOVA	One-way analysis of variance
ARM	Ames Reflectance Meter
ATR-FTIR	Attenuated total reflectance-Fourier transform infrared
BMSC	Bone marrow stromal cell
BSA	Bovine serum albumin
Carbon nanotubes	CNTs
CCD	Charge coupled device
CGM	Continuous glucose monitoring
$-CH_3$	Methyl
CON A	Concanavalin A
-COOH	Carboxyl
Cp	Cyclopentadienyl
D	Distance between the spinneret and the collector
d	Thickness of the membrane
DC	Direct-current
DI water	Distilled water
DLC	Diamond-like carbon
DMF	*N*,*N*-Dimethylformamide
E	Electric field strength
ECM	Extracellular matix
EPU	Epoxy enhanced polyurethane
ESC	Electrospun coating
E_ε	Modulus of elasticity
f	Fraction of solid face area wet by the liquid
FAD	Flavin adenine dinucleotide
$FADH_2$	Hydro-FAD
FEA	Finite Element Analysis
Fmax	Maximum load at failure
FRET	Fluorescence resonance energy transfer
GDH	Glucose dehydrogenases
GDH-PQQ	Glucose dehydrogenase pyrroloquinoline quinone
Ge	Gelatin
GOD	Glucose oxidase

GTA	Glutaraldehyde
H&E	Hematoxylin & Eosin
HDF	Human dermal fibroblast
I_{15mM}	Steady state currents for 15 glucose concentration
I_{5mM}	Steady state currents for 5 glucose concentration
ISF	Interstitial fluid
k, K and a	Constant
m	Mass of the membrane
M	Molecular weight of the polymer
M_∞	Mass/concentration of analyte at time ∞
MIR	Mid infrared
MT	Masson's Trichrome
M_t	Mass/concentration of analyte at time t
NGC	Nerve guidance conduit
$-NH_2$	Amino
NIR	Near infrared
NMP-TCQM	N-methyl phenazinium- Tetracyanoquinodimethane
NPs	Nano-particles
NSC	Neural stem cell
-OH	Hydroxyl
PANEA	Poly(1-(5-aminonapthyl) ethanoic acid)
PBS	Phosphate buffered saline
PCL	Polycaprolactone
PEO-PPO-PEO	The triblock poly(ethylene oxide) and poly(propylene oxide) based system
PHEMA	Hydroxyethyl methacrylate
phi	Constant potential
PLA	Polylactic acid
PLGA	Poly(lactic-co-glycolic acid)
PLLA	Poly-L-Lactic Acid
Pt/-Ir	Platinum/-iridium
PTFE	Polytetrafluoroethylene
Pt-GOD-EPU-ESC	Sensor coated with epoxy-PU (EPU) semi-permeable membrane
Pt-GOD-ESC	Sensor coated without epoxy-PU (EPU) semi-permeable membrane
PU	Polyurethane
PVA	Polyvinyl acetate
PVP	Poly (vinylpyrrolidone)

RBC	Red blood cell
RH	Relative humidity
RHE	Reversible hydrogen electrode
S	Sensor sensitivity
SCC	Static collector configuration
SCE	Saturated calomel electrode
SEM	Scanning Electron Microscopy
SMBG	Self-monitoring of blood glucose
SMC	Smooth muscle cell
TCQM	Tetracyanoquinodimethane
TFE	2,2,2-Trifluoroethanol
THF	Tetrahydrofunan
TMPD	N,N,N',N'-Tetramethyl-p-Phenylenediamine
TTF	Tetrathiafulvalene
TTF-TCNQ	Tetrathiafulvalene-tetracyanoquinodimethane
UTS	Ultimate tensile strength
WHO	World Health Organization
ΔP	Differential pressure
ε	Strain
H	Intrinsic viscosity
θ^*	Apparent contact angle
ρ_b	Bulk density of materials
ρ_{Ge}	Ge bulk density
Σ	Stress
γ_{st}	Surface tension of the wetting liquid
θ	Wetting/contact angle
γ	Surface roughness of a homogeneous surface
r	Core radius of coaxial fibre
R	Total Fibre radius of coaxial fibre
ρ_b	Bulk density
ρ_{PU}	PU density

Chapter 1 Introduction and Literature Review

1.1. Introduction

Reliable continuous monitoring of physiologically relevant molecules using implantable sensors is yet to be achieved. The sensor starts losing sensitivity as soon as it is implanted in the body and the downward drift of sensitivity continues rapidly until the sensor fails. The primary cause for the decrease in sensor sensitivity is the deposition of biological macromolecules, cells and fibrous capsule on the immediate surface of the implanted sensor (Wisniewski *et al.*, 2000). The hypothesis for this thesis was that the tissue composition on the immediate surface of an implanted sensor can be engineered using electrospun coatings to allow reliable long-term continuous monitoring.

The rationale for the above hypothesis was that, electrospun coatings have fibro-porous structure and highly interconnected porosity that can be engineered to closely mimic the 3D architecture of the natural extracellular matrix. The fibrous nature of the electrospun coatings imparts mechanical properties similar to that of the target tissue for implantation, while their highly interconnected porosity and pore volume aids in analyte transport and host cell infiltration necessary to reduce or potentially prevent the deleterious effects of cell and tissue build-up on the immediate surface of the implanted sensor (Sanders, 2011).

For this study, implantable glucose biosensors were chosen as the model sensors to evaluate the efficacy of electrospun coatings, because they are the single most widely researched implantable sensors. The particular sensors used in this study were optimized by the research group of Francis Moussy (Yu et al., 2006, Yu et al., 2005a). They have a needle-type electrochemical sensor design having the working and reference electrodes as coils. The advantage of this design is that its cotton reinforced Pt-Ir working electrode allows loading of excess enzyme to make the sensors durable to suit the intended long-term implantable application.

This thesis presents the research involving the manufacture of electrospun membranes based on Selectophore™ polyurethane and gelatin having tailored fibre diameters, pore volumes, fibre composition, permeability and mechanical properties; their deposition on miniature cylindrical glucose biosensors as uniform and snugly fit coatings; and their *ex vivo* and *in vivo* efficacy as tissue engineering coatings for the implantable glucose biosensors.

The benefits from this research could be profound. Medically, making the long-term implantable sensors a reality would have tremendous socio-economic benefits, especially in

- preventing disease and related complications – both acute and chronic;
- reducing mortality, costs of care, wastage of resources (human, financial and infrastructure); and
- improving quality of life for people.

Technically, the reproducible manufacture of glucose biosensors has been a problem, and the clinical performance of blood glucose monitors in the market are considered acceptable if their readings are within ±20% of the actual blood glucose levels. The huge error margins are primarily caused by the use of traditional solvent cast membranes. Electrospinning provides the opportunity to reproducibly control the porosity and thickness of the deposited membranes, which can potentially lead to reproducible and preferably automated manufacture of sensors.

The aim for the rest of this chapter was to introduce the reader to concepts behind the electrospinning, glucose biosensor and membrane technologies utilized or developed in this study, review the recent developments in the implantable biosensor technologies for implantable biosensors, and define the specific objectives and the scope for this thesis.

1.2. Electrospinning

Electrospinning is a non-woven fibre spinning technology that allows spinning of fibres having diameter ranging from 2 nm to 10s of μm (Bhardwaj and Kundu, 2010). It is different from the conventional dry or wet spinning technologies, in that it generates submicron and nanometer size fibres, and does not require high temperatures or specialised solution chemistries. In addition it also allows spinning of large and complex molecules, as well as combinations of compatible or incompatible polymer solutions.

The principle behind electrospinning is the use of electric charge to create a charged jet of polymer solution. When sufficiently large voltage (+ or –) is applied, electrostatic repulsion of the charged moieties in the polymer solution repel to counteract surface tension resulting in the stretching of the droplet forming a cone shape known as Taylor cone. From the tip of the Taylor cone, a stream of liquid ejects and if the viscosity and the electrical resistivity of the polymer solution are sufficient, the stream does not break up. During the flow, as the solvent dries, the mode of current flow in the jet is said to change from ohmic to convective flow causing it to bend, whip and accelerate towards the grounded collector (http://en.wikipedia.org/wiki/Electrospinning, 2012). The process, as illustrated in Figure 1.1, involves the formation of Taylor cone and jet, followed by the

travel of jet along a straight line during the ohmic flow and then starts bending during the convective flow. The bending during the convective flow of charges within the electrospinning jet is attributed to the mutual repulsive force between the electric charges carried by the jet (Reneker *et al*., 2000). The bending and acceleration stretches the fibre resulting in the thinner fibres observed with non-woven fibres spun using electrospinning.

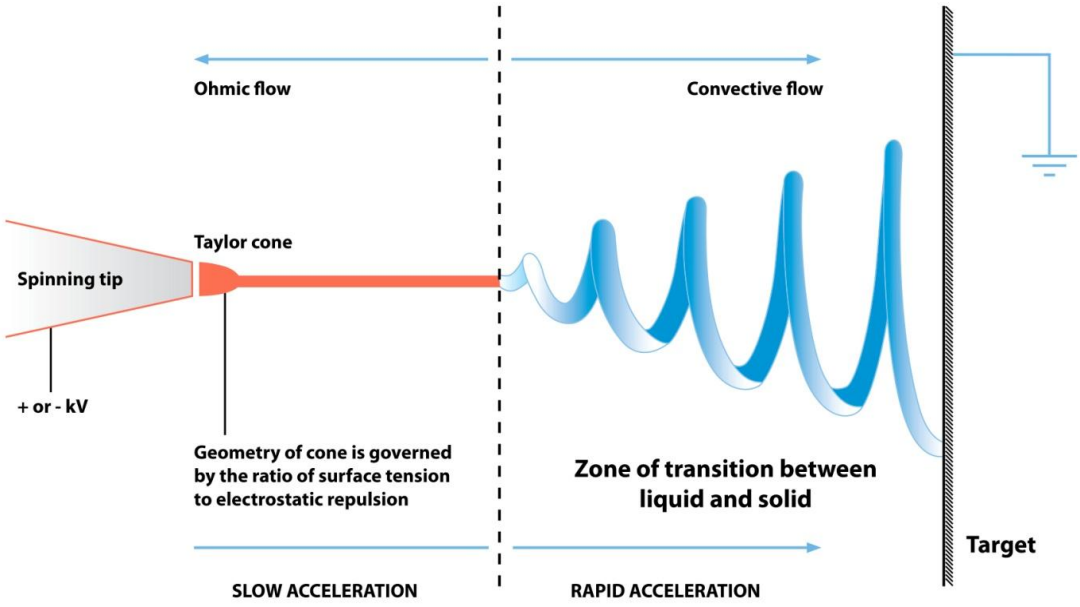

Figure 1.1 Schematic diagram showing the fibre formation dynamics during electrospinning (http://en.wikipedia.org/wiki/Electrospinning, 2012).

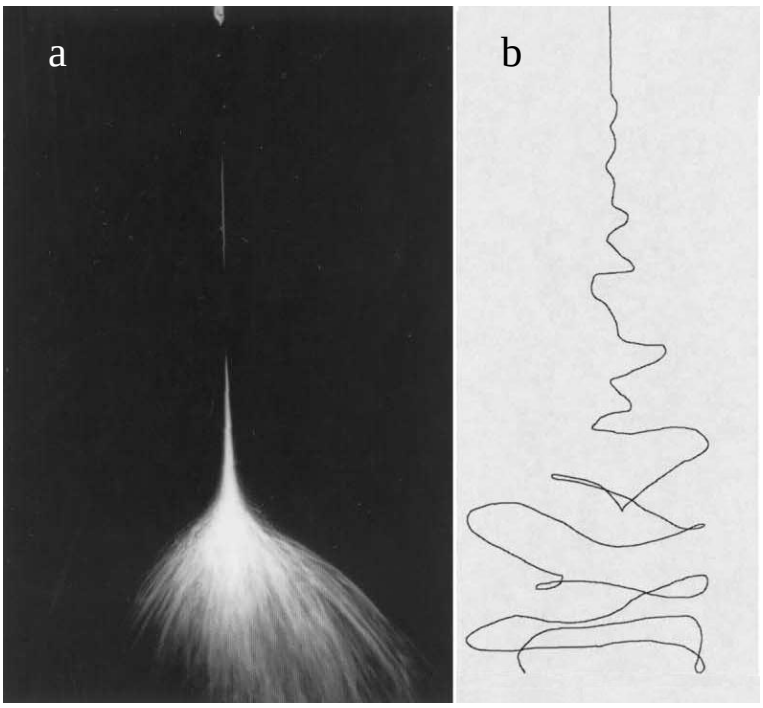

Figure 1.2 The appearance of the electrospinning jet of aqueous poly(ethylene oxide) PEO solution in photos captured using a) conventional and b) high speed cameras camera with exposure times of 1/250 s 18 ns respectively (Shin *et al.*, 2001).

In real-time, the bending instability of the jet appears to naked eye or conventional photography as the single stream of polymer solution splitting into multitude of jets in a cone shape (Figure 1.2a). However, using high speed photography, Shin *et al.* demonstrated that it is essentially a single fibre that bends and whips rapidly to give the illusion of splitting and multiple jets (Figure 1.2b) (Shin *et al.*, 2001).

1.2.1. Electrospinning instrument

The equipment needed for electrospinning is simple in construction and consists of a high voltage power source, a syringe pump with tubing to transport solution from the syringe to the spinneret, and a conducting collector. The spinneret and collector are aligned opposite to each other (Figure 1.1) and together they are usually oriented either horizontally (Figure 1.1) or vertically (Figure 1.2). Any variations in the equipment are primarily concerned with the spinneret and the collector.

1.2.1.1. Spinneret

Spinneret constructions allow greater versatility in the nano-fibre structures. They can be single or multiple and needle-type or needleless configurations (Teo and Ramakrishna, 2006). Typical electrospinning setups are equipped with a single blunt end needle for spinning single polymer fibres (Figure 1.3a). To introduce composite fibre structure, either coaxial (Figure 1.3b) or dual-capillary (side-by-side) (Figure 1.3e) spinnerets are used. The former produce core-shell and the latter side-by-side fused fibre structures respectively. An additional advantage for using coaxial spinnerets is that incompatible or non-electrospinnable polymer solutions can be combined to obtain fibres (Teo and Ramakrishna, 2006). For example, a non-electrospinnable polymer solution can be extruded in the inner capillary, while the spinnable solution extruded in the outer capillary. Thus the inner solution is contained by the outer solution resulting in a core fibre. The shell can then be dissolved to obtain the fibres of the non-electrospinnable solution. This method can also produce hollow fibres by dissolving the core fibre. Overall the coaxial fibre has a reinforcing core polymer fibre encapsulated by a shell of a different polymer, while the side-by-side fused composite fibres have two different polymers side-by-side. The permutations and combinations of the two polymers can be used to engineer membranes for a variety of applications, especially in the emerging field of tissue engineering. In addition, the coaxial spinnerets can further be modified to incorporate, for example, three concentric polymer fibres (Figure 1.3c), or a large fibre reinforced with three different polymer fibres within its composite structure (Figure 1.3d).

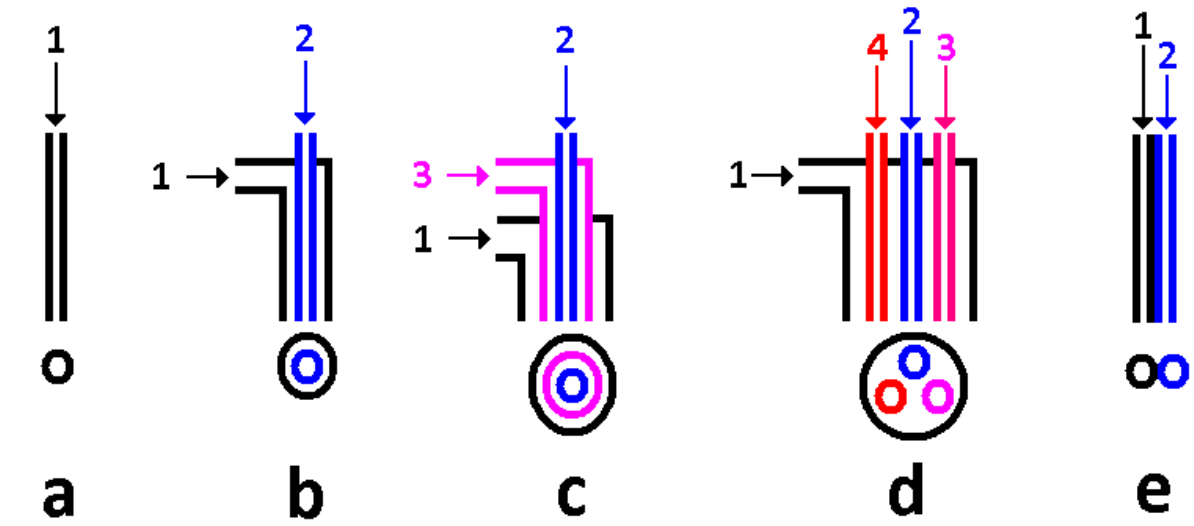

Figure 1.3 Schematic representation of needle-based spinnerets and their cross-sections, a) single needle, b) two concentric needles, c) three concentric needles, d) three side by side needles within a large needle, and e) side-by-side needles. The numbers 1 to 4 indicate different feed polymer solutions (Teo and Ramakrishna, 2006) .

Needleless electrospinning through an orifice in a flat base of a tube is another method, often used for melt-spinning, wherein, the pure polymer is melted by heating, and the molten polymer injected through the orifice.

From the perspective of industrial production, an inherent limitation for electrospinning is that the volume of fibrous meshes or structures produced per unit time is much less when compared that obtained using conventional spinning technologies. To increase productivity, multiple parallel spinnerets (needleless or needle-based) are used. Examples of such spinnerets are shown in Figure 1.4.

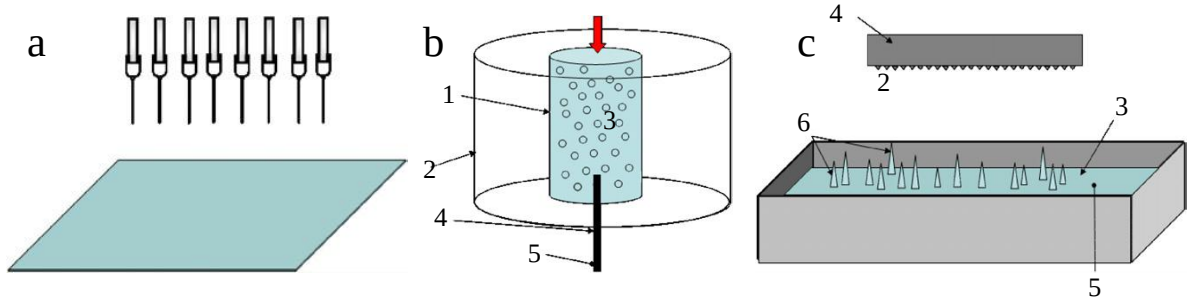

Figure 1.4 Schematic illustrations of electrospinning setups utilizing multiple spinnerets, a) needless, b) porous drum and c) multiple spikes, where 1 is porous drum spinneret, 2 is collector, 3 is polymer solution, 4 is electrode, 5 is positive high voltage, and 6 is spikes (spinnerets) formed by magnetic field. (Figures adapted from (Teo and Ramakrishna, 2006)).

A concern for electrospinning using needle-based or needleless spinnerets is the clogging of the spinneret usually when the solvent used is highly volatile. To avoid clogging, often pointed tip or spike structures (Figure 1.4c) are used.

1.2.1.2. Collector

In a basic configuration, the spinneret needle is aligned perpendicular to a static grounded flat plate (collector). During electrospinning, the seamless fibre is collected as a sheet, typically on an aluminium foil placed on top of the flat plate collector. The resulting sheet has random fibre orientation. However, the orientation, 3D architecture and properties of the electrospun structures can be varied by influencing the electric field between the spinneret and collector or by rotating the collector in the field of electrospinning. A wide variety of collector configurations used in research were collated and represented as schematic representations by Teo and Ramakrishna as illustrated in Figure 1.5 (Teo and Ramakrishna, 2006).

An important collector configuration is the use of a rotating drum in the field of electrospinning as shown in Figure 1.5a. When the speed of rotation matches the speed of the accelerating electrospun fibre, the fibres are primarily aligned along the circumference of the drum. A few thousands of rpm, e.g. 4500 rpm, for the rotating drum is needed for the fibres to align (Matthews *et al.*, 2002). A low rotation speed, e.g. around 500 rpm allows the random orientation of the fibres. When the rotation speed crosses the speed of accelerating electrospun jet, the fibre breaks, thus, disrupting its seamless nature. Increasing the speed of rotation is also reported to influence the mechanical properties of the fibres, e.g. by inducing better alignment of the polymer crystals in the fibres (Kim *et al.*, 2004). In addition, the use of alternating-current (AC) high voltage supply instead of the traditional direct-current (DC) high voltage supply for charging the electrospinning solution is reported to induce better alignment of the fibres (Kessick *et al.*, 2004).

The presence of a conducting object in the field of electrospinning significantly influences the nature of fibre deposition. The use of rings, as shown in Figure 1.5k&l, can control the area in which the fibres are deposited. Similarly, a sharp pin (Figure 1.5j) in the centre of a drum can focus the fibre deposition towards the pin. In addition, significant research has gone into the alignment of fibres. Parallel electrodes (Figure 1.5b) are used exert a pulling force towards the electrodes, thus aligning the fibres perpendicular to the electrodes. Similarly, knife edge electrodes as shown in Figure 1.5 e, f, g &m, also induce highly aligned fibres along the length of the knife edge. Wire drum (Figure 1.5c) and wires wound around a drum (Figure 1.5d) have also been used for generating aligned fibres. Furthermore, special patterning of the fibres was also achieved using collector

configurations such as that shown in Figure 1.5h and i. The former configuration was used to induce twisted or spring like fibre structures, while the latter allowed deposition of aligned fibres perpendicular to each other. For a comprehensive review of the advantages and disadvantages of the different collector configurations, the readers may refer the review by Teo and Ramakrishana (Teo and Ramakrishna, 2006).

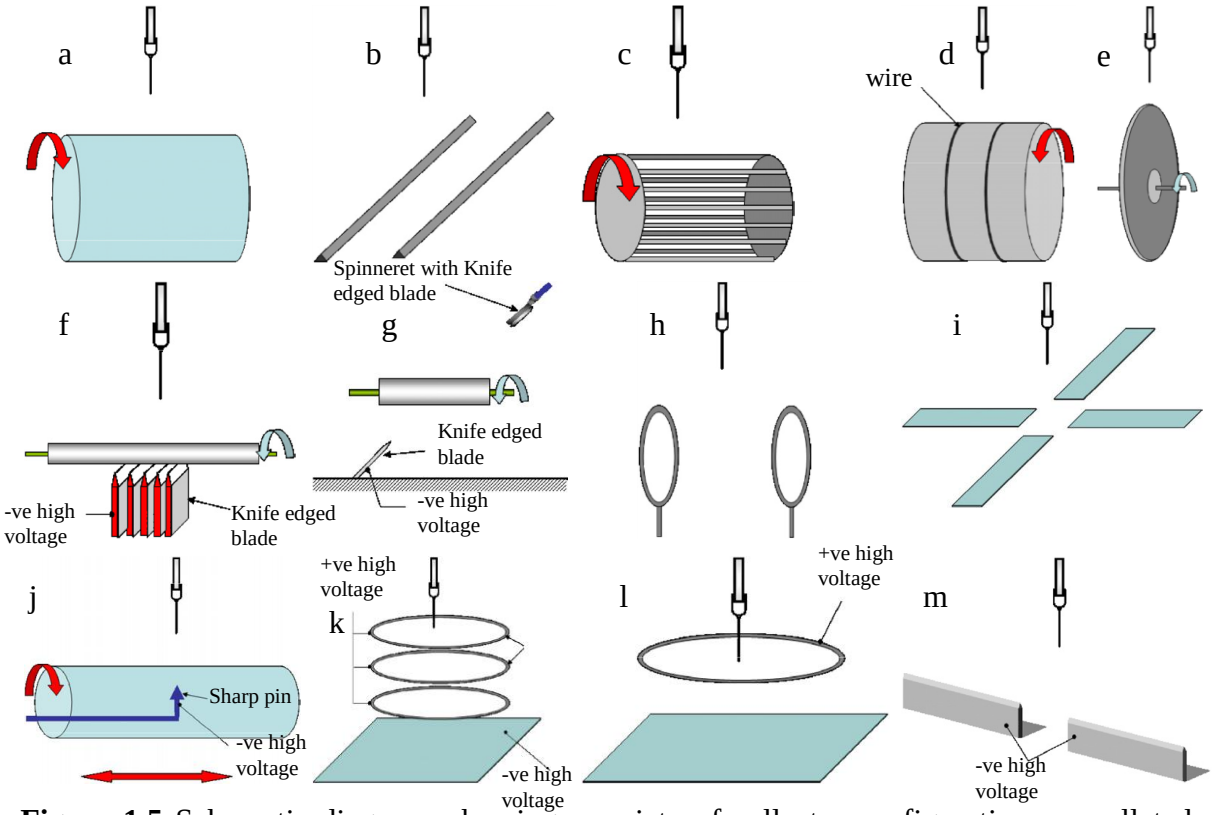

Figure 1.5 Schematic diagrams showing a variety of collector configurations as collated by Teo and Ramakrishna (2006) that have been tested for influence the nature of fibre deposition on the collector.

1.2.2. Parameters effecting electrospinning

The electrospinning of fibres and their resulting morphology and diameter is affected by solution (viscosity, elasticity, conductivity and surface tension), processing (solution flow rate, applied electric potential, and the spinneret and collector) and ambient (temperature and humidity) parameters, and excellent reviews on their effects on electrospinning are available in literature (Ramakrishna *et al.*, 2005a, Huang *et al.*, 2003, Tan *et al.*, 2005, Li and Xia, 2004, Lukas *et al.*, 2009, Theron *et al.*, 2004).

1.2.2.1. Solution Parameters

The electrospinnability of a polymer depends on its solution viscosity and electrical resistivity. If the viscosity is too low, the cohesiveness between the polymer chains (surface tension) is low to hold the fluid jet emerging from the Taylor cone together. Similarly, if the solution is too conductive, the repulsive forces between the polymer

molecules cause the fluid jet to breakdown, forming droplets. With increasing viscosity and electrical resistivity, the breakup of the jet into droplets transitions into the formation of beads-on-string fibre structure before proper fibres form (Shenoy *et al.*, 2005). Further increase in viscosity results in increasing fibre diameter until a maximum viscosity beyond which the Taylor cone becomes too big, causing the jet to become unstable (Megelski *et al.*, 2002, Jarusuwannapoom *et al.*, 2005, Demir *et al.*, 2002, Deitzel *et al.*, 2001a). Thus, for a given polymer, there exists a range of solution viscosity, wherein proper fibres form. This range varies for any specific polymer depending on the solvent it is dissolved in and also varies for different polymers (Huang *et al.*, 2003).

The solution parameters not only determine the electrospinnability of a polymer, but also affect the fibre morphology and diameter. Higher the conductivity of the solution, higher would be the amount of charges carried by the electrospinning jet. Thus, the higher charges' content the higher stretching of the jet, yielding thinner fibres. This aspect has been exploited by introduction of ionic salts to adjust solution conductivity for decreasing the diameter of the electrospun fibres (Zong *et al.*, 2002, Son *et al.*, 2004). Similarly, for making highly conducting polymer solutions electrospinnable, less conductive polymers are added as fillers. Furthermore, the volatility of the dissolving solvent is another dominant factor that affects the formation of nanostructures by influencing the surface tension of the polymer solution (Megelski *et al.*, 2002). Decreasing surface tension has been correlated with the formation of smooth and thicker fibres (Fong *et al.*, 1999, Zeng *et al.*, 2003). In addition, mixtures of solvents can also be used to tune the surface tension of the polymer solution, thus tailoring the morphology and diameter of electrospun fibres.

1.2.2.2. Processing parameters

The next essential group of parameters that affects the structure of electrospun fibres are the electrospinning process variables namely applied voltage, feed rate and distance between spinneret and collector. In most cases, a higher voltage causes greater stretching of solution due to larger columbic forces within the jet and stronger electric field, thus reducing the fibre diameter (Buchko *et al.*, 1999, Lee *et al.*, 2004a, Megelski *et al.*, 2002). However, the higher voltage can also shorten the flight time of electrospinning jet, providing less time for the fibre to stretch before it reaches the collector (Demir *et al.*, 2002). Furthermore, higher voltages are also associated with a greater tendency for bead formation due to greater instability of the jet (Demir *et al.*, 2002, Deitzel *et al.*, 2001a, Deitzel *et al.*, 2001b, Zong *et al.*, 2002). The contrasting effects of the applied voltage can primarily be due to the influence of other process variables. For instance, with increasing

applied voltage, an appropriate increase in polymer solution feed rate is needed to ensure Taylor cone formation.

Furthermore, increasing flow rates increases the amount of polymer in the electrospinning jet, thus increasing the fibre diameters. The increases volume of the jet is also associated with inadequate solvent evaporation leading to a fusion of fibres at contact points between electrospun fibres (Rutledge *et al.*, 2001). Therefore, a lower feed rate is more desirable for bead-free fibre manufacture, as the solvent has more time to evaporate giving more time for the fibre to stretch (Zhang *et al.*, 2009).

Distance between spinneret and collector has a significant influence on the strength and distribution of the electric field. Shorter the distance, stronger is the electric field and vice versa. Typically an intermediate optimum distance is needed for allowing sufficient stretching of the fibre as well as evaporation of solvent.

1.2.2.3. Ambient parameters

In most reported studies, the ambient parameters, namely temperature, humidity and air circulation within the electrospinning chamber, are not controlled. However, they can induce significant variations in fibre morphology and diameter, and sometimes can interfere with the electrospinning process. The temperature increases the rate of solvent evaporation as well as decrease the viscosity of polymer solution. Thus, morphological imperfections such as formation of beads or curly fibres are enhanced by increasing temperature, through speeding up the electrospinning process (Demir *et al.*, 2002). On the other hand, lower viscosity induced by increasing temperature renders higher Columbic forces that further stretch the solution, yielding fibre of small diameter (Mit-uppatham *et al.*, 2004).

The effect of humidity on the average fibre diameter is correlated to the variation in chemical and molecular interactions as well as the rate of solvent evaporation. For water insoluble polymer such as cellulous acetate (CA), the average diameter increases with increasing relative humidity (RH) while for water soluble polymer such as poly (vinylpyrrolidone) (PVP), an opposite trend was shown (De Vrieze *et al.*, 2009). Furthermore, when the humidity was increased to 50%, formation of circular pores on fibre surface was reported for electrospun polysulfone fibres (Casper *et al.*, 2004).

The air circulation within the chamber can impair the electrospinning process, especially when the volatility of the solvent is high. The fast evaporation of the volatile solvent often leads to the clogging of spinneret during electrospinning. Saturation of the atmosphere around the spinneret with the solvent vapour helps avoiding this problem.

1.2.3. History of electrospinning

Electrospinning is the descendent of electro-spraying technology. The first recorded observation of deformation of liquid droplet under the influence of electric field was that reported by William Gilbert in 1600s (Gilbert, 1628). He observed that when a sufficiently electrically charged amber was brought in close proximity of a water droplet on a dry surface, the drop was drawn towards the amber in a cone shape and water droplets lifted off from the tip of the cone. The chronological events since Gilbert's observation of the phenomenon of electrospraying leading to modern day electrospinning are summarised in Figure 1.6. Nollet, in 1749 also demonstrated the disintegration of water jet under the influence of electric field (Nollet, 1749).

The first theoretical work related to electrospinning was reported by Rayleigh in 1882 (Rayleigh, 1882). He calculated the limiting charge at which an isolated drop of water of certain radius became unstable. Thereafter, Larmor in 1898 explained the excitation of dielectric liquid under the influence of electric charge (Larmor, 1898). In 1902, the first patents on electrospinning were granted to Morton and Cooley. Cooley's setup demonstrated the use of rotating collector and auxiliary electrodes, while Morton showed the use of needle and needleless forms of electrospinning (Cooley, 1902, Morton, 1902). However, the exploitation of this method was not possible due to the lack of high voltage power supply technology. Further, experimental work on electrospinning was done by Zeleny between 1914 and 1917, wherein he designed the needle/capillary apparatus to study electrical discharges from liquid points (Zeleny, 1914).

The foundation for modern electrospinning technology was based on the patents of Formhals between 1934 and 1944, for which Formhals is recognised as the father of present day electrospinning (Formhals, 1934, Formhals, 1938a, Formhals, 1938b, Formhals, 1939b, Formhals, 1939a). He developed a variety of innovative electrospinning setups having different spinneret and collector configurations, some of which are still used widely today. In 1936, Norton demonstrated the melt-electrospinning of polymers (Norton, 1936).

The first industrial scale production of electrospun membranes was achieved in 1939 by Natalie Rozenblum and Igor Petrynov-Sokov, who developed cellulose acetate based nano-fibrous meshes as filters for gas masks for military use in former USSR (Filatov, 1977). The filters were popular as 'Petryanov filters'. It was only in 1981 that the commercial production of electrospun products for a variety of filtration applications was achieved by an American company called Donaldson. Finally the commercial manufacture of electrospinning equipment for industrial production and academic research was achieved in 2006, by a Czech company called Elmarco Liberec (Jirsak *et al.*, 2005).

Figure 1.6 Chronological history for electrospinning technology (Lukas *et al.*, 2009, Teo and Ramakrishna, 2006, http://en.wikipedia.org/wiki/Electrospinning, 2012).

Theoretical underpinning of electrospinning method was carried out by Sir Geoffrey Ingram Taylor between 1964 and 1969 (Taylor, 1964, Taylor, 1966, Taylor, 1969). His work was directed towards explaining the electric discharge from rain droplets in clouds. Taylor characterised the cone formed under the influence of electric field and identified the critical angle of 49.3^{o} with respect to the axis of the cone at its apex, which is necessary to balance surface tension and electrostatic forces to form an electrospinning fluid jet. In recognition of his contribution the characteristic liquid cone formed at the tip of the spinneret under the influence of electric field is named 'Taylor cone'. Related theoretical modelling, again concentrated around the effects of electric field on water, was also carried out by Matthews to explain the mass loss and distortion of freely falling water drops in an electric field (Matthews, 1967). Experimental results of Matthews were utilized by Taylor to prove his models for explaining the electrospinning phenomenon. It is also important to note that the foundations for the generalized theoretical modelling of electrospinning is based on the work of Landau and Lifshitz, who modelled the charge density needed to induce surface wave instability for conductive liquids (Landau and Lifshitz, 1984).

Experimental evaluation of electrospinnability and parameter evaluation for a wide variety of polymers has only been initiated in 1970s. In 1971, Baumgarten produced acrylic microfibers with diameters ranging from 500-1100nm (Baumgarten, 1971). He observed the effect of solution viscosity and applied field on the diameter of the jet. But the research picked momentum only in the 1990s, when the groups of Renneker and Rutledge tested a wide spectrum of polymers and popularised the term 'electrospinning' (Doshi and Reneker, 1995, Reneker and Chun, 1996, Shin *et al.*, 2001, Fridrikh *et al.*, 2003, Hohman *et al.*, 2001a, Hohman *et al.*, 2001b). Thereafter, the research expanded worldwide firmly establishing the science and applicability of electrospinning.

1.2.4. Applications of electrospinning in tissue engineering

The practical application of electrospun membranes was first initiated in 1939 by Rozenblum and Petryanov-Sokolov through use as filters for military gas masks. Over the next 30 years Petryanov filters achieved an annual production of 20 million m^2 electrospun filter materials. The commercial production by Donaldson Inc. again concentrated on filtration applications. However, their application as textiles was limited due to their limited productivity 30m/min compared to conventional spinning technologies (~500m/min). The exponential increase in research, through the 1990s and 2000s, lead to the identification of a variety of applications including, filtration, healthcare, building construction, automotive industry, cosmetics, tissue engineering, biosensors, protective

clothing, energy generation, enzyme immobilization, and affinity membranes for non-woven electrospun products. The application for electrospun fibres relevant for this thesis is in tissue engineering. Hence the rest of this section explores the application of electrospun membranes in the emerging interdisciplinary field of tissue engineering.

Animal tissue is made of cells and the extracellular matrix (ECM) that they are embedded in. The natural ECM has a fibro-porous structure, which can be replicated using a simpler and cost effective electrospinning technology. The application of electrospun membranes in tissue engineering has been initiated in 1970s. The first report was published by Annis *et al.*, in 1978, who tested electrospun polyurethane mats as vascular prosthesis (Annis *et al.*, 1978). Later Fisher et al examined their long-term *in vivo* performance as arterial prosthesis (Fisher *et al.*, 1985). It was only in the 1990s that the exploration and exploitation of electrospinning technologies for tissue engineering and drug delivery picked up momentum and involved the use of a wide spectrum of synthetic and natural polymers for electrospinning.

1.2.4.1. Wound dressings and skin tissue engineering

Electrospun nano-fibrous membranes are widely used in wound dressings because of their higher porosity and good barrier. In 2003, Khil *et al.* prepared a nanofibrous PU membrane as a wound dressing exhibiting controllable evaporative water loss, excellent oxygen permeability and fluid drainage. Histological results indicated that epithelialisation occurred quicker and the dermis was better organized in the electrospun PU nanofibrous membrane compared to a commercial wound dressing, Tegaderm™ (Khil *et al.*, 2003). One year later, skin masks made of electrospun nanofibers were claimed as a patent by Reneker and colleagues (Smith *et al.*, 2004). In this design, nanofibres were directly deposited onto skin surface to reduce the fluid accumulation between fibres and wet wound surface. Another example is the co-axial composite fibre containing natural and synthetic polymers to provide a favourable substrate for fibroblasts (Chong *et al.*, 2007b). Biodegradable polycaprolactone (PCL) was the core providing mechanical support while gelatin was the shell for bioactivity providing large surface area for cell attachment, transport, proliferation and function. This nanofibrous scaffold was also directly electrospun onto a polyurethane dressing (Tegaderm TM) to serve as a synthetic epidermis protecting both the wound and the fibroblast-populated nanofibre lattice from infection, while promoting human dermal fibroblast (HDF) proliferation. However, very thin thickness of nanofibrous scaffold is still a shortcoming in the application of replacing the lost dermis. Thus, the author proposed an improved design of the dual-sided fibroblast-seeded scaffolds to reconstitute full dermal thickness (Chong *et al.*, 2007a).

1.2.4.2. Vascular tissue engineering

Electrospun scaffolds/tubes have been recognized as good candidates for artificial blood vessel due to their controllable mechanical and physical properties. The fibre diameter, structure and alignment can be controlled for design of blood vessels. An attempt has been made to use electrospun poly(lactic-co-glycolic acid) (PLGA) tubes with aligned fibres as a scaffold for artificial blood vessels through the hybridization of smooth muscle cells (SMCs) (Kim *et al.*, 2008b). The hybridized scaffold showed formation of neointima with good patency, whereas an occlusion was observed on unhybridized vessel in the first week of implantation in dogs. The importance of fibre alignment for vascular tissue engineering was reported by Xu *et al.* (Xu *et al.*, 2004). They found that the adhesion and proliferation of the coronary artery SMCs were enhanced when compared to the plane polymer films and cells were capable of migrating along the axis of aligned fibres. Surface modification of electrospun nano-fibrous membranes with plasma treatment and collagen coating improved the spreading, viability, attachment and maintenance of phenotype of human coronary artery endothelial cells (He *et al.*, 2005). Such nano-fibre membranes also showed tensile properties suitable for vascular graft.

1.2.4.3. Bone tissue engineering

The design of scaffolds for bone tissue engineering is focused around matching the physical properties of bone tissue including tensile strength, pore size, porosity, hardness, and overall 3D architecture. For bone regeneration applications, scaffolds with a pore size ranging from 100-350 μm and porosity greater than 90% are preferred (Bruder and Caplan, 2000, Hutmacher, 2000). PCL was first considered to be a degradable nano-fibre matrix for bone regeneration, which provided support for rat bone marrow stromal cells (BMSCs) and deposition of native collagen I based connective tissue and calcium phosphate based bone) at 4 weeks. The effect of fibre diameter (0.14-2.1μm) on the MC3T3-E1 cell responses was examined on PLA electrospun nanofibrous scaffold (Badami *et al.*, 2006). It is interesting to note that the biomimetic nano-fibrous topology in conjunction with osteogenic medium significantly enhanced cell density within the scaffold.

The initial adhesion and rapid migration of cells into the bulk of the scaffold is essential for tissue engineering applications. However, due to the innate hydrophobic nature, the initial cell adhesion is limited for most synthetic polymers. Hence, combinations of synthetic and natural polymers were introduced by many researchers to improve cell compatibility. The fibres made of composites of PCL and gelatin at 1:1 ratio exhibited better penetration of BMSCs within the nanofibre matrix compared to the pure PCL nanofibre (Zhang *et al.*, 2004b). Moreover, another study on the blending nanofibers

of PLA with gelatine at various ratios (1:2, 1:1, and 3:1) showed that the osteoblastic cells (MC3T3-E1) were more viable than those on pure polylactic acid (PLA) nanofibre (Kim *et al.*, 2008a). In addition, biomimetic bone collagen and hydroxyapatite were combined with Poly-L-Lactide Acid (PLLA) to produce biomimetic electrospun composite-fibre scaffolds for bone tissue engineering (Zhao *et al.*, 2006, Prabhakaran *et al.*, 2009).

Besides bone tissue engineering, electrospun nanofibres have also been used in engineering other structural tissues including cartilage (Li *et al.*, 2003, Li *et al.*, 2005) ligament (Altman *et al.*, 2002, Yates *et al.*, 2012), and skeletal muscle (Riboldi *et al.*, 2005).

1.2.4.4. Neural tissue engineering

Neural tissue repair is a daunting challenge because almost all neural injuries result in an irreversible loss of function. Therefore, to bridge and enhance nerve regeneration, a variety of ready-to-use nerve guidance conduits (NGCs) having customized sizes and lengths are desired. Numerous studies proved that fibres having diameters of 100-250 nm are capable of directing peripheral neurite growth both *in vitro* and *in vivo* (Lundborg *et al.*, 1997, Rangappa *et al.*, 2000, Smeal *et al.*, 2005, Steuer *et al.*, 1999) and the efficacy is further improved when fibre diameters were lowered to the range of 5-30 nm (Wen and Tresco, 2006). Furthermore, Yang *et al.* found that randomly oriented nano-fibres (150-350 nm) based on electrospun PLLA scaffolds not only supported neural stem cell (NSC) adhesion but also promoted NSC differentiation (Yang *et al.*, 2004a). In a later study, the role of aligned nano-fibres in neural tissue engineering has been further investigated and NSCs were observed to elongate and their neurites grew along the direction of the fiber orientation of the aligned nano-fibres (Yang *et al.*, 2005). Recently, Griffin *et al.* also develop a neutral repairing scaffold composed of aligned PLGA and salicylic acid-derived poly (anhydride-ester) electrospun fibres (Griffin *et al.*, 2011). The addition of the later material, which released salicylic acid during hydrolytic degradation, mitigated the fierce inflammatory cascade invoked by accumulation of the degradation products of glycolic acid and lactic acid in PLGA system.

1.3. Glucose biosensors

Glucose is the fundamental fuel for cells of most living organisms and commercially, it is used as a precursor for the production of molecules such as vitamin C, citric acid, gluconic acid, polylactic acid, sorbitol and bio-ethanol. Such large scale utilization of glucose necessitates the need for efficient feedback control systems, for which the use of glucose sensors is mandatory. This section reviews the different aspects of glucose biosensors, namely, the need for them, the existing technologies, the advantages

and the problems associated with continuous monitoring using implantable sensing technologies, and the strategies employed to make implantable biosensors function reliably in the long-term.

1.3.1. The need for glucose biosensors

The need for glucose sensing has primarily been driven by the medical condition – diabetes, wherein, the normal glucose metabolism is disturbed. The usual blood glucose level in healthy humans varies between 70 to 120 mg/dL or 4 to 8 mM/L. An impaired body's feedback control system causes a wider range, 30 to 500 mg/dL or 2 to 30 mM/L, of blood glucose in people with diabetes. Insulin, the hormone that promotes glucose uptake by cells, is either not produced in enough quantity (Type I) or the glucose absorbing cells develop 'insulin resistance' (Type II), usually causing abnormally high blood glucose levels (hyperglycemia) in diabetics. The opposite effect, wherein hyperinsulinism or lack of counter-regulatory hormones (e.g. cortisol), abnormally lowers blood glucose levels (hypoglycemia). Persistent hyperglycaemia causes dehydration, long-term cardiovascular complications, damage to eyes and kidneys, and impaired would healing; while the hypoglycemia often results in fainting, coma, or death (Heller and Feldman, 2008, Tonyushkina and Nichols, 2009). The conditions hyper- or hypo-glycaemia can also occur due to non-diabetic and genetic causes such as, pregnancy, medication, stress/trauma, haemorrhage, burns, infections, stroke or alcohol consumption (Tonyushkina and Nichols, 2009, Kondepati and Heise, 2007). In either case, it is essential to identify and control the blood glucose levels (glycemic control), to avoid painful and debilitating complications. Tight glycemic control is only possible when reliable, accurate and timely glucose sensing is achieved (Heller and Feldman, 2008, Tonyushkina and Nichols, 2009, Oliver *et al.*, 2009, Kondepati and Heise, 2007).

In addition to medical monitoring of diabetes, glucose sensing has become essential in the process optimization of industrial and research scale microbial and mammalian cell cultures. *In vitro* cell culture processes are complex and difficult to optimize unless a feedback control based on tight monitoring of a wide range of parameters including glucose, lactate, pH and temperature are achieved. An industrial scale glucose sensing is represented in microbial fermentation processes. Traditionally, intermittent sampling of fermentation medium is done, sample processed and used to monitor glucose using a commercial glucose analyser (Yellow Spring Instruments, Yellow Spring, Ohio, USA) (Queinnec *et al.*, 1992). At research scale, focus is on developing mammalian cell culture bioreactors integrated with various sensors including glucose biosensors for regenerative medicine and toxicity testing, especially to reduce animal use for research. Recent

advances in glucose sensing, especially real-time (continuous) glucose monitoring technologies developed for diabetes management, are being explored and utilized for cell culture bioreactors and microfluidic devices (Brooks *et al.*, 1987, Tothill *et al.*, 1997, Lee *et al.*, 2004b, Kimura *et al.*, 2010).

1.3.2. Classification and history of glucose biosensing

Glucose, being a generic sugar, the methods for its sensing often requires the use of special affinity molecules. The glucose binding reaction with the affinity molecule, typically, generates a measurable signal for detecting glucose in complex biological fluid systems. Electrochemical or optical signal transduction based sensors are the most commonly used for glucose sensing technologies, which are the focus for this section.

1.3.2.1. Electrochemical glucose biosensors

Electrochemical technologies have dominated the glucose sensor market since their first use in 1960s. Their advantage is that they are highly sensitive, relatively reproducible and cost effective (Newman and Turner, 2005). Sensors fabricated using this technique can be divided into two main classes, namely enzymatic and non-enzymatic, based on whether they use or not use one or more enzyme(s) as the affinity molecule.

1.3.2.1.1. Electrochemical enzymatic glucose biosensors

To date, four different types of enzymes namely, glucose dehydrogenases (GDH), quinoprotein glucose dehydrogenases, glucose 1-oxidases, and glucose 2-oxidasses have been tested for glucose biosensing (Wilson and Turner, 1992). Among the enzymes, glucose 1-oxidase (GOD) is the most commonly due to its better stability and exclusive specificity to glucose, which properties are attributed to the protection of its redox centres (flavin adenine dinucleotide (FAD)) by a glycoprotein shell. As a result, the glucose molecule and its co-reactant namely O_2 need to diffuse through to a depth of 13Å to reach the reaction centre, which is responsible for its lower reaction turnover (oxidizes about 5000 glucose molecules per second in an electrochemical half-reaction) compared to the other enzymes (Heller and Feldman, 2008). The catalysis reaction for GOD is shown in Figure 1.7.

All sensors utilizing the GOD based catalysis using the natural O_2 as the mediator are called **first generation glucose biosensors** (Figure 1.7). Essentially, these sensors either measure O_2 depletion or H_2O_2 generation, which is proportional to the concentration of glucose, and they can be amperometric, potentiometric or O_2 sensors.

The first glucose biosensor was proposed by Clark and Lyons in 1962 (Clark and Lyons, 1962). This device was based on GOD entrapped on at a Clark oxygen electrode using a semi-permeable dialysis membrane. The depletion of oxygen (proportional to the

glucose concentration) was measured by reducing O_2 at a platinum cathode at a potential of -0.6V against saturated calomel electrode (SCE). The first commercial clinical analyzer, Beckman glucose analyzer introduced in 1968, was based on electroreduction of O_2 at a gold cathode, which later was replaced by a polarographic O_2-electrode (Clark, 1959, Heller and Feldman, 2008). Recently, Gough *et al.* reported the successful use of GOD and catalase based dual enzyme O_2 sensing system for CGM in a subcutaneous animal model for over a year (Gough *et al.*, 2010). The most commonly used and the only sensors currently available for implantable continuous glucose monitoring are amperometric sensors. The H_2O_2, generated in the first generation O_2 mediated reaction, is directly oxidized at an anodic working electrode at potentials between +0.6 to +0.7 V vs saturated calomel (SCE) or silver/silver chloride (Ag/AgCl) reference electrode, which accurately correlates to the oxidised glucose concentration. Potentiometric sensors are typically based on field-effect transistor (FET) sensors, which monitor changes in pH due to either the electrooxidation of H_2O_2 or the hydrolysis of gluconolactone to determine changes in glucose concentrations.

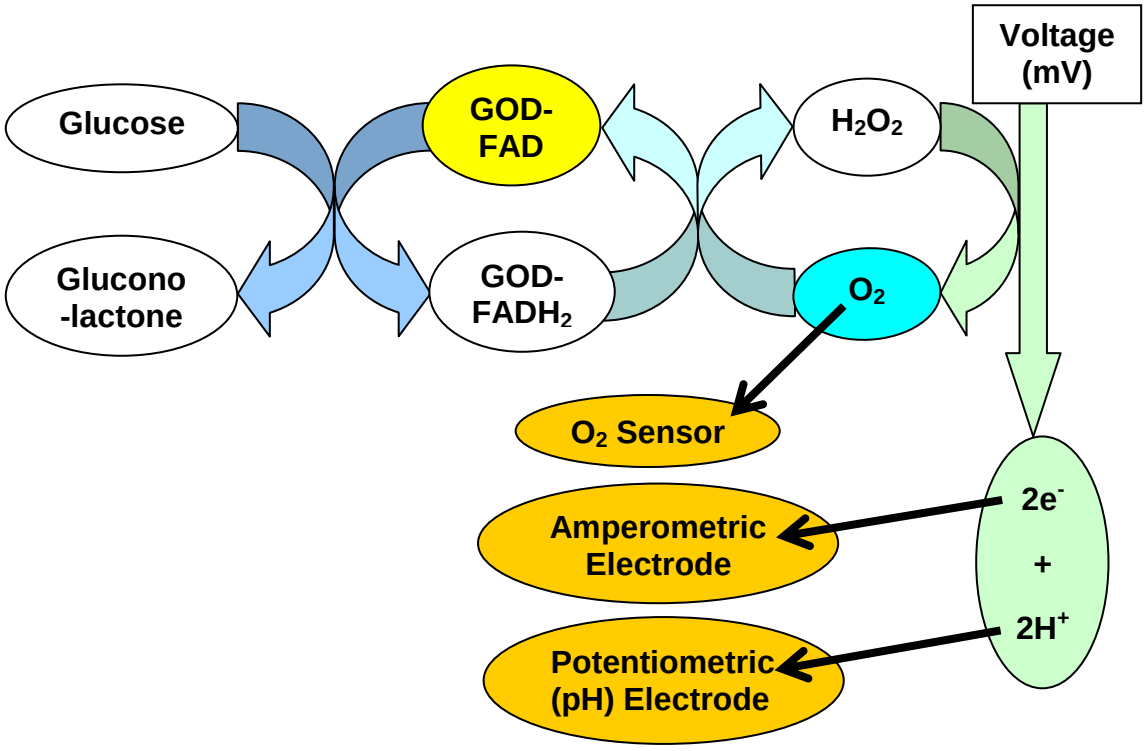

Figure 1.7 First generation glucose sensing reaction and associated sensors

Overall, the main problems for first generation of glucose biosensors exist, namely interference from other redox agents (at the 0.6 to 0.7 V potential used by amperometric sensors) and the high dependency on oxygen. The former is minimized by use of special permselective membranes, while the latter is overcome by use of membranes with high oxygen permeability or by altogether avoiding the use of O_2 as the mediator for GOD

catalyzed glucose oxidation (second generation glucose sensors). In addition, the use of potentiometric sensor is severely limited by the interference from local changes in pH in physiological fluids.

Diminishing the interfering agents such as uric acid, acetaminophen and ascorbic acid in physiological fluids, from reaching the sensor is achieved by use of permselective membranes (Hrapovic *et al.*, 2004). Such selective layer is often applied between the enzyme layer and the electrode. The electropolymerized films such as poly (phenylenediamine) (Sasso *et al.*, 1990) and overoxidized polyrrole (Malitesta *et al.*, 1990) are the commonly used interference eliminating layers on electrode surface. Other widely used coatings include size extrusion cellulose acetate membrane (Reddy and Vadgama, 1997a), negatively charged Nafion (Hrapovic *et al.*, 2004), microporous silicone-based emulsions (D'Orazio, 1996). Interference can also be reduced by lowering the oxidation potential or the use of reduction potential, at which the oxidation of interferants is nearly eliminated. This is achieved by electrode modifications. For example, metal nano-particles (i.e. Pt, Pd, and Ru) dispersed in carbon paste electrodes has been particularly beneficial in obtaining remarkable selectivity towards glucose substrate by means of lowering the oxidation potential of H_2O_2 compared to either pure carbon or pure metal electrodes (Wang *et al.*, 1992, Wang *et al.*, 1994, Newman *et al.*, 1995). On the other hand, the problem of high oxygen dependency that usually results in underestimation of glucose level due to very low physiological oxygen concentrations (0.1 to 0.3 mM) compared to that of glucose (2-30 mM) can be overcome by use of membranes having high permeability to oxygen. A common approach is the use of mass-transport limiting membranes that restrict the amount of glucose reaching the enzyme in relation to O_2. Polymers such as Nafion, polyurethane, poly (vinyl chloride), polycarbonate are the frequently used materials for this purpose (Reddy and Vadgama, 2002, Yu et al., 2005b, Galeska et al., 2000, Moussy et al., 1994, Maines et al., 1996). Gough *et al* designed a two-dimensional sandwich enzyme electrode, with two different membranes on either side of the electrode (Gough *et al.*, 1985). One side is highly permeable for O_2 but not for glucose, while the other side is permeable to both O_2 and glucose. The most efficient method for avoiding O_2 deficiency at the electrode is the use of oxygen rich electrode materials which serve as an internal source of oxygen for glucose oxidation (Wang and Lu, 1998). The sensors consisted of a mixture of graphite powder and a fluorocarbon pasting liquid can provide total oxygen independence even under severe oxygen deprivation. The principle is based on the excellent solubility of oxygen within fluorocarbons which is approximately 25-fold higher than that in water.

Second-generation glucose biosensors, typically, have artificial (non-physiological) mediators replacing O_2 as co-substrates for oxidising GOD or GDH (mediator coupled-electrooxidation, Figure 1.8) (Liu and Wang, 2001, Cass et al., 1984, Mulchandani and Pan, 1999, Di Gleria et al., 1986, Groom et al., 1995, Tsujimura et al., 2006, Chaubey and Malhotra, 2002b, Li et al., 1999, Kulys et al., 1994). Commonly used mediators in the second generation sensors are listed in Table 1.1. The mediators have nano-dimensions capable of directly interacting with $FADH_2$ of GOD, and mediate the direct transfer of electrons to electrode. They obviate the need for O_2 but suffer from competition from O_2 (Toghill and Compton, 2010). To circumvent O_2 competition, large excess of mediator is incorporated, and in most currently available single-use home glucose test strips, GOD is replaced by glucose dehydrogenase pyrroloquinoline quinone (GDH-PQQ). However, sensors with GDH-PQQ suffer from inaccuracy due to competition from non-glucose sugars, such as maltose, xylose, and galactose (found in certain drug and biologic formulations, or can result from the metabolism of a drug or therapeutic product), often leading to falsely elevated blood glucose levels prompting deleterious therapies (FDA, 2009). In addition to O_2 independence, second-generation sensors, depending on the structure of the mediator, require lower electrode potentials for measuring compared to that for direct oxidation of H_2O_2, thus avoiding the common interferants from blood/tissue oxidising at the electrode. In addition, a restrictive membrane to slow down the diffusion of glucose is often not required. However, a membrane to contain or immobilize the mediator and enzyme at the electrode surface is often essential for using the second-generation sensors (Henning, 2010, Li *et al.*, 2007). To solve the problem of mediator leakage, a variety of methods were investigated involving entrapping mediator in a conducting polymer (Foulds and Lowe, 1986), employing high-molecular-weight mediator such as ferrocen derivatives (Schuhmann, 1993) and covalently tethering both the mediator and enzyme to a polymeric materials (Saito and Watanabe, 1998, Koide and Yokoyama, 1999, Kuramoto and Shishido, 1998).

Among the immobilizing membranes, Heller *et al.* demonstrated the efficacy of redox polymers leading to the design of commercial second-generation sensors – FreeStyle Navigator continuous glucose monitoring system (Heller and Feldman, 2010). This design avoided the free diffusion of artificial mediators through their covalent attachment to the enzymes' redox centres and the redox hydrogels. Thus, the enzyme's reaction centres are electrically connected directly to the electrode surface (Heller and Feldman, 2008, Heller, 1990, Heller, 1992, Degani and Heller, 1987). Recently, Wilner's group also developed a similar system where GOD is covalently bound to Au nano-particles (NPs) that are

crosslinked into multiple layers electrically wiring the redox centres of GOD directly on to Au electrode surface(Yehezkeli *et al.*, 2009, Yehezkeli *et al.*, 2010). An added advantage of such direct electrical wiring systems is that the crosslinked redox networks connect multiple enzyme layers, thus increasing the glucose measuring current by 10 to 100 folds and current densities of glucose electrooxidation on conventional solid electrodes can exceed 1 mA/cm^2 at potentials between 0.0-0.1V vs Ag/AgCl (Heller and Feldman, 2008).

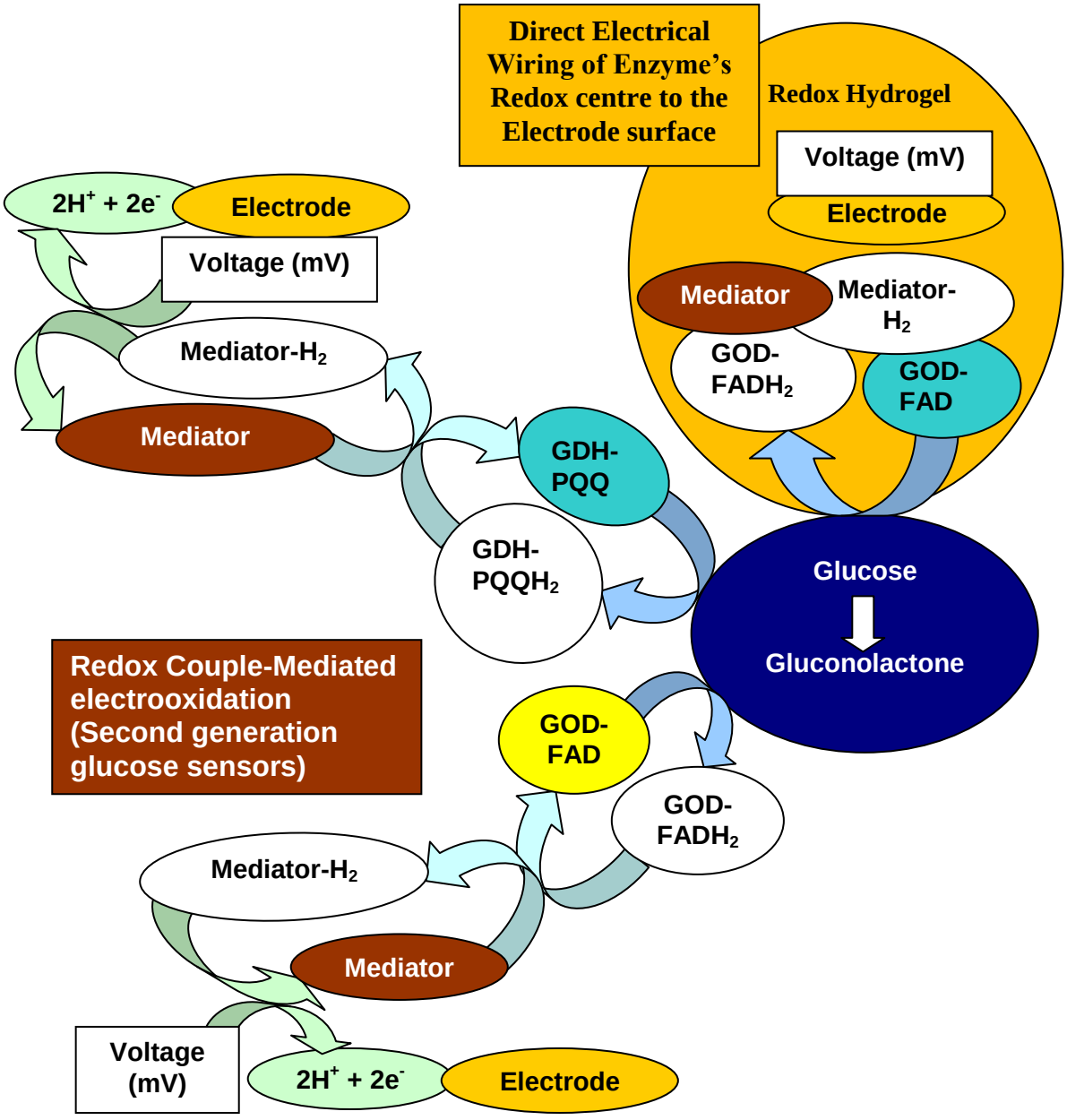

Figure 1.8 Second generation glucose sensing reactions. The associated sensors are typically amperometric

Table 1.1 Artificial mediators – redox couples for electron shuttling from redox centres of enzymes such as GOD-$FADH_2$ and GDH-$PQQH_2$ to electrodes (Heller and Feldman, 2008, Chaubey and Malhotra, 2002a, Švancara et al., 2009)

Type	**Mediators**
Organic	Quinoid dyes: methylene blue, thionine, pyocyanine, Safranine T, brilliant cresyl blue, azure A Quinone and its derivatives including polymeric quinones: hydroquinone, benzoquinone, 1,10-phenanthroline quinine, polyaminonapthoquinone (PANQ) Viologen derivatives: N,N'-Di(4-nitrobenzyl)viologen dichloride, poly(o-xylylviologen dibromide), poly(p-xylylviologen dibromide) Phenothiazines, Phenoxazines, Dithia- & tetrathia- aromatic compounds Phenazines: N-ethyl phenazine, N-methyl phenazine Wurster's salt: N,N,N',N'-Tetramethyl-p-Phenylenediamine (TMPD) Heterocyclic dihydropolyazines: 5,10-dihydro-5,10-dimethylphenazine, 1,4-dihydro-1,3,4,6-tetraphenyl-s-tetrazine Poly(1-(5-aminonapthyl) ethanoic acid) (PANEA) Tetrathiafulvalene (TTF) Tetracyanoquinodimethane (TCQM) Conducting salts: TTF-TCQM, N-methyl phenazinium-TCQM (NMP-TCQM) Carbon materials: Carbon nanotubes (CNTs), powdered graphene, fullerenes
Inorganic	O_2/H_2O_2 Metal hexacyano-complexes: $Fe(CN)_6^{3-/4-}$, $Co(CN)_6^{3-/4-}$, $Ru(CN)_6^{3-/4-}$
Metal-Organic	Pentacyanoferrate(III)-, $Fe^{2+/3+}$-, $Ru^{2+/3+}$-, or $Os^{2+/3+}$- complexes with organic polymers such as pyridine, pyrazole, imidazole, histidine, aza- and thia-heterocycles, benzotriazole, benzimidazole, and aminothiazole Ferrocene and its derivatives: Ferrocene, 1,1-dimethyl ferrocene, vinyl ferrocene, ferrocene carboxylic acid, ferrocene metanol, hydroxymethyl ferrocene, 1,1'-dimethyl 1,3-(2-amino-1-hydroxyethyl) ferrocene Nikelocene Manganese cyclopentadienyl (Cp) half-sandwich, chromium half-sandwich

During the 1980s, intensive efforts were made to develop mediator-based second generation glucose biosensors for sports and clinical applications (Cass *et al.*, 1984, Frew

and Hill, 1987), both for improving *in vivo* sensor performance (Murray *et al.*, 1987) and integrating the technology in test strips for commercial self-monitoring of blood glucose (SMBG) system (Hilditch and Green, 1991, Matthews *et al.*, 1987). In 1982, Shichiri et al (Shichiri *et al.*, 1982) made a prominent contribution to the *in vivo* application of glucose biosensors through the design of the first needle-type enzyme electrode for subcutaneous implantation. The first palm-sized electrochemical blood glucose monitor designed for self-monitoring of diabetics was launched in 1987 as ExacTech by Medisense Inc. (Matthews *et al.*, 1987). It used ferrocene as the mediator and the device was enabled to display a digital glucose reading within 30s after the application of whole blood. In the following decades researchers have increasingly focused on the development of less invasive implantation of sensor device (Henry, 1998, Schmidtke *et al.*, 1998), and the establishment of electron transfer between electrode surface and enzyme redox centre (Degani and Heller, 1988, Ohara *et al.*, 1993, Toghill and Compton, 2010).

The futuristic **third-generation glucose sensors** (Figure 1.9) aim to avoid the redox mediators, yet, achieve direct transfer of electrons from glucose to electrode via the redox centre of the enzyme (Gregg and Heller, 1990, Kulys *et al.*, 1980, Schuhmann, 1995, Khan *et al.*, 1996, Chaubey *et al.*, 2000). The resulting glucose sensors, said to work reagentless, are expected to have a low operating potential that is close to the redox potential of the enzyme (Wang, 2008). The $FADH_2$ redox centre of the conventional GOD enzyme is reported to be buried at a depth of 13-15 Å, due to which, direct electron transfer from GOD to conventional solid state electrodes is reported to be much too slow (Hecht *et al.*, 1993, Heller and Feldman, 2008). Hence, the design of third generation glucose sensors is expected to either utilize other redox enzymes or explore new electrode materials. Wang, and Chaubey and Malhotra provided brief reviews of the different electrode materials being investigated for the design of third-generation sensors (Wang, 2008, Chaubey and Malhotra, 2002a). An example for one such electrode materials is tetrathiafulvalene-tetracyanoquinodimethane (TTF-TCNQ), which is being widely reported for the development of conducting organic salt electrodes for direct transfer of electrons from glucose to electrode through the redox centre of GOD (Wang, 2008, Khan *et al.*, 1996, Koopal *et al.*, 1992, Palmisano *et al.*, 2002). The recent advances in nano and porous materials provide scope for third generation glucose sensors, which could not only improve the sensing performance, but also decrease the cost, size of sensor, use of toxic mediators and avoid dependence on O_2 (Zhou *et al.*, 2008, Bao *et al.*, 2008, Yang *et al.*, 1998, Xu *et al.*, 2003, Zhu *et al.*, 2005, Lee *et al.*, 2005, Yu *et al.*, 2008b, Zhu *et al.*, 2008).

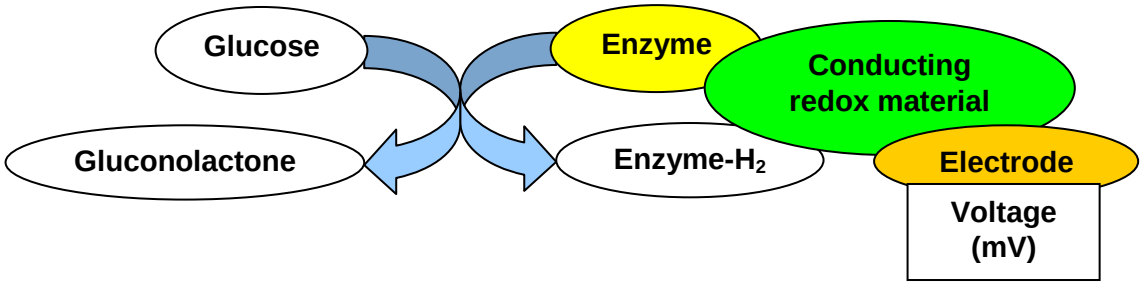

Figure 1.9 Third generation glucose sensing principle, wherein the redox centres of the enzyme are covalently attached to conducting polymers which in turn are covalently attached to electrode surface. This ensures direct transfer of electrons from the enzyme's redox centre to the electrode.

1.3.2.1.2. Electrochemical non-enzymatic glucose sensor

The stability of enzymes in the long-term or during storage has been a concern and methods to eliminate the use of enzyme have been researched (Park *et al.*, 2006). Walther Loeb first studied the means of electrochemically oxidizing glucose in the presence of sulphuric acid at an anode a century ago (Toghill and Compton, 2010). Since then, a variety of methods were tested. Direct electrooxidation or reduction of glucose in an electrolytic cell usually require extreme conditions, such as pH>11, pH<1 and high voltages, or suffer from electrode poisoning, inhibition and interference at physiological pH (Table 1.2) (Heller and Feldman, 2008, Park *et al.*, 2006). The different isomeric (α-, β-, γ-) forms of glucose get electrooxidized at a metal electrode, whether they involve intermediates or not, to form gluconic acid as the final stable product of a two-electron oxidation of glucose (Park *et al.*, 2006, Ernst *et al.*, 1980, Beden *et al.*, 1996) The resulting gluconic acid is reported to have a half-life of 10min and rate constant of 10^{-3}/s at pH 7.5.(Park *et al.*, 2006) Furthermore, the electrooxidation of glucose was shown to have three potential ranges vs reversible hydrogen electrode (RHE) of relevance to glucose sensing (Table 1.2) (Ernst *et al.*, 1979, Park *et al.*, 2006). The first, between 0.15 and 0.35V, called 'hydrogen region', provides strong oxidation peak potentials unique to glucose, observed primarily with Pt electrode. However, flat platinum electrodes rapidly lose sensitivity to glucose due to poisoning by chloride ions and various organic agents including amino acids, acetaminophen, creatinine, epinephrine, urea and uric acid in physiological solutions, which normally block the catalytic sites on platinum, inhibiting glucose oxidation. The second, between 0.4 and 0.8V vs RHE, called 'double layer region' lowers the adsorptive capacity of the poisoning agents, but other electroactive (interfering) agents also get oxidized at the electrode. Finally, the third, 'Pt oxide region', between 1.1

and 1.5V produces a Pt oxide layer, with which glucose reacts, while poisoning products similar to lactones are decomposed by further oxidation.

Thus glucose, a monosaccharide, can indeed be directly electrooxidized at conventional electrodes. However, its rate of oxidation is much slower than common interfering substances such as uric acid and ascorbic acid in biological fluids. Though the normal concentration of glucose in blood (3 to 8 mM) is much higher than the interfering substances (0.1mM), the faradic current generated by oxidation of interfering agents is much higher than that for glucose.(Park *et al.*, 2006) Attempts have been made to avoid interference by lowering the over-potential for oxidation of glucose through the development of electrodes based on alloys of Pt, Pb, Au, Pd, Rh, Cu, Mn, Ni, Fe, Ag etc. (Vassilyev *et al.*, 1985, Beden *et al.*, 1996, Park *et al.*, 2006, Sakamoto and Takamura, 1982, Kokkinidis and Xonoglou, 1985, Wittstock *et al.*, 1998, Zhang *et al.*, 1997, Yeo and Johnson, 2000). Glucose oxidized at Pt_2Pb alloy surface at remarkably lower potentials (than pure platinum) at which the electrode is insensitive to common interfering substances (Sun *et al.*, 2001). Nevertheless, they failed to prevent electrode poisoning by chloride ions and other electroactive components abundant in physiological solutions as well as by the various glucose oxidation products.

The advent of nanotechnology provided new hope for non-enzymatic glucose sensing, and combining nano-materials with conventional electrodes not only avoided interference from interfering substances, but also lowered or prevented electrode poisoning. Carbon-based materials such as carbon paste, diamond-like carbon, graphite, graphene and carbon nanotubes (CNTs) are widely being explored for glucose sensing, often in combination with NPs. Among the carbon materials, CNTs are widely researched due to their exceptional chemical and physical properties including high surface to volume ratios, chemical stability, electrical conductivity and electron transfer kinetics. Different combinations of carbon based materials and/or NPs, with or without polymer fillers are being tested as coatings on common electrodes such as Pt, Au and glassy carbon for non-enzymatic glucose sensing (You *et al.*, 2003, Ye *et al.*, 2004, Jianxiong *et al.*, 2007, Tan *et al.*, 2008, Yang *et al.*, 2010, Jiang and Zhang, 2010, Kang *et al.*, 2007, Zhu *et al.*, 2009, Rong *et al.*, 2007, Wang *et al.*, 2009a, Chen *et al.*, 2008, Cui *et al.*, 2006, Chen *et al.*, 2010b, Liu *et al.*, 2010). However, the electrocatalytic effects of almost all of the nano-material coatings are observed in basic conditions usually at pH>9.

Table 1.2: Direct electro-oxidation of glucose at electrodes (Heller and Feldman, 2008, Park *et al.*, 2006, Ernst *et al.*, 1979)

Electrode	**Conditions**	**Disadvantages**
Conventional electrodes (e.g. Pt and Au)	pH>11, pH<1, High voltages	• Electrode poisoning, Inhibition • Interference • Extreme conditions
Reversible Hydrogen Electrode (RHE)	0.15 to 0.35 V (hydrogen region)	• Electrode poisoning, agents such as chloride ions, acetaminophen, creatinine, epinephrine, urea and uric acid, bind and block catalytic sites on electrodes • Selectivity not exclusive to glucose
Reversible Hydrogen Electrode (RHE)	0.4 to 0.8 V (double layer region)	• Electrode poisoning is reduced but there is interference due to oxidation of other electroactive agents including ascorbic acid, acetaminophen and uric acid • Selectivity not exclusive to glucose
Reversible Hydrogen Electrode (RHE)	1.1 to 1.5 V (Pt oxide region)	• High voltages decompose interferants but not glucose, but selectivity not exclusive to glucose

One of the simplest, yet effective, enzyme-free sensor is based on nano-porous Pt electrode, whose surface nano-pores have diameter in the range of 2-50 nm (Park *et al.*, 2003, Boo *et al.*, 2004). This electrode is reported to selectively enhance the faradic current of the sluggish glucose oxidation reaction through kinetic controlled electrochemical mechanism. Interfering agents – ascorbic acid and acetaminophen gave negligible response, while signal amplification was observed for glucose oxidation at the nano-porous Pt electrode (Park *et al.*, 2003). Thus nano-porosity on Pt not only reversed the analyte selectivity, but also prevented electrode poisoning by chloride ions. Unlike other non-enzymatic glucose biosensor, the elimination of interference from common interfering

agents at the nano-porous Pt electrode is not a function of potential applied but of the dynamics of mass transport near the novel morphology of the electrode surface (Park *et al.*, 2006). Compared to the enzymatic sensors, the nano-porous Pt sensor is mechanically and chemically stable, resistant to humidity and temperature, has longer storage shelf-time, allows thermal and chemical sterilization process, and favourable for mass production due to simpler quality control (Park *et al.*, 2006).

1.3.2.2. Optical glucose biosensors

Spectroscopic measurements of direct or indirect interactions of different properties of light with glucose molecules alone; colour generating glucose-dye complexes; or fluorescence systems based on glucose–receptor molecule complexes form the firm basis for the optical methods.

A direct method to measure blood glucose levels is to irradiate tissues such as skin, eye, or whole blood, with different forms of light, and detect the resulting absorption, transmission, reflection, scattering or emission signals (Oliver *et al.*, 2009). Mid infrared (MIR) with wavelengths (λ) between 2.5 to 50 μm and near infrared (NIR) λ – 0.7 to 1.4 μm are widely studied for this purpose. Although the tissue penetration depth for MIR is much low (superficial compared to NIR that reaches up to the subcutaneous space), MIR was successfully used in glucose measurements, ex vivo, in whole blood in intensive care units (Shen *et al.*, 2003, Nelson *et al.*, 2006). Other commonly investigated forms of light for glucose detection include, plain polarized, coherent (light in which emitted photons are synchronised in time and space), single wavelength (Raman) and He-Ne laser light (Cameron and Anumula, 2006, Esenaliev *et al.*, 2001, Dieringer *et al.*, 2006, Ashok *et al.*, 2010). Despite being non-invasive, these methods failed to reach the standards for CGM *in vivo*, because of their, usually, >20% error in glucose measurements (Kondepati and Heise, 2007, Clarke *et al.*, 1987). The large error is caused by factors including interferants; heterogeneity of tissue; temperature; heterogeneous distribution of glucose between cells, interstitium and blood; changes in water, free fatty acids, chylomicrons, fats or protein content in tissue; motion artefacts (including blood flow); and drug treatments (Kondepati and Heise, 2007, Oliver *et al.*, 2009, Pickup *et al.*, 2005). Often the glucose measuring signal is weak (esp. for Raman spectroscopy), and to quantify the single solute, the signal requires screening of multiple wavelengths and multivariate statistical analysis with calibration (Oliver *et al.*, 2009).

Glucose can also be measured by indirect methods, where glucose molecules modify a specific tissue property that can be detected. Photo-acoustic and impedance spectroscopy are two such methods used for measuring the glucose-mediated decrease in

specific heat capacity and the glucose-red blood cell (RBC) interactions causing concentration-dependent changes in dielectric properties of tissue respectively (Weiss *et al.*, 2007, Pfutzner *et al.*, 2004). These methods also suffer from similar problems faced by the above described direct methods.

By far the most efficient, reliable and practical way to measure glucose is to use glucose specific interactions (Heller and Feldman, 2008, Oliver *et al.*, 2009). Most fluorescence based optical methods utilize affinity based sensing principle, where glucose competitively displaces a fluorescently labelled binding agent (e.g., dextran, α-methyl mannoside or glycated protein) from a receptor, specific to both glucose and binding agent, resulting in a concentration-dependent change in fluorescence emission or quenching signal (Oliver *et al.*, 2009, Pickup *et al.*, 2005). The receptor materials can be broadly classified into four categories: Concanavalin A (CON A), enzyme based (glucose oxidase/dehydrogenase, hexokinase), synthetic boronic acid derivatives, and bacterial glucose specific proteins. While the former two are well established, newer and better molecules of the latter two categories are being developed for glucose sensing. Further, an advanced and extremely sensitive fluorescent method is the fluorescence resonance energy transfer (FRET) based on Angstrom level dipole-dipole interactions between fluorescence donor and acceptor molecules leading to a decrease in fluorescence or life-span of a donor molecule. In spite of their huge promise, fluorescence based glucose detection methods are yet to reach the clinics for CGM *in vivo*.

1.4. Commercial glucose biosensors

Broadly, the commercial glucose biosensors available for home and clinical use can be classified into self-monitoring of blood glucose (SMBG) and continuous glucose monitoring (CGM) devices. The former use test strips, on which, a drop of blood usually drawn by finger pricking is applied, to detect blood glucose concentration. The later involves non-invasive, minimally invasive or invasive methods for CGM. However, the only devices available commercially for CGM are the invasive devices, wherein, needle type electrochemical glucose biosensors are inserted in the dermal or subcutaneous space of skin, which function for a maximum of 7 days.

SMBG measurements are discontinuous and often miss the deleterious episodes of hypo- or hyper-glycaemia, which are further be exacerbated by the patient unwilling to do the required number of tests (compliance). In contrast, CGM avoids the need for patient compliance, and provides 24/7 monitoring of glucose to alert the patient and physicians to prevent hypo- or hyper-glycaemia.

SMBG is currently the indispensable part of the disease management programme for diabetes patients recommended by the American Diabetes Association (ADA, 2008). The first blood glucose meter and glucose self-monitoring system, the Ames Reflectance Meter (ARM) was invented by Anton H. Clemens in 1970, using a single drop of blood and providing a reading in 1 minute (Tonyushkina and Nichols, 2009). Since then a large number of test strip based SMBG devices have been introduced in the market and reviewed widely in the literature (Heller and Feldman, 2008).

The CGM systems available commercially include Guardian REAL-Time, Minimed Paradigm REAL-Time, Minimed CGMS system Gold, SEVEN by Dexcom (San Diego, CA, USA) and Freestyle Navigator by Abbott (Abbott Park, IL, USA). All of these systems are based on enzymatic, amperometric glucose biosensors. They measure glucose in the interstitial fluid (ISF). Glucoday is another system which uses the principle of microdialysis, wherein ISF is drawn using a minimally invasive dialysis tubing, to an amperometric device outside the body. This device is relatively bulky and hence its use is limited to hospitals. The reliable use of these devices for CGM is limited to 2 to 7 days, due to biocompatibility problems.

1.5. Biocompatibility – the bottleneck for implantable glucose biosensors

The foreign body interactions associated with implantation of sensor in the body are the primary barrier for the development of reliable, long-term implantable biosensors. As soon as the sensor is implanted in the body, a cascade of reactions, including the normal wound healing process and the host responses to the implanted sensors, are triggered. Proteins, cells and other biological components adsorb on the sensor surface and block the pores on the mass-transport limiting membrane on sensor surface (Wisniewski *et al.*, 2000). This phenomenon called biofouling severely affects the sensor function by lowering the amount of analyte (glucose) reaching the sensor. The biofouling layer is typically 1 to 3 cells thick (~5 to 30 μm) and its composition continually changes from the time of implantation. In addition to biofouling, the normal wound healing process also deposits a thick layer of fibrous capsule that further impairs glucose from reaching the sensor.

The typical foreign body reaction can be divided into four stages: haemostasis; inflammation; repair; and encapsulation (Wisniewski and Reichert, 2000). The length and characteristics of each stage depend on the nature of the implant (Reichert and Sharkawy, 1999, Sharkawy *et al.*, 1997a). In the first few minutes to hours, post implantation, proteins and platelet from blood foul the sensor surface, restricting the diffusion of glucose. Within an hour blood clot (haemostasis) made of crosslinked fibrin and platelets forms, integrating the implant with the surrounding intact host tissue. This clot, called provisional matrix

(framework) aids cell attachment and migration. The first cells to be recruited are neutrophils, which arrive at the wound site within an hour. This phase called acute inflammation usually lasts for two days, wherein neutrophils engulf and digest small debris in the wound area, following which they die and require to be cleared by long-living macrophages. The recruitment of monocytes from blood, which change into macrophages in the tissue, starts the chronic inflammation (Morais *et al.*, 2010). The macrophages not only remove the debris, including dead neutrophils, but also attack the sensor surface. Within a week, the provisional matrix is degraded and replaced by fibrous tissue called granulation tissue (repair). Angiogenesis, or infiltration of the provisional matrix with blood capillaries and vessels to sustain the repair process. Once the repair is complete, cell activity reduces drastically, thus lowering the blood vascular supply to this tissue and the fibrous tissue matures in to a dense avascular capsule segregating the implant from surrounding tissue.

Starting immediately after implantation in the body, the sensors lose sensitivity, which further drifts gradually until the sensor fails in the body. Brauker *et al.* associate this decrease primarily due to the cell layer on the immediate surface of the sensor (Brauker *et al.*, 2012). This cell layer is primarily composed of macrophages and giant cells, which are closely opposed on sensor surfaces that are smooth or microporous (less than about 1 μm). The overlying fibrous tissue apparently produces a downward contracture resulting in the compaction of the cell layer. Irrespective of the vasculature close to the sensor surface, Brauker *et al.* suggest that this cell layer acts as a barrier blocking the transport of analytes across the tissue-device interface.

1.6. Strategies to reliably lengthen the *in vivo* clinical life of implantable glucose biosensors

Traditionally, surface modifications or deposition of additional polymeric coatings were used as the strategies to combat the effects of biofouling, fibrous encapsulation and blood vessel regression (Wisniewski *et al.*, 2001). Surface chemistry plays an important role in the initial adsorption of proteins and cells on implant surface. Hence, initial studies were directed at reducing biofouling with the introduction of surface functional groups such as carboxyl (-COOH), hydroxyl (-OH), amino ($-NH_2$) and methyl ($-CH_3$) groups. The -NH2 (hydrophilic) showed the highest protein and cell adsorption, which was higher even with hydrophobic surfaces ($–CH_3$) (Tang *et al.*, 1998). The hydrophobic $–CH_3$ and hydrophilic $–NH_2$ functionalities induced thicker fibrous capsules compared to –OH and –COOH groups (Barbosa et al., 2006). Hence hydrophilic surface composed of neutral hydroxyl (crosslinked poly (hyddroxyethl methacrylate) (PHEMA)) or acidic

perfluorosulfonic acid (Nafion) based membranes were popular as biocompatible surfaces (McKinley *et al.*, 1981, Margules *et al.*, 1983, Shimada *et al.*, 1980, Wisniewski and Reichert, 2000). However, the acid groups caused calcification limiting their use as biocompatible surfaces for implantable glucose biosensors (Mercado and Moussy, 1998). Other hydrophilic (e.g. the triblock poly(ethylene oxide) and poly(propylene oxide) based system (PEO-PPO-PEO) and Polyvinyl acetate (PVA)), phospholipid and diamond like-carbon (DLC) surfaces have also been tested as anti-bifouling surfaces (Neff and Caldwell, 1999, Lee *et al.*, 1989, Espadas-Torre and Meyerhoff, 1995, Reddy and Vadgama, 1997b, Lindner *et al.*, 1994, Ruckenstein and Li, 2005, Higson and Vadgama, 1995, Treloar *et al.*, 1995). However, they failed to address the deleterious effects of foreign body reactions. This is attributed to the formation of barrier cell layer that is compacted on the surface due to the pressure exerted by the contracting fibrous capsule layer (Brauker *et al.*, 2012).

Another focus for the surface modification was to ensure blood vessel supply close to the sensor surface. This was achieved with porous polymer coatings that disrupt fibrous tissue formation and thus ensures vasculature close to the sensor. Porous polymers PVA and PLGA, as well as other nanoporous structures composed of titania, silicon, anodic alumina and DLC were tested for this purpose (Koschwanez *et al.*, 2008, Sharkawy *et al.*, 1997b, Sharkawy *et al.*, 1998a, Sharkawy *et al.*, 1998b, Brauker *et al.*, 1995). However, the presence of blood supply in conjunction with mild chronic inflammation, did not show any improvement in sensor function, further reiterating the suggestion of the effects of barrier cell layer formation (Brauker *et al.*, 2012). Therefore, the need for biocompatible coatings for reliably extending the *in vivo* lifetime of implantable glucose biosensors is still unmet.

1.7. Scope of this work

Reliable long-term CGM using implantable biosensors is not a reality yet. *In vivo* sensor function is hindered by the deleterious effects of the host's foreign body responses. As discussed in section 1.6, several approaches have been tested for overcoming the effects of host responses. A promising approach is the use of porous polymer coatings.

Koschwanez *et al.* suggested that the use of porous PLGA coatings did not improve the sensor performance *in vivo*. Brauker *et al.* utilize similar principle, but with different polymers PTFE and silicone, and claim *in vivo* efficacy for up to 30 weeks (Brauker *et al.*, 2012). However, porous polymeric coatings tested are primarily solvent cast films whose porosity is increased with the use of salt. The disadvantage with such membranes is that their mechanical properties become increasingly poor with increasing porosity. Moreover,

the reproducibility of their manufacture, in terms of porosity and thickness, can also be very poor.

Electrospinning provides a unique opportunity to precisely control the porosity and thickness of electrospun membrane, which in principle can be adapted for the development of biocompatible coatings for implantable biosensors. In their fibro-porous 3D architecture, extensively interconnected pores, high pore volumes and mechanical properties, electrospun membranes mimic the natural extracellular matrix. Moreover, electrospun membrane composed of fibres of diameters 1 to 5.9 µm were shown to prevent fibrous capsule formation (Sanders *et al.*, 2003). Thus, the biomimetic properties of electrospun membranes mimicking natural ECM prompted the overall goal for this thesis to establish the applicability of electrospun membranes as coatings to improve the reliability and the longevity of glucose biosensors when implanted in the body.

The glucose biosensors for implantable applications must be robust, durable and have constant sensitivity for several months. The sensors usually function with more or less constant sensitivity for several months, when tested ex vivo in simulated physiological fluids, e.g. phosphate buffer saline (PBS), pH7.4. However, when implanted in the body, in addition to the effects of tissue build-up on sensor surface (described in section 1.5), the activity of the immobilized enzyme also deteriorates (Valdes and Moussy, 2000). Moussy's group have developed a sensor design that allows loading of excess enzyme to cope with the demands for long-term implantation, which design has been adapted for this study (Yu et al., 2005a). These sensors were shown to function with stable sensitivity under continuous polarization of the electrodes with applied voltage of +700mV for a test period of 12 weeks (Yu et al., 2007, Yu et al., 2005b). The design and its working principle are shown in Figure 1.10. The sensors are dual electrode systems consisting of Platinum-Iridium (Pt-Ir) coil as the working electrode and Silver/Silver Chloride (Ag/AgCl) as the reference electrode. GOD is immobilized on Pt-Ir coil reinforced with cotton using bovine serum albumin (BSA) and glutaraldehyde (GTA). An epoxy enhanced polyurethane (EPU) layer is used as the mass-transport limiting membrane for the sensors to detect glucose levels in the range of 2 to 30 mM/L glucose. An added advantage of such sensors is that the sensor sensitivities are in the nA/mM levels which is much better compared to most sensors tested in the literature (including commercial implantable glucose biosensors (Brauker *et al.*, 2012, Reddy and Vadgama, 1997b), since current measurements in pA/mM are susceptible to large fluctuations.

Selectophore™ PU and Type-A gelatin (Ge) were chosen as the materials for electrospun membranes prepared in this study. The former was chosen because it is a

component of the sensor design described above, is a relatively inert (does not elicit immune response when implanted and any inflammation is very mild), slow degrading and hyperelastic material. Moreover, its use also minimizes the number of components in the sensor design, each of which would have an influence in the foreign body responses of the host tissues when implanted in the body. Ge is a derivative of collagen, the main component of natural ECM. The incorporation of Ge in the electrospun fibre structure is intended to aid cell adhesion and infiltration into the bulk of the membrane structure, thus preventing the formation of fibrous tissue surrounding the implanted biosensor.

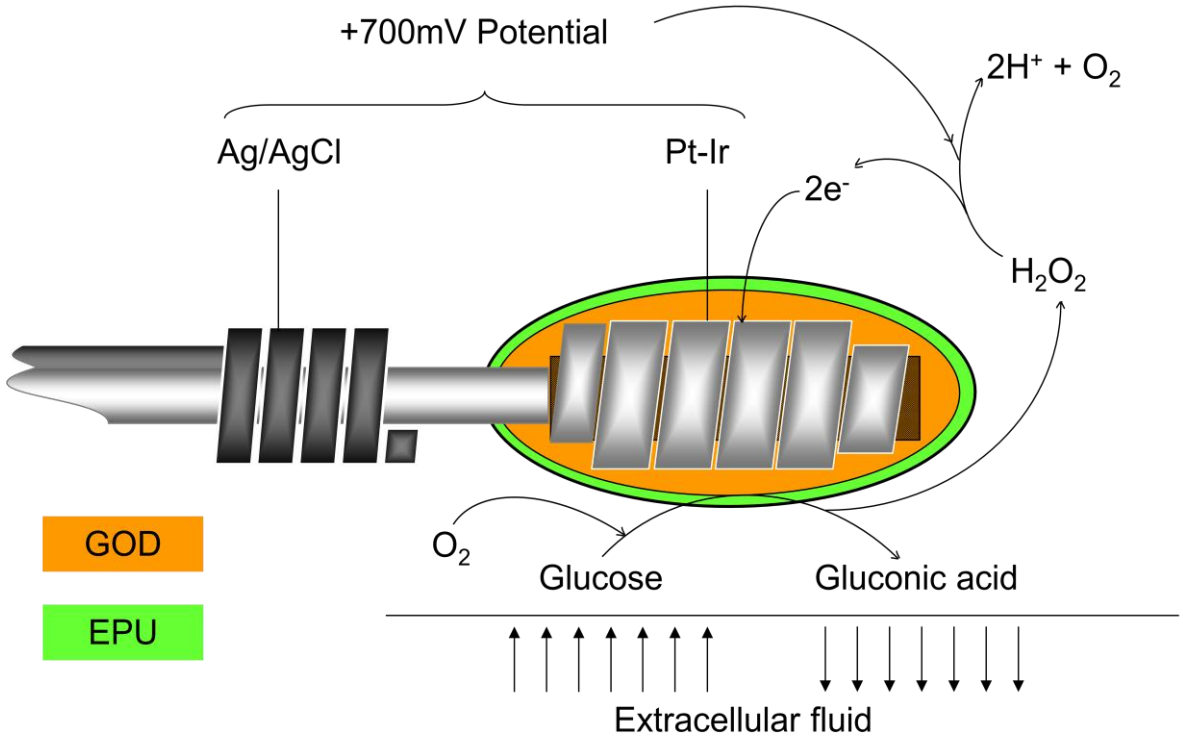

Figure 1.10 Schematic diagram showing the design of the coil-type implantable glucose biosensor used in this study and its sensing principle, where GOD – glucose oxidase, EPU – epoxy-enhanced polyurethane, Pt-Ir – platinum–iridium working electrode coil reinforced with cotton, Ag/AgCl – sliver/silver chloride reference electrode coil.

The diameters of the fibres spun using electrospinning can be varied in the range of 20 nm to 10s of µm. As coatings for implantable glucose biosensors, the objective was to test their efficacy as mass-transport limiting membranes and as biocompatible coatings. The former requires submicron porosity while that for latter requires pore sizes in the range of 3 to 10 µm. The focus for this thesis has been the preparation of electrospun membranes having fibres of about a micron or submicron diameters (for both pure PU and PU-Ge coaxial fibres). The work achieved included the manufacture of an electrospinning setup, and extensive studies on the optimization of electrospinning parameters, membrane

characterization, application on sensor, effects on sensor function ex vivo and pilot *in vivo* assessments for biocompatibility and sensor function.

1.8. Socio-economic implications on UK and World economies

The most direct application of the sensor coatings developed in this study is in the CGM for diabetes patients. Diabetes is growing at epidemic proportions both in UK and worldwide. The diabetes prevalence 2011 report for UK reports about 2.9 million people diagnosed with diabetes (Diabetes-Prevalence, 2011). The corresponding population of people diagnosed with diabetes for the years 1996 and 2004 were 1.4 and 1.8 million respectively. Similarly, worldwide, there were about 171 million people estimated to have diabetes in 2000, 285 million in 2010 and is expected to reach 439 million by 2030 (Shaw *et al.*, 2010). In other words the number of people diagnosed with diabetes is doubling every generation.

Such exploding incidence of diabetes is leading to a great demand for cheaper and better glucose detection methods and devices. The NHS recently reported that costs of diabetes monitoring and drugs alone in England increased from £458.6 million in 2004–2005 to £649.2 million in 2009–2010 (Bottomley, 2010). United Kingdom, together with Germany and France, possessed 55.3% of the biosensors market estimated in 2008 (Jose, 2008). Sale of glucose biosensors in United States is expected to reach US$1.28 billion (~ £794.4 million) by 2012. Europe and US dominate the glucose biosensor market for medical biosensors, collectively collaring 69.73% share estimated in 2008 (Jose, 2008). According to recent report by Global Industry Analyst, Inc., the global market for strips and glucose biosensors will reach $11.5 billion USD (almost £7.2 billion) by 2012 (Yoo and Lee, 2010). With rapidly growing of glucose biosensor market, the competition among manufacturers becomes much fiercer.

Making long-term reliable CGM technologies a reality would have huge socio-economic implications for UK and World economies. The above listed costs are only limited to diabetes monitoring. The lack of patient compliance with conventional testing using finger-prick methods is a key concern that results in long-term medical complications requiring hospitalization of the patients. The complications have been a significant cause for overall deaths around the world. CGM technologies would drastically reduce the cost of care for diabetes and also reduce a bulk of the strain on healthcare institutions, carers and the patients in general. For patients, it would mean less GP/hospital visits, early diagnosis, avoids medical complications, better lifestyle and longer lifespan;

for clinicians, better patient management, faster and accurate diagnosis and therapy; for the wider public, better nursing and homecare of patients.

If successful, the electrospun membrane technologies would open up a huge market for implantable biosensors for a wide range of disease, trauma, diagnosis and therapeutic markers. They can also be developed as coatings for other implantable biomedical devices and as novel biomimetic tissue constructs for tissue engineering and regenerative medicine.

1.9. Specific objectives for this work

The overall aims for this thesis were:

1. To maximise the pre-implantation sensor sensitivity, through the use of electrospun coatings having large pore volumes and highly interconnected porosity replacing traditional solvent-cast mass-transport limiting membranes
2. To prevent fibrous capsule formation around the implanted sensors, through the use of bioactive electrospun membranes that mimic the natural extracellular matrix

Specific objectives were:

- To design and manufacture an electrospinning setup
- To optimize the parameters for electrospinning Selectophore™ PU membranes having tailorable fibre diameters, porosity and thickness
- To characterise the electrospun PU membranes for morphology, fibre diameters, porosity, thickness, permeability to glucose, mechanical and chemical properties, and hydrophilicity
- To develop a method to electrospin fibres directly on miniature coil-type implantable glucose biosensor
- To evaluate the effects of electrospun PU coatings on sensor function
- To optimize the parameters for electrospinning coaxial fibre membranes based on PU and Ge
- To characterise the electrospun PU core – Ge shell coaxial fibre membranes for morphology, fibre diameters, porosity, thickness, permeability to glucose, mechanical and chemical properties, and hydrophilicity
- To evaluate the biocompatibility of certain optimized PU and PUGe (coaxial fibre) membranes in a rat subcutaneous implantation model
- To evaluate the *in vivo* efficacy of implantable glucose biosensors coated with the certain optimized PU and PUGe (coaxial fibre) membranes in a rat subcutaneous implantation model

Chapter 2 Materials and Methods

2.1. Introduction

This chapter presents the materials, instrumentation and techniques used to prepare, characterize and evaluate electrospun membranes as mass-transport limiting and biomimetic membranes on a model implantable glucose biosensor. A versatile electro-spinning set-up, including a rotational collecting rig to electrospin fibres directly on the surface of miniature biosensors, was designed and built in-house, which has been the workhorse throughout the project. A coaxial-needle spinneret was also made and used for electrospinning coaxial fibres.

2.2. Materials

Electrodes: Platinum–iridium (Pt:Ir, 9:1 weight ratio) and silver wires, each having a diameter of 0.125 mm and covered with an insulating Teflon-coating, were obtained from World Precision Instruments, Inc. (Sarasota, FL).

Sensor Coatings: Bovine serum albumin (BSA), glutaraldehyde (GTA) grade I (50%), glucose oxidase (GOD) (EC 1.1.3.4, Type X-S, Aspergillus niger, 157,500U/g, Sigma), ATACS 5104/4013 epoxy adhesive, non-ionic surfactant Brij 30, Selectophore® polyurethane (PU, a medical-grade aliphatic polyether polyurethanes), Gelatin (GE) from porcine skin (type A), Tetrahydrofunan (THF), *N*,*N*-Dimethylformamide (DMF), 2,2,2-Trifluoroethanol (puriss., ≥99.0% (GC)), were purchased from Sigma–Aldrich–Fluka. GTA (25%, BioReagent) was bought from Fisher Scientific.

Sensor Function Testing: D-(+)-Glucose and phosphate buffered saline (PBS) tablets (0.01 M containing 0.0027 M potassium chloride and 0.137 M sodium chloride, pH 7.4, at 25 °C) were purchased from Sigma-Aldrich-Fluka, UK.

Animals, anaesthetics and analgesics: Ketamine hydrochloride (Ketaset®, Fort Dodge Animal Health Ltd.), xylazine (Chanazine, Channelle Vet. Ltd.), isoflurane (ISOFlo®-, Abbott Laboratories Ltd.), Buprenorphine Hydrochloride (Vetergesic, Reckitt Benckiser Healthcare), Carprofen (RIMADYL, Pfizer Ltd), Atipamezole Hydrochloride (ATIPAM, Dechra Veterinary Products) were procured through Lab Services Ltd, Watford, UK. Sprague Dawley rats weighing between 175 and 200g were purchased from Harlan UK Ltd., Oxon, UK. Routine surgical consumables were obtained from NU-CARE products Ltd., and Barrier Healthcare Ltd., UK. Surgical sutures, Ethicon 5-0 Vicryl Rapide polygalactin sutures were obtained from Vet-Tech Solutions Ltd.

Histology: Histology grade xylenes, Mayer's Hematoxylin, Eosin Y (alcoholic), DPX mountant for histology, and Masson's Trichrome kit (HT15) were procured from

Sigma-Aldrich, UK. RCL-2 formalin free fixative, an ALPHELYS Lab Tech product, was obtained from Mitogen, UK. Absolute ethanol and industrial methylated spirit were purchased from Fisher-Scientific.

Deionised (DI) water purified with a Barnstead water purification system was used for all experiments.

2.3. Glucose Biosensor

A miniature coil-type implantable glucose biosensor, developed in Moussy's group (Yu et al., 2005a), is used as model sensor in this study. The basic design of the sensing element is shown in Figure 2.1. The amperometric sensor is a two electrode system based on Pt/Ir working and silver/silver chloride (Ag/AgCl) reference electrodes.

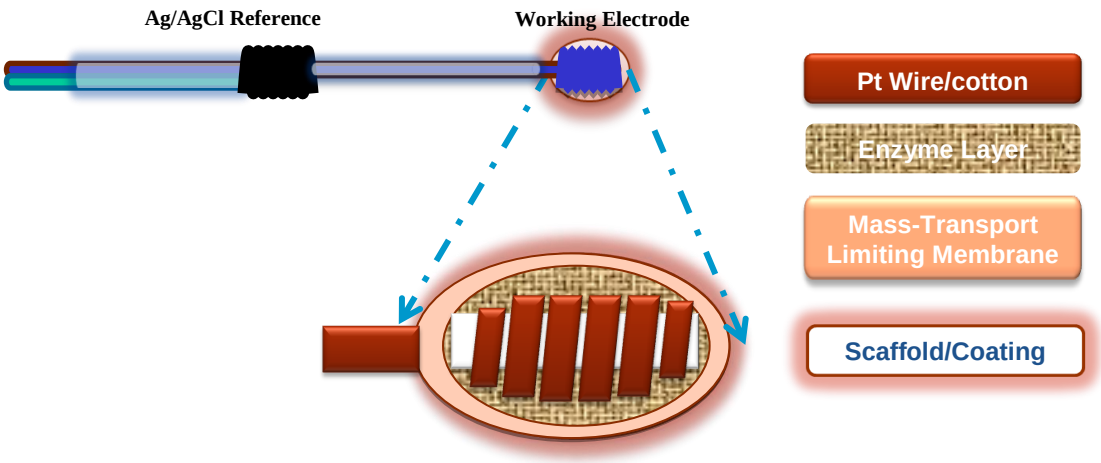

Figure 2.1 Schematic diagram showing the implantable glucose biosensor design

Working electrode: It was prepared by first removing 1 cm length of Teflon-coating at either ends of an 8 cm long Pt-Ir wire. On one end, the bare Pt-Ir wire was wound around an 18 gauge needle (1/2 inch, BD) to make the working electrode coil. The core of the coil was filled with cotton to enhance the immobilization of enzyme and prevent air bubble formation. The cotton reinforced coils were washed in DI water for 30 min under continuous sonication followed by washing in ethanol for 20 min.

Enzyme Loading: For immobilizing GOD on the working electrode coil, 1.0-1.5 µl of the enzyme loading solution (39.3 mg/ml BSA, 8.2 mg/ml GOD and 1.6% (v/v) GTA (50%, v/v) dissolved in DI water) was coated on the cotton reinforced Pt-Ir coil and allowed to dry at room-temperature for 30 min. This enzyme loading procedure was repeated for 4-6 times. After the last coating, the enzyme layer was left overnight to allow GTA crosslinking to complete.

Mass-transport limiting membrane: To coat epoxy-PU (EPU) mass-transport limiting membrane, 1.5 µl of the EPU loading solution (26.7mg of PU, 8.9mg each of Part

A and Part B of epoxy adhesive and 1 µl of Brij 30 dissolved in 4ml THF) was applied on the enzyme layer (Yu *et al.*, 2007). After air-drying at room temperature, the solvent cast EPU layer was cured at 80^{o}C for 20 minutes.

Electrospun fibro-porous membranes: The methods for electrospinning membranes on flat-plate collector and directly on sensor surface are described in section 4.4. The efficacy of the membranes as mass-transport limiting (without EPU) and as biomimetic coatings (on top of EPU membrane) was tested.

Reference electrode: The reference electrode was prepared by stripping 1 cm of Teflon coating from each end of a 7 cm long Teflon coated silver wire. One end was carefully wound around a 30 gauge 1/2 inch hypodermic needle to obtain the coil end. The Ag coil was treated with ammonia solution for 30 s followed by 10 s in 6 M nitric acid. The coil was then washed in DI water and electroplated in 0.01 M HCl at a constant current of 0.1 mA using a galvanostat (263A, Princeton Applied Research, TN, US) overnight. The resulting Ag/AgCl reference electrode coils were rinsed with DI water.

Sensor Assembly: The sensors were assembled by inserting the Pt-Ir wire of working electrode through the coil of reference electrode until the two electrode were separated by 5 mm and the Teflon-covered part of the two wires were intertwined along their entire length.

2.4. Electrospinning Setup

Basic setup: The electrospinning setup utilized for this study was manufactured at our workshop (Figure 2.2). It was a vertical setup consisting of a 22G stainless steel needle (spinneret) (BD, flat-tip, FISHMAN, UK) aligned perpendicularly above a grounded steel plate (collector, 16x16 cm^2). The spinneret needle was secured and height (the distance between the needle tip and the collector) adjusted using a stand as shown in Figure 2.2. A high voltage power supply (EL30R1.5, Glassman High Voltage Inc., Hampshire, UK) was used to charge high electrical potential between the spinneret and the collector. This basic vertical setup was enclosed in a transparent Plexiglass box equipped with a safety lock for protection from high voltages. The top of the Plexiglass box was perforated to vent organic solvent fumes. Furthermore, a syringe pump (Fusion 100), also positioned inside the Perplex box, was used to pump polymer feed solution in a 10 ml plastic syringe (BD), allowing a uniform, constant and stable mass flow through a Polytetrafluoroethylene (PTFE) tube (Ø 1/16') connecting the syringe (on the syringe pump) to the spinneret needle (in the plexiglass box).

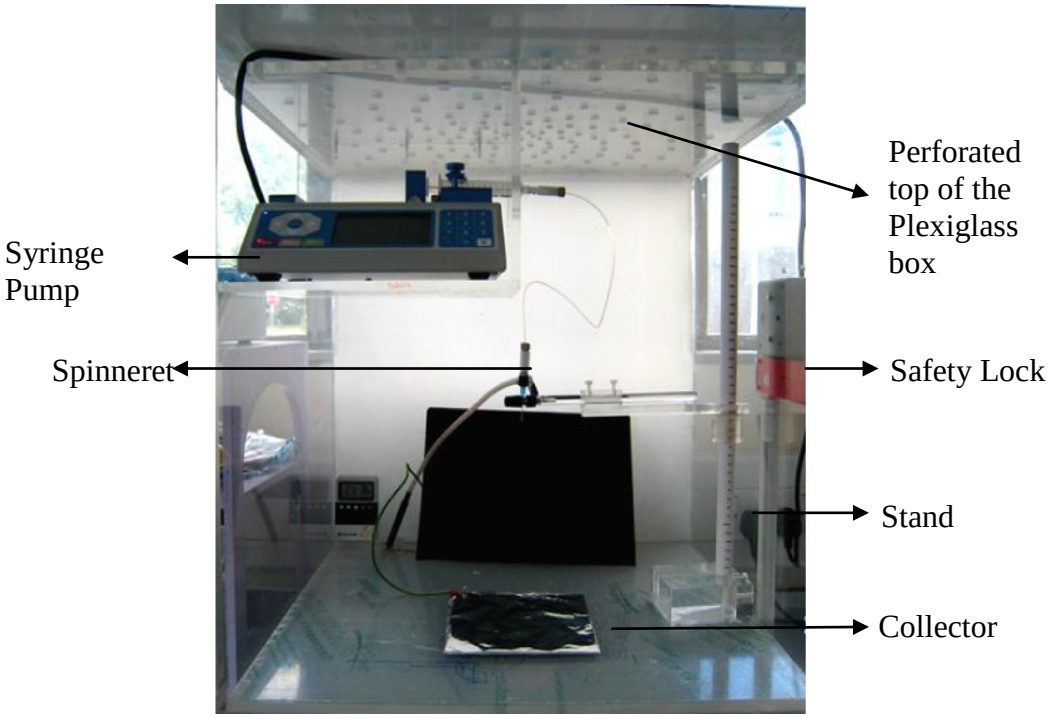

Figure 2.2 The basic electrospinning setup

To facilitate electrospinning of co-axial fibres, a second syringe pump (fusion 100) was integrated to the basic setup. This pump was positioned outside the Pelxiglass box to deliver second polymer solution to a co-axial spinneret through 1/18" OD PTFE tubing.

Co-axial spinneret: To spin co-axial fibres, a coaxial electrospinneret was custom-made (Figure 2.3). It consisted of a stainless steel Tee-Union (1/8" Swagelok, UK), a PTFE union set (1/16", a PTFE union, two PTFE cones and two PEEK adaptors), and two stainless steel concentric tubes that allow coaxial extrusion of two fluids simultaneously. The inner tube has an inner diameter of 0.508mm and an outer diameter of 0.711mm, while the outer tube has an inner diameter of 2.88 mm and an outer diameter of 3.0mm. This design is to separate two fluids before they eject from the spinneret nozzle, offering the advantage of fabrication of unique core-sheath structure of the co-axial fibres, especially when the two fluids are immiscible or the two types of feeding polymers are incompatible.

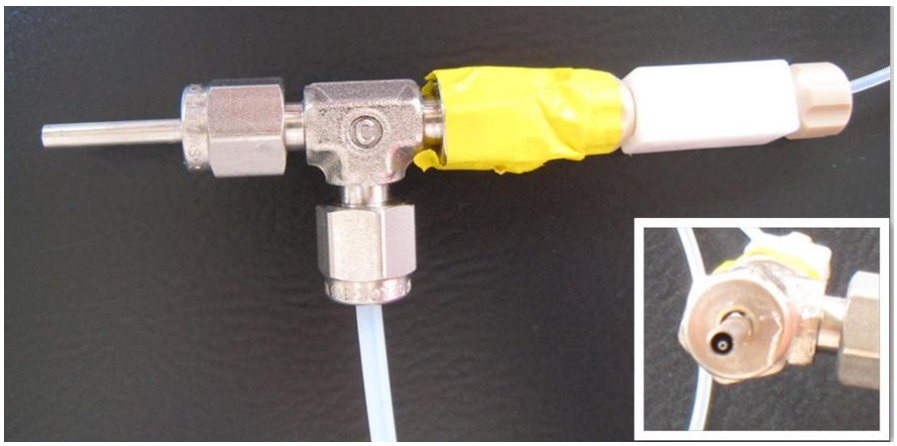

Figure 2.3 Coaxial electro-spinneret

Electrospinning spinning fibres directly on miniature sensor surface: Two different collector configurations were designed and tested (Figure 2.4). The first was a static model using an auxiliary electrode, wherein a 1.5 inch stainless steel needle (23G blunt-tip) was fixed vertically at the centre of the flat-plate. Both the sensor (inserted in the needle) and the plate were grounded (Figure 2.4a). To verify the suitable gap between spinneret needle tip and sensor tip for fibre deposition on sensor surface, Maxwell SV software was used to simulate the electric field distribution between the spinneret and collector needles using a 2D model. For solving the simulation, the appropriate electrode materials, simulation parameters and boundary conditions were defined using the software's GUI and materials database.

The second collector configuration was dynamic, wherein the sensor was inserted in 0.5 inch stainless steel needle (23G blunt-tip) and the needle fixed at the end of a custom-made rotator (Figure 2.4b). The rotator consisted of a mini motor and wood protective shield. The mini motor was driven by a low voltage power supply unit (Model: LA100.2, Coutant), whose rotation speed was calibrated using a stroboscope (RS components, UK) by systematically varying the voltage and current settings. A rotation speed between 660 – 690 rpm, obtained by setting both voltage and current constant at 5V and 0.11A respectively, was chosen to obtain random orientation of the electrospun fibres.

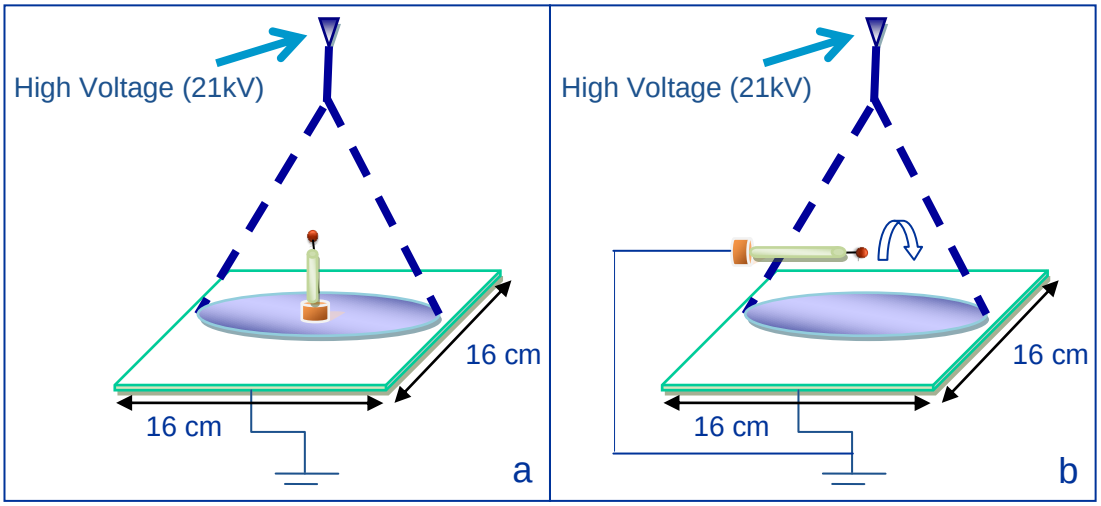

Figure 2.4 Schematic diagrams showing (a) static collector and (b) rotating collector system set ups used in our experiment to coat glucose biosensors. The distance between the tip of the spinneret and the working electrode surface was considered the distance between the spinneret and collector.

2.5. Optimization of Electrospinning parameters

2.5.1. Polyurethane

The electrospinning parameters, specifically, solvents, polymer solution concentration, flow rate, applied electric potential and distance between the spinneret and the collector, were first optimized for spinning uniform fibro-porous polyurethane (Selectophore™) membranes on a grounded flat-plate collector. Then, the optimized parameters were adapted for spinning fibro-porous PU and coatings directly on miniature glucose biosensors.

THF and DMF mixed in weight ratios of 100:0, 70:30, 50:50, 30:70 and 0:100 were tested as the solvent mixtures for the polyurethane electrospinning solution. Other parameters varied for optimization of electrospun PU membranes on flat grounded plate include polyurethane solution concentrations of 8, 10 and 12%, solution feed flow rates from 0.1 to 1.2 ml/h, an applied voltage ranging from 11 to 25 kV and a distance of 18 to 24 cm between the spinneret and collector. The electrospinning was essentially processed at ambient conditions (23±3.32^{o}C room temperature and 35 to 47% relative humidity). Electrospinning time was varied from 1 to 120 min to obtain membranes of different thicknesses. For ease of harvesting and handling, the electrospun membranes were collected on aluminium foils placed on the flat plate collector. The electrospun membranes were dried for 24h at room temperature in a power assisted vacuum desiccator and then stored in a vacuum desiccator until further use.

Electrospinning directly on sensor surface: The electrospinning parameters used for spinning PU membranes directly on sensor surface are summarised in Table 2.1. The PU solution concentration was varied to study the effect of fibre diameter and porosity on sensor function. Similarly, the electrospinning times were varied (2.5, 5 and 10 min) to study the effect of thickness of electrospun coating (ESC). Furthermore, the fibro-porous PU membranes were electrospun both on sensors coated with epoxy-PU (EPU) mass-transport limiting membrane (Pt-GOD-EPU-ESC) and those without (Pt-GOD-ESC) to study the ability of electrospun membranes to function as semi-permeable membranes. The designations of the sensors, as presented in Table 2.1, are based on the final sensor configuration. For example, Pt-GOD-EPU-8PU indicates the concentric working electrode components from inside to out. Pt indicates Pt-Ir coil, GOD – glucose oxidase, EPU – epoxy polyurethane mass transport limiting membrane, and 8PU – electrospun membrane spun using 8% PU solution. In addition, to indicate the time of electrospinning a suffix, -2.5", -5" or -10" is added to the designations in Table 2.1(e.g., Pt-GOD-EPU-8PU-2.5"). To study the effect of different ESC configurations on sensor function, n=6 for each

electrospun PU coating configuration were tested and 6 Pt-GOD-EPU sensors without any electrospun coatings as controls.

Table 2.1 Electrospinning conditions used for spinning PU fibres directly on biosensor surface. D is distance between spinneret and collector

Designation	Concentration (wt %)	Solvent THF:DMF (w/w)	Voltage (kV)	Feed rate (ml/h)	D (cm)
Pt-GOD-EPU-8PU, Pt-GOD-8PU	8	40:60	21	0.6	22
Pt-GOD-EPU-10PU, Pt-GOD-10PU	10	50:50	20	1.0	22
Pt-GOD-EPU-12PU, Pt-GOD-12PU	12	50:50	20	1.2	22

2.5.2. Co-axial fibres with polyurethane core and gelatin sheath

In this study, a fluorinated alcohol, TFE (100%), was used for dissolving both gelatin and PU. Gelatin was dissolved in TFE under continuous stirring at room temperature for at least 10 h. PU solutions of different concentrations (2, 4, 6, and 8 w/v%) were also prepared in TFE at room temperature, under continuous stirring for 6 h. For spinning co-axial fibres, gelatin and PU solutions were separately fed to the outer and the inner needles of co-axial spinneret respectively, using two programmed syringe pumps through 1/8" OD and 1/16" OD PTFE tubing with the feed rate of 1.2ml/h and 0.8ml/h respectively. Applied voltage between 11.25-14kV and a tip-to-collector distance of 15cm were used to ensure the formation of a steady coaxial jet with an external meniscus surrounding the inner one erupting from a stable Taylor Cone for the different PU solution concentrations. The fibres were spun at ambient room temperature (20±2°C) and humidity (40±5%).

Crosslinking of gelatin: Gelatin, being water soluble, needed stabilization by crosslinking to maintain the co-axial fibre structure. Two methods were tested for GTA crosslinking of the gelatin sheath of the co-axial fibres. First, the coaxial fibre membranes on Al foils were immersed in aqueous glutaraldehyde (25% GTA solution diluted with DI water at 1:99 volume), under continuous shaking for 12 hours at room temperature. The membranes were washed in several changes of DI water, dried over night at 40°C and then stored in a vacuum desiccator until further use. Secondly, GTA crosslinking of gelatin was achieved by incubating the co-axial fibre membranes on Al foils in a vacuum desiccator

with the desiccant replaced by 10 ml of 25% aqueous GTA solution (in a petri dish) for 3 days at room temperature. The samples were then transferred to a power-assisted vacuum desiccator for removal of excess GTA and stored in desiccator until further use.

Electrospinning co-axial fibres directly on sensor surface: Two types of Gelatin-PU coaxial fibrous membrane were electrospun on both sensors coated with epoxy-PU (EPU) semi-permeable membrane (Pt-GOD-EPU-ESC) and those without (Pt-GOD-ESC) to study the ability of coelectrospun membranes as mass-transport limiting membranes. The designations and electrospinning conditions for co-axial fibre membranes directly on sensor surface are summarised in Table 2.2. GTA crosslinking of gelatin in the co-axial fibres was achieved by incubating the sensors in vacuum desiccator saturated with GTA fumes as described above in this section. Six sensors per electrospinning coating configuration (Pt-GOD-EPU-ESC or Pt-GOD-ESC) were tested for *ex vivo* functional efficacy and six sensors without any electrospun coatings (Pt-GOD-EPU) used as controls.

Table 2.2 Electrospinning conditions used for spinning coaxial PU-GE fibres directly on biosensor surface (n=6)

Designation	Concentration (w/v %)		Voltage (kV)	Feed Rate (ml/h)		D (cm)
	PU	GE		PU	GE	
Pt-GOD-EPU-6PU10GE Pt-GOD-6PU10GE	6	10	13.25	0.8	1.2	15
Pt-GOD-EPU-2PU10 GE Pt-GOD-2PU10GE	2	10	14	0.8	1.2	15

2.6. Characterization of electrospun membranes

2.6.1. Infrared spectroscopy

An ATR-FTIR spectrophotometer (PerkinElmer Inc.) was used to investigate the residual solvents and polymer structure of the electrospun membranes (after drying cycles). The core-shell fibre structure of electrospun coaxial fibres was also verified. Each spectrum, acquired in transmittance mode, was an average of 128 scans at a resolution of 4 cm^{-1}.

2.6.2. Morphology

The quality of electrospun membranes being prepared was first screened visually under an optical microscope (LEICA S60) to ascertain the uniformity of the fibres being

formed. Thereafter, morphology of small samples of the different electrospun membranes were sputter coated for 30 sec with gold using an AGAR high-resolution sputter-coater and observed under SEM (Zeiss Supra 35VP field emission SEM (FESEM) in SE mode).

2.6.3. Fibre diameter and membrane thickness

The fibre diameters were measured on SEM images using a user friendly application developed (by a colleague in our department) using Matlab for length measurements. For each measurement, the software first requires a line to be drawn at one edge along the length of the fibre followed by a second line perpendicular to the first line drawn across to the other edge of the fibre to obtain the actual and the accurate measurement for fibre diameter. The accuracy of these measurements was cross-confirmed with Image J image analysis software. For the measurement of fibre diameter, a total of 160 measurements were made on 8 different SEM images, each representing a non-overlapping random field of view for each electrospun membrane configuration.

To obtain the fine cross section images for the electrospun membranes (both sheets and on sensors) were snap-frozen using liquid nitrogen, followed by cutting using a scalpel. The resulting samples were processed for SEM and oriented appropriately to obtain image of cross-sections of the membranes. The above-mentioned software for length measurements was also used to measure the thicknesses of the membrane using SEM images captured showing their cross-sections. The effect of PU solution concentrations (8, 10 and 12%) and electrospinning time (1 to 120 min) on the thickness of the resulting electrospun membranes was evaluated.

The thickness of the electrospun membranes were also measured using a digital micrometer having a resolution of 0.001mm. The membranes were sandwiched between two slides and their thickness determined by subtracting the glass slides' thickness.

2.6.4. Pore size and Porosity

The pore size for the different membranes was measured using extrusion porosimetry (also called bubble point measurement) as reported earlier (Gopal *et al.*, 2006). The pressure needed to blow air through a liquid filled membrane was used to determine the bubble point. Water (surface tension – 72kJ/m^2) was used as the wetting liquid. A 2 h electrospinning time was used to obtain membranes thick enough for bubble point measurements.

A schematic representation of the bubble point measuring apparatus is shown in Figure 2.5. Electrospun fibrous membranes were sealed on a porous metal disk and loaded in the sample chamber filled with water, where in the samples were incubated for 30 min

to allow complete wetting of the membrane. The gas in mould was then completely extracted using vacuum prior to test. After placing the mould back to the system, pressure was gradually increased with Nitrogen gas and the appearance of bubbles across the membrane and their flow rate as a function of pressure was measured. The range of pore sizes (radius a) were calculated using the Young-Laplace equation (2.1):

$$a = \frac{2\gamma_{st}\cos\theta}{\Delta P} \qquad \text{(Eq. 2.1)}$$

where ΔP is the differential pressure, γ_{st} the surface tension of the wetting liquid and θ the wetting angle. For a completely wetted membrane having all pores filled with the wetting liquid, cos θ is 1 (Gopal *et al.*, 2006), which is valid assuming the walls of the pores are straight having sharp edges and the wetting liquid forms a flat film on the pore walls. In this study, a contact angle of 20°C was used giving a value of 0.94 (cos 20).

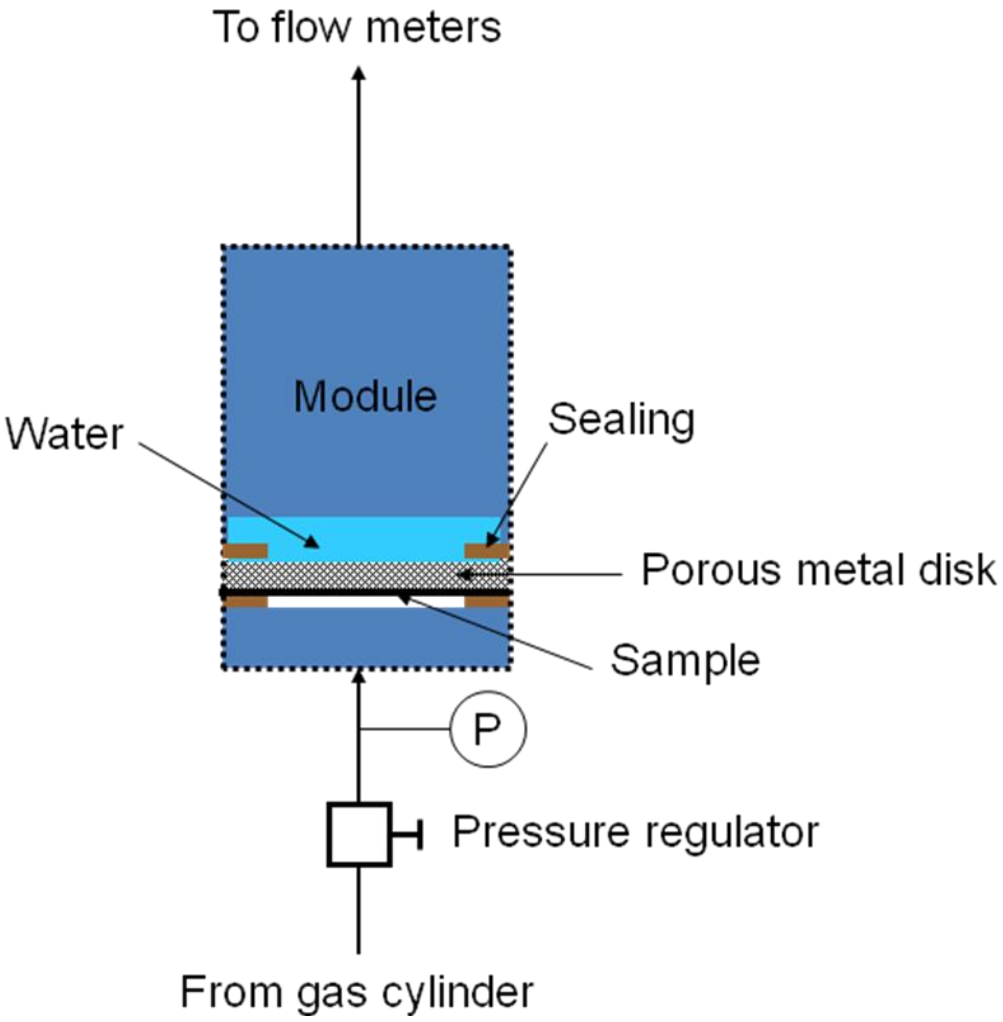

Figure 2.5 A schematic representation of the bubble point measuring apparatus.

The porosity of the membranes was also determined using gravimetry. The dimensions of the membranes were measured using micrometer (No. 293-832 Mitutoyo, Japan) and ruler to obtain thickness and surface area. The weight of the sample was

measured using a high sensitivity balance (Fisher Scientific, resolution 0.01 mg). The resulting data was fitted in equations 2.2 and 2.3 to obtain the apparent density and porosity of the membranes.

$$\rho_{app} = \frac{m}{d \times A} \qquad \text{(Eq. 2.2)}$$

$$\varepsilon = 1 - \frac{\rho_{app}}{\rho_b} \qquad \text{(Eq. 2.3)}$$

where m = the mass of the membrane (g), d = the thickness of the membrane (cm), A= the area of nanofibrous mat (cm^2), ρ_b = the bulk density of materials (g/cm^3). The bulk density for Selectophore™ PU as reported by the manufacturer was 1.04 g/cm^3, and crosslinked Gelatin type A (GE) 1.36 g/cm^3.(Mwangi and Ofner Iii, 2004)

2.6.5. Diffusion test

Permeability of the electrospun membranes to glucose is essential for the performance of the membrane coated glucose biosensors. To study the effect of membrane structure and composition on its permeability to glucose, diffusion tests were done using a biodialyser (singled-sided biodialyser with magnet, 1ml, Sigma-Aldrich). The biodialyser has an integrated magnet, 1 ml sample well and a threaded cap ring to mount a membrane on top of the sample well exposing a 113.14 mm^2 membrane area for diffusion as shown in Figure 2.6.

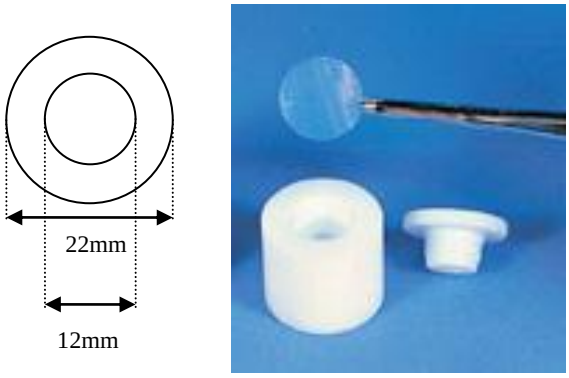

A B

Figure 2.6 (A) the aluminium template used to prepare diffusion membrane and (B) the microdialysis chamber.

Membranes for diffusion test were prepared using a ring-shaped aluminium template (in principle similar to the rectangular paper template used for strips for mechanical testing) having an inner circle of 12 mm diameter cut out and an outer diameter of 22 cm was flattened and placed on aluminium foil covered flat-plate collector. Following electrospinning, to fix the membrane on the template ring, super dry glue was applied on top of the electrospun membrane on the ring. After overnight drying in air, the template with membrane was cut along the outer circle edge using a scalpel. Then, then the

underlying supporting Al foil was carefully peeled off. Finally, the membranes were soaked in PBS (pH 7.4) at 37°C for seven days to ensure equilibrium swelling of the hydrophilic membranes before the diffusion test.

For diffusion test, the donor solution chamber of the biodialyser was filled with 1ml of glucose solution in PBS and the wet membrane (on the ring template) was mounted and secured with the treaded cap ring. The assembly was then placed in a 100 ml glass beaker containing 49 ml of receiving PBS. The beaker was placed on a magnetic stirrer plate to assist the continuously rotation of the biodialyser at 250 to 300 rpm. Pre-calibrated amperometric glucose sensor made in-house was immersed in the receiving PBS to monitor the changes in glucose concentration (as described in section 2.7). The concentration of glucose solution in donor biodialyser chamber was chosen such that the eventual equilibrium glucose concentration of receiver solution reaches 30 mM. The experiment was run overnight to ensure equilibrium was reached. The resulting sensor response currents were converted to concentration vs time (flux) curve and the first 60% of the data was fitted in equation 2.4 (Korsmeyer et al., 1983, Ritger and Peppas, 1987a, Ritger and Peppas, 1987b) to determine the glucose diffusion kinetics across the membrane.

$$M_t / M_\infty = kt^n \qquad \text{(Eq. 2.4)}$$

where M_t and M_∞ are mass/concentration of analyte at time t and ∞ (typically concentration at equilibrium), k is a constant, and n is the diffusion exponent. The n value is used to define the mechanism of diffusion across the membrane.

2.6.6. Uniaxial tensile testing

A two hour electrospinning time was used to obtain membranes thick enough for easy handling for mechanical testing. For the tensile tests, the membranes were first cut into 50 mm long and 10 mm wide strips following a method reported earlier (Huang *et al.*, 2004) as illustrated in Figure 2.7. Briefly, a rectangular paper template constituting an outer 10 mm wide rim on four sides with the central region of the paper cut out. Two 10 mm wide double sided tapes were glued on the top and bottom rim of the paper template, which was then glued on top of the electrospun membrane. Using this template, 10 x 50 mm rectangular strips were cut out without damaging the membrane. Thereafter, the aluminium foil on the other side of the membrane was carefully peeled off, and both the gripping ends of the membrane strips were reinforced with single sided transparent tape. The thickness of the membrane was measured using a digital micrometer having a resolution of 0.001mm.

For the tensile testing, the ten mm wide strips were soaked overnight in distilled water. The wet strips were mounted onto an Instron tester (Model 5542) fitted with

automatic clamps (30 or 10 mm apart). Preload of 0.01 N upper force limit was applied to each strip to precondition the samples followed by the test to failure using a 10N static load cell and test speed of 10 mm/min at room temperature. PU films were tested with a crosshead clamping distance of 30 and 10 mm. The Young's modulus was similar, but the sample only failed when the crosshead distance was reduced to 10 mm. Load/extension data were logged throughout testing to failure, using a computer equipped with mechanical testing data acquisition and analysis software (Instron's Bluehill ® Lite software). These data were used to construct a load-deformation curve, from which the maximum load at failure (Fmax) was obtained. At least four samples were tested for each type of electrospun membrane.

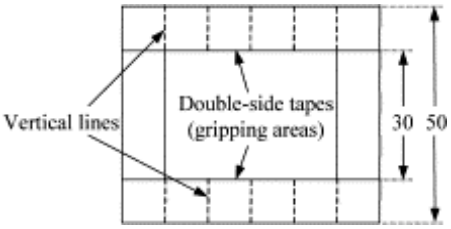

Figure 2.7 A paper template used to prepare tensile testing specimens of the electrospun non-woven fiber mat. (Huang *et al.*, 2004)

The ultimate tensile strength (UTS) (Fmax/original cross-sectional area, N/mm^2) and modulus of elasticity (from the relationship σ) Eϵ, where σ is the stress, ϵ is the strain, and E is the modulus of elasticity, N/mm^2) and strain at UTS were then determined.

2.6.7. Contact angle measurement

To evaluate the hydrophilic and hydrophobic properties of electrospun polyurethane fibrous membranes, the contact angles were measured using a contact angle instrument (OCA15+, Data-physics, Germany) equipped with a CCD camera at room temperature. The sample were prepared by cutting the electrospun membrane with aluminium foil into a square with length of sides larger than 10mm in order to provide enough space for four testing points without interference between. Moreover, completely flat surface of samples were required and confirmed by the fact that opposite sides of surface were projected in the same line. A single drop of 1µL DI water was dropped on the surface of flat fibrous membrane using a syringe perpendicular fitted upon and the picture was taken immediately (<1s) after the water droplet became stable on the surface. This process was repeated four times on four different points on each membrane tested. The contact angles were then determined using the instrument's SCA20 software. Contact angles (θ) less than 90^o are indicative of hydrophilic surface and greater than 90^o indicative

of a relatively hydrophobic surface. A zero contact angle represents rapid and complete wetting.

2.7. Sensor function testing

Basic Test: Sensor function was tested by amperometric measurements of glucose in PBS using Apollo 4000 Amperometric Analyser (World Precision Instruments Inc., Sarasota, FL) at 0.7 V versus Ag/AgCl reference electrode. The buffer solution was continuously stirred to ensure mixing of glucose in solution. Calibration plots for the sensors were obtained by measuring the current while increasing the glucose concentration from 0–30 mM (stepwise). The response time was calculated as 90% of the maximum response time after increasing the glucose concentration from 5 to 15 mM. The sensitivity (S) of each sensor was calculated using equation 2.5:

$$S = (I_{15mM} - I_{5mM}) / 10 \qquad \text{(Eq. 2.5)}$$

where I_{15mM} and I_{5mM} are the steady state currents for 15 and 5 mM glucose concentration respectively. All experiments were carried out at room temperature.

Efficacy of electrospun membrane coatings on sensor function and longevity: To test the efficacy of electrospun membranes on sensor function, each sensor was tested before and after applying the electrospun coating. In addition, the sensor function test on each sensor was repeated several times up to 84 days to test their longevity. The sensors (Pt-GOD-EPU-ESC, Pt-GOD-ESC and Pt-GOD-EPU,) were calibrated at 7, 3 and 1 day before and on 1, 3, 7, 14, 21, 28, 35, 42, 56, 70, and 84 days after applying the electrospun coatings. The control sensors, Pt-GOD-EPU sensors without ESC were also processed and tested similar to those with ESC. Between the tests, sensors were washed and stored in PBS at 37^{o}C. The storage PBS was replaced with fresh PBS every 2 to 5 days. The change in sensitivity and linearity as a function of electrospun coating configuration and time was investigated.

2.8. Biocompatibility assessment for electrospun meshes

Sprague Dawley rats (Harlan UK Ltd., Oxon, UK) weighing between 175 and 200 g were housed in the experimental animal facility at Brunel University. All animal procedures had ethical approval from the Animal Ethics Committee of Brunel University and covered under the appropriate project and personal licences from Home Office. The rats were acclimatized to local environment for 1 week prior to surgery.

2.8.1. Subcutaneous implantation

The rats were anaesthetized with ketamine (100 mg/kg) and xylazine (5 mg/kg) and the dorsal skin shaved and disinfected. Along the dorsal midline, three 15 mm longitudinal

incisions were made, about 30 mm apart. At each incision, two lateral subcutaneous pockets were made. In each pocket one 10 x 15 mm membrane scaffold was inserted at the subcutaneous level about 10 mm away from the incision. Prior to implantation, the different scaffolds were sterilised by their incubation in 70% ethanol for 1 h followed by washing in several changes of sterile saline. The incisions were closed using a degradable Ethicon™ 4-0 Vicryl Rapide® (Johnson & Johnson Ltd., UK). The rats were given standard pellet diet and fresh water. The implant sites were physically observed at regular intervals.

A total of six rats were divided into two groups of three each. Each animal received six implants. The two groups of animals were killed after 4 and 9 weeks respectively, and subsequently the implant sites were harvested and fixed in RCL-2 formalin free fixative (ALPHELYS Lab Tech product, Mitogen, UK). Four implant variables were assessed for this study, namely polyurethane film, electrospun polyurethane membranes – 8PU and 12PU, and gelatin-polyurethane co-electrospun membrane 6PU10Ge. Per time point, 3 samples of each type of scaffold were implanted.

2.8.2. Histology

RCL-2 fixed tissues were dehydrated through graded ethyl alcohol solutions (70%, 95%, and 100%), cleared with xylene and embedded in paraffin. Seven-micrometer thick paraffin sections were stained with hematoxylin and eosin (H&E), and Masson's trichrome (MT). The stained stains were used to evaluate the general histomorphology of the implant sites. The differentially stained sections were observed under light microscope and digital images were captured for stereological analysis (SP-500 POL microscope, equipped with Minicam DCM 1.3M USB 2.0 digital camera, Brunel Microscopes Ltd, Bristol, UK).

2.9. *In vivo* sensor function testing

2.9.1. *In vivo* sensor modification

Glucose biosensors described in section 2.3 were modified prior to implantation. The modification was performed by first electropolymerization of the m-phenylenediamine on the surface of a platinum electrode (working electrode) as an internal interference-limiting layer. The coil-type working and reference electrodes were placed in a modifying solution containing PBS (8ml), 1,3-phenylenediamine (4mg), glucose oxidase (1ml) and glutaraldehyde (8ul) and the electropolymerizaiton on the Pt electrode were carried out by applying a potential of 0.7V to the cell using the galavanostat mentioned in section 2.3 for 5mins. The coils were then washed in DI water and dried at 60ºC for 20mins.

To prevent the exposed wires from breaking during *in vivo* testing, the glucose sensors were secondly reinforced through shielding wires with silicon tubing (Φ1/16') and sealing the ends with silver epoxy. A knot was then made in the middle of this section to secure lodging in tissue.

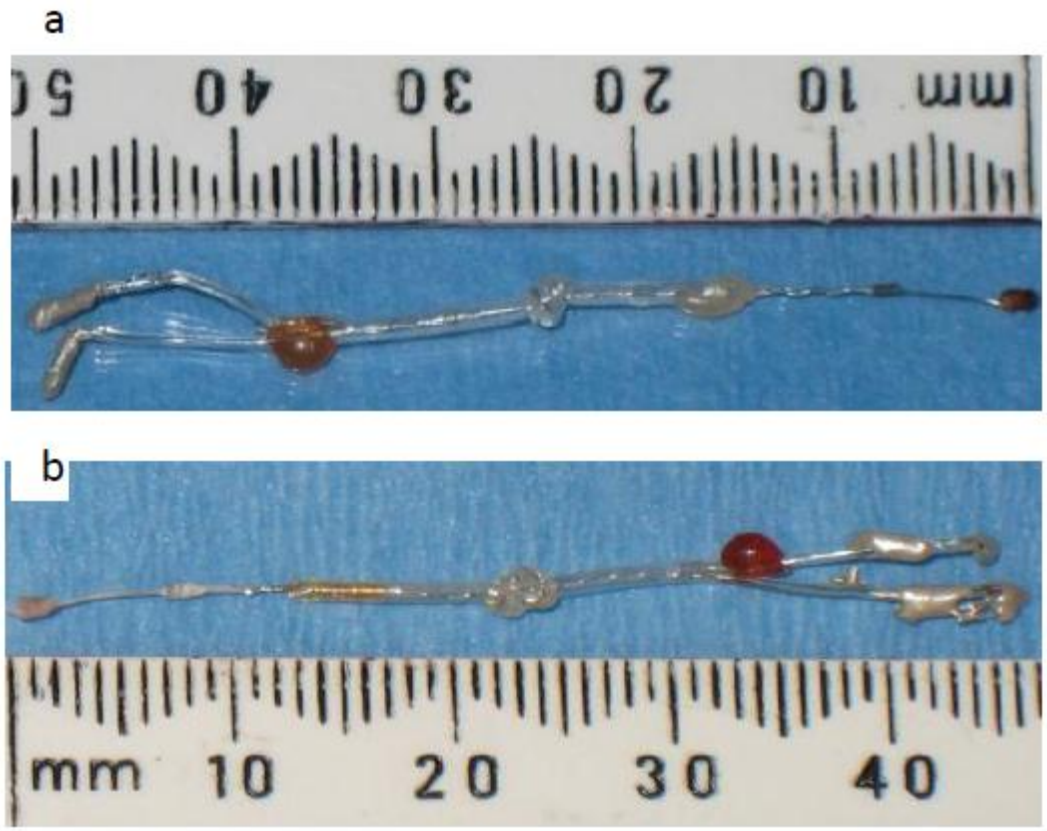

Figure 2.8 The modified implantable glucose biosensors used for in vivo test a) Pt-GOD-EPU b) Pt-GOD-ESC

2.9.2. Glucose biosensor implantation

The rats were anaesthetized in the similar way as described in section 2.8.1. During surgery, a continuous flow gas anaesthesia system reported earlier (Yu et al, 2006) was introduced to prolong the anaesthetic time, wherein isoflurane (1.5%) with oxygen (2.0L/min) were delivered. In either side of the dorsal midline, two 5mm transversal incisions were made. In each pocket, the sensor with the knot threaded by non-degradable polypropylene suture was inserted at subcutaneous level and the incision was then closed by a degradable polyglactin suture. Prior to implantation, the different sensors were sterilised in absolute ethanol for 30mins followed by washing in several changes of sterile saline. After the initial implantation, the devices were not repaired or reconnected in the period of testing and the implant sites were physically monitored at regular intervals.

2.9.3. *In vivo* function test of glucose biosensor

Sensor configurations Pt-GOD-8PU-12PU, Pt-GOD-EPU-12PU, Pt-GOD-EPU-6PU10Ge, and Pt-GOD-EPU (4 sensors made for each configuration) were chosen to implant in the rat subcutaneous tissue for studying the effects of electrospun membranes on function of implanted glucose biosensor. Two different sensors were randomly selected to implant in one rat on the position detailed above. Sensor testing were performed at 1, 3 and 9weeks after implantation. Similar with ex-vivo tests, sensor function was verified by ampermetric measurements of glucose in interstitial fluid (IF) using Apollo 4000 Amperometric Analyzer. To calibrate IF glucose concentration with that of blood, blood glucose concentration was measured using a commercial glucose monitor- Freestyle Lite by withdrawing blood drops from an incision made at the tip of rat's tail. When current became stable, two readings were recorded using the glucose monitor. An injection of 0.7ml glucose/saline solution (a 50:50 w/w dilution with saline) was made in the peritoneum of rat. Blood glucose was monitored at regular intervals as a calibration reference. Sensor sensitivity was calculated using equation below:

$$S = \frac{\Delta I}{\Delta C} \quad \text{(Eq. 2.6)}$$

where ΔI is the difference of current between the peak and the baseline, ΔC the variation in concentration of corresponding blood glucose.

2.10. Statistical analysis

Statistical analyses were carried out using statistical software (SPSS v.15). Statistical variances between groups were determined by one-way analysis of variance (ANOVA). Tukey's test was used for post hoc evaluation of differences between groups. A P value of <0.05 was considered to be statistically significant. Unless otherwise mentioned, all data presented is expressed as mean ± standard deviation.

Chapter 3 Electrospun Selectophore™ Polyurethane membranes

3.1. Introduction

Electrospinning is a well-established science, and significant research has gone into the process optimization for a variety of polymers. Each of the electrospinning parameters namely, solvent(s), polymer and its solution concentration, flow rate, applied potential, distance from spinneret to collector, static or dynamic state and shape of the collector, ambient temperature and humidity significantly influence the electrospun fibre structure. The general influence of each parameter on the final fibre structure is well characterised. However, to realise our objective of reproducibly controlling the fibre diameter and porosity, it was essential to identify the right combinations of electrospinning parameters for the commercial Selectophore™ PU polymer.

This chapter addresses the process optimization for electrospinning PU. The parameters – solvents, flow rate, applied electric potential, distance from spinneret to collector and solution concentration, were varied. Light microscopy and SEM were used to monitor the morphology and diameter of the electrospun fibres. Three sets of electrospinning parameters were shortlisted for spinning PU membranes having desired fibre diameters. The membranes were characterised for morphology, pore sizes, porosity, hydrophilicity, solute diffusion, chemical and mechanical properties.

3.2. Electrospinning setup

A typical vertical setup having a blunt end 22G stainless steel needle as spinneret and a stainless steel plate as collector was used for the optimization of electrospinning parameters (Figure 2.2). Electrospun PU membranes were collected as sheets on aluminium foil placed on top of the flat collecting counter electrode.

3.3. Process optimization for electrospinning PU

Each of the electrospinning parameters: solvents, flow rate, applied potential, distance from spinneret to collector and solution concentration was individually varied while keeping all the other parameters constant to study each of their influence on fibre structure and diameter. Temperature and humidity were not controlled, but were closely monitored during each electrospinning experiment.

3.3.1. Solvents

Solvent selection is critical and it determines the electrospinnability of a polymer. In order to yield continuous fibres, the solvent must have optimal volatility, dielectric property, boiling point and ability to maintain the integrity of the polymer solution. The

intrinsic viscosity (η) of a polymer solution is defined by the Mark–Houwinck equation (Eq. 3.1).

$\eta = KM^a$ (Eq. 3.1)

where constant K and a are determined by polymer, solvent and temperature, while M is the molecular weight of the polymer. Therefore, with a given M, solvent can impact viscosity by changing constants *a* and K. Moreover, other solution properties such as surface tension and conductivity can be adjusted by selecting solvent system.

In this study, two solvents, namely THF and DMF were tested either alone or in combinations. For assessing the solvent effects on electrospun PU fibre structure, 20 kV applied voltage, 1ml/h flow rate, 22 cm distance to collector and 10 % (w/w) solution concentration were used, while varying the solvent composition, having THF and DMF at ratios of 100:0, 70:30, 50:50, 30:70 and 0:100 (w/w). The morphology and fiber diameter distribution histograms for the electrospun membranes as a function of solvent composition are presented in Figure 3.1.

When the PU was electrospun with its solution in 100 % THF, bead formation was observed and the spinneret needle tip often got blocked during the electrospinning process. Apparently, it was due to the rapid evaporation of THF, which has a low boiling point (Table 3.1). The beads as observed under SEM (Figure 3.1A) had a hollow elongated spheroid shape and were 2 to 10 μm in diameter. Similar bead structure was also reported for electrospun polystyrene (Lee *et al.*, 2003). A combination of rapid jet acceleration and solvent evaporation is thought to cause phase separation resulting in the unusual hollow bead structures (Lee *et al.*, 2003, Bognitzki *et al.*, 2001). This problem was overcome by mixing THF with DMF, which has higher boiling point, surface tension, dielectric constant, dipole moment and viscosity. The higher polarity of DMF (dielectric constant of 38.3) is expected to increase the surface tension and decrease the volatility of the THF-DMF solvent mixture, thus preventing bead formation and clogging of spinneret (Lee, 2002, Lee *et al.*, 2003).

Table 3.1 Solvents used in this study and their properties.

Solvent	Structure	Boiling Point (°C)	Surface Tension (mN/m)	Dielectric Constant	Dipole Moment	Viscosity (Pa.s)
THF	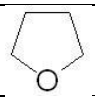	66	26.4	7.5	1.63	5.5×10^{-4}
DMF	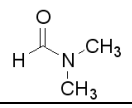	153	37.1	38.3	3.82	9.2×10^{-4}

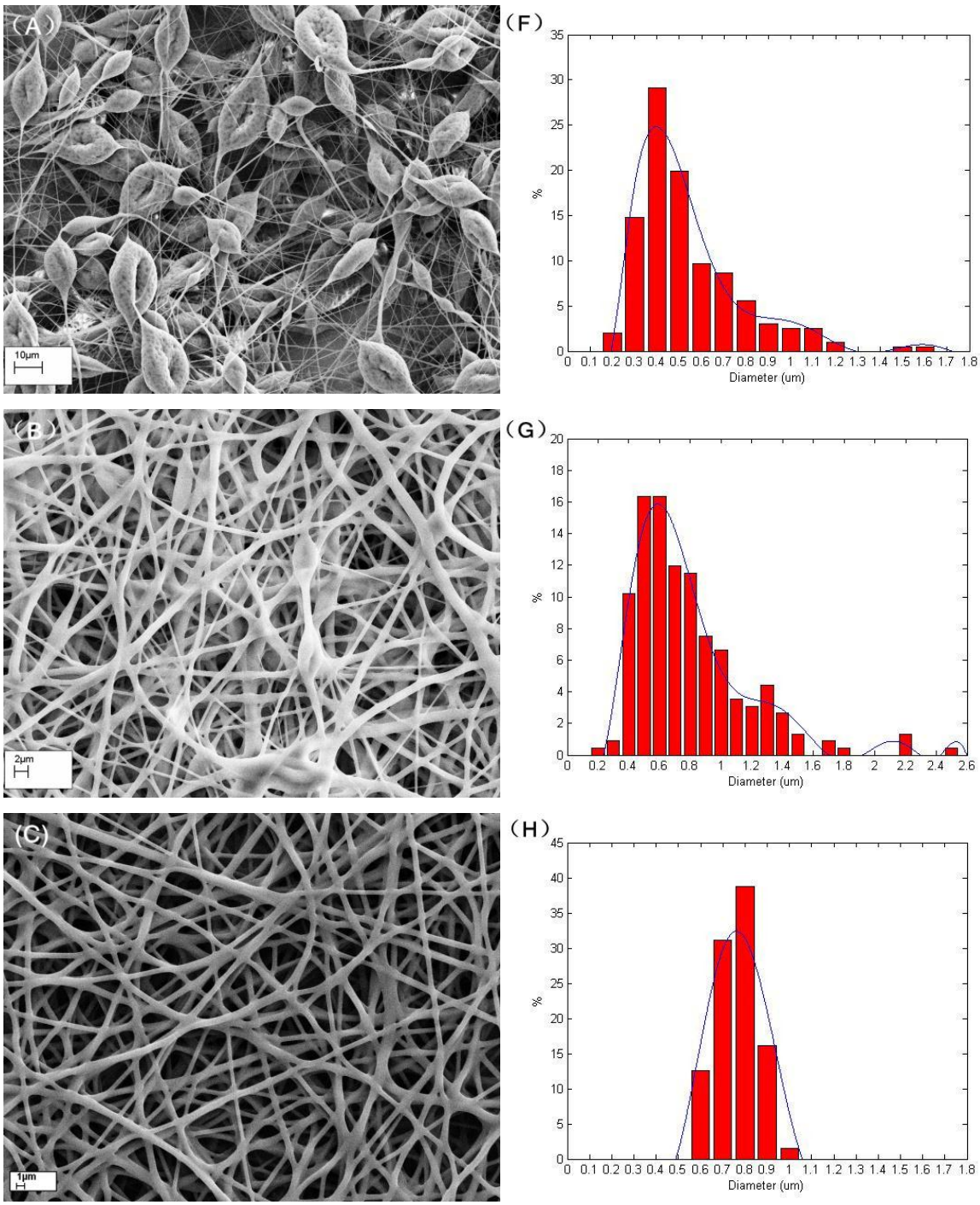

Figure 3.1 Morphology and fibre diameter distribution histograms for the electrospun membranes as a function of solvent composition - ratios of THF: DMF at 100:0 (A, F) , 70: 30 (B, G), 50:50 (C, H), 30:70 (D, I), 0:100 (E, J). PU solution concentration of 10 % (w/w), 20kV applied voltage, flow rate of 1 ml/h and 22 cm distance to collector, were kept constant.

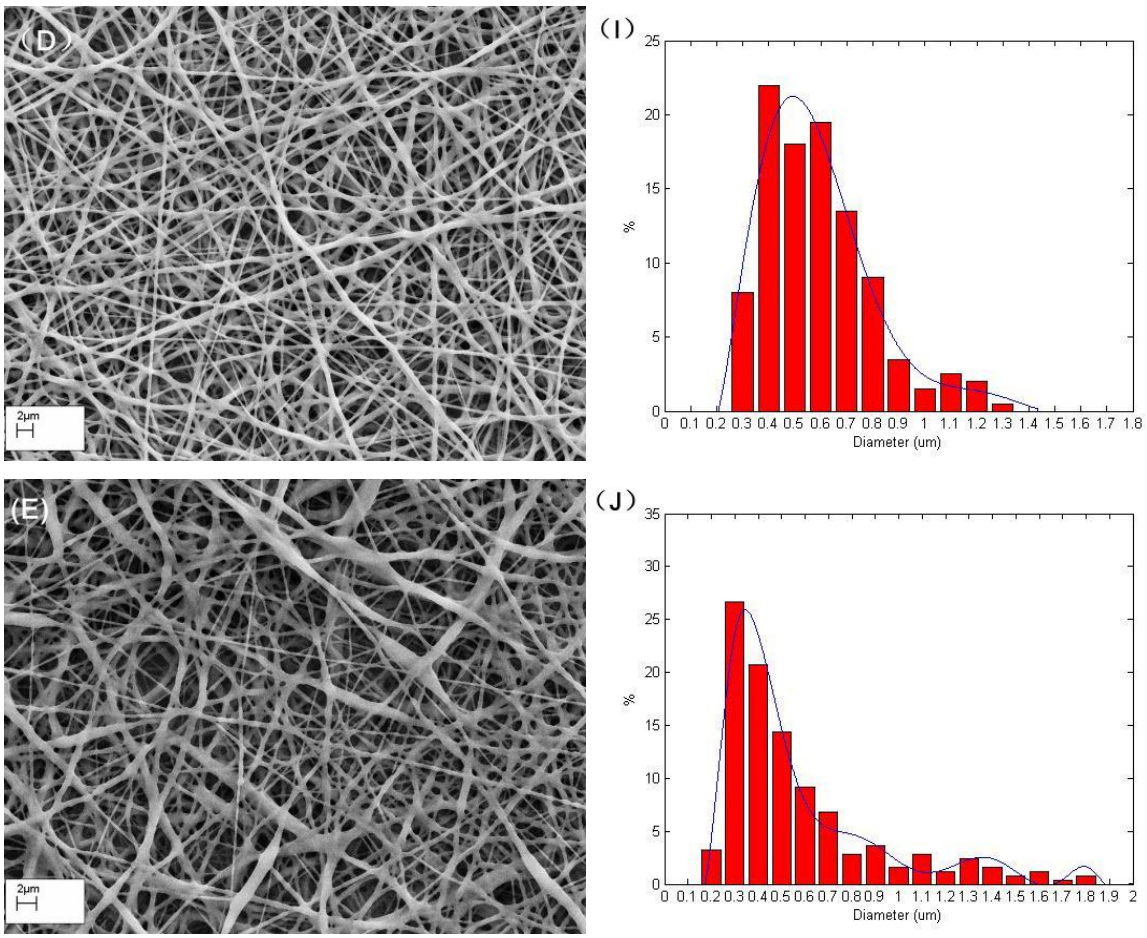

Figure 3.1 **(continued)**

Although much less prominent, the hollow spheroid shaped beads still formed when a 70:30 ratio THF:DMF solvent mixture was used (Figure 3.1B), indicating an insufficient solvent polarity. At 50:50 (1:1) and 30:70 THF to DMF solvent ratios, the bead formation was eliminated (Figure 3.1C & D). But when PU was electrospun in 100% DMF spindle shaped beads formed (Figure 3.1E). Overall, the fibre diameter measurements (Figure 3.1F to 3.1J) in conjunction with morphology (Figure 3.1A to 3.1E) reveal an increase in fibre diameter with a corresponding narrower fibre diameter distribution until 50:50 THF: DMF and vice versa, clearly indicate the effect of solvent polarity on the electrospinning of PU. Higher solvent polarity (dielectric constant) induces higher conductivity for polymer solutions, which, in turn, causes the beads to stretch sufficiently to form continuous and thicker fibres until an optimal conductivity is reached at 50:50 THF: DMF weight ratio. Beyond the optimal conductivity the higher charge density in the electrospinning jet causes bending instability, increased jet path and stretching, resulting in a reduction in fibre diameter (Hsu and Shivkumar, 2004). However, when PU was electrospun in pure DMF, although not phase-separated and hollow, beads formed (Figure 3.1E). The resulting spindle shaped bead morphology, also reported in other studies (Srivastava *et al.*, 2007, Yang *et al.*, 2004b, Lee *et al.*, 2003), is attributed to the higher

surface tension but relatively lower viscosity of PU solution in 100% DMF. Under the influence of high surface tension, low viscosity allows solvent molecules to aggregate causing beads to form along fibres. Moreover, the low PU concentration is another factor to induce the formation of beaded fibre (Lee *et al.*, 2003). Zou *et al.* reported that 14%-20% was the optimal range of PU/DMF concentration for electrospinning fibres without beads (Zou *et al.*, 2007). To sum up, the desired continuous fibres with narrow fibre diameter distribution were obtained with an optimum solvent mixture of 1:1 weight ratio of THF:DMF for electrospinning PU with 10% solution concentration, 20 kV applied voltage, 1ml/h flow rate, and 22 cm distance to collector.

3.3.2. Solution Flow Rate

The solution flow rate plays a key role in the formation of Taylor cone, at the tip of the spinneret needle, the size of which influences the diameter of the fibres deposited on the collector (Ramakrishna *et al.*, 2005b). In this study we changed the flow rate from 0.1 to 2 ml/h while maintaining PU solution concentration at 10%, operating voltage at 20 kV and distance to flat-plate collector at 22 cm. For flow rates from 0.1 to 1.2 ml/h, no bead formation was observed (SEM images not shown). The size of the Taylor cone increased with increasing the flow rate. But when the flow rate reached 2 ml/h, the size of droplet was too big to suspend at the tip of the needle resulting in the free fall of droplets on the collector. As illustrated in Figure 3.2, the average fibre diameter increased up to a flow rate of 1 ml/h and thereafter it appeared to decrease. For the flow rates less than 1 ml/h, at the set applied voltage of 20 kV, the electrospinning jet emerging from the Taylor cone was not stable enough and continuous to provide uniform fibre structure across the electrospinning duration. The increase in fibre diameters with increasing the flow rate up to 1 ml/h can be attributed to the increasing volume of polymer solution in the Taylor cone. However, the increase peaked and started to decrease by further increasing flow rate. Such insignificant decrease is apparent from the fact that for the increasing volume of polymer solution in the Taylor cone with increasing the flow rate, a corresponding increase in surface charge (induced by the high applied voltage) is essential to stretch the Taylor cone, stabilize the jet and reduce the fibre diameter (Rutledge *et al.*, 2001).

3.3.3. Applied Voltage between Spinneret and Flat-Plate Collector

In contrast to the flow rate, an increase in applied voltage resulted in a significant decrease in average fibre diameters. As shown in Fig 3.3, at 25 kV, the fibre diameter was about half that at 15 kV. The membranes were electrospun with 10% solution concentration, 1 ml/h flow rate and 22 cm distance from the collector.

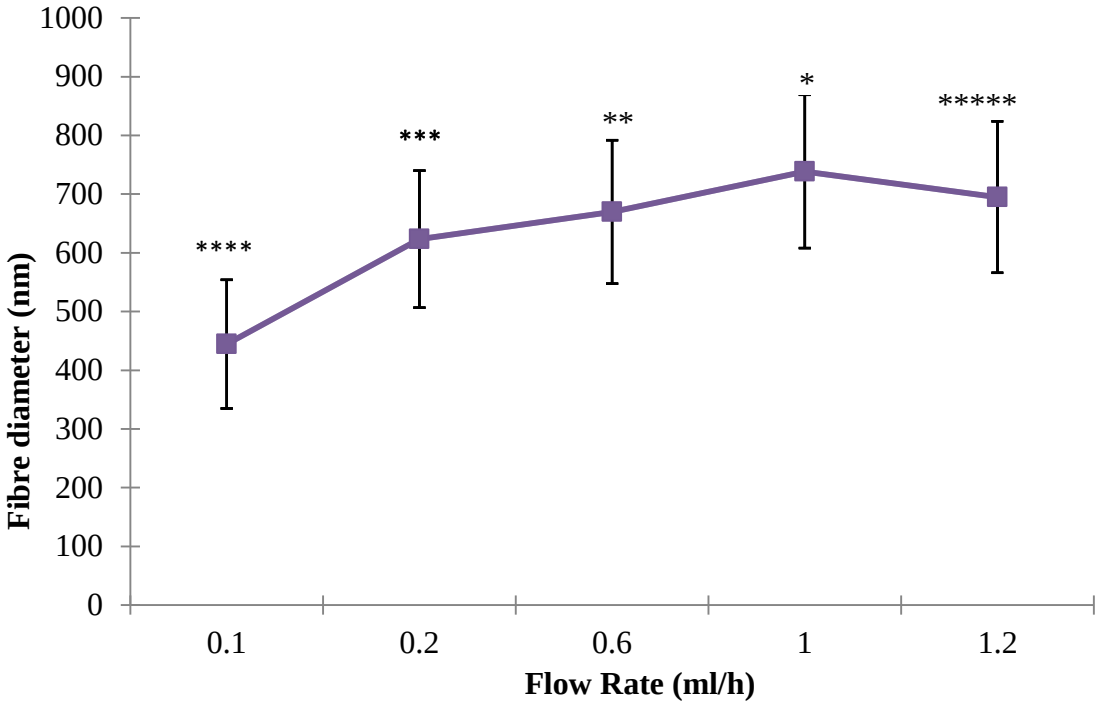

Figure 3.2 Average fibre diameters for electrospun PU membranes as a function of solution flow rate. The membranes were spun using 10% (w/w) PU solution in 1:1 THF:DMF, applied voltage of 20kV and distance to collector maintained at 22 cm. $p<0.05$ for each flow rate with the exception of *****, which was not statistically different from * and **.

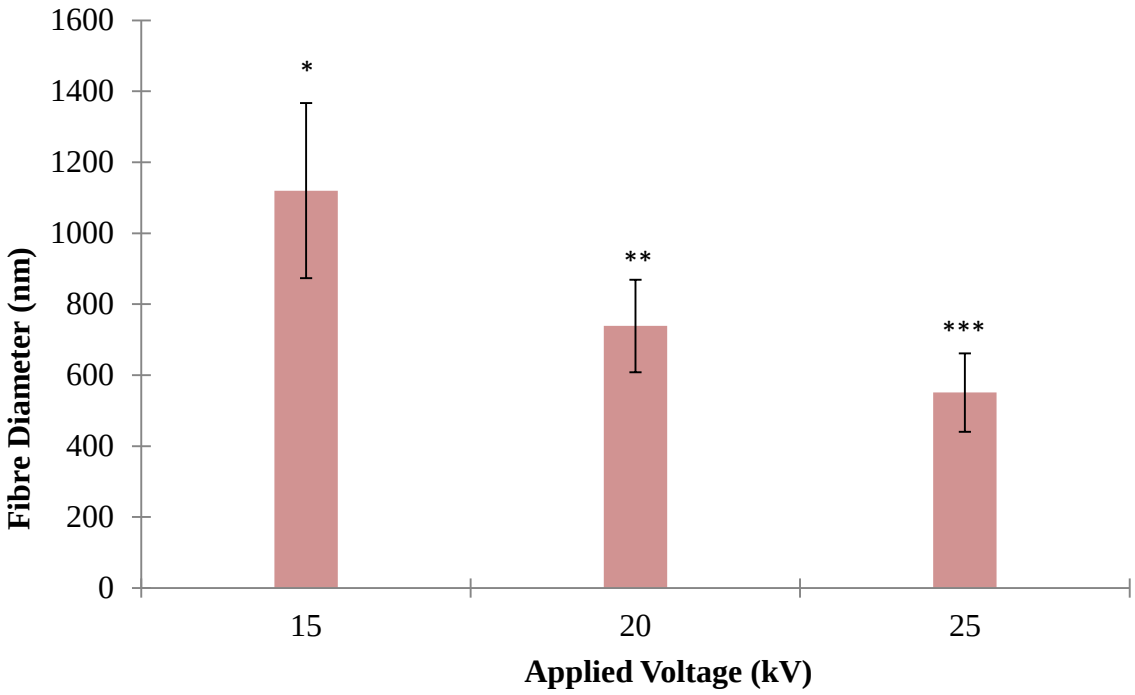

Figure 3.3 Average fibre diameters for electrospun PU membranes as a function of applied voltage. The membranes were spun using 10 % (w/w) PU solution with 1:1 of THF:DMF, 1 ml/h flow rate and 22 cm distance from the collector. ($p<0.05$ between * and **, ** and ***)

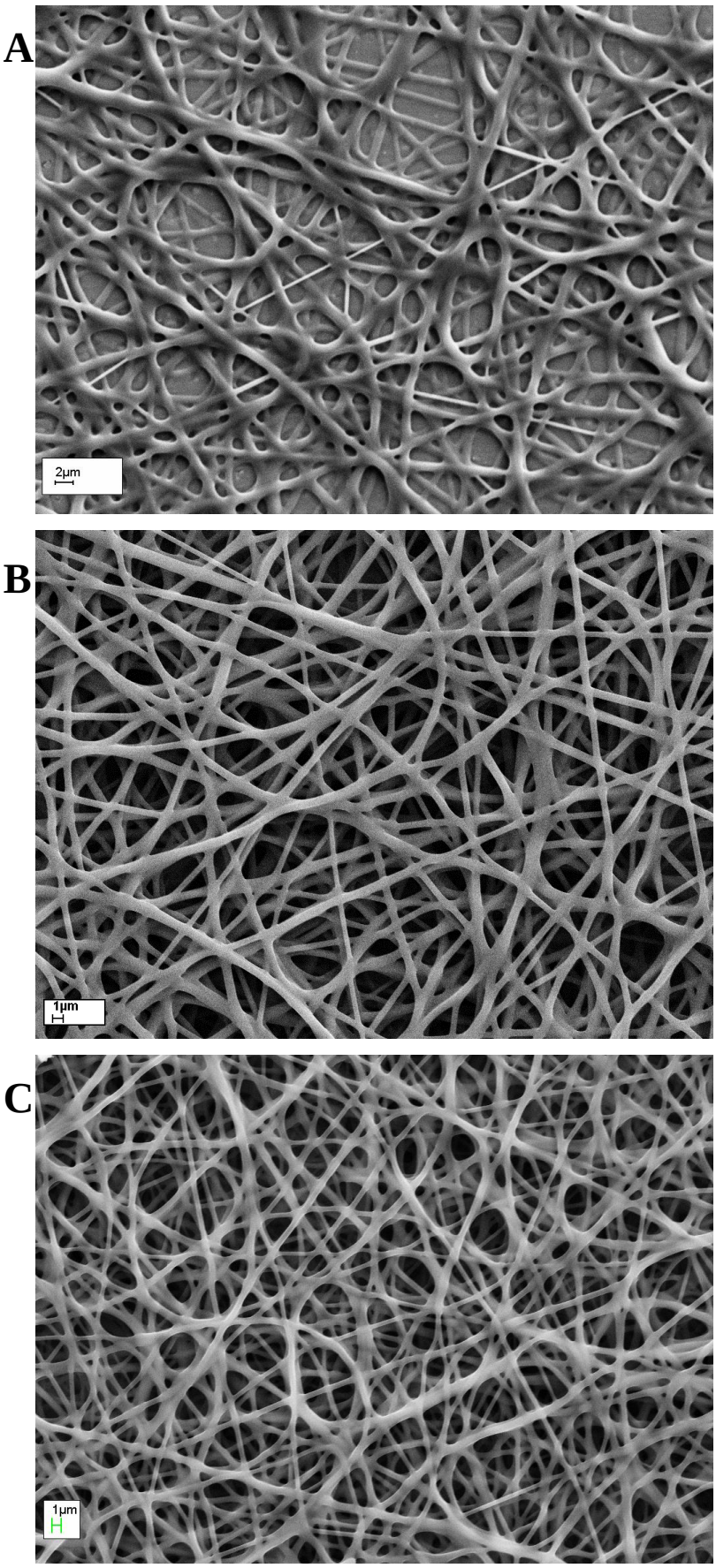

Figure 3.4 Morphology of electrospun PU membranes as a function of applied voltage, a) 15kV, b) 20kV, and c) 25kV. PU solution concentration of 10 % (w/w), 1:1 THF:DMF, 22 cm distance to collector and flow rate of 1 ml/h were kept constant.

At voltages below 11 kV, no jet emerged from Taylor Cone and the PU solution dripped on to the grounded collector. Further, with an increase in applied voltage the Taylor Cone was observed to recede closer to the tip of the needle. Also at 25kV, occasionally, secondary jets formed during electrospinning. The different jets repelled each other due to the flowing charge on their surface causing fibre deposition on a larger area on the collector. The secondary jets are also considered to cause smaller fibre diameters (Demir *et al.*, 2002). It is worthwhile to note that higher voltages resulted in a more uniform and narrow fibre diameter distributions (Figure 3.4).

The effect of applied voltage on the diameter and structure of fibres has been a debatable issue. This study as well as other reports in the literature suggested a decrease in fibre diameter with an increase in applied voltage (Buchko *et al.*, 1999, Megelski *et al.*, 2002). This could be due to the higher surface charge and the lower volume of polymer solution available in the receding Taylor cone with increasing applied voltage. In contrast, some studies report increasing applied voltage to cause no change or even an increase in fibre diameter. Lower voltages are thought to lower the jet acceleration, thereby allowing more time for the jet to stretch and elongate before the smaller diameter fibres distribute on the collector and vice versa (Zhao *et al.*, 2004, Zhang *et al.*, 2005, Demir *et al.*, 2002, Lee *et al.*, 2004a, Lee, 2002). Reneker and Chun reported that there is not much influence of electric field on the fibre size for the electrospinning of polyethylene oxide (Reneker and Chun, 1996). In addition, some studies also reported a greater possibility of bead formation in stronger external electric fields as a result of the increased stretching of the jet (Deitzel *et al.*, 2001a, Zong *et al.*, 2002, Demir *et al.*, 2002). However, this study with 10% PU solution, 1 ml/h flow rate and 22 cm distance from the collector demonstrated bead-less fibres for the voltage range of 15 to 25kV. The divergent observations on the effects of applied voltage on fibre characteristics are proposed to be influenced by the polymer properties and choice of solvents, further supporting the need for polymer specific process optimization for electrospinning.

3.3.4. Distance between the spinneret tip and collector

Distance between the spinneret needle tip and collector influences the flight time for the electrospinning jet and the electric field strength. As shown in Figure 3.5, increasing the distance up to 22 cm lead to a decrease in the average fibre diameter and thereafter the reverse trend was observed.

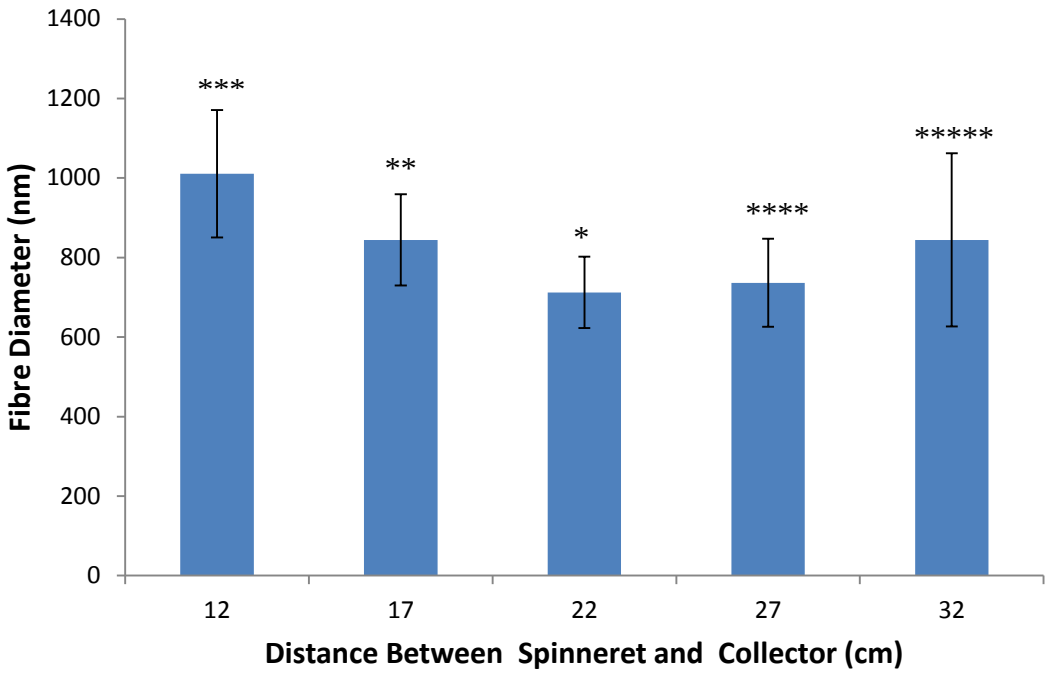

Figure 3.5 Average fibre diameter for electrospun PU membranes as a function of distance from spinneret tip to collector. The membranes were spun using 10 % (w/w) PU solution in 1:1 THF:DMF solvent system, 1 ml/h flow rate and an applied voltage of 20kV. ($p<0.05$ between * and **, ** and ***, **** and ******; $p>0.05$ between *** and ****, ** and *****)

To obtain independent fibres, the electrospinning jet must be allowed enough time for most of the solvent to evaporate. Short distances between the spinneret and collector cause stronger electric fields, which in turn accelerate the jet. As a result, there may not be sufficient time for solvent to evaporate before the fibre hits the collector (Ramakrishna *et al.*, 2005a). The excess solvent usually induces inter- and intra-layer fusion of fibres as illustrated in Figure 3.6A. Provided there is sufficient electrostatic field strength, increasing the distance between the spinneret and needle causes stretching of fibres, reducing the fibre diameter (Figure 3.6B). However, beyond an optimum distance, the strength of the electrostatic field decreases, thus lowering the stretching effect and increase in fibre diameter (Figure 3.6C) (Lee *et al.*, 2004a). Moreover, too large a distance would cause a lower density of fibres deposited on the collector as indicated in Figure 3.6C. The lowest average fibre diameter with fibres forming an evenly distributed nano-web was obtained at 22cm (Figure 3.6B).

3.3.5. Solution Concentration

For a given molecular weight of a polymer, concentration is the primary factor affecting the solution viscosity (Eq. 3.1) and therefore its electrospinnability. For the

electrospinning of PU, 3 concentrations, namely 8%, 10% and 12% were tested, while having 1:1 for THF:DMF solvent ratio, 22 kV applied voltage, 1 ml/h flow rate and 22 cm distance to the collector constant. The morphology and fibre diameter distribution histograms are presented in Figure 3.7A-C. Bead formation was observed for an 8% PU solution in 1:1 THF: DMF (Figure 3.7A), indicating a lesser viscosity solution. At 10 and 12 % PU solution concentrations, the viscosity was sufficient to prevent bead formation (Figure 3.7B & C). Higher viscosity allows ionic charge distribution among the polymer chains and solvent molecules such that the polymer solution is stretched to form uniform fibres (Demir, 2010). As illustrated in Figure 3.7D-F, an increase in the average fibre diameter having wider distribution was observed with increasing polymer solution concentration. This was in accordance with reported literatures (Megelski *et al.*, 2002, Jarusuwannapoom *et al.*, 2005, Demir *et al.*, 2002, Deitzel *et al.*, 2001a). The increasing viscosity with increasing concentration is said to prevent the charged jet from splaying and splitting, thus reducing the jet's path and bending instability (Mit-uppatham *et al.*, 2004) resulting in increasing fibre diameter. The lower splaying, in turn, also causes the fibres to be deposited in a smaller area on the collector. Srivastava *et al.* explain the increasing fibre diameter with increasing polymer solution concentration to be induced by the faster evaporation of low solvent content and the greater viscoelastic forces acting against the columbic forces of the charges results in the less stretching of fibres and thus the formation of thicker fibres (Srivastava *et al.*, 2007). The results achieved in this work further reiterate that the polymer solution concentration and the choice of solvents play a critical role on the resultant structure and diameter of the resultant electrospun fibres.

3.3.6. Further reduction in fibre diameter

To generate finer fibres, 8wt% PU solutions in three different solvent mixture of THF to DMF ratios of 3:1, 1:1 and 2:3 (w/w) were tested. For the 8% PU solution in 3:1 THF: DMF solvent mixture, the external electrostatic strength was varied by applied voltages between 9 and 27 kV. The flow rate was also varied to suit the applied voltage such that the electrospinning jet forms, while maintaining the distance to collector constant at 22 cm. Irrespective of the changes in the applied voltage and flow rates, 8% PU solution in 3:1 THF: DMF solvent mixture always resulted in bead formation (an example in Figure 3.8A), with the exception when the applied voltage was less than 10kV, where no jet formed. Similarly, 8% PU in 1:1 THF: DMF solvent mixture also caused bead formation irrespective of the applied voltage and flow rate (Figure 3.8B), with the exception of 27kV, where beads began to join to form thick fibres. Moreover, the bead density increased with

increasing applied voltage. Finally, an 8% PU solution in 2:3 THF to DMF produced beadless and uniform fibres (Figure 3.8C).

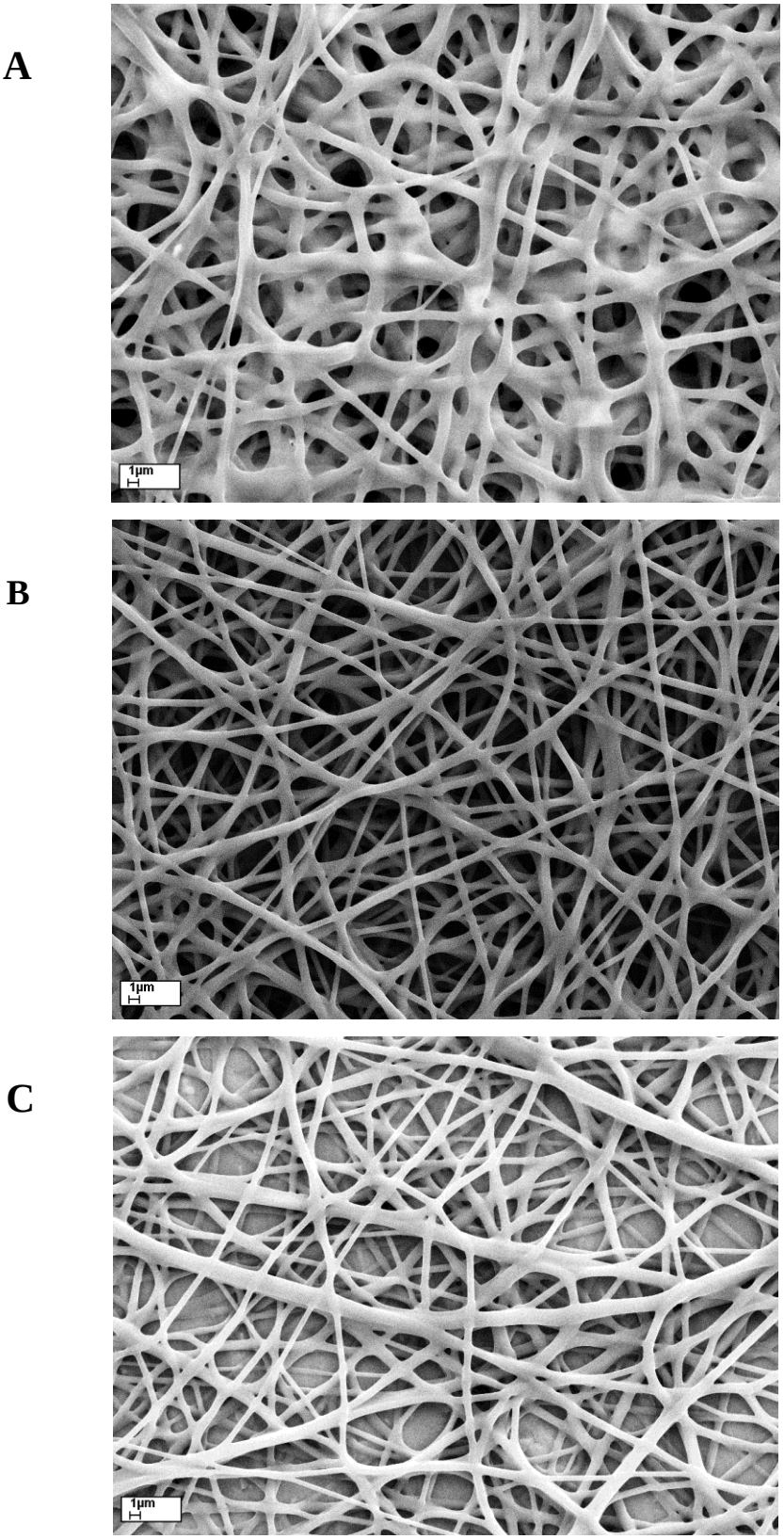

Figure 3.6 Morphology of electrospun PU membranes as a function of distance to collector, a) 12 cm, b) 22 cm, and c) 32 cm. PU solution concentration of 10 % (w/w), 1:1 THF:DMF, 20kV applied voltage, and flow rate of 1 ml/h were kept constant.

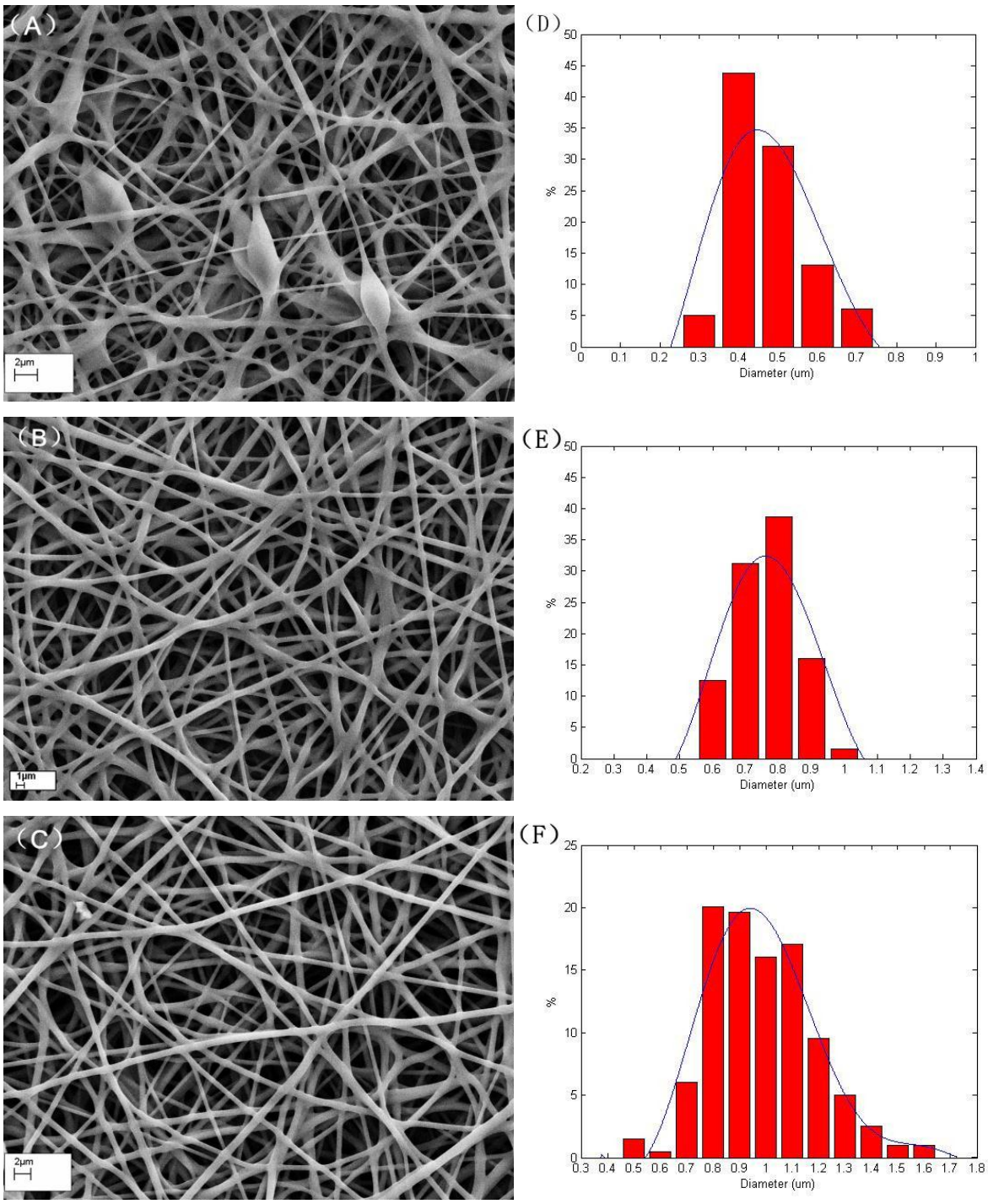

Figure 3.7 SEM images of the PU electrospun fibrous webs and their fibre diameter distribution with different concentration at 8wt% (A,D), 10wt% (B,E), 12wt% (C,F) , constant THF:DMF solvent ratio of 50:50, voltage of 20kV, DTC of 22cm, and flow rate of 1.0ml/h

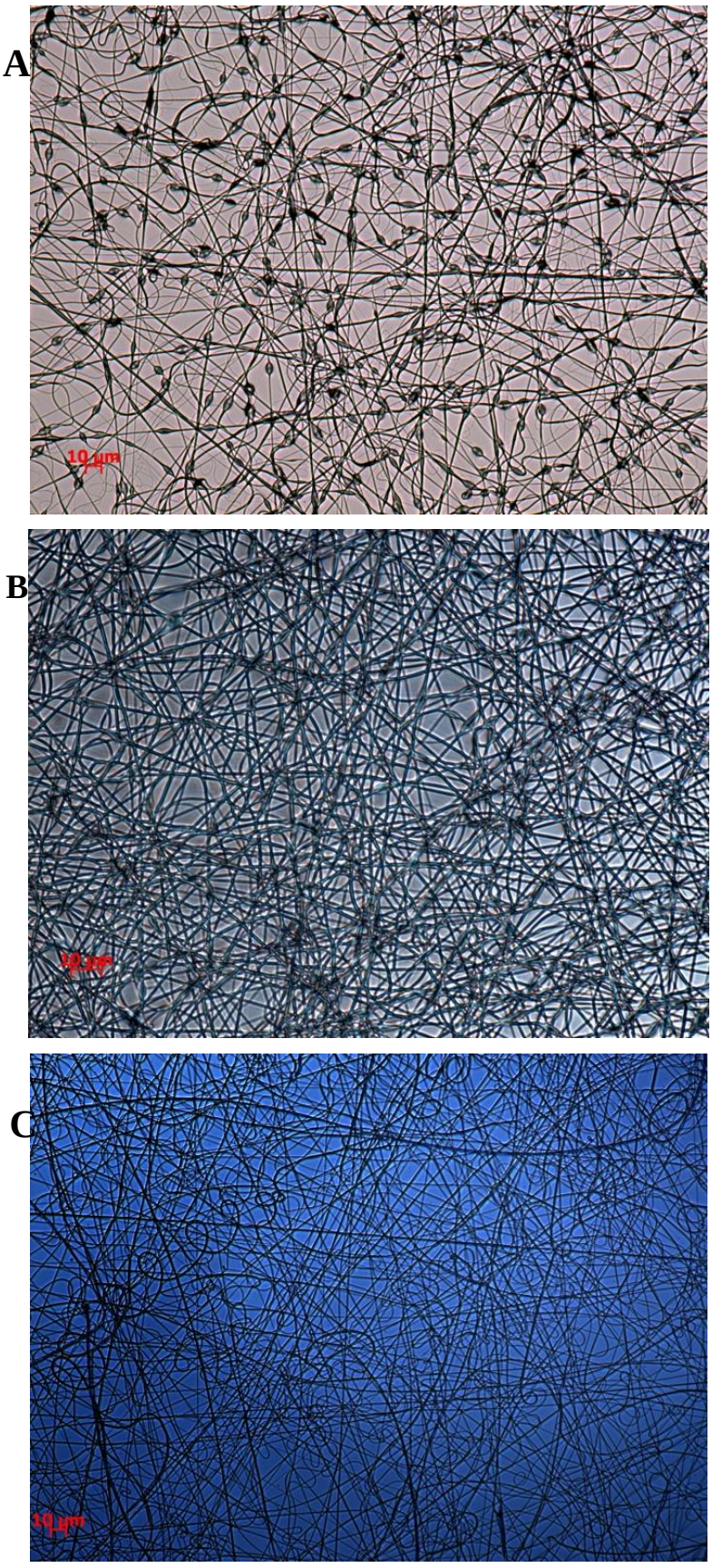

Figure 3.8 Light microscopy images showing the morphology of fibres electro-spun from 8% polyurethane solution in A) 3:1, B) 1:1 and C) 2:3 w/w THF:DMF solvent mixtures while maintaining applied voltage at 21kV, flow rate at 0.6 ml/h and distance to collector at 22cm.

The results for electrospinning of PU using 8% solutions in 3:1, 1:1 and 2:3 THF: DMF solvent mixture is illustrative of the importance of solution parameters (solvents and solution parameters) in comparison to process parameters (applied voltage, flow rate and distance to collector). A threshold viscosity is essential to obtain proper polymer fibres using electrospinning irrespective of the process parameters.

3.3.7. Optimized parameters

Based on the extensive electrospinning process optimization experiments presented above, it is evident that electrospinning can be used to generate membranes with desired fibre diameters. Towards the goals of achieving membrane with different fibre diameters and interconnected porous structures and understanding their structure effect on the coated glucose biosensor function, three membrane configurations having average fibre diameters of 347.4nm, 738.4nm and 1102.3nm, designated as 8PU, 10PU and 12PU membranes respectively, were shortlisted for further studies. The electrospinning conditions for the shortlisted membranes are presented in Table 3.2. Their morphology and fibre diameters are represented in Figure 3.9A-D.

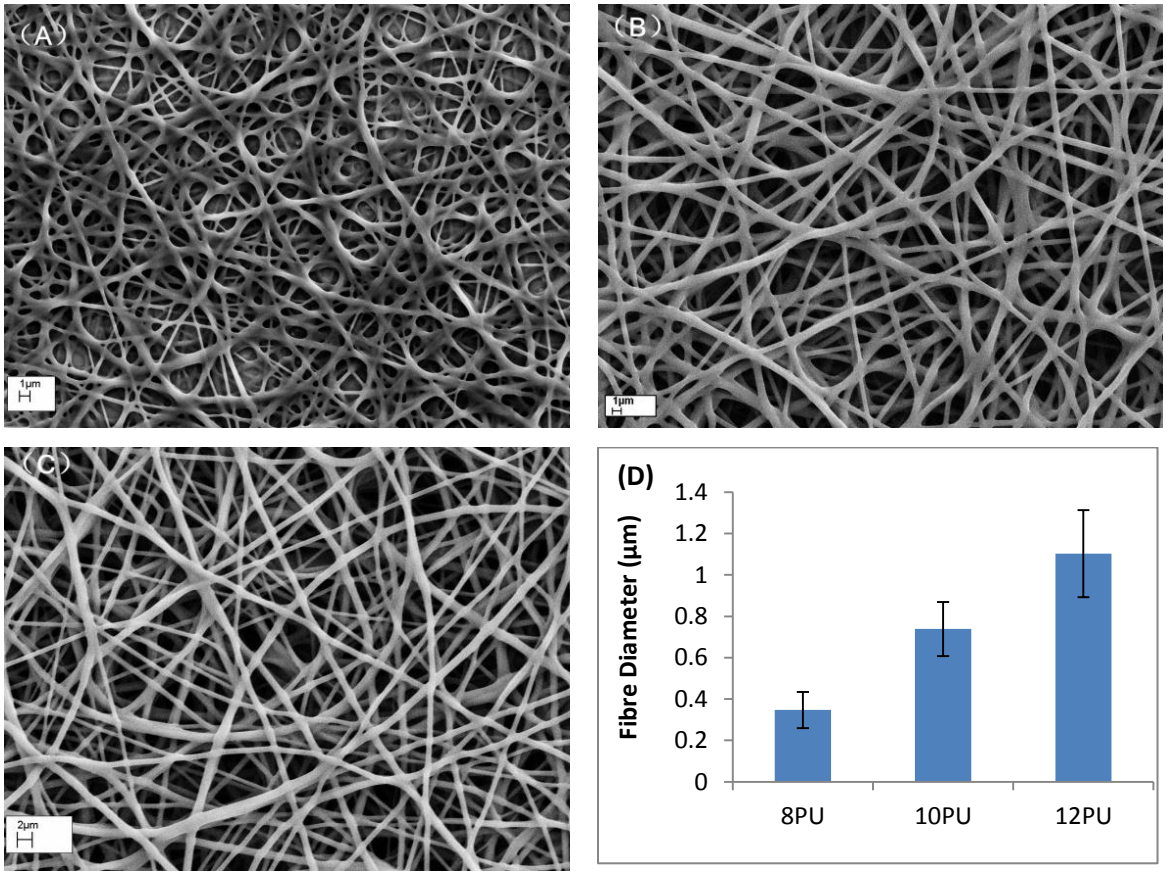

Figure 3.9 Morphology of the membranes A) 8PU, B) 10PU, and C) 12PU and D) their respective fibre diameters. The average fibre diameter for each membrane configuration is statistically different from the other two membranes.

Table 3.2 Electrospinning parameters for the three shortlisted membrane configurations

Designation	PU Solution Concentration (wt %)	Solvent THF: DMF (wt%:wt%)	Voltage (kV)	Feed Rate (ml/h)	Distance to Collector (cm)
8PU	8	40:60	21	0.6	22
10PU	10	50:50	20	1.0	22
12PU	12	50:50	20	1.2	22

3.4. Characterization of Electrospun PU Membranes

3.4.1. Residual solvent detection using FTIR Spectroscopy

The chemical structure and residual solvents in the electrospun membranes were assessed using ATR-FTIR spectroscopy and were compared with that of solvents, solvent cast PU and as-supplied PU. IR absorption spectra were recorded for the range of 650 to 4000 cm^{-1} (Figure 3.10). The FTIR spectra of electrospun PU membranes had the characteristic absorption peaks at 3324, 2855, 1715, 1530, 1232, 1111 and 779 cm^{-1} which are assigned to *v* (N-H), *v* (C-H), *v* (C=O), *v* (C=C), *v* (C-C), *v* (C-O) and *v* (C-H) on substituted benzene respectively (James *et al.*, 2006, Jiang *et al.*, 2006). The spectra of solvent cast PU, as-supplied PU Pellet and electropun PU membranes all had similar absorption peaks with the exception of the absorption peak at about 1111 cm^{-1} concerning the C-O-C stretching vibration, which shifted slightly to a higher wave number after electrospinning. Therefore, it can be confirmed the original chemical structure was not affected by the electrospinning process involving huge applied voltages. Furthermore, as illustrated in Figure 3.10, the strong absorption peaks characteristic for DMF, C═N at 1657 cm^{-1}, and THF, C-F at 1065 cm^{-1}, were not observed in the spectra for solvent cast films or electrospun PU membranes, indicating that drying cycles employed removed any residual solvents in the films and membrane.

3.4.2. Thickness versus electrospinning time

Substrate thickness is an essential parameter that influences the permeability and transport properties of a membrane. For the chosen three membrane configurations, namely 8PU, 10PU and 12PU, the electrospinning time was varied from 1 to 120 min to study its influence on membrane thicknesses. Thickness increased as a function of electrospinning time and polymer solution concentration (Figure 3.11). The former is obvious, since the longer the electrospinning time, the more the polymer that is deposited on the collector. On the other hand, the increase as a function of polymer solution concentration can be attributed to not only the increased volume of polymer being pumped per unit time, but also due to the stacking of fibres with larger diameters (Figure 3.9) on the collector.

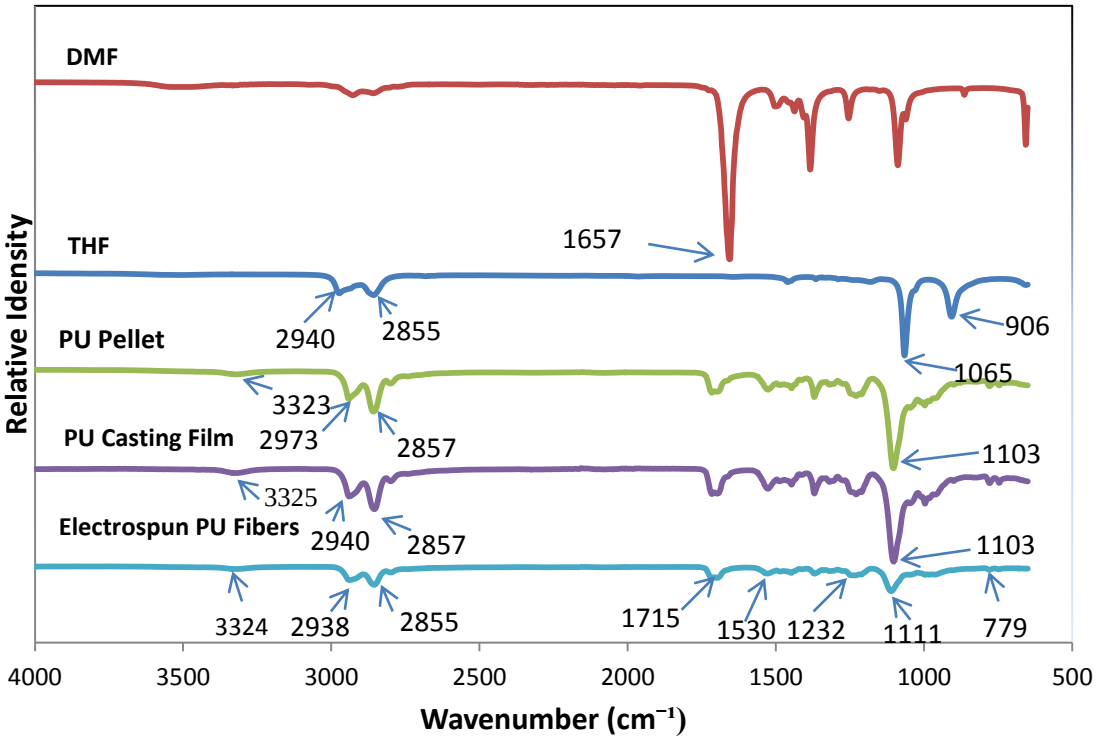

Figure 3.10 ATR-FTIR spectra for DMF, THF, as-supplied PU pellets, solvent cast PU film and electrospun PU membrane.

Considering the stacking of crisp fibres on top of each other, one can expect a linear increase in the membrane thickness with an increasing electrospinning time. However, the linearity decreased with decreasing polymer solution concentration, with R^2 of 0.9931, 0.9893 and 0.9166 for 12PU, 10PU and 8PU respectively (Figure 3.11), indicating a partial fusion of fibres in neighbouring stacks. The R^2 values of about 0.99 for 12 PU and 10PU suggest minimal fusion of fibres, while a lower R^2 of 0.9166 for 8PU suggests fusion of fibres which can be clearly visualised in Figure 3.9A. The latter can be attributed to a lower viscosity of its feed PU solution concentration.

3.4.3. Pore Size and Porosity

The membranes 8PU, 10PU and 12PU were prepared using a 2h electrospinning time to obtain membranes thick enough to meet the safety requirement for the bubble point measuring apparatus (Figure 2.5). Bubble point measurements of the pore radii revealed an increase of the average pore size with increasing fibre diameter (Figure 3.12). The pore size distribution was very narrow for 8PU compared to wide distributions for 10PU and 12PU membranes. The results for fibre packing density and pore volume determined by gravimetry shown in Table 3.3 also reiterate the increasing porosity as a function of fibre diameter.

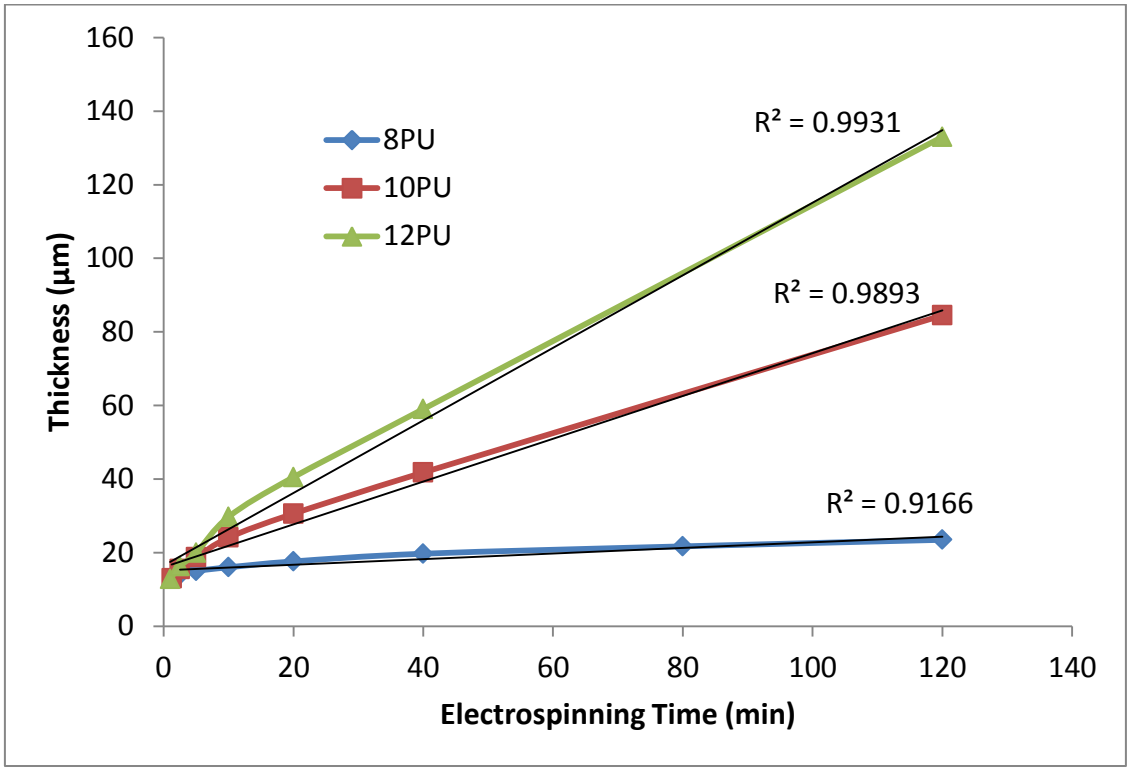

Figure 3.11 Thickness of the electrospun membranes: A) 8PU, B) 10PU, and C) 12PU as a function of electrospinning time.

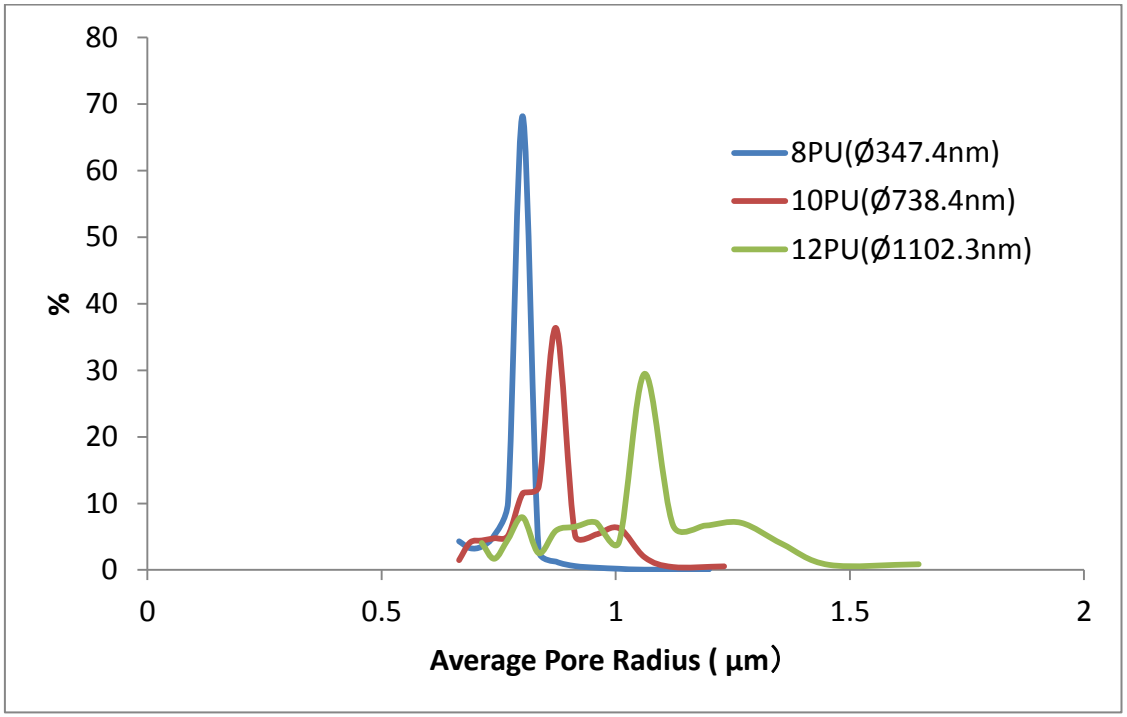

Figure 3.12 Pore size distributions for the electrospun membranes 8PU, 10PU and 12PU, as determined by bubble extrusion porosimetry. The pore size were obtained by averaging the result calculated using two adjacent pressure, while the percentages of particular pore sizes were estimated by the ratio of subinterval and all area of flow rate.

The advantage for electrospun membranes is that they have a fibrous mesh structure that ensures surface to surface interconnected and continuous pores. In addition, if the pores size distribution is narrow and porosity in sub-micron dimension, they could function as size or molecular weight cut-off membranes. Having significantly smaller fibre diameters (~0.347 μm), pore size (~0.8μm), narrow fibre diameter and pore size distribution (68% between 0.7 and 0.9 μm), and about 44% pore volume (Figure 3.12 and Table 3.3), 8PU is anticipated to allow high flux/flow of solvents or solutes across, while acting as a mass-transport limiting membrane.

In general, our results demonstrate that the porosity and the pore size distribution in the electrospun membrane are dependent on the diameter and packing density of fibres. Furthermore, the fibre diameter and its distribution can be tailored by appropriate electrospinning conditions.

Table 3.3 Porosity estimations for electrospun PU membranes based on gravimetry, calculated using equations 2.2 and 2.3. The electrospinning time for the membranes was 2h, and n=3 per test membrane. The fibre packing density (*) and pore volume ($^{\#}$) was significantly lower for 8PU when compared to 10PU and 12PU membranes.

Sample Designation	Thickness (μm)	Fibre Diameter (μm)	Fibre Packing Density (g/cm^3)	Pore Volume (%)
8PU	28.4 ± 5.4	0.347 ± 0.087	0.580 ± 0.028*	44.19± 2.54$^{\#}$
10PU	86.0 ± 12.9	0.738 ± 0.131	0.408 ± 0.013	62.87± 1.18
12PU	180.6 ± 42.2	1.102 ± 0.210	0.381 ± 0.020	65.40± 1.85

3.4.4. Diffusion Test

The permeability of the electrospun membranes to glucose was tested as a function of membrane porosity and thickness using rotating biodialysers. Three different electrospinning times namely 2.5, 5 and 10 min were used to obtain 8PU, 10PU and 12PU membranes having fine differences in thickness to test their efficacy as mass-transport limiting membranes for sensor with minimal effects on sensor function. The membranes were equilibrated in PBS (pH 7.4) at 37^{o}C prior to diffusion tests. Electrochemical glucose sensors were used to measure the changes in glucose in the receiving buffer (PBS). The thickness for the various membranes is listed in Table 3.4 and glucose diffusion profile results for the different membranes are shown in Fig 3.13.

The original glucose diffusion profiles had 10 data points recorded per second. To minimize the enormity of the data for statistical analysis, we extracted readings for the

time points 2, 5, 10, 20, and 40 min for each of the membranes and comparisons were made, using one-way ANOVA, to differentiate the effects of membrane thickness on glucose diffusion across the membranes (Figure 3.13A-C).

Table 3.4 The thickness of electrospun membranes used for diffusion tests. (n=5)

Electrospinning Time (min)	Thickness of electrospun membranes (μm)		
	8PU	10PU	12PU
2.5’	0.0139 ± 0.0042	0.0155 ± 0.0024	0.0163 ± 0.0030
5’	0.0149 ± 0.0027	0.0187 ± 0.0040	0.0199 ± 0.0041°
10’	0.0160 ± 0.0037	0.0241 ± 0.0031	0.0297 ± 0.0025°

° Statistically significant difference in thickness compared to that of 8PU-2.5’

As a function of membrane thickness (electrospinning time), there appeared to be a decrease in the rate of diffusion of glucose across each of the three membrane configurations 8PU, 10PU and 12PU (Figure 3.13A-C). However, the decrease was statistically significant only for 10PU-10’, when compared to 10PU-2.5’ and 10PU-5’. It is also interesting to note that between the membrane configurations, for each electrospinning time, there were no statistically significant differences. For example, no significant differences were observed between 8PU-2.5’, 10PU-2.5’ and 12PU-2.5’ for the trans-membrane diffusion of glucose, in spite of significantly differences for their corresponding fibre diameters and membrane thicknesses.

Diffusion kinetics analysis further reiterated the free diffusion of glucose across the 8PU, 10PU and 12PU membranes irrespective of their thicknesses. The first 60% of the glucose transport data was fitted in the Power Law (Korsmeyer-Peppas) model, equation 2.4. The ‘n’ value is an exponent used to describe diffusion mechanisms. When the values of ‘n’ lies between 0.5 and 1, the diffusion mechanism through a polymer is anomalous, where the solute diffusion rate (i.e. glucose) is about the same order of magnitude with the polymer relaxation. In this case, the glucose transport is fast but also restricted by the structure and viscoelastic properties of the polymer materials. On the other hand, when ‘n’ is greater than 1 the rate of diffusion becomes faster which means that the glucose can diffuse through polymer materials more freely. The ‘n’ values for the membranes 8PU, 10PU and 12PU as a function of electrospinning time are plotted in Figure 3.14. Although statistically insignificant, the ‘n’ values showed a decreasing trend with increasing membrane thicknesses for all membrane configurations. The average ‘n’ values were closer to 1 for membrane configurations spun with 2.5’ electrospinning time, indicating a near-zero order (Case-II) glucose diffusion. With increasing thickness, the diffusion was tending towards anomalous diffusion (non-Fickian). Besides, the results also revealled that no significant variation in the diffusion exponent (‘n’) can be found by changing the pore

volume, with the exception of membrane made by 2.5'electrospinning. The significant increase in values 'n' from 8PU-2.5' to 12PU-2.5' may be due to the ultrathin membrane thickness and less fibre production within a short time electrospinning process.

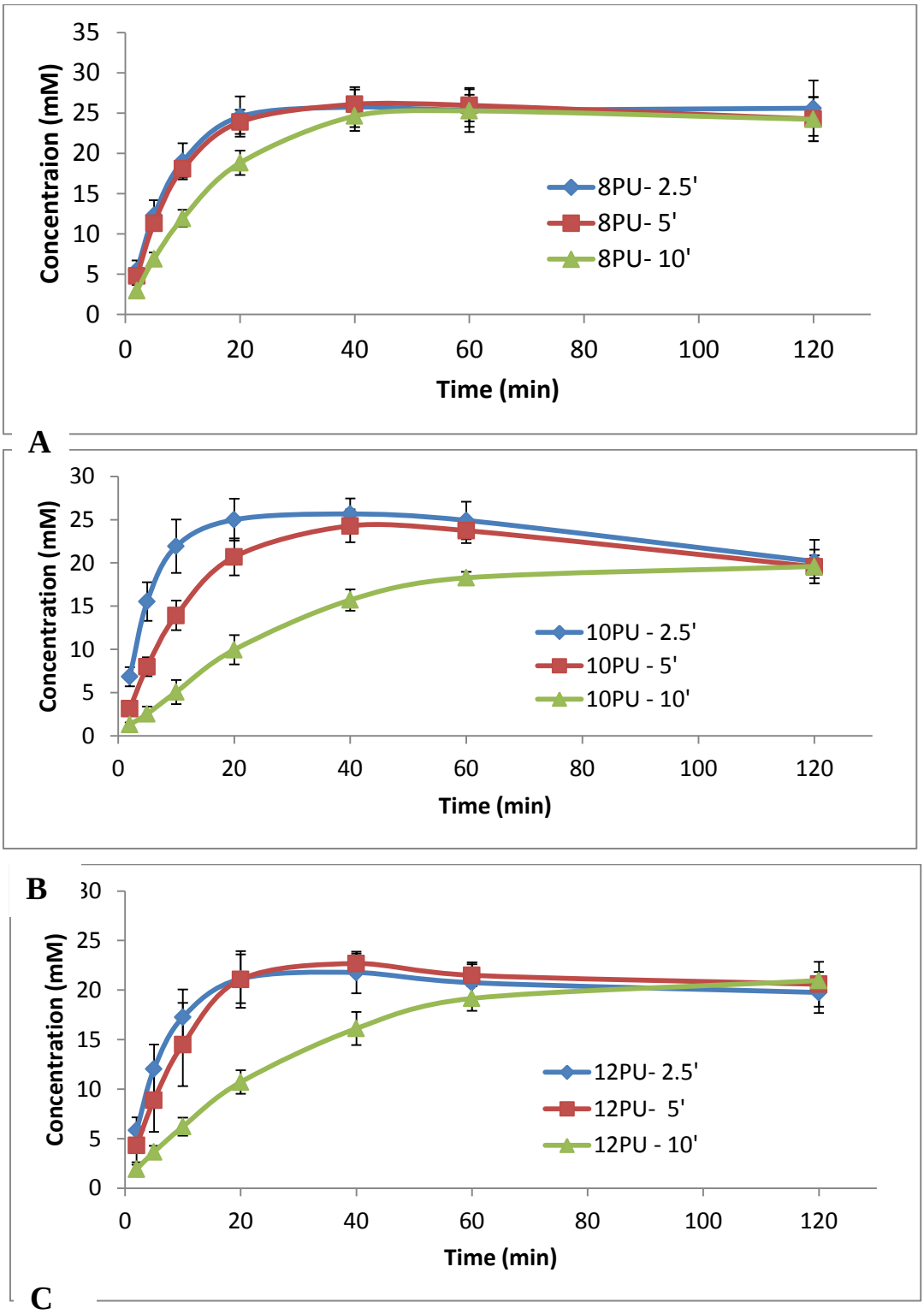

Figure 3.13 Glucose diffusion across A) 8PU, B) 10PU and C) 12PU membranes as a function of time, and thickness (electrospinning times of 2.5, 5 and 10 min). Data is represented as Mean ± SE (standard error) of mean, n=5.

Over all the permeability (flux) for glucose transport across electrospun PU membranes was high, and fine changes to membrane thicknesses and porosities did not induce any statistically significant changes in diffusion kinetics. Such behaviour can be attributed to the highly interconnected porous network structure having about 44 to 69 % pore volume of the fibro-porous electrospun membranes, which is significantly different to conventional porous membranes that have pore volume up to 34% (Yoon *et al.*, 2006).

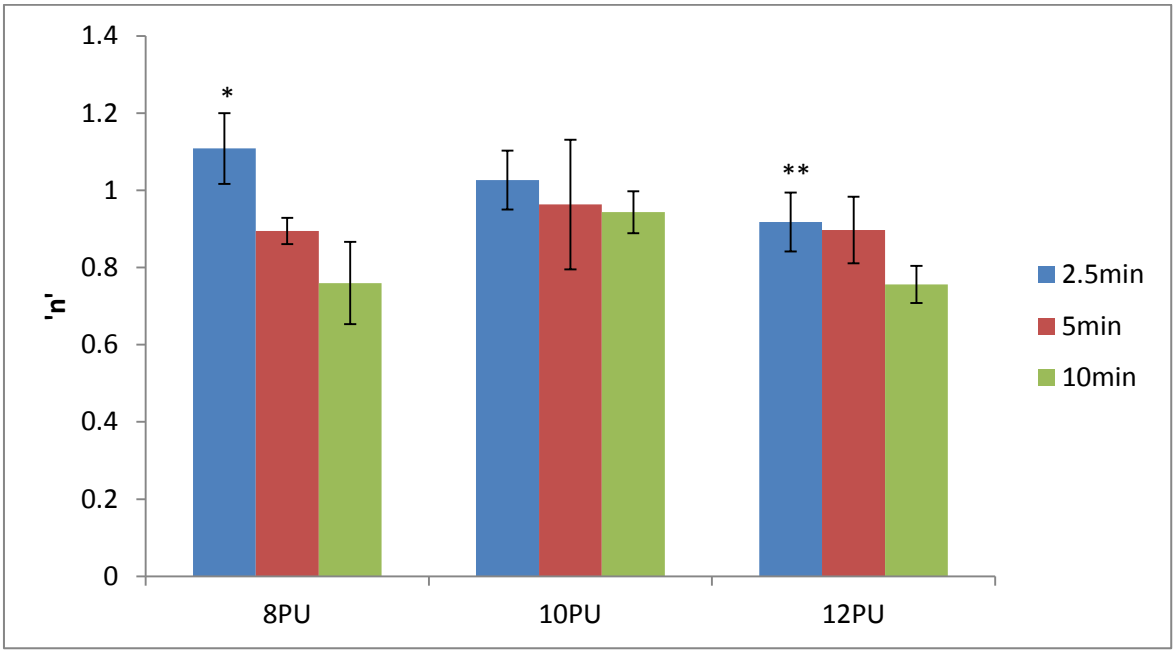

Figure 3.14 Diffusion exponent 'n' values for the different membrane configurations as a function of electrospinning time (thickness). n=5, $p<0.05$ between * and **.

3.4.5. Uniaxial mechanical properties of electrospun PU membranes

The typical stress-strain behaviours observed for electrospun PU membranes are shown in Figure 3.15. Solvent cast PU films were used as controls. Some of the samples were tested both in wet and dry forms. The results for tensile properties namely, ultimate tensile strength (UST, *i.e.* engineering tensile strength, calculated assuming the original cross-sectional area before necking), Young's modulus (between recoverable strain 0%-20%), and strain at break are presented in Table 3.5. The necking is not taken into account in calculation of UTS as the neck dimension during the deformation could not be measured directly using the existing capacity of the Instron tester available in the lab.

The solvent cast PU films showed a typical response for a thermoplastic elastomeric material-sigmoid in shape and displayed hyperelastic characteristics with higher elastic (Young's) modulus (2.8 MPa), UTS (7.04 MPa) and a huge strain (754%)

compared to the electrospun materials. In contrast, the electrospun PU membranes showed fairly linear stress-strain curves until they failed, although they were also elastomeric in nature, undergoing a relatively large strain (up to 260%). No significant difference in tensile properties was observed between dry and wet 8PU samples, which can be attributed to the relatively higher hydrophobicity of PU (see following Section 3.4.6 Surface Contact Angle Measurement). For the dry membranes, as the fibre diameter decreased, the ultimate tensile strength and Young's Modulus increased, and elongation at break decreased (Fig 3.15 & Table 3.5).

The mechanical properties of non-woven electrospun polymeric membranes are mainly determined by macromolecular chain structure, packing and orientation of the chains as well as dimensions and packing morphology of the fibres (Lee, 2002). The typical elastomeric stress-strain sigmoidal profile of thermoplastic PU bulk film is a result of corresponding movements of unique poly-ether-urethane block-copolymer chains and their soft-hard-phase-separated morphology under tensile stress at different length scales with different relaxation times (Fig 7A). Polyurethane hard segment domains in either crystalline or psesudo-crystalline state acted as physical cross-links incorporated with polyether soft segment domains in rubbery state, contributing to the high elasticity. The initial linear elasticity before yield point (around 100-150% strain) was attributed to reversible transient movements of covalent bond stretching (<20%) and entropic elasticity due to the orientation (reduction of conformations) of the soft polyether chain segments. After the yield point (necking started), the large strain (up to 450-500%) involved viscoelastic deformation, a combination of both reversible elastic and irreversible plastic deformation as hard chain segments started to move, resulting in collapse of hard-domains and orientation of polyurethane hard segments in response to the increasing stress. Finally the whole chains were completely extended, aligned and then started to move. Consequently, the modulus increased on account of strain hardening until it reached ultimate strength at 754% strain. Distinctly different stress-strain behaviour for the

electrospun membranes lies in the fibrous porous structure and higher degree of chain orientation within the electrospun fibres than in the bulk film. The strain applied to the electrospun membranes involved both fibre orientation and elongation. The initial lower stress observed with electrospun membranes may be attributed to porous structure with lower bulk density (i.e. fibre packing density, 0.38-0.58 g/cm^3, Table 4) in comparison with PU bulk film and the rotation of random fibres at the beginning of the stretch (Pedicini and Farris, 2003). Nevertheless, the stress in the electrospun PU increased more rapidly than that in the bulk film depending on the fibre diameter, which was attributed to the stress-induced alignment of the fibres and possible chain orientation of individual fibres with less plastic deformation involved. Without a sign of yield point, the membrane prematurely failed before profoundly viscoelastic deformation and stain stiffening occurred. The fibre ends or weak fibre interconnections may play a critical role as defects causing the lower ultimate strength (3.2 to 6.7 MPa) of the fibrous membranes at a lower strain (190-260%) compared with the bulk film (8.2 MPa at 754%).

A range of tensile strength and modulus with the relatively higher linearity of hyperelasticity and lower strain at break of the membranes were obtained depending on the fibre diameter (Fig 3.15). For the dry membranes, as the fibre diameter decreased, the ultimate tensile strength and Young's Modulus increased, and elongation at break decreased, which could be due to a corresponding increase in Young's Modulus of thinner individual fibres, fibre packing, thus reduction in pore volume (Figure 3.15 & Table 3.5). The higher chain orientation in the fibre formed during electrospinning is believed to account for high Young's modulus of individual electrospun fibres with smaller diamter (Wong *et al*., 2008, Baji *et al.*, 2010). In this work, the stronger interconnection between fibres due to fibre fusion may also contribute to the highest mechanical properties of 8PU membrane among the samples tested. Overall, the elastic modulus and tensile strengths for the different PU membranes tested here are higher than that of soft tissues (~2.75kPa) and

therefore the tough and strong membranes could be suitable for implantable applications (Iatridis et al., 2003).

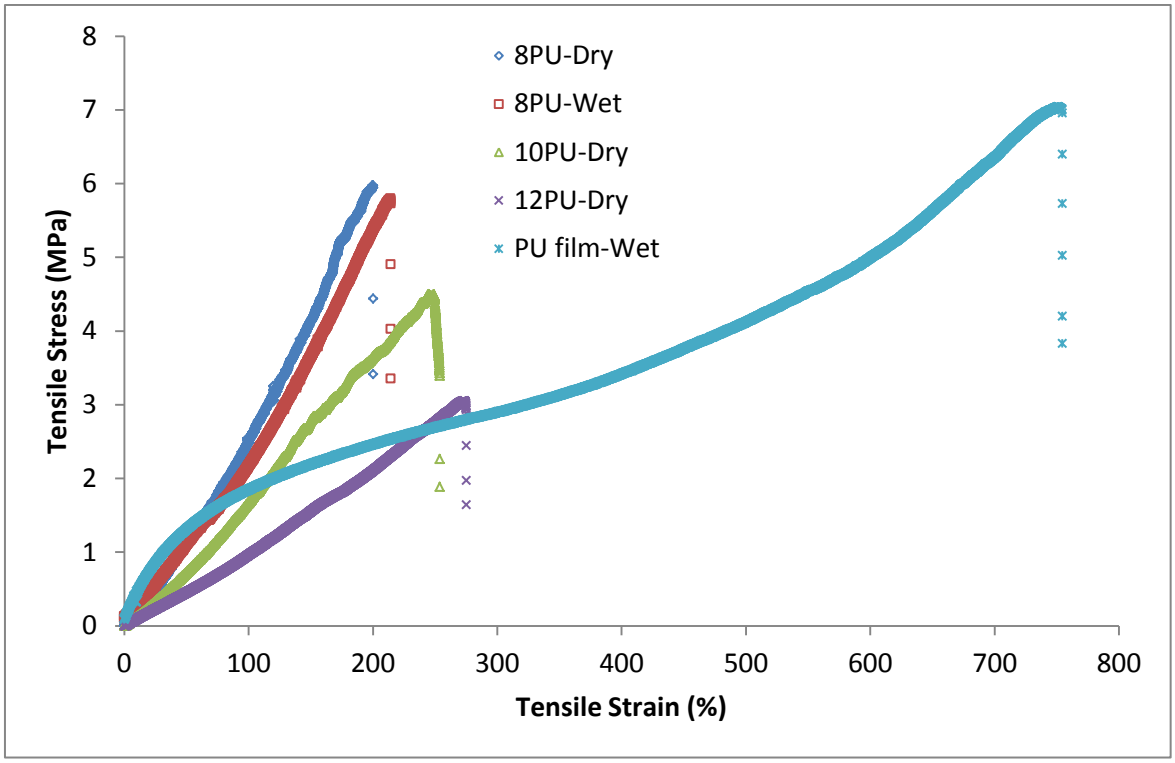

Figure 3.15 Typical stress-strain curves for different PU membranes

Table 3.5 Tensile Properties of Electrospun and solvent cast PU Membranes, n= 4.

	8PU - Dry	8PU - Wet	10PU - Dry	12PU - Dry	PU film – wet
Fibre Diameter (nm)	347.6 ± 87.3		738.4 ± 130.71	1102.3 ± 210.33	-
Thickness (µm)	23.5 ± 4.81	45.0 ± 8.54	84.5 ± 17.45	133.3 ± 28.34	71.6 ± 16.8
Young's Modulus 0-20% (MPa)	1.9 ± 0.24	2.3 ± 0.85	1.3 ± 0.05	0.97 ± 0.049	2.8 ± 0.43
Ultimate Tensile Strength (MPa)	6.7 ± 0.93	5.8± 2.13	5.3 ± 0.54	3.1 ± 0.06	8.1 ± 2.00
Strain at Break (%)	192.9 ± 23.00	191.2 ± 61.10	248.1 ± 10.73	261.0 ± 12.09	849.7 ± 258.8

3.4.6. Surface Contact Angle Measurement

The hydrophobic and hydrophilic natures of membranes have an important role in biosensor applications through their effects on the diffusion of analytes, protein adsorption and foreign body reactions (Allen et al., 1994, Yu et al., 2005a, Tang et al., 1998, Krishnan et al., 2008). The most direct means for measuring hydrophilicity is via surface contact

angle measurements. Figure 3.16A&B illustrate the typical morphology of a 1µl droplet of DI water on the different PU membranes and their corresponding contact angles. The solvent cast non-porous PU film showed the smallest contact angle of about 86°, while the electrospun PU membranes, 8PU, 10PU and 12PU had 104.3°, 116.1° and 122.5° respectively. Clearly, porous structures had higher hydrophobicity and among the fibro-porous membranes, statistically significant increase in hydrophobicity was observed with increasing fibre diameters and porosity. The static contact angle measured is determined by the surface chemistry and the surface roughness of the membrane. Cassie-Baxter model (Cassie's law) (Marmur, 2003) describes the contact angle as a function of the surface roughness and contact surface area of a textured surface:

$$cos\theta^* = \gamma_f f cos\theta + f - 1$$

Where:

θ^* is the apparent contact angle on a textured surface which corresponds to the stable equilibrium state.

θ is the contact angle on a ideal solid surface to the stable equilibrium state

γ_f is the roughness ratio of the wet surface,

f is the fraction of solid face area wet by the liquid (for flat homogeneous surface, f=1 and $\gamma_f=\gamma$, γ is the surface roughness of a homogeneous surface)

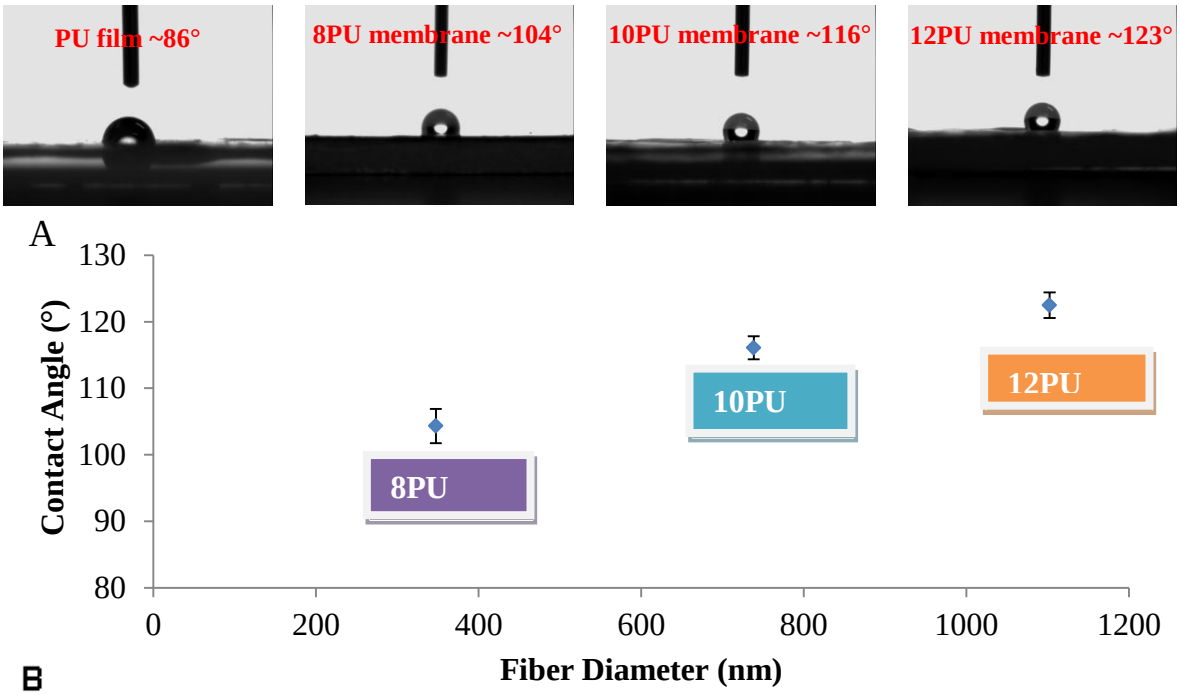

Figure 3.16 Contact angle measurement: (A) the morphology of water droplet (1µL) on solvent cast PU film and the three electrospun PU membrane variables; and (B) contact angles as a function of fibre diameter.

It is obvious that the surface roughness of the electrospun PU membranes with different diameters and porous surface contributes to the change of their contact angles. In consistence with the equation, the larger diameter of 12PU membrane provides a larger porosity and higher roughness (i.e. high γ_f), therefore based on the above equation, the trend of f can be estimated.

The similar observations were also reported earlier (Acatay *et al.*, 2004, Han and Steckl, 2009). The bigger pores on the electrospun membrane surface are said to entrap more air causing the surface to be more hydrophobic (Ma *et al.*, 2005, Kim *et al.*, 2009, Cui *et al.*, 2008). Liu *et al.* also suggest that the smaller the pore in the material, the higher their capillary effect contributing to faster water absorption, thus decreasing the contact angle with decreasing pore sizes (Liu *et al.*, 2008).

3.5. Chapter summary

In this work, ultra-fine elastic fibres having micro- and nano- scaled diameters were successfully prepared using electrospinning technology. Fibre diameters in the electrospun membranes are significantly influenced by the electrospinning conditions, namely, solution (solvents and solution concentration), processing (flow rate, applied voltage, spinneret tip to collector distance) and ambient (temperature and humidity) parameters. The typical influence of the different solution and processing parameters on fibre structure and porosity of the electrospun membranes was further reiterated by our study results with a commercial PU. More importantly, the solvent compositions, solution concentrations, flow rates, applied voltages, and distances to collector were identified for preparing electrospun PU membranes having desired fibre diameters. Here three membranes having statistically different average fibre diameters of 347, 738 and 1102 nm were chosen to study their effects on chemistry, morphology, porosity, solute diffusion, mechanical and hydrophilicity properties.

Analysis using FTIR spectroscopy revealed that the electrospinning process involving huge applied voltages did not affect the chemical structure of PU. A slight shift in the C–O–C stretching on the polymer backbone was suggestive of the change from non-porous to fibrous membrane structure. In addition, FTIR spectra of electrospun membranes also confirmed the removal of any residual solvents following the drying cycles in vacuum desiccator.

The duration of electrospinning had a near-linear increase in thickness of the electrospun membranes. Fusion of fibres in neighbouring stacking layers due to incomplete evaporation of solvents when the fibres are deposited on the collector could be the cause

for reduced linearity in the thickness of electrospun membranes as a function of electrospinning time, but enhance the mechanical properties of the membranes..

The three electrospun membrane configurations, 8PU, 10PU and 12PU having fibre diameters of about 347, 738 and 1102 nm respectively had radii for majority of their pores at about 800 (68%), 870 (36%) and 1060 (29%) nm respectively as determined using bubble point measurements. The reducing percentage of the majority of pores having uniform size is indicative of wider pore size distributions with increasing fibre diameters. As expected, gravimetry method revealed a decreasing fibre packing density and increasing pore volume as a function of fibre diameters. The pore volumes were about 44%, 63% and 68% respectively for 8PU, 10PU and 12PU, which with the added advantage of extensively interconnected pores is anticipated to contribute to high solute/solvent transport flux across their cross-section when used as membranes compared to conventional porous membranes that usually have up to 34% pore having lesser pore interconnectivity.

Diffusion tests using rotating biodialysers confirmed the high flux rates associated with electrospun membranes with extensive pore interconnectivity. Moreover, slight variations in membrane thicknesses and porosities did not significantly affect the rate of transport of glucose across the electrospun PU membranes. Our studies showed that ultra-thin membranes of tailored thicknesses can be by varying the electrospinning time, while causing minimal loss in solute transport flux across the membranes.

Uniaxial tensile tests showed that the electrospun PU membranes had a linear hyperelasticity and tensile strengths higher than soft tissues, making them suitable candidates for implantable biomedical device applications.

The surface wetting analysis using contact angle measurements demonstrated an increase in hydrophobicity as a function of increasing fibre diameters and porosity for electrospun PU membranes indicating that the hydrophilicity-hydrophobicity balance for a particular polymer can be adjusts for biocompatible surfaces using electrospinning technology.

In conclusion, electrospinning parameters were optimized and certain combinations of parameters for obtaining tailored fibre diameters, porosity and thickness were identified for electrospinning the commercial Selectophore™ PU. The resulting ultra-thin fibro-porous membranes support high solute transport flux and have mechanical properties better than soft tissues. Hence, these membranes are anticipated to find applications as membranes for sensors requiring analyte exchange, while having minimal (insignificant) effects on sensor function, especially for implantable applications.

Chapter 4 Electrospun Polyurethane Membranes on Miniature Biosensors

4.1. Introduction

Polymeric coatings are commonly used as mechanical and chemical buffer zones at the sensor-tissue interface and are intended to prevent biofouling, fibrous encapsulation and blood vessel regression on the immediate surface of the implant. However, it must be emphasised that any additional biocompatibility coatings on sensor surface would adversely affect their sensitivity, even before they can be implanted in the body. Hence, the design of such coatings should not only address the deleterious host tissue effects on sensor's *in vivo* function, but also have minimal effect on its sensitivity. The hypothesis for this study was that electrospun polymer membranes, due to their unique fibro-porous structure with interconnected pores and high porosity (40 to 70%) would have minimal effect on sensor's *ex vivo* sensitivity.

This chapter addresses the electrospinning of membranes directly on the miniature sensor surfaces and their effects on sensor function, *ex vivo*. Finite element analysis simulations were used to identify the right distance from the spinneret to the sensing element tip. Thereafter, static and dynamic collection systems were integrated to the basic electrospinning setup (Figure 2.2) described in Chapter 2, to electrospin PU fibres directly on coil-type amperometric glucose biosensors. Light microscopy and SEM were used to visualize the morphology of the electrospun membranes on sensors. The three membrane configurations, namely 8PU, 10PU, and 12 PU shortlisted in Chapter 3, were applied on coil-type amperometric glucose biosensors to study their efficacy as additional biocompatibility or mass-transport limiting membranes on sensor function.

4.2. Glucose biosensor

The sensor is amperometric, enzymatic, and has a coil-type design standardized by Moussy's group (Yu et al., 2005a). It is a two electrode system based on Pt-Ir coil working and Ag/AgCl coil reference electrodes (Fig 2.1). The coil design was intended for loading excess enzyme to meet the demand for implantable application. Further, it uses an epoxy-polyurethane (EPU) membrane as the mass-transport limiting membrane, the crosslinking density and thickness of which can be varied to tune the sensitivity of the enzymatic sensor. For this study, the glucose sensors with (Pt-GOD-EPU) and without (Pt-GOD) EPU membrane were coated with electrospun PU membranes to test their ability to function as mass-transport limiting membranes and their effect on sensitivity.

4.2. Electrospinning setup

Electrospinning has been extensively used to generate polymer fibres having large surface to volume ratios, excellent physical and chemical properties and fibro-porous structure mimicking the natural extracelluar matrix (ECM) to suit a variety of applications including biosensing and tissue engineering (Wang *et al.*, 2009b, Ren *et al.*, 2006, Manesh *et al.*, 2008, Shults *et al.*, 2010). However, in most of these studies, electrospun fibres were collected as two dimensional membranes on flat electrodes. In the present study, the main challenge was assembling fibres on miniature 3D ellipsoid shaped sensing element. Moreover, the resulting electrospun coatings should have uniform thickness, completely cover and fit snugly on the sensor surface, while having random fibre orientation (for mechanical integrity) and uniform pore size distribution (for uniform permeability to analyte).

The assembly of electrospun fibres in the form of macroscopic 3D tubular structures is commonly done by using a rotating collector (Stitzel *et al.*, 2006, Matsuda *et al.*, 2005). Furthermore, the alignment of fibres can be controlled by varying the rotation speed of the collecting mandrel and thus tailor the material properties of engineered membrane/matrix (Matthews *et al.*, 2002, Kim *et al.*, 2004). Nevertheless, this method has limitations, especially in the fabrication of tiny tubes of less than 0.3 mm diameter having one end closed, and tubes with multiple interconnected tubes (Teo and Ramakrishna, 2006). Zhang et al utilized novel static methods in the electrospinning setup to overcome these limitations. They used multiple collecting elements (assistant collectors together with working collectors) to alter the electric field to generate the desired tubular electrospun structures (Zhang and Chang, 2007). To identify the optimum collecting system for spinning polymer fibres directly on miniature sensors, in this study, two collecting systems were designed as illustrated in Figure 2.4. In either case, the sensor was grounded and when used the grounded flat plate was the auxiliary collecting electrode.

4.3. Static collector system optimization for electrospinning fibres directly on miniature sensing element

The spatial pattern and magnitude of the electric field generated between the spinneret and collector has significant influence on the 3D architecture of the electrospun structures, especially when static collecting systems are used. Hence, in this study, FEA simulations were first done using Maxwell ® SV 2D software (Ansoft Corporation) to identify the electrostatic field distribution (magnitude of electric field, vectors of electric field, and contours of constant voltage) around a vertically aligned collecting sensor.

4.4.1. Finite Element Analysis (FEA) Simulation of electric field distribution around static collector systems

The FEA simulations were tested using two different collecting system configurations. In addition, two distances between the spinneret tip and the tip of the collecting sensor were also used for the simulations. The limitation for the simulations was that they were 2D. However, the 2D simulation can be considered as a planar slice through the three dimensional apparatus, so as to identify the optimum collector position and distance from the spinneret. The y-z plane that passes through the axis of the spinneret needle and the collector was chosen to model the electric field distribution. Three simulations were done using two types of collector systems. First collector system consisted of the sensor and its holding needle (23G) and only the sensor is grounded, while having the distance between the tip of the spinneret and the collecting sensor tip at 22 cm (static collector configuration (SCC) - 1). In the second collector system, the sensor and its holding needle were integrated vertically in the centre of a stainless steel plate. The plate and the sensor were grounded, wherein the plate was functioning as an auxiliary electrode. The distance between the spinneret tip and the tip of the sensing element was varied to identify its effects on the strength of generated electric field. The sensor tip to the spinneret was either 16 cm (SCC-2) or 22 cm (SCC-3). After model definition, materials have been filled in each element. The background was fixed by air. An applied voltage of 21 KV set on spinneret was used for all three simulations (SCC-1, SCC-2 and SCC-3) while 0 KV was assigned on all grounded collectors. A balloon boundary was assigned to the background since our electrospinning system can be estimated as a electrically insulated system with all objects being far away from all other sources in all directions. After solving the problem, calculation of the capacitance can be achieved through defining a capacitance matrix using Setup Executive Parameters command. The grounded collector components were assigned as ground whereas the other objects were assigned as signal lines. The finite element mesh was automatically generated by changing percent refinement per pass to 45. After modify solution criteria, the problem was solved and the respective results are presented in Figures 4.1, 4.2 and 4.3. The decrease of energy error after each adaptive pass was found in each above problem indicating the simulator converges on an accurate solution and all problems were well defined.

Surface plots were used to show the spatial distribution and magnitude, while electric field vector plots for direction and magnitude of the magnetic field around and between the electrodes. The field strength is illustrated with a gradient of 25 colours from

blue (minimum) to red (maximum). In addition to colour coding, the increasing vector arrow thickness and length also indicates increasing electric field strength.

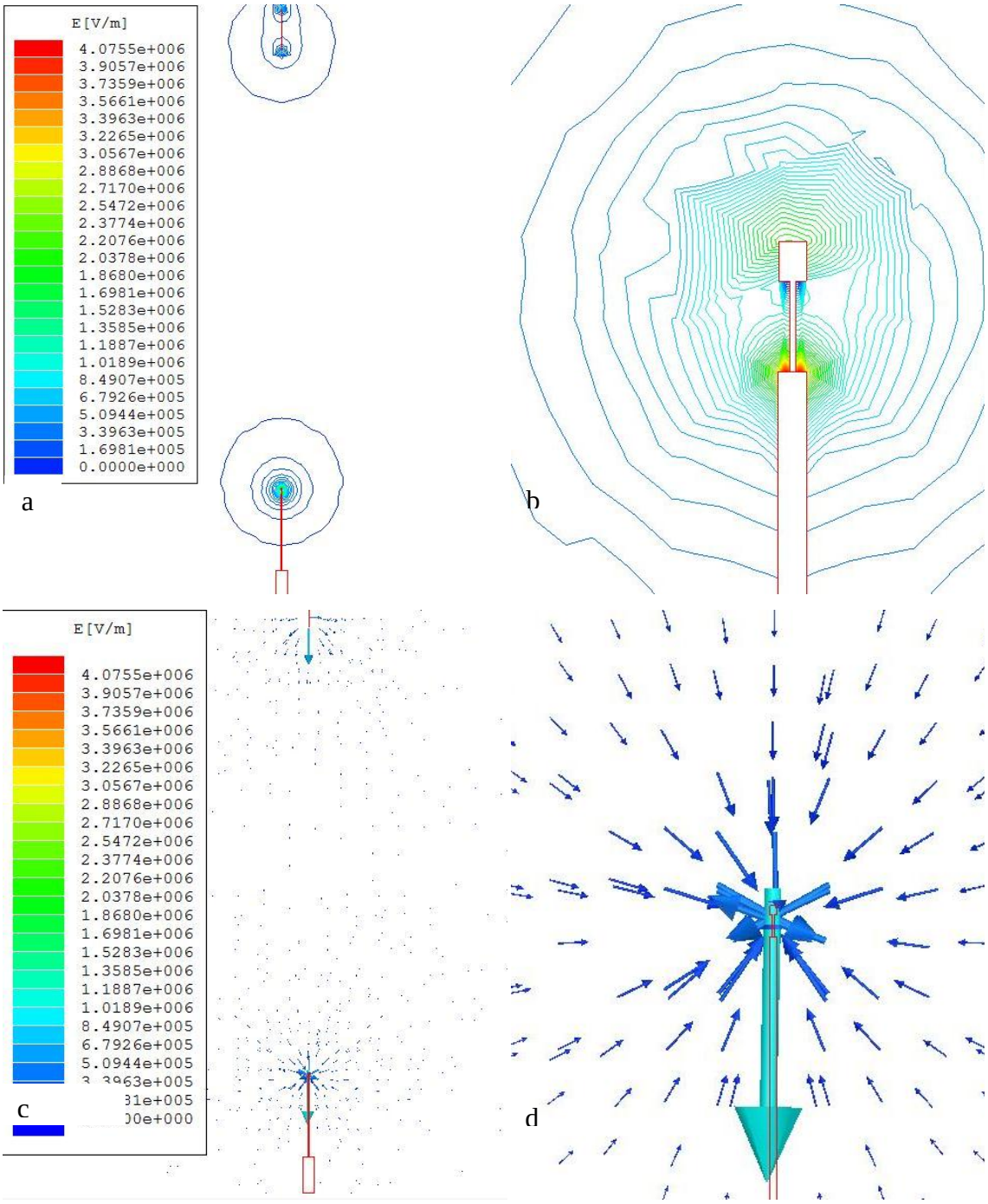

Figure 4.1 FEA simulation result showing electric field distribution between the spinneret and SCC-1. The legend in a and c shows the electric field strength represented by an increasing gradient of 25 colours from blue to red, illustrating the field strength (surface plots in a, b) and direction (electric field vector plots in c, b) between spinneret and collector system (a, c) and around the sensor's sensing element (b). The length and thickness of the electric field vector arrows indicate the field strength.

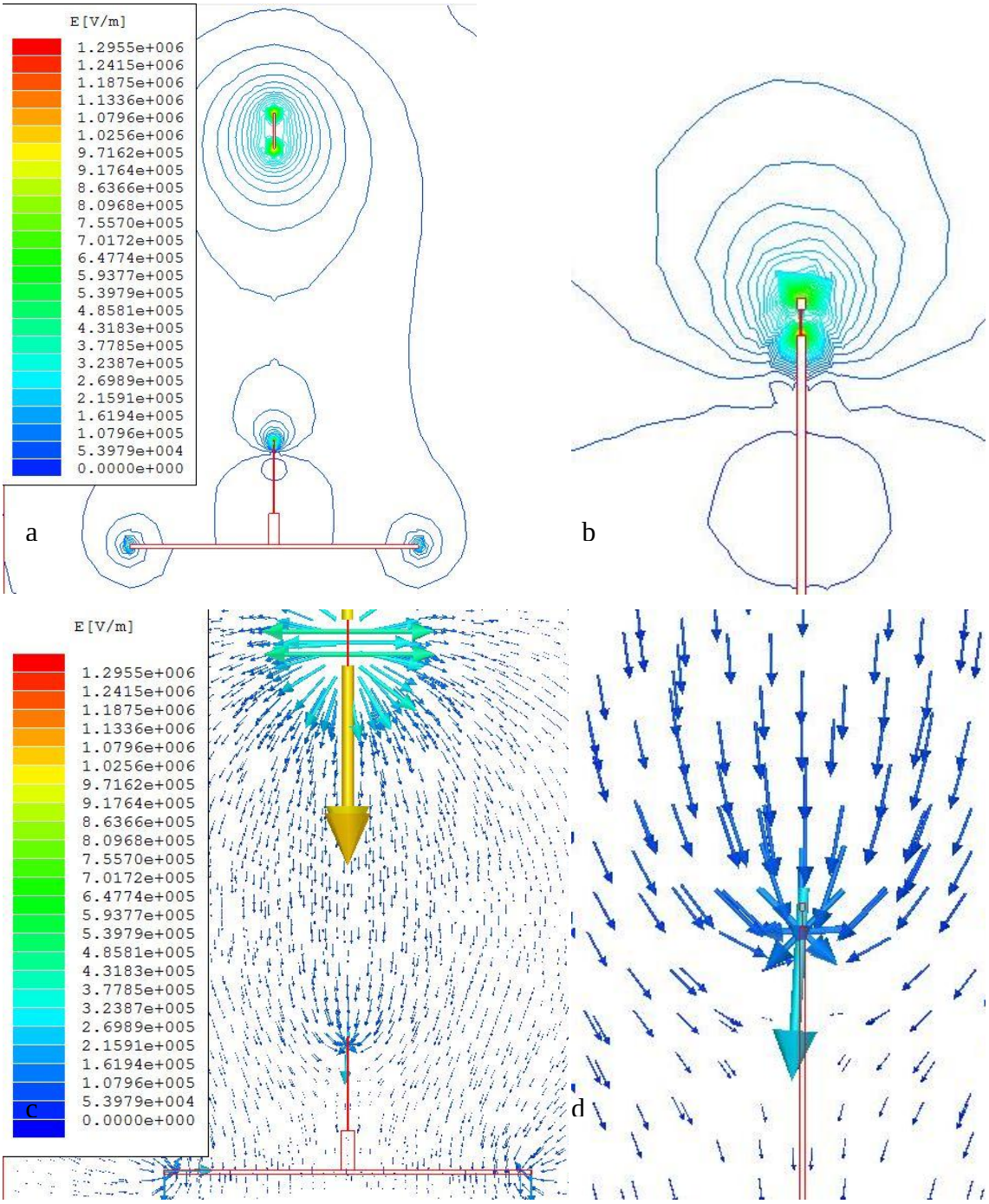

Figure 4.2 FEA simulation result showing electric field distribution between the spinneret and SCC-2. The legend in a and c shows the electric field strength represented by an increasing gradient of 25 colours from blue to red, illustrating the field strength (surface plots in a, b) and direction (electric field vector plots in c, b) between spinneret and collector system (a, c) and around the sensor's sensing element (b, d). The length and thickness of the electric field vector arrows indicate the field strength.

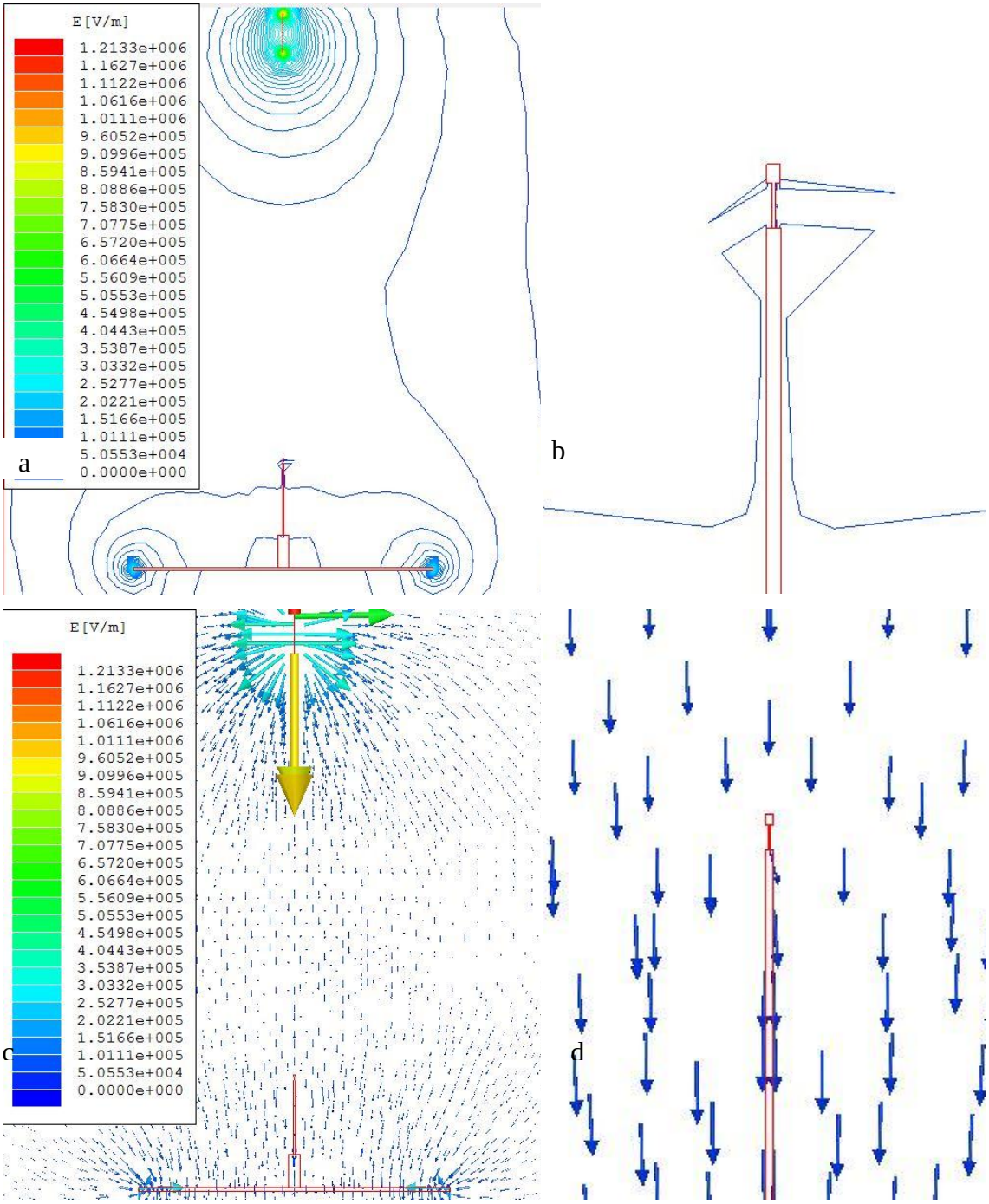

Figure 4.3 FEA simulation result showing electric field distribution between the spinneret and SCC-3. The legend in a and c shows the electric field strength represented by an increasing gradient of 25 colours from blue to red, illustrating the field strength (surface plots in a, b) and direction (electric field vector plots in c, b) between spinneret and collector system (a, c) and around the sensor's sensing element (b, d). The length and thickness of the electric field vector arrows indicate the field strength.

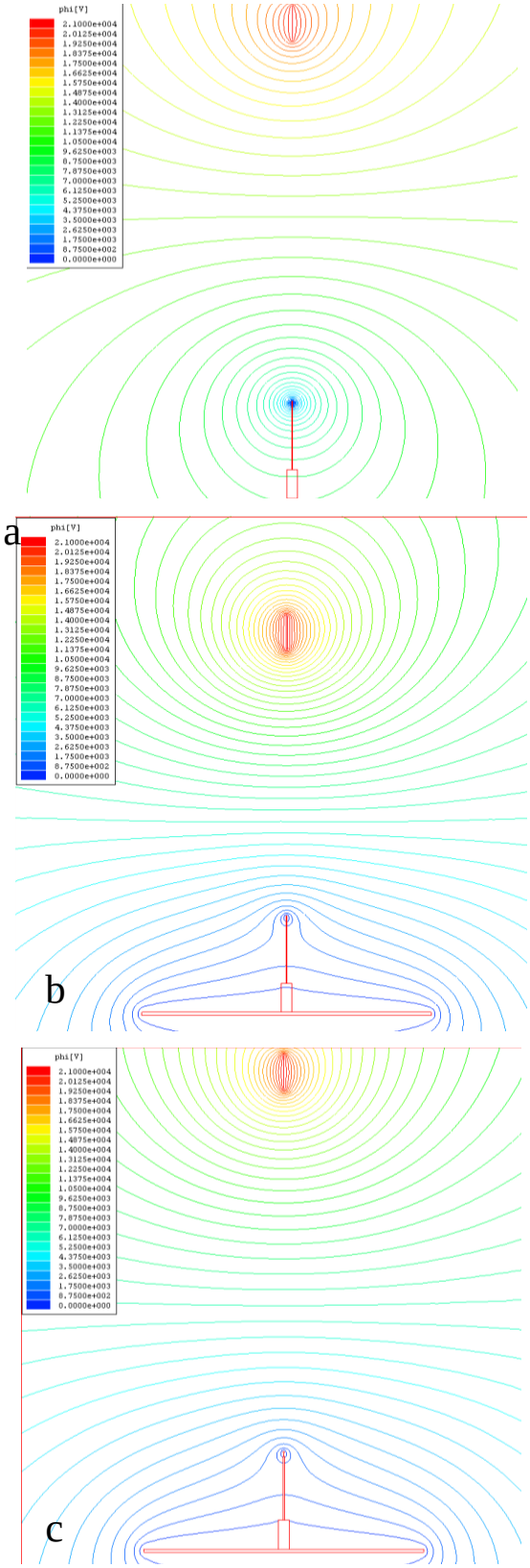

Figure 4.4 FEA simulation results showing the spatial distribution of electric potential between the spinneret and collectors systems, a) SCC-1, b) SCC-2 and c) SCC-3. The legend indicates an increasing gradient of colours corresponding to an increasing electric potential (from 0 to 21kv).

In the SCC-1, where the sensor alone was used as the grounded collector (Figure 4.1 a-d), the electric field strength around the sensor tip was higher than that observed for SCC-2 or SCC-3. Thus, if the ejected jet with electrons on its surface flies to the grounded collector along the electric line of strength, an electrospun coating with a large diameter may be produced (Kong *et al.*, 2007). For the same reason, SCC-2 and SCC-3 design may decrease the diameter of deposited fibres. The distribution of local electric field lines for SCC-1 was symmetric. The electric field lines start diverging at the tip of the spinneret needle and then all the vectors turn perpendicular to the collector (Figure 4.1c).

As the electric field reaches the collector, the vectors converge to the sensor tip. Where the electric field vectors are perpendicular to the collector, the polymer jet is expected to move in a vortex-like loop. But as it approaches the sensor tip, the converging field would stretch the polymer jet. At the tip of sensor, the electric field vector plot (Figure 4.1d) illustrates an extremely high electric field, which could be due to the sharp edge effect. Since the charge density is highest at convex regions of greatest curvature, fibres would preferably deposit on the sensor tip and not cover the entire sensing element. Moreover, the electric field distribution on the lateral sides of sensing element was not uniform which is thought to be the result of the strong influence from the electric field originating at tip of the holding needle, causing huge instability of approaching jet to prevent an even deposition of fibres. Thus, to avoid the focus of electric field on one point on the collector (causing reflection), a grounded flat plate auxiliary electrode was added to the collector system for further FEA simulations (SCC-2 and SCC-3).

A shorter distance (16 cm) between the spinneret needle and the sensing element tip coupled with a flat plate auxiliary electrode (22 cm from the spinneret tip), in the SCC-2 (Figure 4.2 a-d), induced an intense and spread-out electric field compared to SCC-1 and SCC-3. Again, the spatial distribution of the electric field at the collector was not uniform with the maximum intensity of electric field observed on the tip of sensor, indicating a strong influence of electric field around the spinneret (Figure 4.2 a & b). The electric field typically diverges from spinneret needle and eventually converges on to the collector system. The use of the flat plate coupled with the shorter distance between electrodes apparently caused wider spreading of the electric field, allowing deposition of fibres over a larger surface area on the collector system. In the SCC-2, the relatively high intensity of electric field was also observed at the tip of its holding needle (Figure 4.2b) indicating a shift in focus of the electric field away from the sensing element. However, at the tip of the holding needle opposing electric field vectors of different but relatively high intensity emerge perpendicular to the needle axis, potentially preventing the fibres from depositing

on the lateral surface of the sensing element (Figure 4.2d). As a result, the fibre deposition was expected to spread out from the tip of the sensing element to the flat plate below to form a 3D umbrella shaped membrane.

When the spacing between the spinneret tip and collecting sensor tip was increased to 22 cm, in the SCC-3 (Figure 4.3 a-d), the intensity of the electric field reduced. A symmetric and uniform electric field resulted around the sensing element, having the electric field vectors pointing perpendicularly to the surface of the assistant electrode, stainless steel plate, below the sensing element (Figure 4.3d). Also, the intensity of the electric field vector originating along the spinneret axis decreased, suggesting a lesser opposing influence from the electric field around the collector. Apparently, the direction of electric field at the sensing element was preferentially along the axis away from the spinneret. This was anticipated to ensure the complete covering of the ellipsoid sensing element with rounded and closed tip.

The spatial distribution of potential between the electrodes (spinneret and collector system), illustrated by the surface plots for SCC-1, SCC-2 and SCC-3 respectively in Figure 4.4a-c, wherein each line represents a fixed potential (referred to as equipotential lines), further reiterates the observations for electric field strength and direction shown in Figures 4.1 to 4.3. The focus of electrical potential gradually shifted from a single point on the sensing element in SCC-1 to the flat-plate auxiliary electrode in SCC-3 (Figure 4.4a-c), allowing a symmetric, uniform and well spread out electric potential and strength for SCC-3. As additional advantage for such uniform spatial distribution of electric potential, as suggested by Yang *et al.*, was that it aids in the formation of fibres with small diameters (Yang *et al.*, 2008). Thus, the simulations helped the identification of an optimum spinneret to sensing element tip distance of 22cm, while using a flat plate as the auxiliary collector on which sensor – the main collector, was mounted perpendicularly. This was anticipated to aid in the complete coating of the sensing element with electrospun membranes.

4.4.2. Morphology of coatings electrospun on sensor surface using static collector

Figure 4.5 shows the morphology of electrospun coatings on the sensing element of biosensor as a function of electrospinning time. The fibres were spun using 8% PU solution, electrospinning times of 5, 10 and 30 min, static collecting system (SCC-3, where the sensor was mounted perpendicularly on a flat plate using holding needle, the sensor and plate were grounded), the distance between the spinneret tip and sensing element tip was 22 cm and the applied voltage was 21kV. The coating covered the entire surface of the

sensing element and half of its holding stainless steel needle from where a uniform fibrous membrane spread out forming an umbrella-like structure having an air gap between the flat plate and the holding needle.

Although completely covering the sensing element, as required, the coating thickness was not uniform (Figure 4.5). The coating had ridges and groves with interspersed rounded spikes, which structure could be indicative of the 3D electric field distribution around the collecting sensing element. Zhang et al reported that during the electrospinning process, fibres are driven by electrostatic forces to move towards the earthed substrate. But, as the fibres reach the collector surface, their deposition pattern would be determined by Coulomb interactions (Zhang and Chang, 2007). In addition, following deposition, any residual charge on the deposited fibres would also influence further deposition patterns for the fibres (Deitzel *et al.*, 2001a). The formation of ridges and grooves could be attributed to the distortion in electric field around the sensing element due to the square shape of the flat plate auxiliary electrode. On the other hand, the formation of rounded spikes could be due to the 3D shape and static nature of the sensing element. As the fibre touches the static 3D collector, the accelerating fibre, under the influence of gravity could form a loop such that the entire length of the fibre is not in contact with the sensor surface. This looping could be responsible for the formation of the rounded spikes with enclosed air pockets as shown in Figure 4.6.

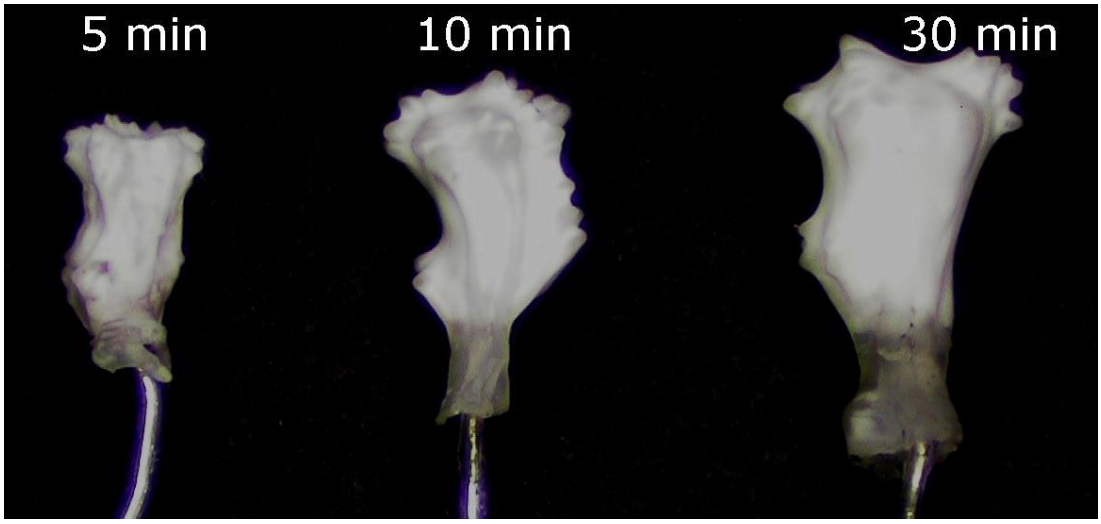

Figure 4.5 Optical microscopic images showing the morphology of coatings on the sensing element of the biosensor. The coatings were 8PU spun for 5, 10 and 30 min using the static collector configuration 3 (SCC-3).

The thickness and volume of the coating increased significantly with increasing electrospinning time (Figure 4.5). Further, the examination of the cross-section of the

coating revealed a solid coating snugly fitting on the sensors (Figure 4.6a), but with some air pockets primarily under the rounded spike structures (Figure 4.6b).

4.5. Dynamic collector and spinning uniform fibrous coating on miniature sensing element

To overcome the effects of electric field on the fibre deposition patterns on the immediate surface of the collecting sensing element, the static collector system was replaced by a rotating mandrel holding the sensing element parallel to the flat plate auxiliary electrode as illustrated in Figure 4.7a&b. The motor of the rotating mandrel was en-capsulated within a wooden casing (Figure 4.7b) to reduce its influence on the applied electric field. Irrespective of the electric field distribution, the rotation of the grounded sensor resulted in uniform electrospun coatings on the sensor (Figure 4.8& 4.9), for the tested spinneret tip to sensor tip distance of 22 cm.

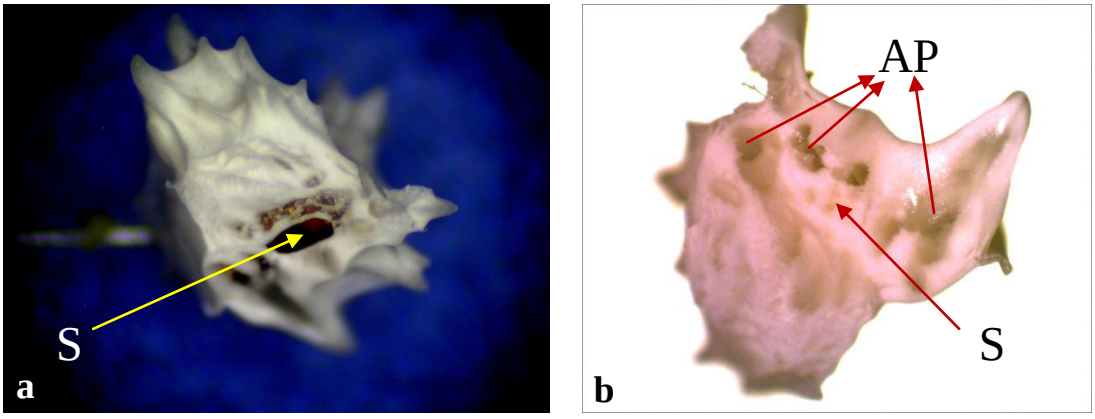

Figure 4.6 Optical microscopic images showing the cross-section of coating on a sensing element of coil-type biosensor electrospun with 8PU for 10 min using the static collector configuration 3 (SCC-3). S – Sensing element, AP – Air Pockets.

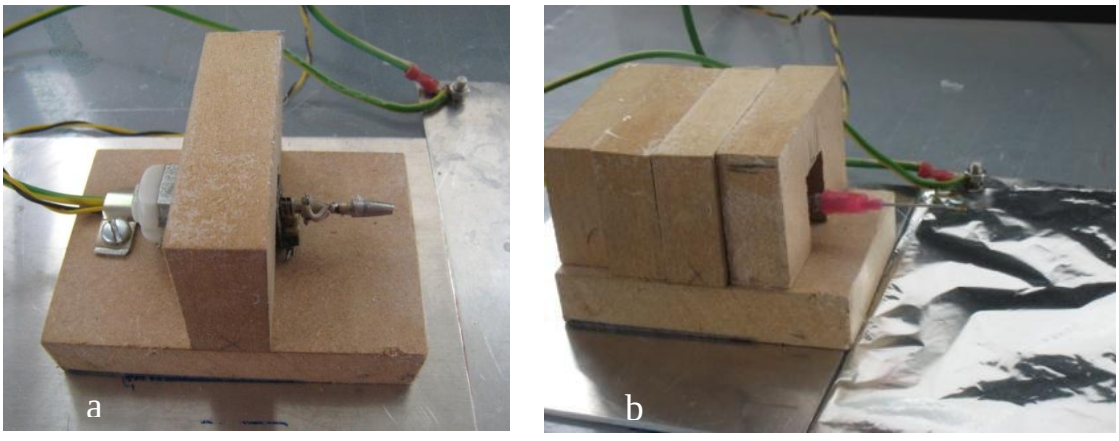

Figure 4.7 The rotating mandrel (a) for the dynamic collector system enclosed in a wooden casing (b) to reduce electromagnetic effect of the motor on electrospinning.

4.5.1. Morphology of coatings on sensor surface electrospun with dynamic collector

The morphology of the fibrous coating electrospun using a dynamic collector is shown in Figure 4.8 & 4.9. The contour of the sensing element is clear even after coating with electrospun membrane (Figure 4.8) indicating a coating of uniform thickness. The coating was also uniform at the convex tip of the sensing element (Figure 4.9a), which could be due to the choice of rotating speed of the mandrel. The examination of cross-section of the membranes, as shown in Figure 4.9b, revealed uniform and interconnected porosity in the membrane. A rotation speed of 660-690 rpm was chosen to ensure random orientation of the fibres on the collector (Figure 4.9c).

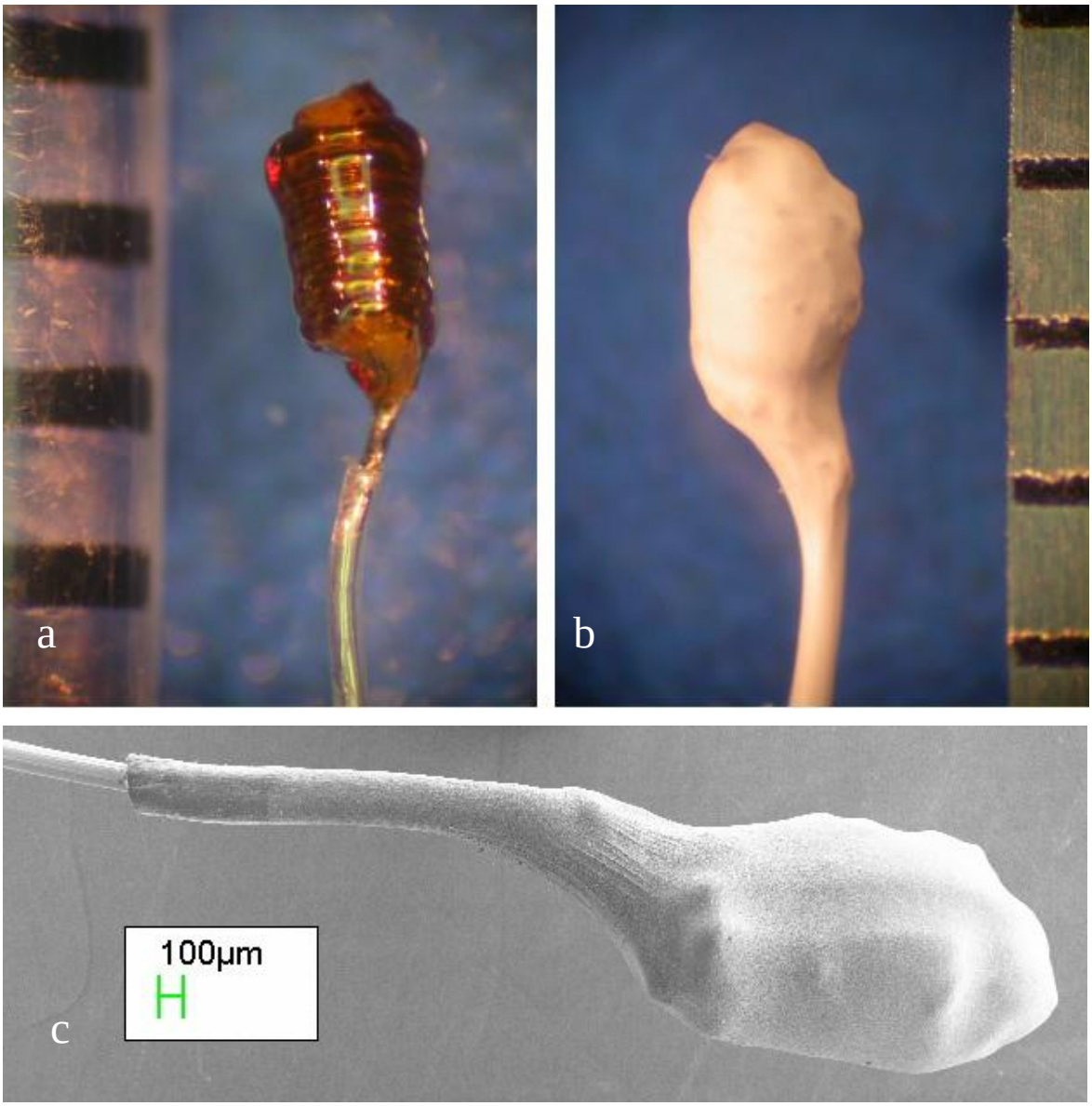

Figure 4.8 Optical microscope (a & b) and SEM (c) images showing the morphology of a coil-type biosensor without (a) and with (b & c) electrospun 8PU membrane coating spun using a dynamic collector.

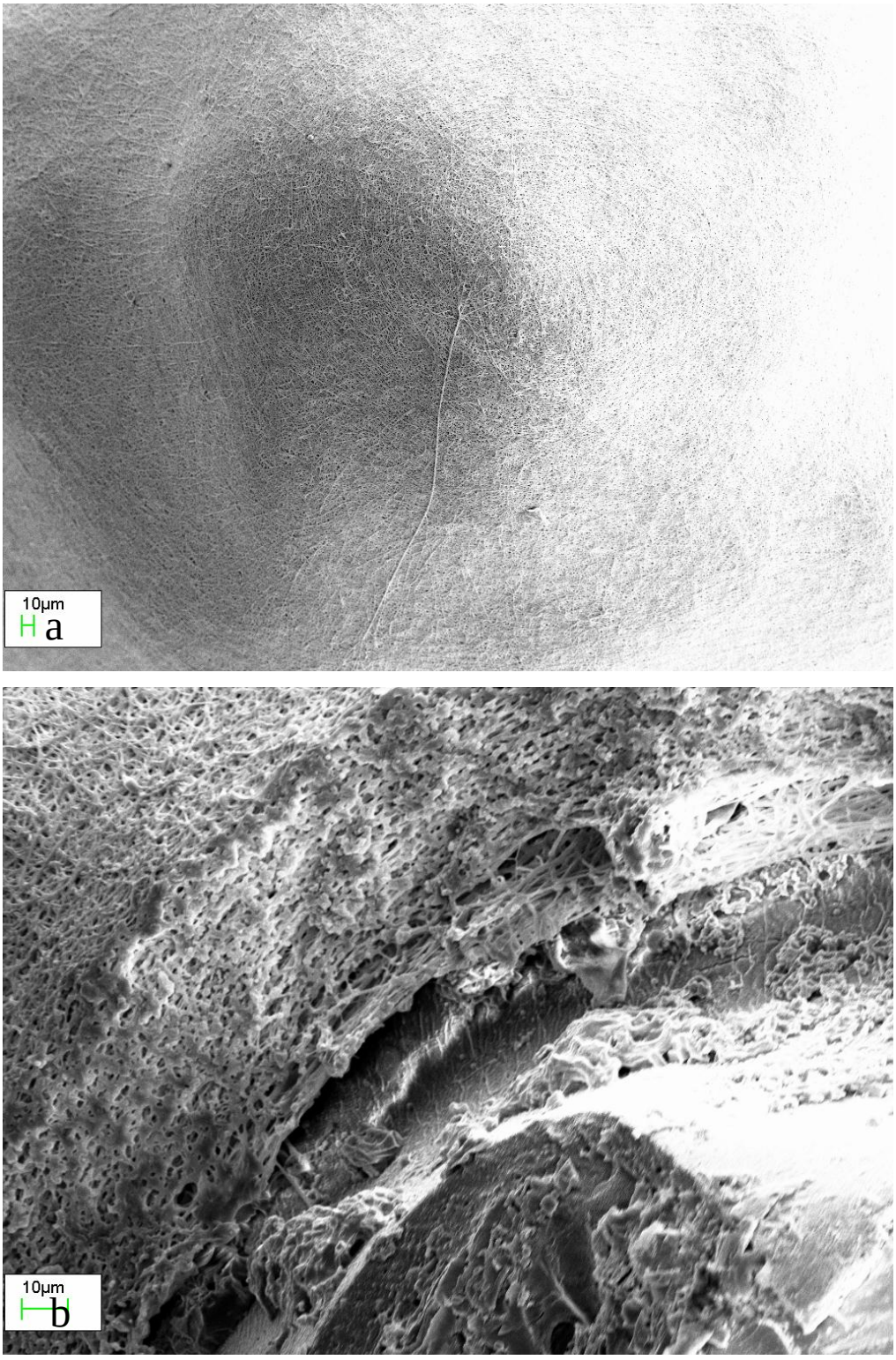

Figure 4.9 SEM images showing the morphology of 8PU membrane spun using dynamic collector on coil-type implantable glucose biosensor: a) uniform covering of the convex tip of sensor, b) cross-section of 8PU membrane on sensor and c) surface morphology showing random orientation of electrospun fibres.

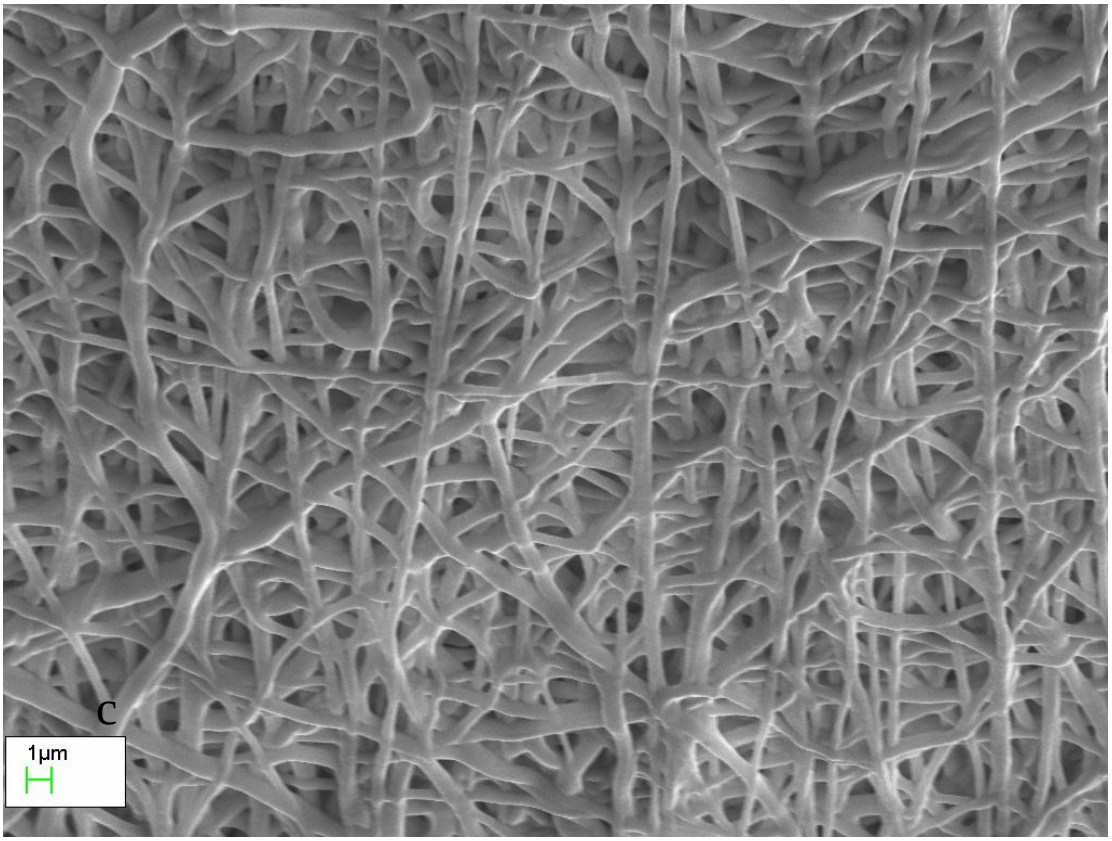

Figure 4.9 (*Continued*)

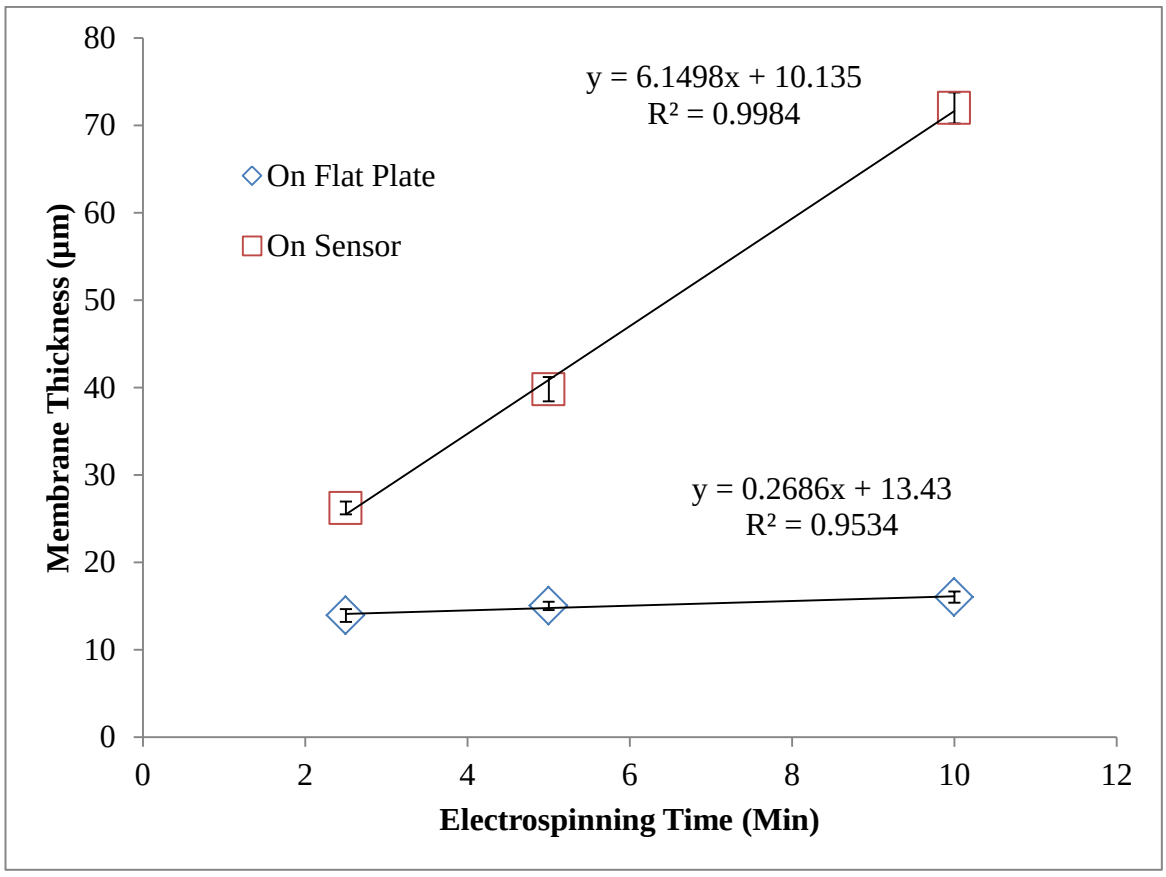

Figure 4.10 Thickness of 8PU membranes electrospun on flat plate (static collector) or directly on sensor surface (dynamic collector) as a function of electrospinning time.

The seamless fibre being generated by the electrospinning, due to the medium rotation speed, resulting in random fibre orientation was also reported earlier (Teo and Ramakrishna, 2006). The diameter of fibres of 8PU membrane electrospun directly on sensors (Figure 4.9c) varied between 260 - 690nm (mean ± SD: 484 ± 108.9nm), which was not statistically different from those collected directly on a static flat plate (200 – 560nm; mean ± SD: 342.6 ± 91.0 nm). Thus, the objective of snugly fit and uniform coating on the entire surface of the ellipsoid sensing element, having uniform and interconnected porosity, was achieved.

4.6. Efficacy of electrospun membranes as coatings for implantable coil-type glucose biosensors

To study the effects of electrospun coatings on sensor function, the sensor configurations: Pt-GOD or Pt-GOD-EPU were first tested for *ex vivo* function, and then coated with the test electrospun membrane(s), followed by repeated *ex vivo* function testing. Results of *ex vivo* function before and after coating with electrospun membranes for each sensor were compared and reported.

4.6.1. Calculation of sensitivity and linearity for a typical glucose sensor

The effect of electrospun membrane on sensor *ex vivo* function was studied in terms of sensor sensitivity and linearity. Sensor calibrations were performed by measuring the current while stepwise changing the glucose concentration from 0–30 mM. The trend of current was automatically plotted as a function of time by software APPLO 4000 as shown in Figure 4.11a. The sensitivity (S) of each sensor was defined by equation 2.5. The linearity of signal concentration dependence (R^2) was determined based on the plot of data points taken from the curve of current (Figure 4.11a) every 300 sec after each concentration jump as illustrated in Figure 4.11b.

4.6.2. Effects of electrospun coatings using static collector on *ex vivo* sensor function

Pt-GOD-EPU sensors coated with 8PU membranes using static collector (SCC-3) were tested for *ex vivo* sensitivity and linear detection range. The electrospinning times of 5, 10 and 30 min was varied and a significant increase in coating volume was observed. Relative change in sensitivity and linearity over the range of 2 to 30 mM for sensors with electrospun coatings from that before coating is expressed as % change and plotted in Figure 4.12.

Huge variation in sensitivity, as illustrated by the standard error of mean (Figure 4.12), was observed between the sensors for each electrospinning time. Between the

electrospinning times, statistically different decrease in sensitivity was only observed between 5 and 30 min electrospinning times. Irrespective of the electrospinning time or the 3D structure of the coating, the linearity for the working range of 2 to 30 mM glucose solution concentration was not affected (Figure 4.12). The uneven structure and very thick fibrous coating obtained using static collecting system is probably the primary factor that affects sensor sensitivity.

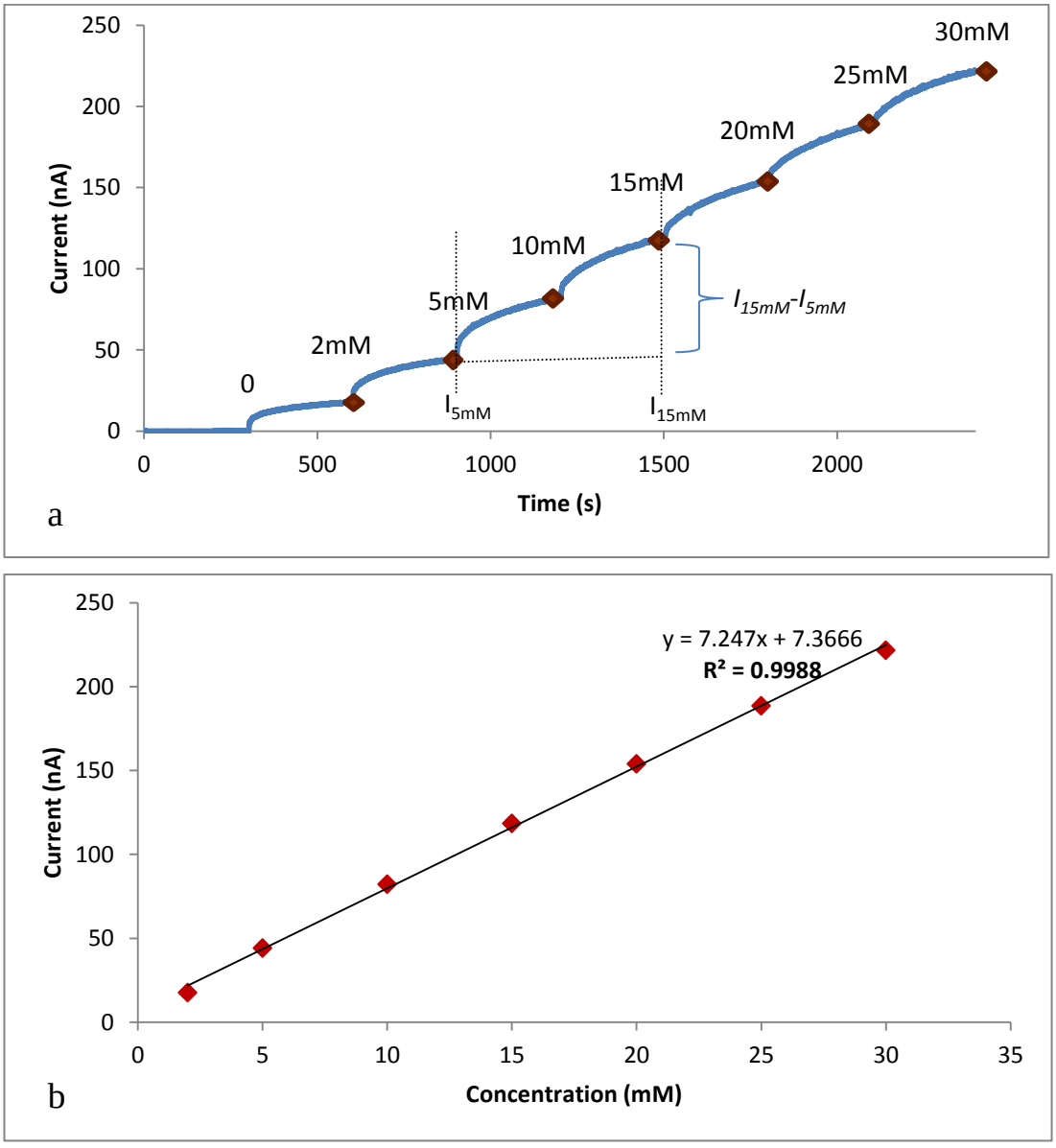

Figure 4.11 The plot of current as a function of time (a) and concentration (b) respectively for a typical glucose biosensor.

4.6.3. Effects of electrospun coatings using dynamic collector on *ex vivo* sensor function

From literature it is clear that increasing thickness of coatings, typically, decrease the sensitivity of sensors (Yu *et al.*, 2008a). However, due to the uneven nature of the coating obtained using the static collection system it would be difficult to ascertain a

quantitative relationship between thickness and sensitivity. Hence in the choice of electrospinning times for thickness effects using dynamic collector, time points around 5 min (~20% decrease in sensitivity while using static collector, Figure 4.12), i.e., 2.5, 5 and 10 min were anticipated to cause minimal decrease in sensitivity. The resulting electrospun coatings had a linear increase in thickness with increasing electrospinning time (Figure 4.10).

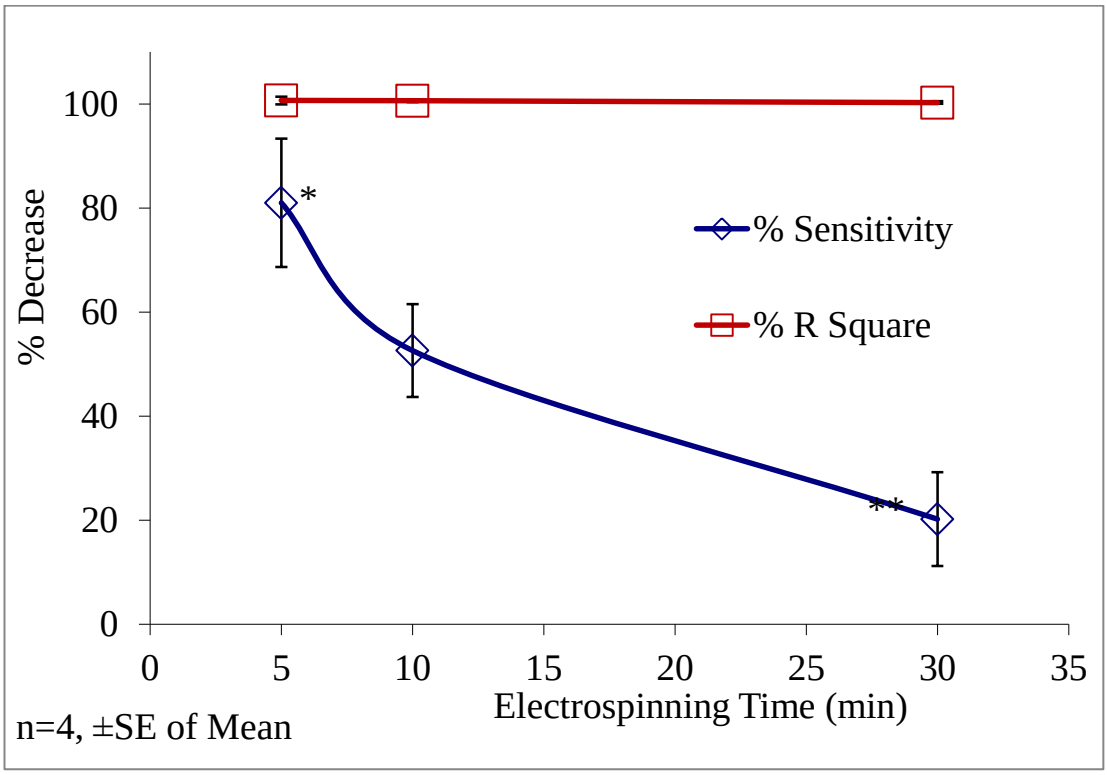

Figure 4.12 Effect of electrospun membrane on *ex vivo* function of sensor (Pt-GOD-EPU-ESC) as a function of electrospinning time expressed as % change of sensitivity and R^2 (2 to 30mM) for each sensor from that before coating (Pt-GOD-EPU). Membranes were spun with 8% PU solution (8PU), 22 cm distance between spinneret tip and sensing element tip, 21kV applied voltage and a static collector (SCC-3). $p<0.5$ between * and **

4.6.3.1. Effect of increasing thickness of electrospun membranes on sensor function

Pt-GOD-EPU sensors were first immersed in PBS pH 7.4 and incubated at 37^{o}C to ensure rapid swelling of enzyme and mass-transport limiting membranes and their function tested on 1, 3 and 7 days. Following testing on day 7 the sensors were rinsed in DI water and dried overnight in a fan assisted incubator at 37^{o}C. The sensors were then coated with electrospun membranes. For testing the effect of thickness while maintaining porosity, 8PU membranes were electrospun for 2.5, 5 and 10 mins on sensors. The respective sensors were designated as Pt-GOD-EPU-8PU-2.5', Pt-GOD-EPU-8PU-5', Pt-GOD-EPU-

8PU-10'. For each sensor configuration 6 sensors were prepared and tested. Pt-GOD-EPU sensors were used as controls (n=6) and were processed similar to the electrospun coated sensors. Following electrospinning the sensors were re-immersed in PBS pH 7.4 and incubated at 37^{o}C and tested for sensor function on 1, 3 and 7 days and thereafter weekly until six weeks (42 days) and biweekly until 12 weeks (84 days). The results for the effects of electrospun membranes on sensitivity and linearity (for the detection range of 2 to 30mM) of sensors are presented in Figure 4.14 and Figure 4.14 respectively.

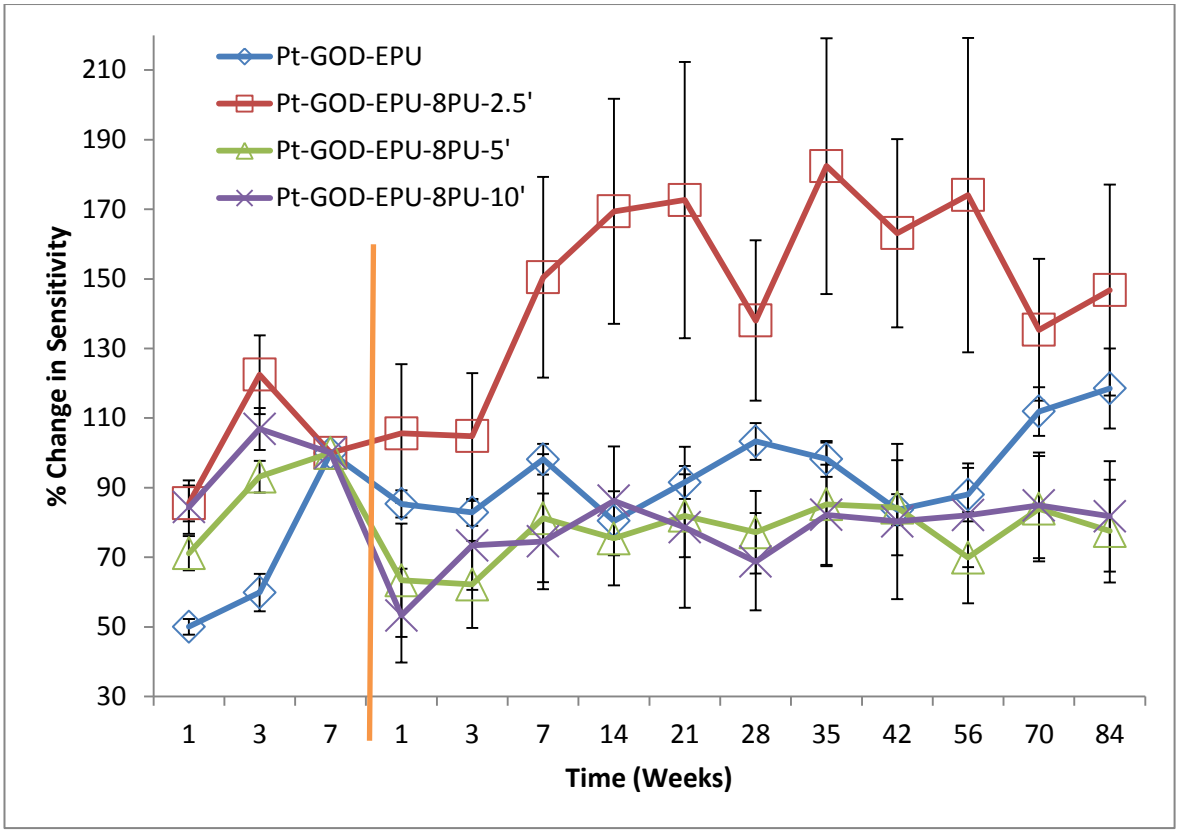

Figure 4.13: Effect of electrospun membrane on *ex vivo* function of sensor (Pt-GOD-EPU-8PU) as a function of electrospinning time expressed as % change in sensitivity for each sensor from that before coating (Pt-GOD-EPU) normalised to that on day 7 (100%) before applying electrospun coatings (data point left of the orange line).

When the sensors were immersed in PBS for the first time, there was an increase in sensitivity with time. The increase was often significant until 7 days and thereafter the sensor sensitivity plateaus off when the sensors were incubated at 37^{o}C. Moreover, sensor to sensor variation in sensitivity is also significant for within the (manufacture) batch for Pt-GOD-EPU sensors (Trzebinski *et al.*, 2011). Hence, to avoid the effects of sensor to sensor function variability, the sensitivity and linearity results for all time points were normalised to that on day 7 before coating with electrospun membranes and expressed as % change (Figure 4.14, Figure 4.15 and Figure 4.15).

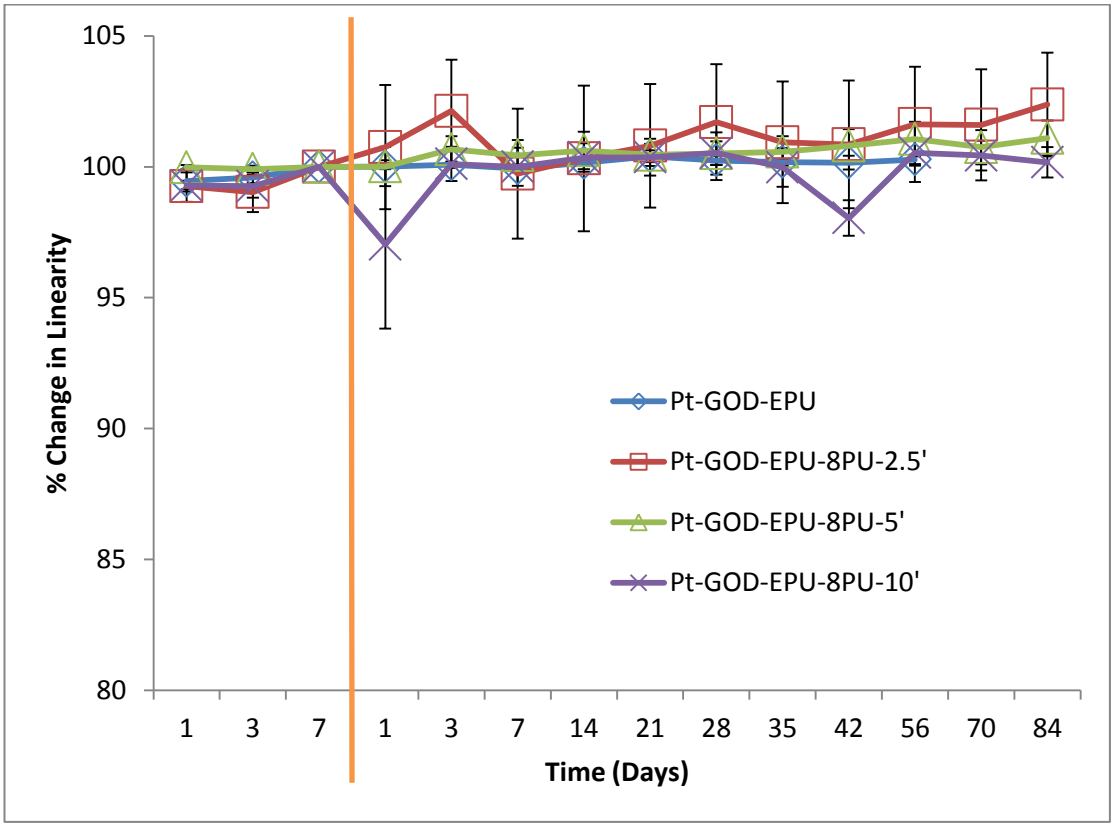

Figure 4.14: Effect of electrospun membrane on *ex vivo* function of sensor (Pt-GOD-EPU-8PU) as a function of electrospinning time expressed as % change in linearity (R^2) for each sensor from that before coating (Pt-GOD-EPU) normalised to that on day 7 (100%) before applying electrospun coatings (data point left of the orange line).

Following coating, the sensitivity of Pt-GOD-EPU-8PU-5' and Pt-GOD-EPU-8PU-10' sensors showed a slight but statistically insignificant decrease at 1 and 3 days after coating compared to the corresponding time points before coating; while that for Pt-GOD-EPU-8PU-2.5' did not show any change (Figure 4.13). By 7 days after coating, the sensitivity for all sensors appeared to reach a maximum and plateaued off thereafter until 12 weeks (84 days) of testing (Figure 4.13). The linearity for the detection range of 2 to 30 mM glucose was stable (R^2 close to 0.99) across all the time points before and after the coating for all sensors including Pt-GOD-EPU controls (Figure 4.14). When all the sensor sensitivity readings for each sensor (normalised to the 7^{th} day testing before applying electrospun coating) in the plateaued region of 7 to 84 days after applying electrospun coating were averaged, the trend for effect of coating thickness on sensor sensitivity was evident as shown in Figure 4.15.

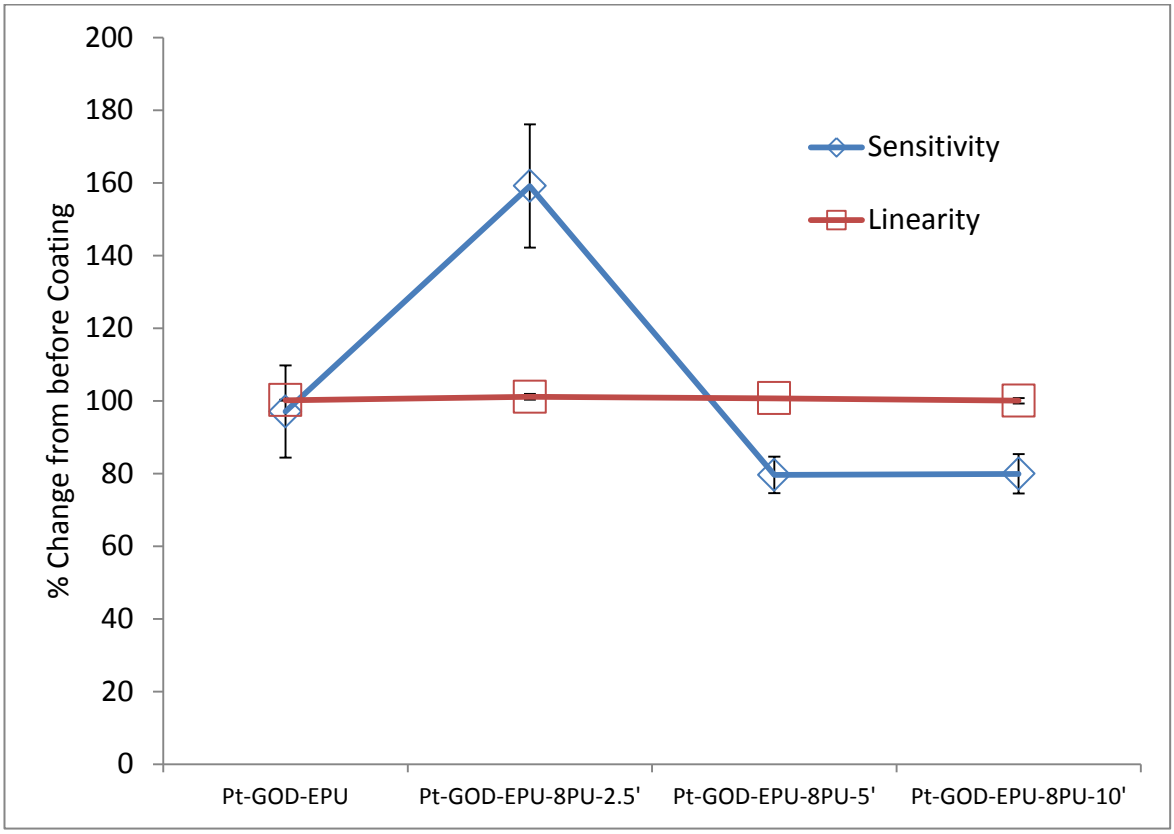

Figure 4.15: Effect of electrospun membrane on *ex vivo* function of sensor (Pt-GOD-EPU-ESC) as a function of electrospinning time expressed as % change of sensitivity and R^2 (2 to 30mM) for each sensor from that before coating (Pt-GOD-EPU). Membranes were spun with 8% PU solution (8PU), 22 cm distance between spinneret tip and sensing element tip, 21kV applied voltage and a dynamic collector.

The Pt-GOD-EPU-8PU-2.5' sensors showed significantly higher sensitivity compared to all the other sensor configurations including controls (Pt-GOD-EPU) (Figure 4.15). This was un-expected and could be due to the permeability kinetics of the thin fibro-porous 8PU membrane on the immediate surface of EPU mass-transport limiting membrane. Between, the Pt-GOD-EPU-8PU-5' and Pt-GOD-EPU-8PU-10' sensors there were no significant differences in sensitivity. However, their average sensitivity was lower, but not statistically different when compared to Pt-GOD-EPU (controls). Moreover, the change in linearity for the 2 to 30 mM glucose detection range was negligible at all times tested for all sensors. Thus, excluding the anomaly of 2.5' electrospun 8PU membrane, an increase in the tested coating thickness up to about 72µm for fibro-porous electrospun 8PU membrane did not cause a statistically significant decrease in sensor sensitivity.

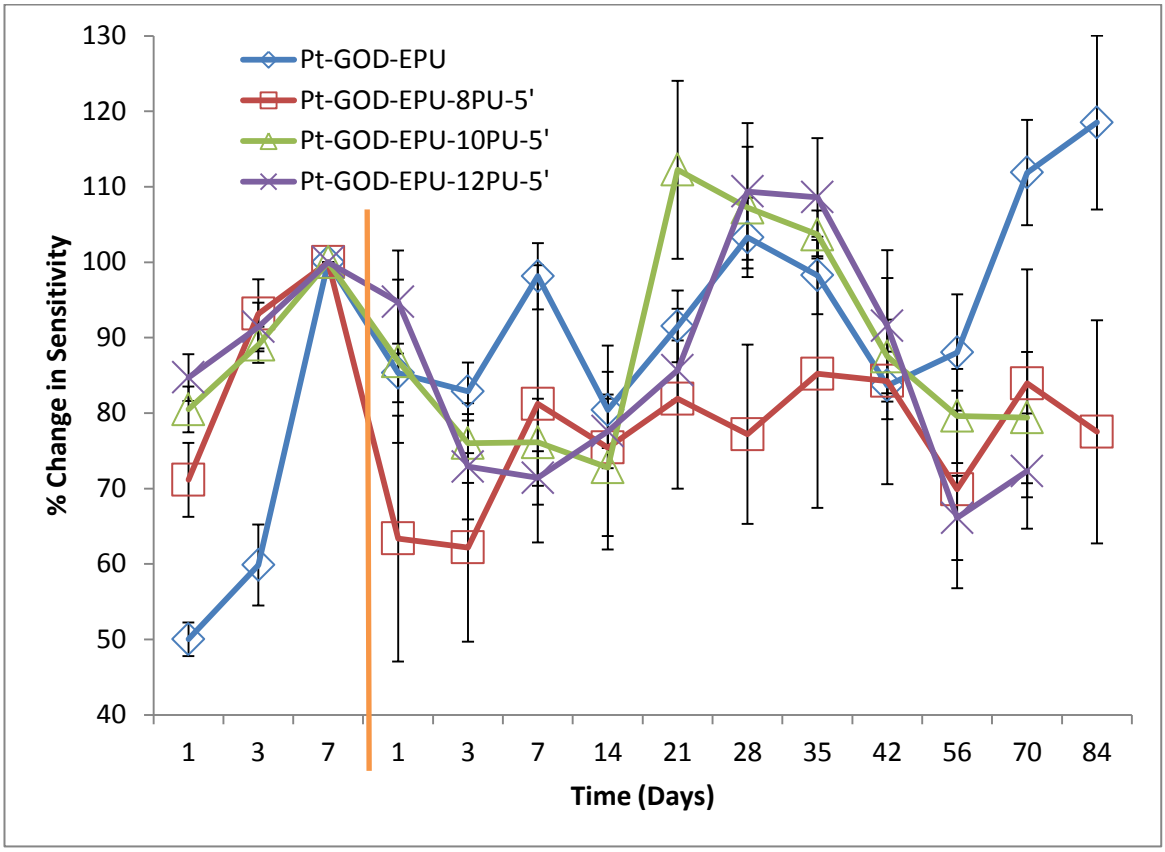

Figure 4.16: Effect of electrospun membrane on *ex vivo* function of sensor (Pt-GOD-EPU-ESC) as a function of membrane thickness and porosity expressed as % change in sensitivity for each sensor from that before coating (Pt-GOD-EPU) normalised to that on day 7 (100%) before applying electrospun coatings (data point left of the orange line indicating drying of Pt-GOD-EPU sensor and coating with electrospun membrane).

4.6.3.2. Effect of increasing porosity of electrospun membranes on sensor function

The efficacy of electrospun membranes as a function of increasing thickness and porosity on Pt-GOD-EPU sensors was tested similar to that described in section 4.6.2.1 above. The sensors were coated with 8PU, 10PU and 12PU membranes with an electrospinning time of 5 min. The respective sensors are designated as Pt-GOD-EPU-8PU-5', Pt-GOD-EPU-10PU-5', Pt-GOD-EPU-12PU-5'. For each sensor configuration 6 sensors were prepared and tested, and Pt-GOD-EPU sensors were used as controls processed similar to the electrospun coated sensors. The results for the effects of increasing thickness and porosity of electrospun membranes on sensor function are presented in Figure 4.17, Figure 4.18 and Figure 4.18.

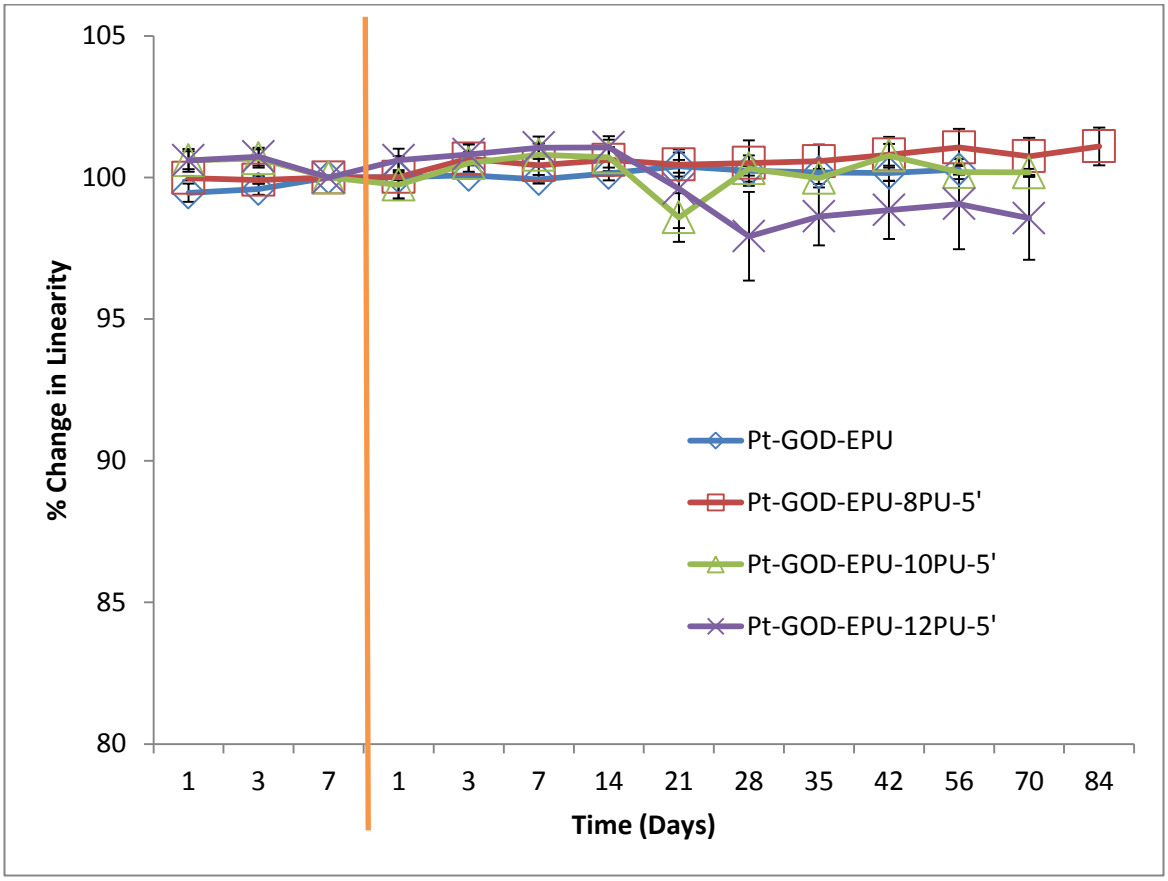

Figure 4.17 : Effect of electrospun membrane on *ex vivo* function of sensor (Pt-GOD-EPU-ESC) as a function of membrane thickness and porosity expressed as % change in sensitivity for each sensor from that before coating (Pt-GOD-EPU) normalised to that on day 7 (100%) before applying electrospun coatings (data point left of the orange line indicating drying of Pt-GOD-EPU sensor and coating with electrospun membrane).

The trend in the chronological changes in sensor sensitivity was similar to that described in section 4.6.2.1 above for 8PU membranes. Among the three sensor configurations, Pt-GOD-EPU-8PU-5', Pt-GOD-EPU-10PU-5', and Pt-GOD-EPU-12PU-5', no statistically significant differences in sensitivity or linearity were observed (Figure 4.16 to Figure 4.18), suggesting that the combined increase in thickness and porosity of electrospun fibro-porous coatings did not have any effect on sensor function. Compared to the Pt-GOD-EPU control sensors, although lower, the average sensitivities for the electrospun membranes coated sensors were not statistically significant (Figure 4.18).

Overall, it is interesting to note that fibro-porous electrospun membranes were causing <20% decrease in sensitivity of implantable coil-type glucose biosensors, and the decrease was similar irrespective of thickness and porosity of the tested electrospun membranes.

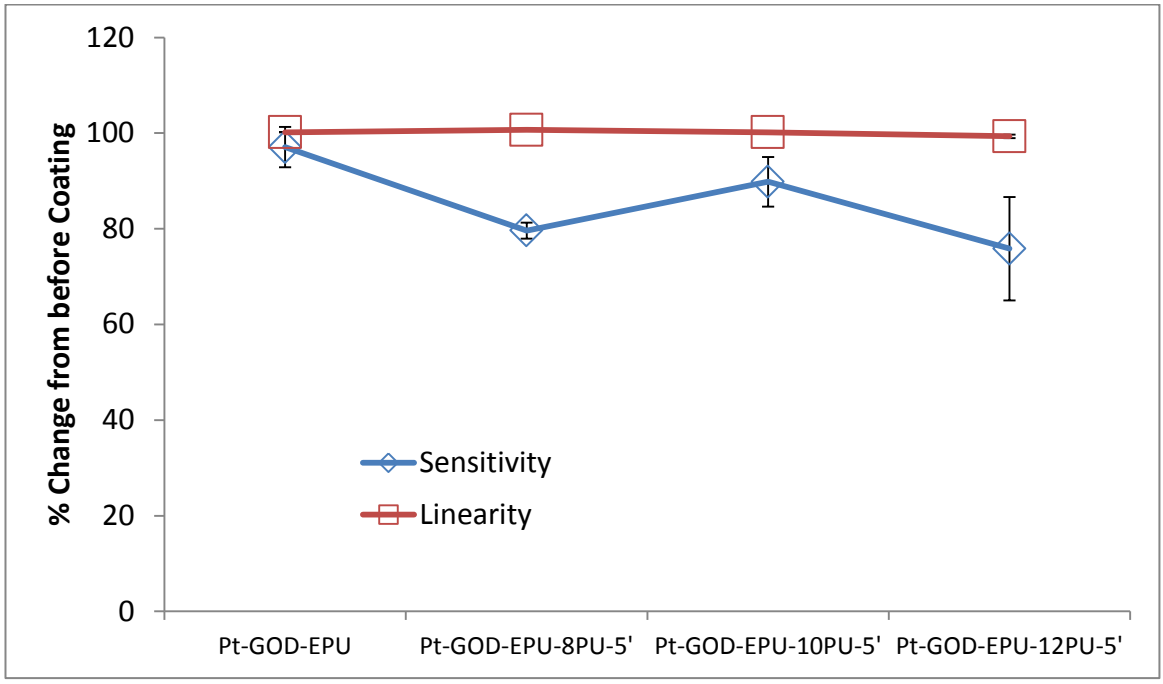

Figure 4.18: Effect of electrospun membrane on *ex vivo* function of sensor (Pt-GOD-EPU-ESC) as a function of membrane thickness and porosity expressed as % change of sensitivity and R^2 (2 to 30mM) for each sensor from that before coating (Pt-GOD-EPU). 8PU, 10PU and 12PU membranes were spun with, 22 cm distance between spinneret tip and sensing element tip, 21kV applied voltage and a dynamic collector.

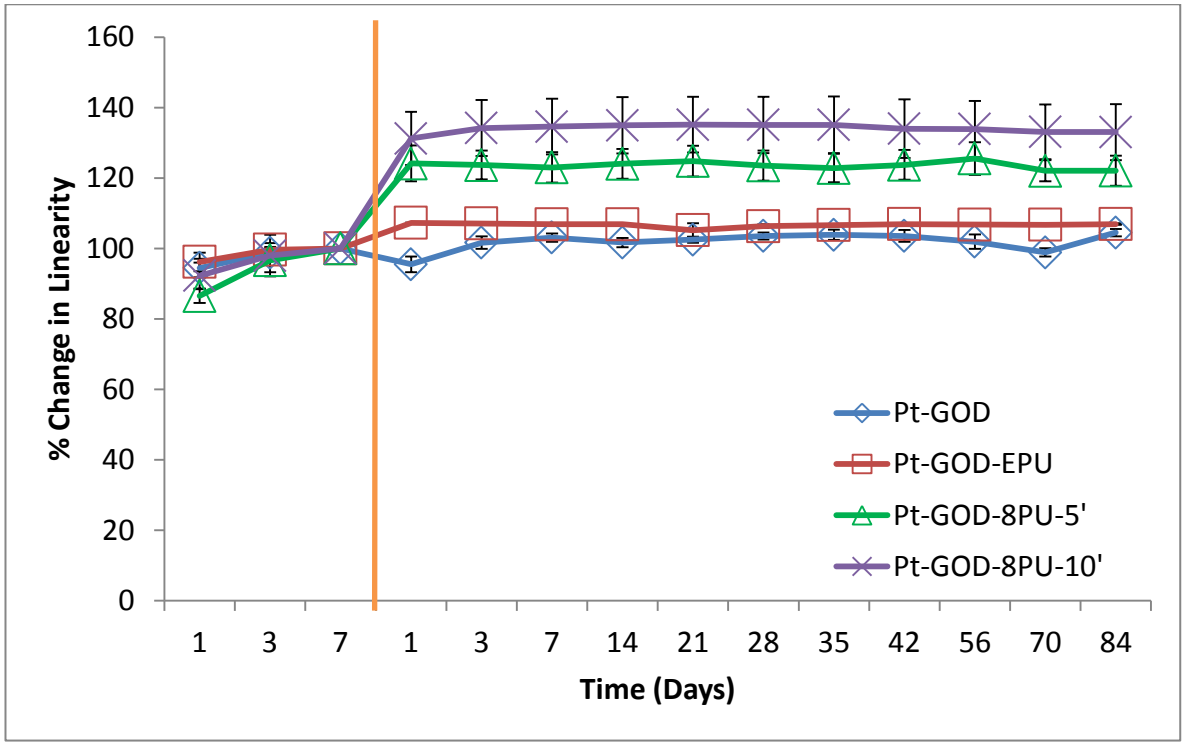

Figure 4.19: The ability of electrospun 8PU-5' and 8PU-10' membranes to function as mass-transport limiting membranes as illustrated by the increase in R^2 for the linear detection of glucose in the range of 2 to 30 mM using coil-type implantable glucose biosensors (Pt-GOD-EPU and Pt-GOD used as control groups).

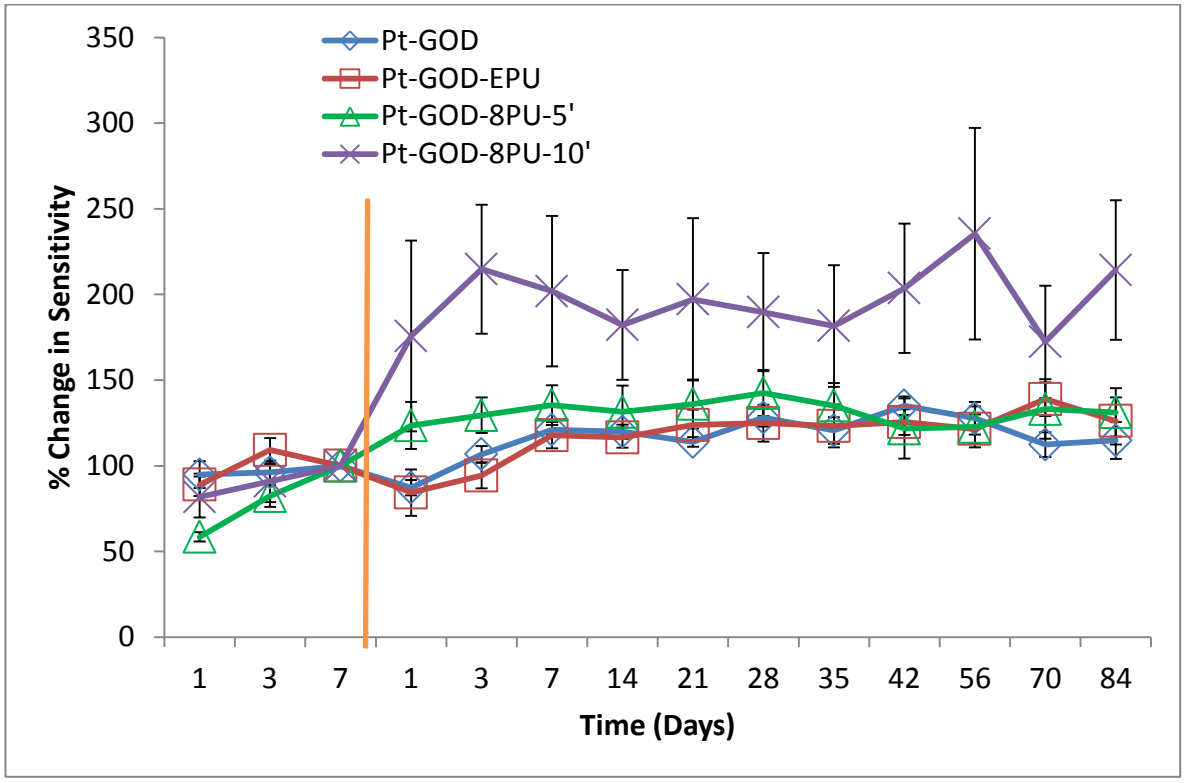

Figure 4.20: Effect of electrospun membrane on *ex vivo* function of sensor (Pt-GOD-ESC) expressed as % change in sensitivity for each sensor from that before coating (Pt-GOD) normalised to that on day 7 (100%) before applying electrospun coatings (data point left of the orange line; Pt-GOD-EPU and Pt-GOD used as control groups).

4.7. Efficacy of electrospun coatings as mass-transport limiting membranes for glucose biosensors

The Pt-GOD sensors were directly coated with electrospun membranes in order to test the ability of electrospun membranes to function as mass-transport limiting membrane. As illustrated by the increase in R^2 for Pt-GOD sensors from before to after applying electrospun coatings in Figure 4.19, the tested 8PU-5' and 8PU-10' membranes extended the linear detection range from about 2 to 10 mM to 2 to 30 mM for glucose detection. In addition, the extension of linear detection range also resulted in an increase in sensor sensitivity calculated for change in sensitivity between 5 and 15 mM.

4.8. Long-term stability of sensor function for glucose biosensors before and after coating with electrospun membranes

The long-term stability in sensor function for all sensor configurations illustrated in Figure 4.13, Figure 4.16& Figure 4.20 was tested for up to 12 weeks. All sensor configurations tested maintained stable sensitivity for the test period of 12 weeks. It must be emphasised that when electrospun membranes were used as mass-transport limiting membranes, they not only extended the linear glucose detection range to cover the desired 2 to 30 mM, but also maintained the stable sensor sensitivity till 12 weeks of testing.

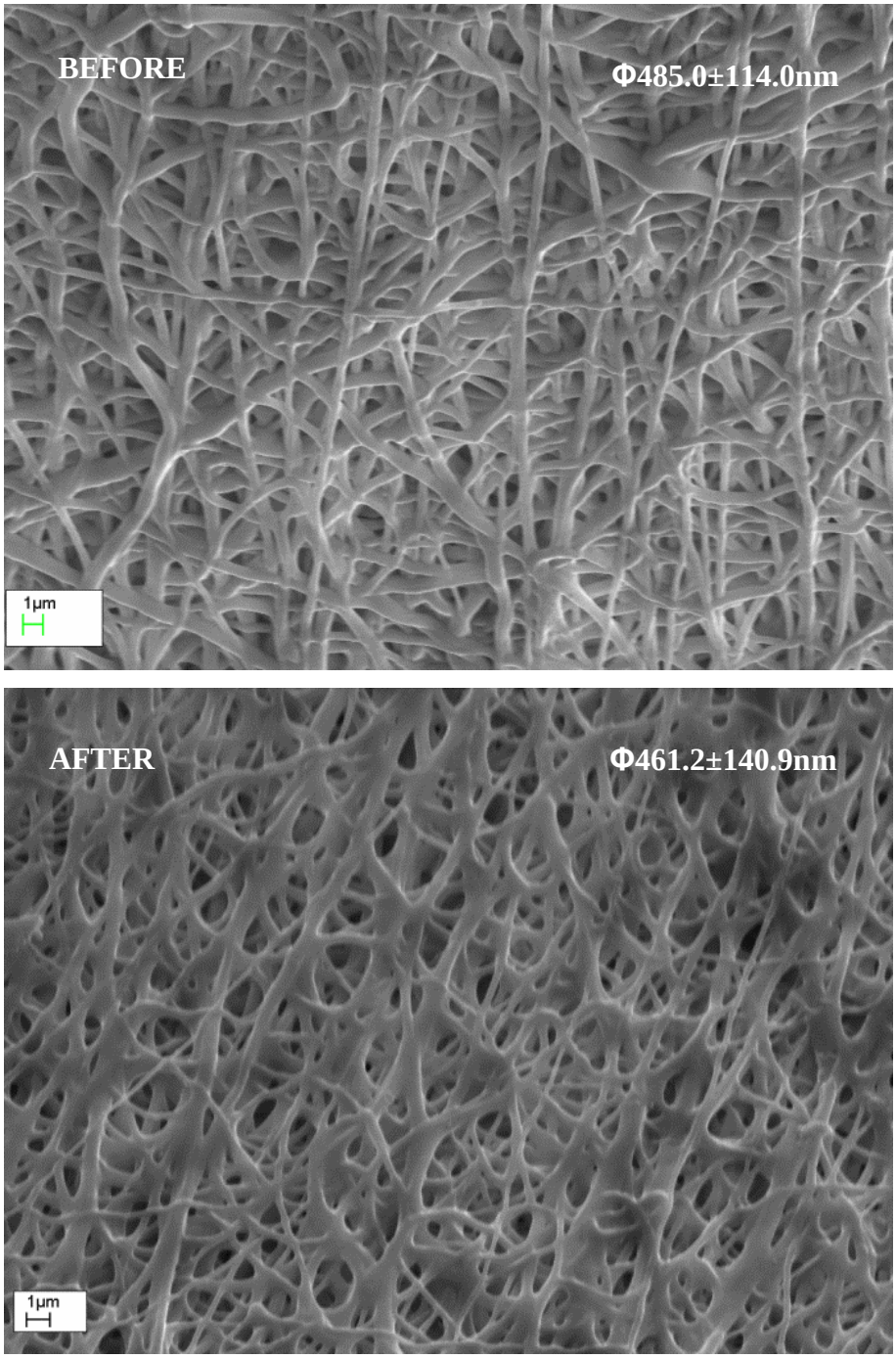

Figure 4.21 SEM images showing surface morphology on 8PU-5' electrospun membrane on sensors a) before and b) after long-term *ex vivo* sensor functional efficacy testing.

4.9. Effect of long-term incubation of electrospun membrane coated sensors in physiological solution on the diameter of PU fibres

The fibres remained stable for up to 12 weeks, and only a slight but statistically insignificant decrease in fibre diameter was observed (Figure 4.21). 8PU-5' membranes showed average fibre diameters of 485±114 and 461±141 nm before and after the long-term incubation in PBS pH 7.4 at 37^{o}C, which also included intermittent sensor function tests exposing the sensors to 0 to 30 mM glucose solution and polarization with 0.7V

electrical potential. The slight decrease in fibre diameter can be attributed to the slow degradation of PU fibre through surface erosion.

4.10. Chapter Summary

The research focus for this chapter was to develop a method for electrospinning fibres directly on miniature coil-type glucose biosensor and to test the effects of the resulting coatings on sensor function. Considering the disparity in size, shape and surface area available for deposition of fibres on the surface of a miniature biosensor compared to that of a flat plate, it was first essential to identify the optimum collector configuration and distance from the spinneret for electrospinning fibres directly on biosensor surface. Finite element modelling was used to identify an optimum static collector configuration. Thereafter, methods were optimized for electrospinning fibres directly on the sensing element of the biosensors using both static and dynamic collector systems. Following on from Chapter 3, the effects of membrane thickness (using 8PU membranes spun for different electrospinning time) and porosity (using 8PU, 10PU and 12PU having increasing fibre diameters and corresponding increase in thickness and porosity) on sensor function was tested.

For a flat plate collector, as reported in chapter 3, an optimum distance between spinneret tip and collector was identified to be about 22 cm. To identify the optimum collector configuration for electrospinning fibres directly on sensor surface, initially, the same 22 cm air gap between the spinneret tip and the collector tip was adapted. However, the grounded flat plate collector was replaced with the miniature coil-type glucose biosensor. The thin sensor wire was not rigid enough to be held perpendicular to the ground along the axis of the spinneret needle. Hence, the length of the thin working electrode wire was inserted into a 23G needle, such that the working electrode (sensing) element along with about 5 mm wire was exposed outside the tip of the holding needle for deposition of electrospun fibre. Only the sensor wire was grounded for electrospinning purpose and its stainless steel holding needle was not. The specifications for this configuration referred as SCC-1 (Figure 4.1), were then fed in the Maxwell ® SV FEA simulation software to simulate the electric field distribution between the spinneret needle and the grounded sensor.

It was observed that the edges/ends of the spinneret, sensor and even the non-grounded conducting stainless steel holding needle caused focal points for higher electric field strength (Figure 4.1). Due to the small volume and area of the collecting sensor (<5mm diameter and about 8 cm length) compared to the large flat plate (16 x 16 x 0.5 mm), the electric field focused at one point at the sensing element for SCC-1. Essentially,

the electric field vectors converged on the sensing element and then were strongly reflected in all directions (Figure 4.1d), indicating that the uniform distribution for fibres on the sensor surface would be difficult to achieve.

In order to shift the focus of strong electric field from the collecting sensing element, the sensor along with its holding needle was integrated perpendicularly at the centre of a flat stainless steel plate. Both the sensor and the flat plate were grounded, where the sensor was the main electrode while the flat plate the auxiliary electrode. For this static collector system, first the distance between the spinneret tip and the flat plate was kept at 22cm, such that the air gap between the spinneret tip and the sensing element tip was 16 cm. In this configuration, referred to as SCC-2 (Figure 4.2), again the edge effects were prominent, but an additional two focal points at the either ends of the flat plate formed (Figure 4.2 a & b), thus lowering the electric field strength at the sensing element compared to that observed with SCC-1. However the short distance between the spinneret and the sensor, combined with the wider auxiliary electrode caused an intense electric field coupled with a wider lateral spread (Figure 4.2c). The intensity of electric field was still high and its distortion at the sensing element was also high due to its proximity to the electric field around the spinneret needle tip (Figure 4.2b). The focus of electric field shifted from the sensing element (observed with SCC-1) to the tip of the holding needle in SCC-2. However, the stronger electric field due to shorter air gap between spinneret and sensing element meant that the electric field vectors still deflected, but the preferential direction now is perpendicular to the holding needle axis. The reflection of electric field again was thought to prevent the uniform distribution of fibres on the sensing element surface.

Finally, the distance between the spinneret tip and the sensing element tip was kept at 22cm, while using the flat plate (as in SCC-2) as the auxiliary electrode. This configuration, referred to as SCC-3 (Figure 4.3), significantly shifted the focus of the electric field strength from the sensing element to the auxiliary electrode (flat plate) (Figure 4.4c). Essentially, this resulted in the preferential orientation of electric field vectors predominantly downwards to the flat plate along the axis of the sensor and its holding needle (Figure 4.3d), thus potentially ensuring a uniform distribution of electrospun fibres on the entire surface of the sensing element. Hence, for the actual electrospinning experiments the SCC-3 was chosen as the static collection system.

True to the FEA simulation results observed for SCC-3, the sensing element was completely covered by the electrospun fibres. In fact, the coating was extended to about half the length on the holding needle (the boundary of the electric field around the tip of

the sensor holding needle closer to the flat plate), from where, the fibrous membrane spread out in an umbrella shape.

Although completely covering the sensing element, the coating was not uniform (Figure 4.5). The coating increased significantly in volume and thickness with increasing electrospinning time, and had grove-ridge structure on the lateral surface, which could be due to the square shape of the auxiliary electrode. In addition, at the cylindrical edges on both the tip and the base of the sensing element, spike-like structures with rounded ends and hollow cores formed. The formation of the spike-like structures could be attributed to the 3D structure and static nature of the sensor. The accelerating polymer jet, when hits the tip of the stationary sensing element tip, would bend forming a loop such that, the entire length of polymer fibre doesn't contact the electrode surface. The looping of fibres could be responsible for the hollow spike-like structures (Figure 4.6).

To overcome the limitation due to static nature of the collector, the sensor was placed parallel to the auxiliary electrode and rotated at about 660 to 690 rpm in the electrospinning field (Figure 4.7). The distance between the spinneret tip and the sensor surface was kept constant at 22 cm. This resulted in the uniform coating of the sensing element with the electrospun membranes. The coating thickness appeared to be uniform on the entire ellipsoid sensing element surface including its closed tip (Figure 4.8). The morphology as observed under SEM (Figure 4.9) revealed a uniform fibre size distribution and interconnected porosity across the cross-section of the 8PU membrane electrospun on the sensor. Thus, the objective of applying uniform electrospun membranes having controllable fibre diameters, porosity and thickness was achieved.

Thereafter the effect of electrospun coatings on biosensor function was assessed. Initially, the efficacy of the membranes collected for 5, 10 and 30 minutes using static collector system (SCC-3) was tested. The large volume of the fibrous membrane on sensor surface meant a significant decrease in sensor sensitivity (Figure 4.12). Further studies using the static collector system were abandoned because of the very uneven shape and thickness of the coatings (Figure 4.5).

Anticipating a <20% decrease in sensor sensitivity (as observed with 5 min coating using the static collector, Figure 4.12), the electrospinning times of 2.5, 5 and 10 min were chosen to obtain membranes of varying thickness on sensors using the dynamic collector system. Initially, the effects of thickness on sensors' *ex vivo* function were assessed, while maintaining fibre diameter by electrospinning 8PU membranes for 2.5, 5 and 10 min on Pt-GOD-EPU sensors. Thereafter, the effect of increasing fibre diameter, porosity and associated increase in thickness for 8PU, 10PU and 12PU membranes electrospun for 5

min on the function of Pt-GOD-EPU sensors was assessed. The sensors were tested for sensitivity and linearity in the glucose detection range of 2 to 30 mM, before and after coating with electrospun membranes.

Following their manufacture, when Pt-GOD and Pt-GOD-EPU sensors are immersed in a physiological fluid for the first time, their sensitivity increases initially with time and then plateaus off. In this study, when the sensors were incubated at 37^{o}C, the time taken for the sensors to attain stable sensitivity was less than 7 days. Hence the sensors were tested on 1, 3 and 7 days, before coating for *ex vivo* function, to allow for enzyme and any additional layers on the sensors' working electrode to attain equilibrium swelling and sensor polarization. The sensors were dried overnight and then coated with electrospun coatings. Following the coating, the sensor function was tested at 1, 3, 7 days, then weekly until 6 weeks (42 days) and thereafter biweekly till 12 weeks (84 days). For all sensor configurations tested in this study, the sensitivity increased for up to 7 days and stabilised thereafter. Furthermore, there was no statistically different change in linearity (R^2) for all sensors for the entire duration of testing – both before and after applying electrospun coatings.

As a function of thickness, there was a significant increase in sensor sensitivity when Pt-GOD-EPU sensors were coated with 8PU membrane for 2.5 min, which was unexpected, and could be associated with the membrane's permeability kinetics. However, for both Pt-GOD-EPU-8PU-5' and Pt-GOD-EPU-8PU-10', although the average sensitivity was slightly lower after applying the electrospun coatings, there was not statistical difference from that observed for the Pt-GOD-EPU control sensors processed similarly but without applying any additional coatings. Similar results for changes in sensitivity were also observed when Pt-GOD-EPU sensors were coated with 8PU-5', 10PU-5' or 12PU-5' membranes. Essentially, the electrospun coatings, irrespective of their thickness (about 22 to 100 μm) and porosity (between 44 to 70%), did not cause any statistically significant decrease in sensitivity of the Pt-GOD-EPU sensors.

Furthermore, considering their submicron and uniform porosity, 8PU membranes were also anticipated to function as mass-transport limiting membranes for glucose biosensors. In fact, when the 8PU-5' and 8PU-10' membranes were tested on Pt-GOD sensors, they significantly increased the linearity (Figure 4.19) for the detection range of 2 to 30 mM for glucose, proving their efficacy as mass-transport limiting membranes.

A linear increase in thickness was observed for 8PU membranes on sensor as a function of electrospinning time (Figure 4.10). The increasing trend of membrane thickness on sensors was similar (R^2 about 0.99) to that observed for the corresponding

membranes electrospun on flat plate spun for 2.5, 5 and 10 min. However, the thicknesses were significantly higher on sensors compared to that on flat plate, due to the smaller area available for the deposition of fibres on miniature sensors. For the thicknesses of membranes electrospun on flat plate, diffusion kinetic analysis described in chapter 3, indicated a Case II Fickian diffusion mechanism for transport of glucose across the membrane. However, a tendency for the diffusion mechanism to shift towards anomalous diffusion (non-Fickian) was noted with increasing thickness of the membranes. As a result, the diffusion across the much thicker membranes on sensors could be diffusion controlled (Fickian diffusion).

Long-term stability of sensor function was also tested for up to 12 weeks. All sensor configurations tested in this study maintained a stable sensitivity and linearity for the entire duration of the testing. The stability can be attributed to the stability of the PU fibres in the membrane. Morphology observations on the membranes following incubation at 37^{o}C in PBS of pH 7.4 and repeated sensor function testing for 12 weeks revealed the surface etching resulting in rough fibre surface. However, the decrease in fibre diameter was insignificant to have any significant effect on sensor function until 12 weeks of testing.

To conclude, a method for spinning uniform and snugly fitting electrospun membranes having tailorable fibre diameters, thickness and porosity directly on miniature biosensor surface was optimized. Initially, FEA simulations were used to identify the right static collector configuration and distance from the spinneret for obtaining coatings that cover the entire surface of the sensing element of the biosensor. Although completely covering the sensor surface, the coating was not uniform when electrospun using a static collecting system. Rotating the sensor in the electrospinning field (dynamic collecting system) helped achieve the objective of spinning desired electrospun coating configurations. The resulting coatings were demonstrated to cause negligible decrease in sensitivity for glucose biosensors. The electrospun coatings with sub-micron porosity were also shown to function as mass transport limiting membranes. Long-term stability of the fibres and the *ex vivo* function of the electrospun membrane coated sensors were demonstrated for the study period of 12 weeks. Overall, electrospun membranes having highly interconnected porous network (with approximately 44 to 70% porosity) of wide range of thicknesses were shown to cause negligible effect on sensor's sensitivity, which finding is unique and widely desired for coating applications requiring free solute flux across membranes.

Chapter 5 Electrospun PU-Core and Ge-Shell Coaxial Fibre Membranes for Miniature Biosensors

5.1. Introduction

The synthetic polymer, PU has desirable mechanical properties for implantable biomedical device applications, but is relatively inert. In contrast, extracellular matrix derivatives, collagen and gelatine (Ge) are bioactive, but lack the desired mechanical properties. Electrospinning provides an opportunity to combine the synthetic and natural materials as co-axial fibre composites that combine bioactivity and mechanical strength.

The objective for this chapter was to electrospin co-axial composite fibres constituting of gelatin sheaths reinforced with PU core as biomimetic membranes for implantable biosensors. A specialised spinneret, made of concentric tubes connected to two separate fluid sources, such that coaxial fibres can be electrospun, was designed. The solution and process parameters for electrospinning coaxial fibres were varied. The gelatin sheaths were stabilized by crosslinking. The membranes were characterised for morphology, pore sizes, porosity, hydrophilicity, solute diffusion, chemical and mechanical properties. Glucose biosensors were then coated with optimized co-axial fibre membranes and their effects on sensor function evaluated.

5.2. Glucose biosensor

The coil-type implantable glucose biosensor described in section 4.2 of Chapter 4 was used for characterizing the effects of PU-core and GE-sheath co-axial fibre membranes on sensor function.

5.3. Electrospinning setup

The basic vertical electrospinning setup (Figure 2.2) described in chapter 2 was used for optimizing solution and processing parameters for spinning co-axial fibre membrane sheets on flat-plate collector. However, to obtain coaxial fibres a coaxial spinneret was used (Figure 2.3). For spinning co-axial fibres directly on glucose biosensors, the rotating collector system shown in Figure 2.4B was used.

5.4. Process optimization for electrospinning PU-GE co-axial fibres

The solubility of Ge in a variety of organic solvents in very poor and a highly polar solvent TFE was essential for making an electrospinnable solution of Ge. At the same time, its incompatibility with other solvents meant, it was also essential to prepare the co-electrospinning PU solution in TFE. However, the solubility of PU in TFE was poor and only a maximum of 8% (wt/v) was possible. For the optimization of parameters for

electrospinning co-axial fibres, a 10% (wt/v) Ge solution was chosen. Due to the lower solubility of PU in TFE, PU solution concentrations were varied from 2 to 8% (wt/v) for electrospinning co-axial fibres.

The solution viscosity for the different PU and Ge solutions are summarised in Table 5.1. TFE had a viscosity of 7.68 x 10^{-4} pa/s, which was similar to that observed with THF (7.55 x 10^{-4} pa/s) and its volatility was high. Hence, in this study, to obtain a Taylor cone that remains stable and maintains its shape throughout the electrospinning process, it was essential to use the following combinations of parameters: electrical voltage in a range of 11-15kV, a working distance (between spinneret and collector) of 15cm to prepare solvent-free fibres, and flow rates of inner (PU) and outer (Gelatin) solution were constant at 0.8ml/h and 1.2ml/h respectively for electrospinning PU-core and Ge-shell co-axial fibres. The ambient temperature and humidity were not controlled.

Table 5.1 Dynamic viscosity of the different PU and Ge solutions used for electrospinning co-axial fibre membranes, * viscosity was higher than measuring limit for the instrument.

Solvent/Solution	**Concentration - wt/v (wt/wt) (%)**	**Dynamic Viscosity x 10^{-4} (pa/s)**
TFE	100	7.684±0.0084
PU	2 (1.5)	332.763±1.0382
PU	4 (2.9)	1373.714±0.9675
PU	6 (4.3)	3764.733±6.0548
PU	8 (5.8)	*
Ge	10 (6.8)	797.122±1.0056

The designations for the different co-axial fibre membranes electrospun in this study are 2PU10Ge, 4PU10Ge, 6PU10Ge and 8PU10Ge. The formation of the core-shell fibre structure was first ascertained using TEM. As illustrated in Figure 5.1a core-shell structure was demonstrated for 8PU10Ge membranes.

Furthermore, to make Ge insoluble and maintain the co-axial fibre structure, it was essential to stabilize the Ge-shell through crosslinking; using glutaraldehyde (GTA). The morphology of the as-spun 8PU10Ge membranes is shown in Figure 5.2a. Two methods were tested for GTA crosslinking of Ge-shell. Firstly the membrane was immersed in GTA solution. However, this resulted in the disruption of the coaxial fibre structure, forming a Ge sheet reinforced with PU fibres (Figure 5.2b). Secondly, the membranes were incubated in a GTA saturated air for 3 days to allow crosslinking of Ge-shell of the co-axial fibres, which preserved the co-axial fibre structure (Figure 5.2c).

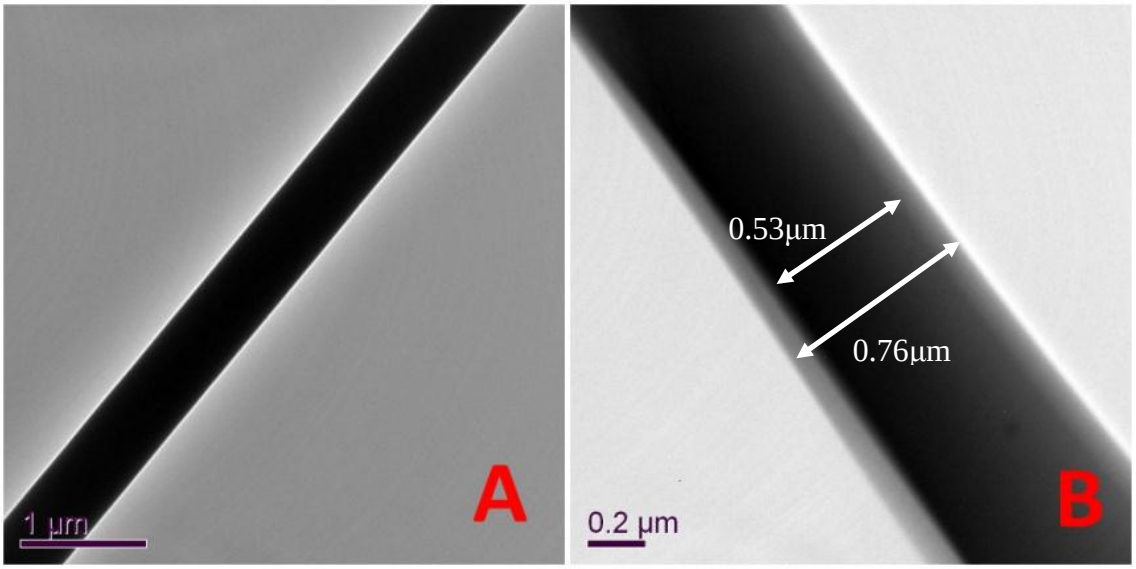

Figure 5.1 TEM images showing A) PU and B) 8PU10Ge fibres electrospun using TFE as the solvent.

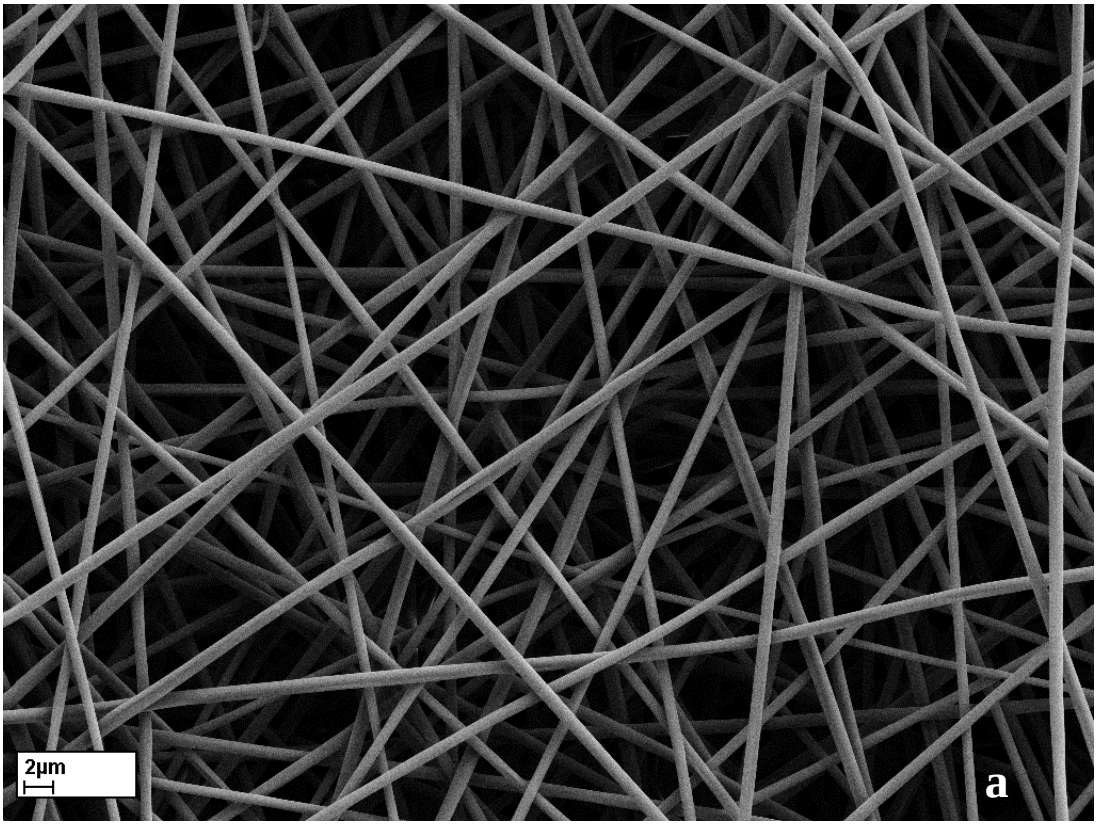

Figure 5.2 SEM images showing co-axial fibres of 8PU10Ge membranes: a) as-spun, b) crosslinked by immersing in GTA solution, and c) co-axial fibres crosslinked using GTA vapour.

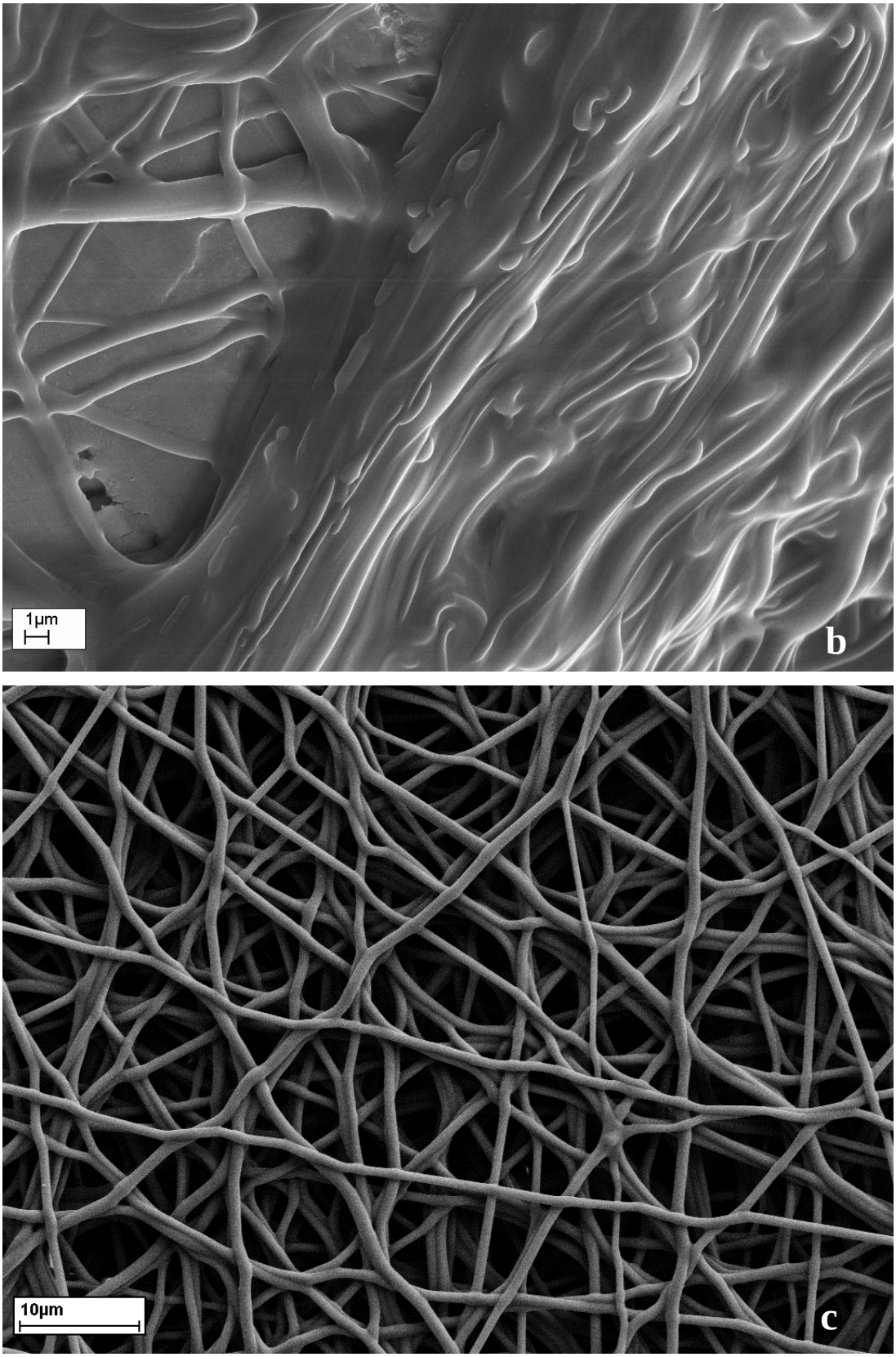

Figure 5.2 (*Continued*)

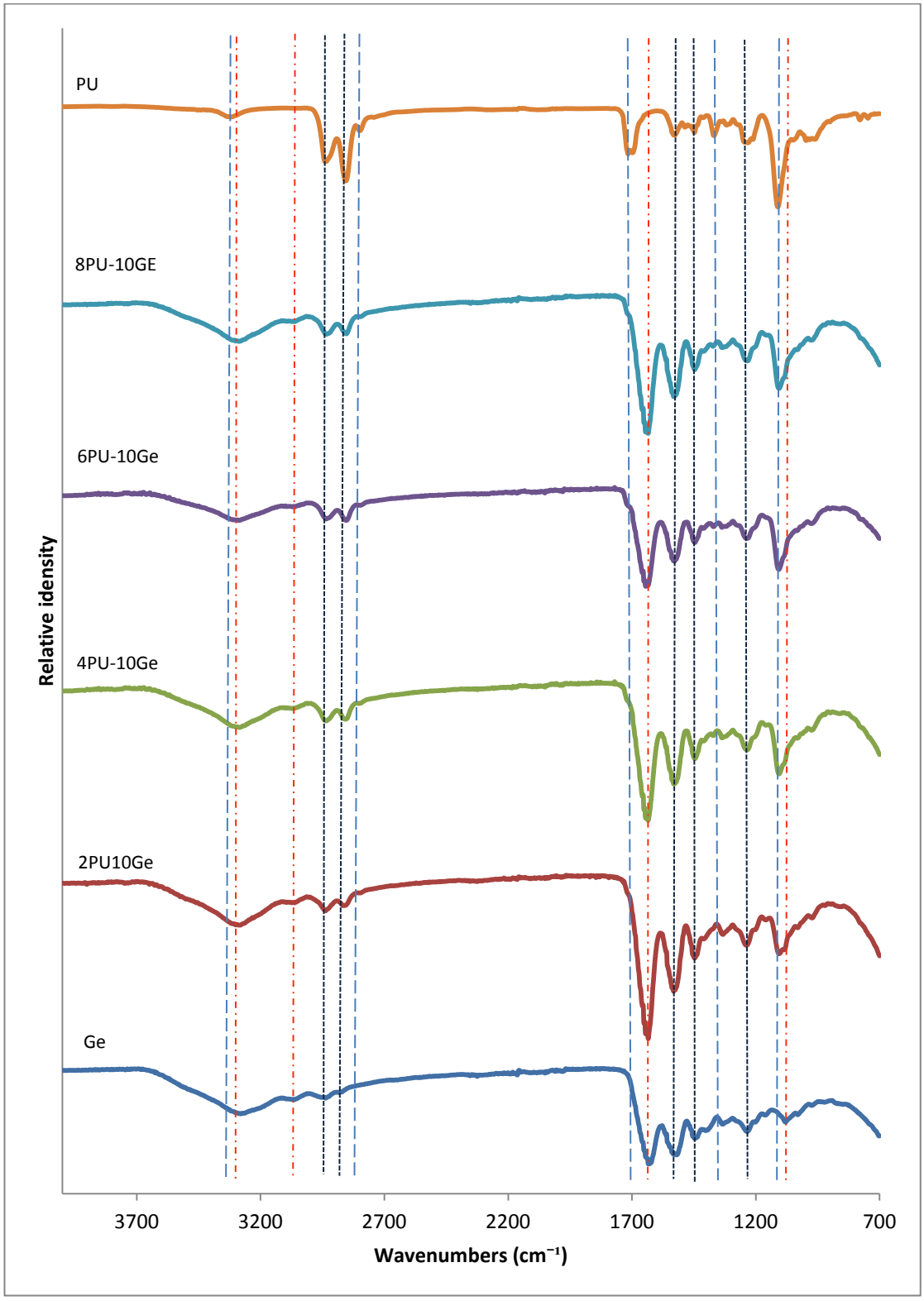

Figure 5.3 FTIR spectra electrospun co-axial fibre membranes having Ge shell non-crosslinked and the spectra of PU and Ge were used as controls. The dotted blue and red vertical lines represent the typical peaks of PU and Ge respectively, while the dotted dark blue line represents common peaks.

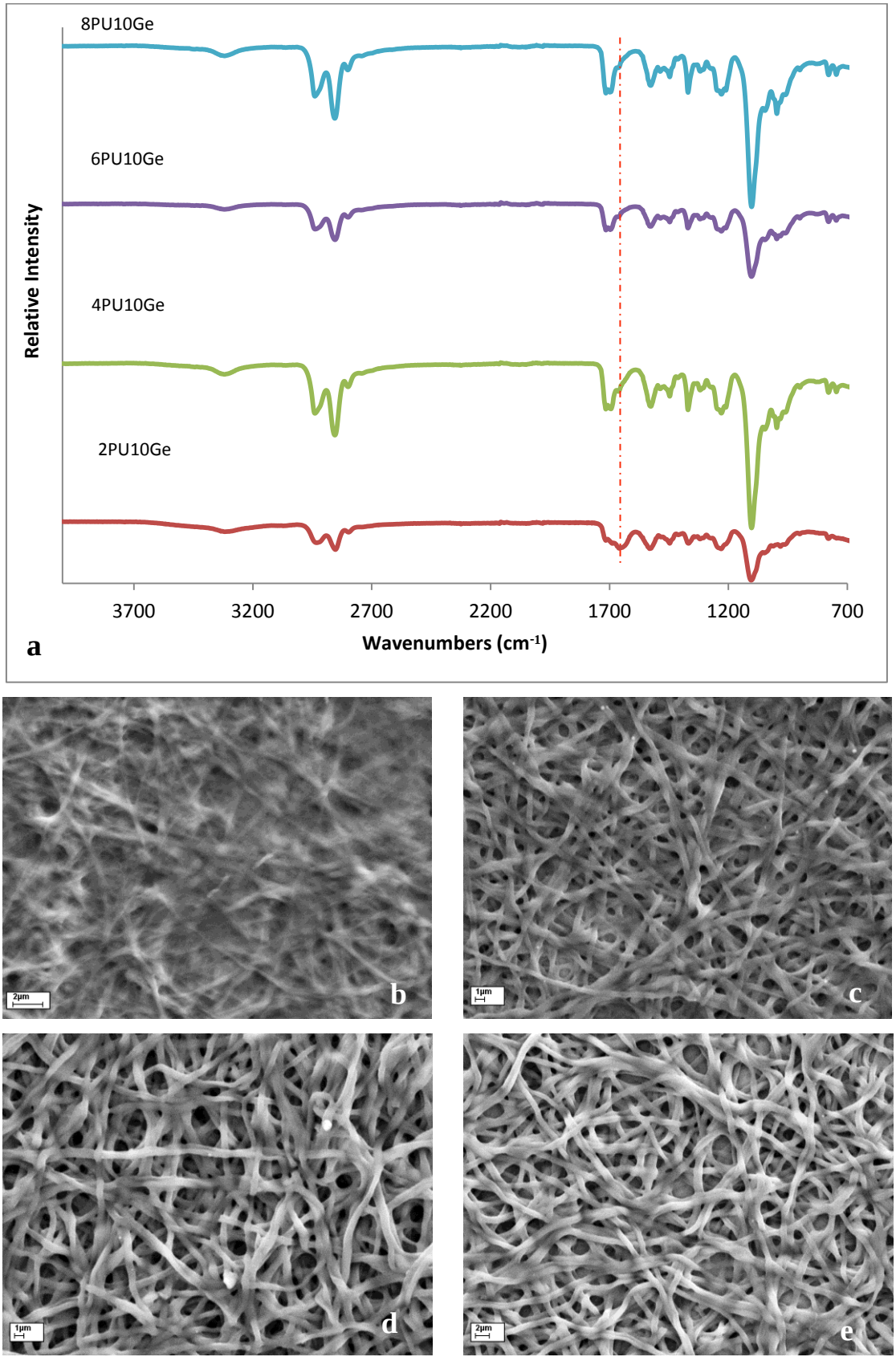

Figure 5.4 FTIR spectra (a) and respective morphologies for electrospun coaxial fibre membranes: 2PU10Ge (b), 4PU10Ge (c), 6PU10Ge (d) and 8PU10Ge (e) after washing off the gelatin shell layer in DI water at 40ºC for 1 week, with immersion DI water changed every 24h.

5.5. Characterization of the electrospun co-axial fibre membranes

5.5.1. Surface chemical composition of co-axial fibres using FTIR spectroscopy

ATR-FTIR spectra (Figure 5.3) were recorded for the different coaxial fibres without crosslinking the Ge shell, and their feed components – Ge powder and PU pellets (as supplied) were used as controls to examine any interaction between core (PU) and shell (GE) due to the electrospinning process. The gelatin showed its typical bands at 1634 cm^{-1} (amide I), 1531 cm^{-1} (amide II) and 1233 cm^{-1} (amide III) corresponding to C=O stretching, N–H bending and C–N stretching vibrations respectively pertaining to the triple helical structure of gelatin (Chang *et al.*, 2003). The typical PU peaks included the C-H stretching vibrations between 2825 and 2946 cm^{-1}, ~1731 cm^{-1} the free urethane carbonyl peak, ~1106 cm^{-1} the soft segment ether peak and ~1033 cm^{-1} the hard segment ether peak. The spectra for co-axial fibres showed the unique peaks of both PU and Ge indicating the presence of both PU and Ge in the co-axial fibre membranes. The broad absorption band centred at about 3288 cm^{-1} was found in the FTIR spectra of all PU/GE coaxial fibres, which can be attributed to overlapping peaks of the N-H and OH-O stretching vibration. Moreover, no shift in characteristic peaks of either PU or Ge was observed for any of the electrospun coaxial fibre membranes, suggesting that there may be no obvious interaction between PU and GE. This is consistent with the observation on electrospun Ge/PU blended nanofibres reported earlier (Kim *et al.*, 2009).

Furthermore, the ATR-FTIR spectra were also recorded for co-axial fibre membranes from which the Ge shell was washed off using DI water at 40^{o}C for 1 week with water changes every 24h. The FTIR spectra and morphology for the different coaxial fibre membranes is shown in Figure 5.4. The spectra for all membranes were similar to that of pure PU, with the exception of 2PU10Ge samples, which showed a prominent peak, at about 1633 cm^{-1} unique to pure Ge. Moreover, the morphology of 2PU10Ge showed spreading of the polymer between the fibres. Although, not spreading out as observed with 2PU10GE, the fibres of the other membranes appeared to fuse with neighbouring fibres, which could be indicative of some degree of blending of PU and Ge at the interface between the PU core and Ge shell during electrospinning. When the Ge is washed off, the residual PU in the transition layer could accumulate on the surface of PU core causing neighbouring fibres to fuse.

5.5.2. Co-axial fibre morphology and diameter distribution

The morphology and fibre diameter distributions for co-axial fibre membranes as a function of increasing feed concentration of PU solution from 2 to 8% (wt/v) while

maintaining a constant 10% Ge solution in TFE are presented in Figure 5.5. For the 2PU10Ge membranes having the lowest feed concentration for PU-core, occasional spindle shaped beads formed (Figure 5.5a). The bead formation could be due to the disparity in solvent content in the core PU solution compared to the shell Ge solution. The core PU solution containing higher solvent content, due to its low viscosity (about 33.28 x 10^{-4} pa/s, Table 5.1) breaks into droplets as the polymer solution accelerates toward the collector, while the gelatin shell solidifies containing the PU droplets, resulting in beads. Similar result is reported earlier (Diaz *et al.*, 2008). However, for the rest of the membranes, namely 4PU10Ge, 6PU10Ge and 8PU10Ge, an increasing viscosity (Table 5.1) resulted in coaxial fibres were seamless and without any beads (Figure 5.5b to d).

It is interesting to note that the fibre diameter distributions were quite narrow, indicating a stable electrospinning process for spinning co-axial fibres (Figure 5.5e to h). Furthermore, the average fibre diameters increased significantly with increasing feed solution concentration of the core PU solution. Fibre diameters were submicron only for 2PU10Ge membranes. The increase in fibre diameters is well recognised to be caused by the increasing concentration of the feed polymer solution(s) ((Huang *et al.*, 2003, Yu *et al.*, 2004, Huang *et al.*, 2005).

5.5.3. Core-shell fibre structure

To visualise the core-shell structure of the co-axial fibres under SEM and quantify the thickness of the Ge-shell and diameter of the PU-core, one of the components, either Ge or PU, was dissolved while preserving the other component. In the first instance, following crosslinking of Ge-shell with GTA vapour, the PU core was dissolved using THF. The resulting hollow fibres for the different membranes are shown in Figure 5.6. The tubular structure was prominent for all membranes. However, for 4PU10Ge membranes some of the fibres did not form complete tubes (Ge-shell) (Figure 5.6b), which could be due to an observed experimental anomaly, wherein the fast evaporation of solvent could accelerate solidification of gelatin on the tip of the nozzle either blocking or significantly slowing the shell fluid flow. The amount of the shell liquid in Taylor cone thus decreases to a point where the viscous drag applied by the sheath solution could be insufficient to confine the core solution within the Taylor cone. To slow down the evaporation of the Ge solution at the Taylor cone and thus ensuring formation of proper co-axial fibre, a solvent soaked tissue paper was wrapped around the spinneret needle holder close to the spinneret tip.

For quantifying the thickness of Ge-shell and diameter of PU-core, Ge-shell (non-crosslinked) was washed off using DI water at 40^{o}C. The diameters for the resulting PU

core were measured on SEM images. The total thickness of the Ge-shell on coaxial fibres was obtained by subtracting the diameter of PU core with that of the whole coaxial fibre having its Ge-Shell layer crosslinked using GTA vapour. The results are presented in graphs in Figure 5.7. The data for core diameter and shell thickness was excluded for 2PU10Ge membranes, because its PU core fibres were obscured by the polymer spreading out due to the DI water washings into sheets as shown in Figure 5.4b.

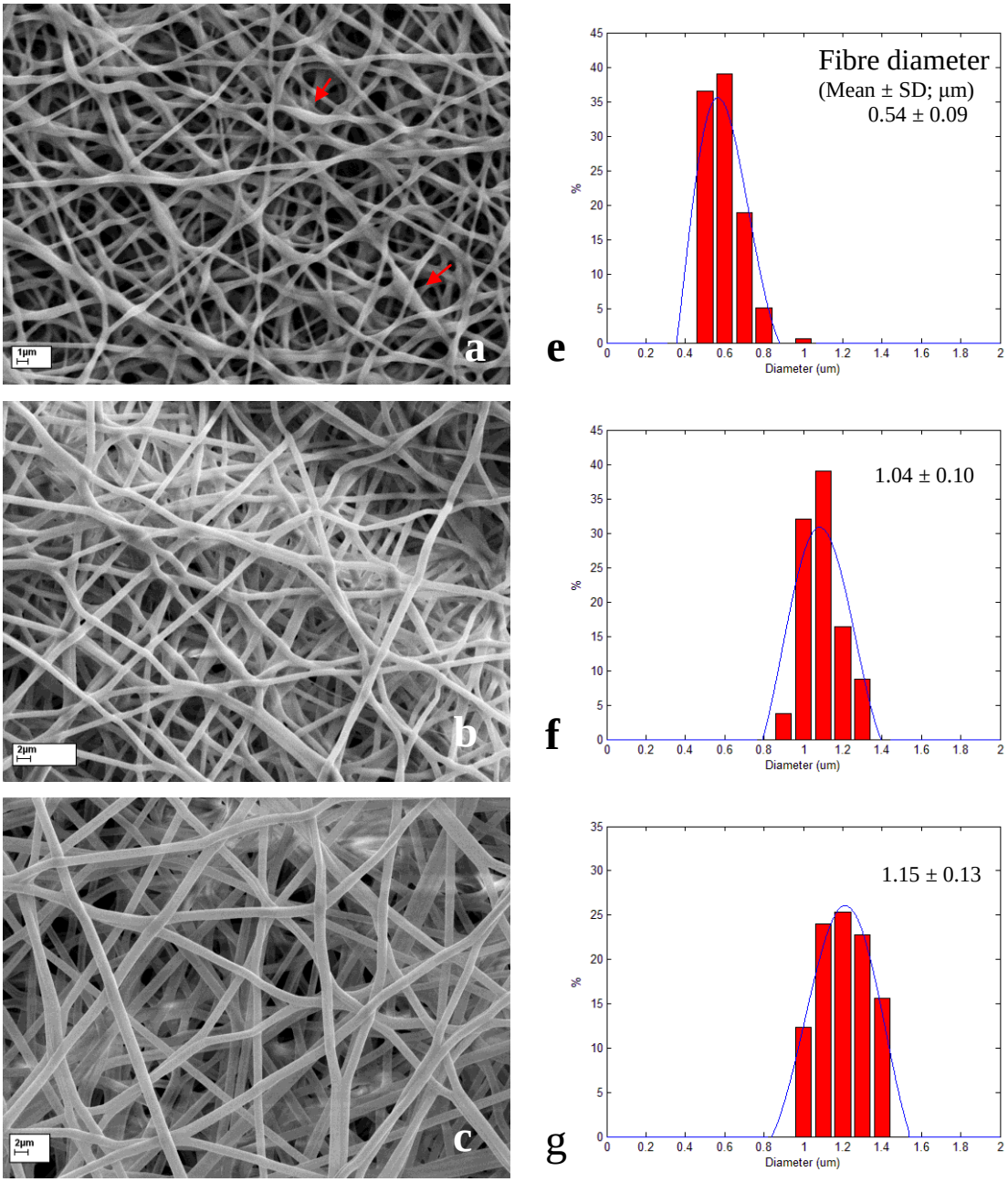

Figure 5.5 SEM images (a to d) and fibre diameter distribution histograms (e to h) for the different co-axial fibre membranes: 2PU10Ge (a & e), 4PU10Ge (b & f), 6PU10Ge (c & g) and 8PU10Ge (d & h) respectively. Red arrows indicate spindle-shaped beads. Average fibre diameters for each membrane were significantly different from all other membranes ($p<0.05$).

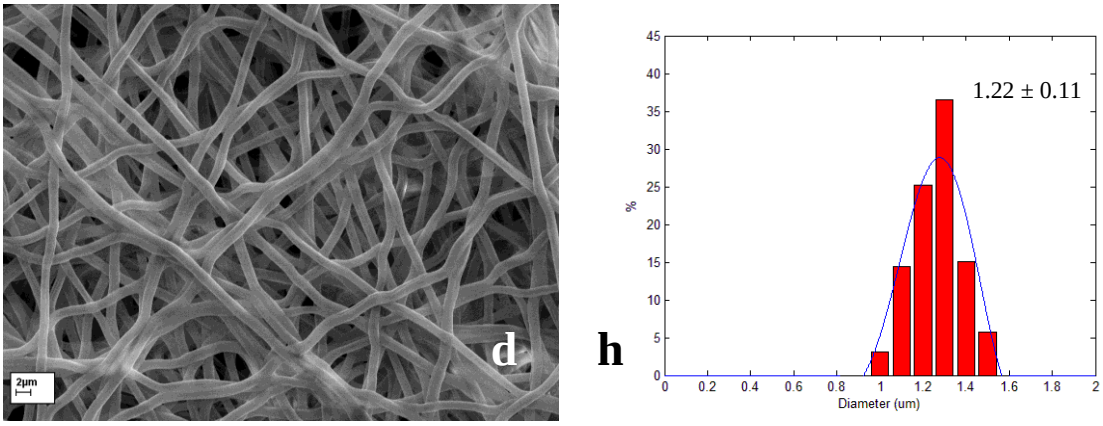

Figure 5.5 (*Continued*)

However, the rest of the membranes that had intact fibres, the increase in concentration of feed PU solution significantly increased the diameter of the PU-core in the coaxial fibre, while the thickness of its Ge-shell showed a gradual decrease (Figure 5.7). The ratio of the diameter of PU core to the total thickness of Ge shell on the co-axial fibres further reiterates the increasing volume of PU core with increasing feed PU solution concentration (Figure 5.7). The increase in the diameter of PU core and a parallel decrease in Ge shell thickness were also reported by Zhang *et al.*, who explain the decrease in the shell thickness to be due the same mass of the shell layer distributed over a larger core (Zhang *et al.*, 2004a).

5.5.4. Pore size and porosity

The co-axial fibre membranes attained sufficient thickness for measuring pore sizes using bubble point method when electrospun for 10 min. To study the effect of thickness on pore sizes, two electrospinning times, 10 and 40 min were chosen for spinning coaxial fibre membranes. The pore size distributions are presented in Figure 5.8. For membranes electrospun for 10 minutes, an increasing pore size was observed with increasing fibre diameter (Table 5.2), ranging from 920.70 nm for 2PU10Ge-10', 1964.34 nm for 4PU10Ge-10', 2624.23 nm for 6PU10Ge-10' through to 3051.74 nm for 8PU10Ge-10'. Furthermore the pore size distribution was narrow and sharp for 2PU10Ge-10', which became broader for other coaxial fibre membranes with increasing fibre diameters (Figure 5.8a). The membranes having smaller fibre diameters have been widely reported to have smaller pore sizes and narrower pore size distribution (Hartman *et al.*, 2009, Dotti *et al.*, 2007, Soliman *et al.*, 2011)

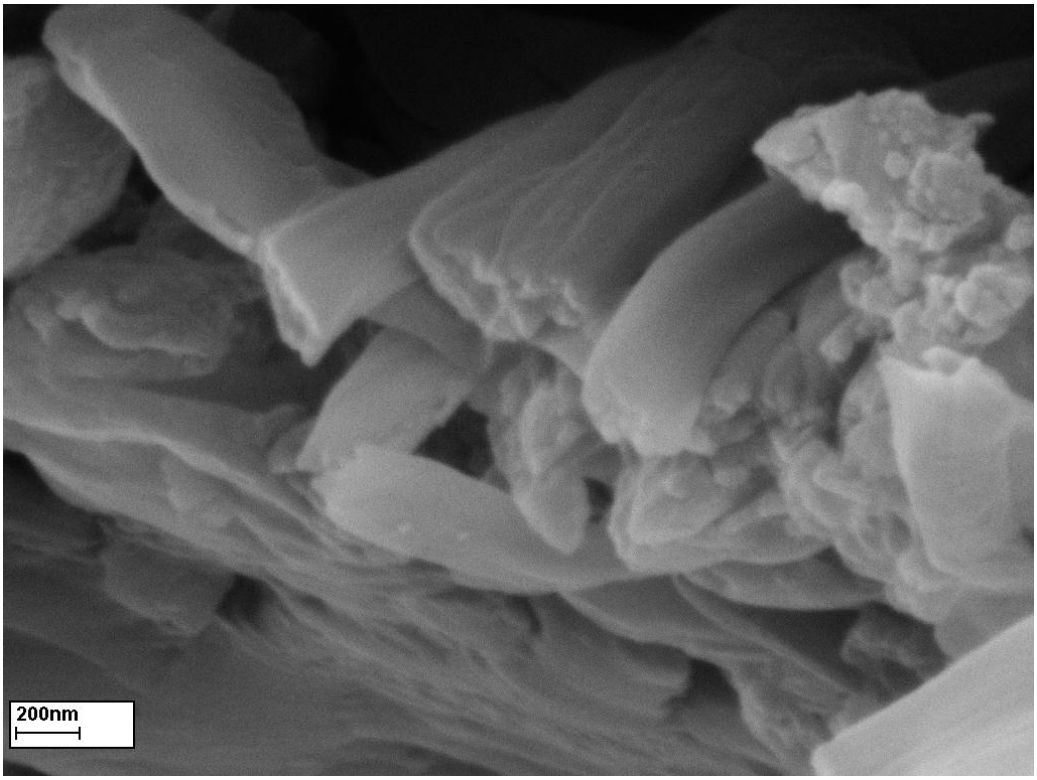

a

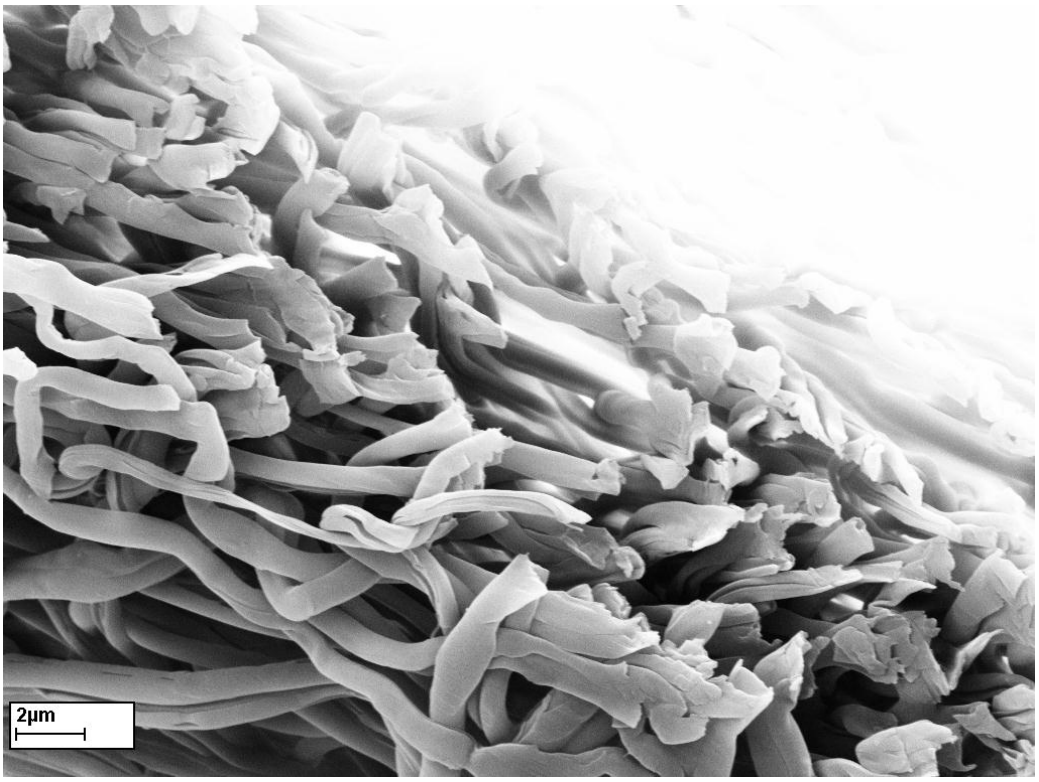

b

Figure 5.6 SEM images showing the hollow fibres (with PU core removed by dissolving in THF) for a) 2PU10Ge, b) 4PU10Ge, c) 6PU10Ge and d) 8PU10Ge electrospun co-axial fibre membranes.

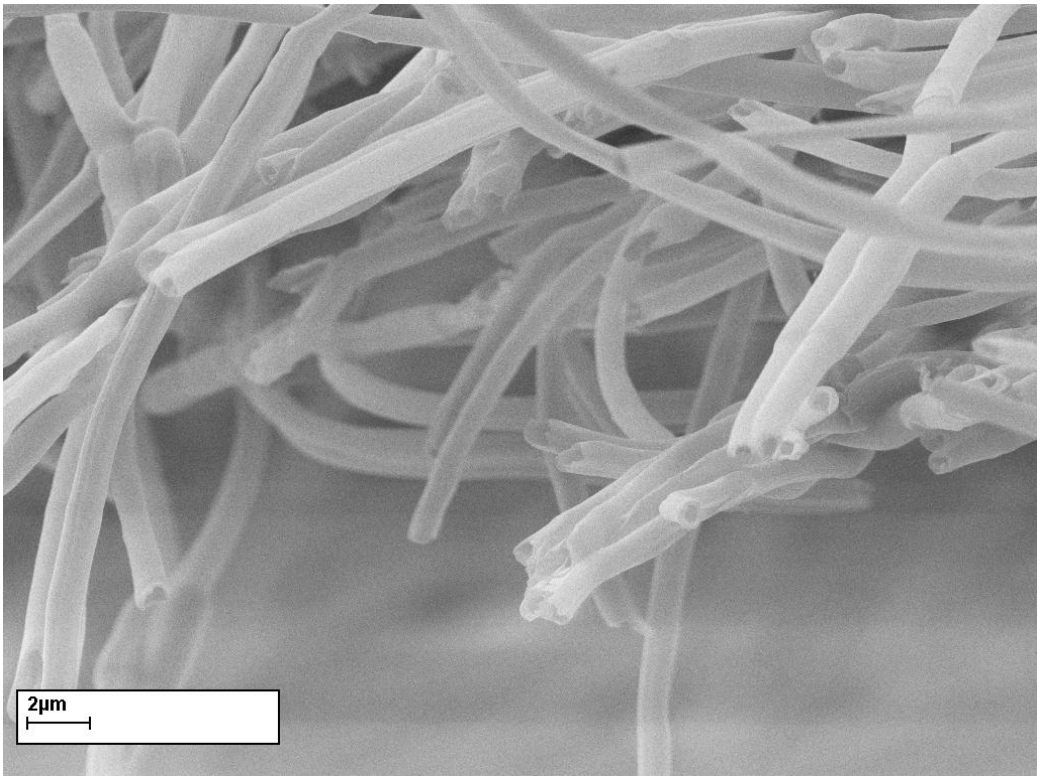

c

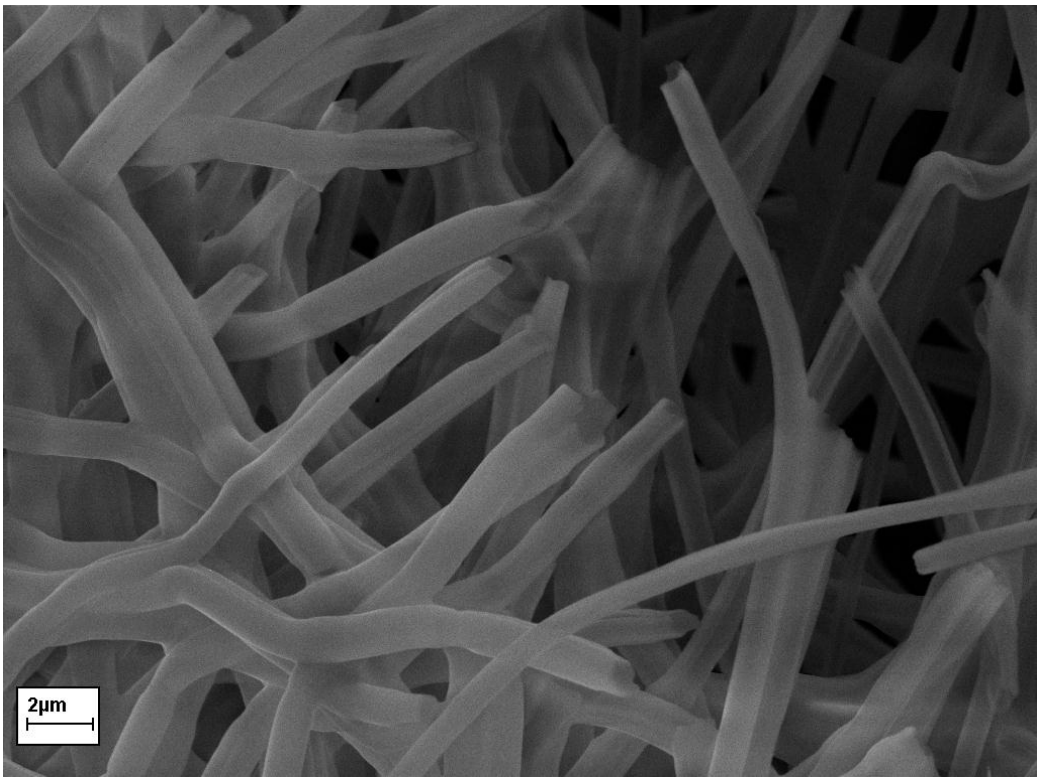

d

Figure 5.6 (*continued*)

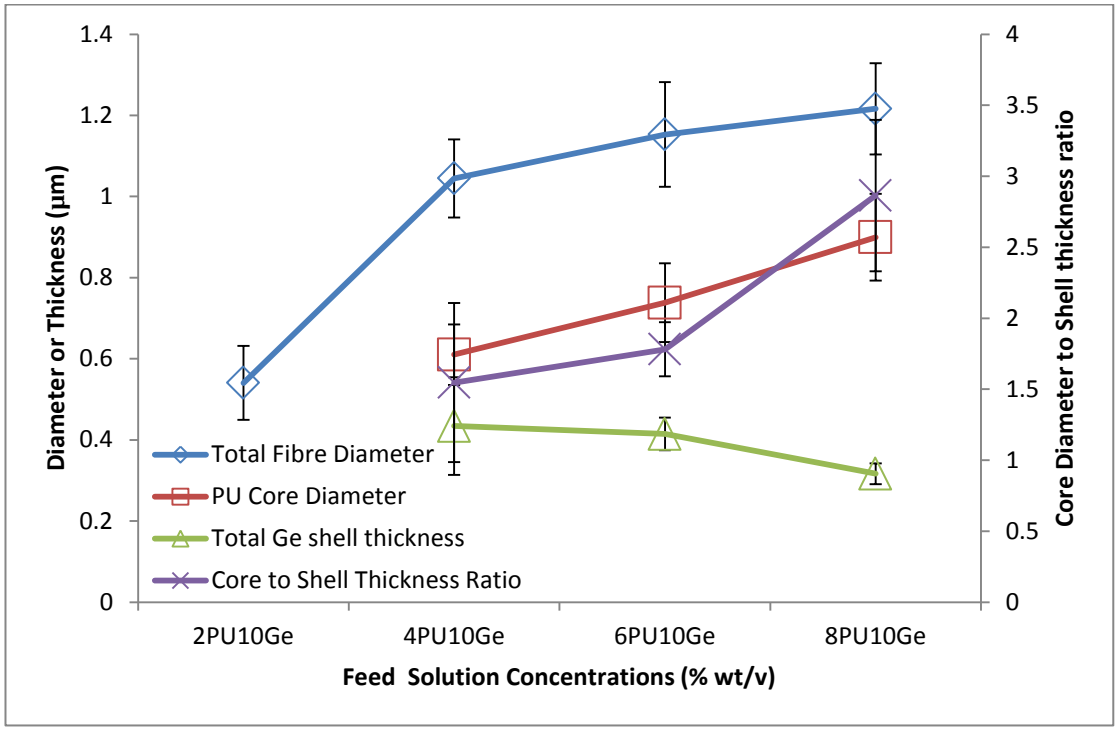

Figure 5.7 Cross-sectional dimensions for coaxial fibres electrospun on a flat plate collector as a function of increasing PU (core) feed solution concentrations (% wt/v), while maintaining the Ge (shell) feed solution concentration. For each of total fibre diameter, PU core diameter, total Ge shell thickness and PU core diameter to total Ge shell thickness ratios, statistical differences were observed between each of the membrane configurations (±SD, n=160) ($p<0.05$).

When the thickness of the coaxial fibre membranes was increased by increasing the electrospinning time to 40 min, the pore sizes again increased with increasing fibre diameter (Table 5.2), with the exception of 8PU10Ge membranes which had pore sizes smaller than 4PU10Ge (Figure 5.8b). However, compared to membranes electrospun for 10 min, the thicker membranes showed smaller pore sizes: 333.85, 1444.32, 1535.61 and 1028.91 nm respectively for 2PU10Ge-40', 4PU10Ge-40', 6PU10Ge-40' and 8PU10Ge-40' (Figure 5.8b). Such influence of electrospinning duration on pore size was also observed by Chiu *et al.*, who fabricated electrospun polyacrylonitrile ion-exchange membranes (Chiu *et al.*, 2011). They reported a sharp decrease in average pore diameter in the first 1 to 3h electrospinning time following which the pore sizes stabilized. The decrease in pore sizes with increasing membrane thickness could be due to the tighter packing of fibres induced by the increasing weight of the fibres being continuously deposited. The notably lower porosity of 8PU10GE-40' membranes (Figure 5.8b) can also be attributed to the densely accumulated fibres leading to smaller pore sizes similar to that observed by Soliman *et al.* (Soliman *et al.*, 2011).

The denser fibre packing causing lower porosity was also supported by the membrane thickness measurements and the gravimetry based porosity estimations (Table 5.2). Thickness of the membranes was measured using a digital micrometer.

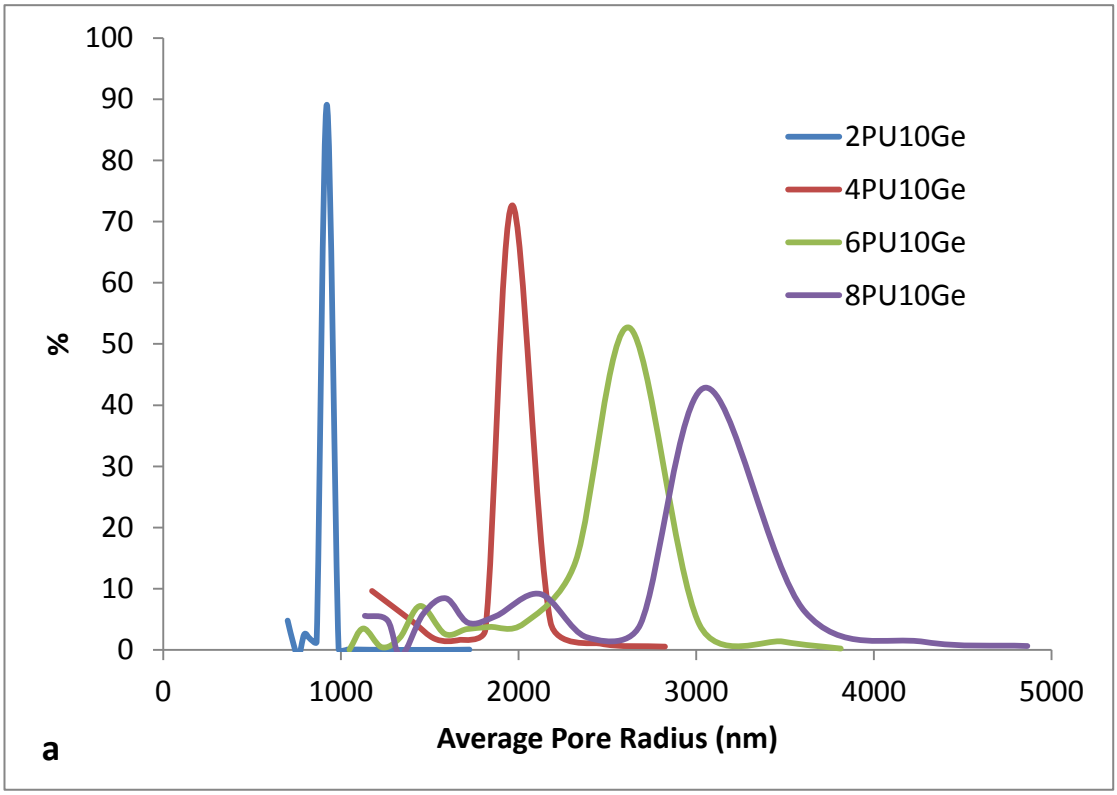

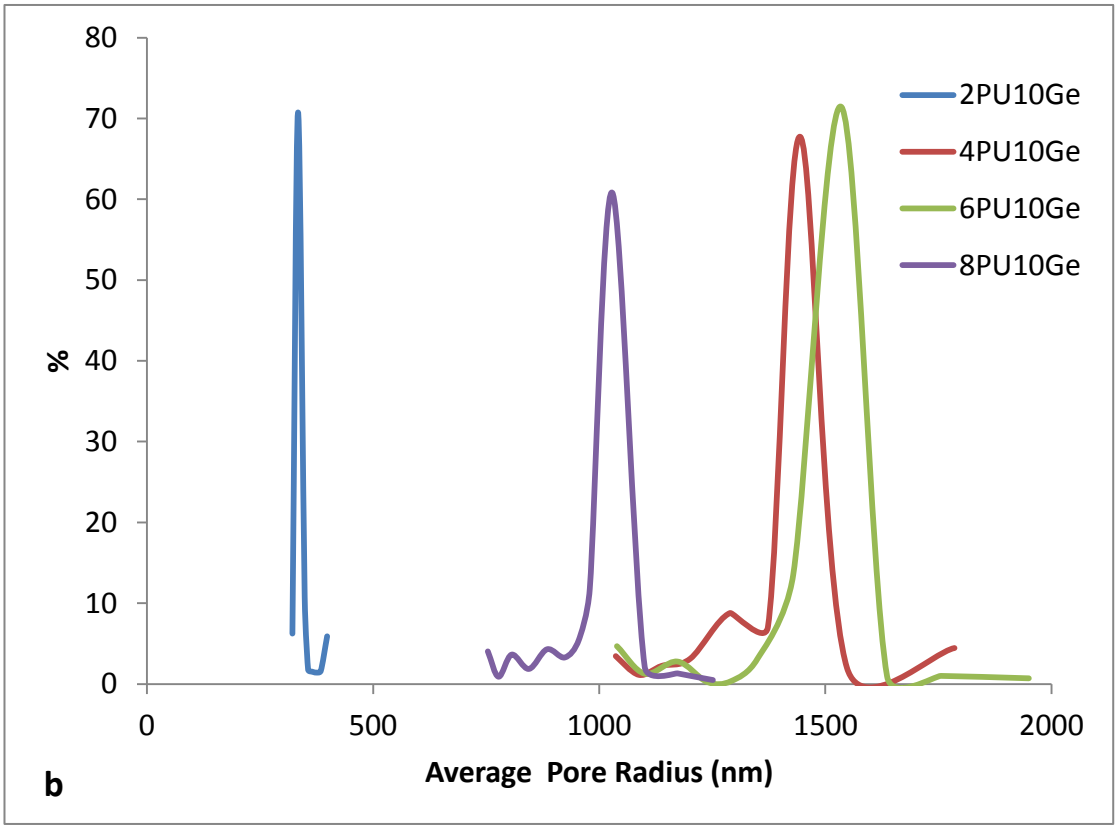

Figure 5.8 Pore size distributions for the co-axial fibre membranes 2PU10Ge, 4PU10Ge, 6PU10Ge and 8PU10Ge electrospun for a) 10 and b) 40 min.

Table 5.2 Porosity estimations for electrospun coaxial fibre membranes based on gravimetry, calculated using equations 2.2 and 2.3. n=3.

	2PU10GE	**4PU10GE**	**6PU10GE**	**8PU10GE**
Fibre Diameter (μm)	0.54±0.06	1.04±0.10	1.15±0.13	1.22±0.11
Fibre Bulk density (g/cm^3)	-	1.26	1.29	1.18
Membranes electrospun for 10 min				
Thickness (μm)	21.6±4.0	23.4±2.6	25.1±5.2	22.2±14.0
Fibre packing density º(g/cm^3)	0.285±0.068	0.276±0.009	0.257±0.066	0.214±0.079
Porosity (%)	-	78.02±0.68	80.14±5.09	82.02±6.67
Membranes electrospun for 40 min				
Thickness (μm)	56.8±4.9	40.3±5.7	36.0±5.4	67.7±6.7
Fibre packing density º(g/cm^3)	0.595±0.045	0.539±0.057	0.474±0.017	0.469±0.056
Porosity (%)	-	57.05±4.58	63.33±1.34	60.60±4.74

º the fibre packing density can be also called the apparent density as defined in Section 2.6.4

The apparent density (fibre packing density) and porosity of membranes was estimated using equations 2.2 and 2.3. The pore volume was calculated based on the apparent density (mass/volume) and bulk density of their corresponding PU/gelatin blends. The latter (ρ_b) was predicted by the thickness of core/shell layers of the fibre (Figure 5.7 and Table 5.2) and the bulk density of both materials (PU at 1.04g/cm^3 and Ge at 1.369g/cm^3 (Mwangi and Ofner Iii, 2004) as shown in the equation below:

$$\rho_b = \frac{\rho_{PU} r^2 + \rho_{Ge}(R^2 - r^2)}{R^2} \qquad \text{(Eq.5.1)}$$

Where r is PU core radius, R the total fibre radius, and ρ_{PU} and ρ_{Ge} referring to the bulk density of PU and Ge respectively.

Membrane thickness, material bulk density, fibre packing density and pore volume estimations are summarised in Table 5.2 for the different electrospun coaxial fibre

membranes electrospun for 10 and 40 min. As the core diameter in 2PU10Ge cannot be detected, its corresponding porosity cannot be calculated.

No significant change in the overall thickness was observed when the coaxial fibre membranes (4PU10Ge to 8PU10Ge) were electrospun for 10 min. In addition, they had apparent densities (or fibre packing density) in the range of 0.21-0.28 g/cm^3, which change was again not statistically significant, in spite of increasing feed PU solution concentration. Therefore, the comparable resultant percent in pore volumes can primarily be ascribed to their corresponding similar bulk density of the composite PU-Ge fibres (Table 5.2). All the coaxial fibre membranes electrospun for 10 min had pore-volumes greater than 60%, which could be useful for tissue engineering application requiring cellular infiltration to the bulk of porous scaffolds (Chong *et al.*, 2007b).

However, when the electrospinning time was increased, inconsistent membrane thickness, fibre packing densities and pore volumes were observed (Table 5.2). The thickness of the membranes decrease from 2PU10Ge to 6PU10Ge, and that of 8PU10Ge was higher than all the other membranes. The fibre packing densities also followed the trend observed with thickness measurements, but the fibre packing density for 8PU10Ge was comparable to that observed for 6PU10Ge. The pore volume estimations revealed a steady trend similar to that observed with membranes electrospun for 10 min. However, the pore volumes of coaxial fibre membranes electrospun for 40 min was significantly lower than those electrospun for 10 min. Overall, the insignificant variations in pore volumes with decreasing PU core volumes from 8PU10Ge to 4PU10Ge can be due to PU in the inner layer. Although the porosity (pore volume) would decrease with the shrinking of Ge shell due to GTA crosslinking as demonstrated for hydrogels in general (Wang et al., 2005, Yao et al., 2003, Jin and Hsieh, 2005, Zhao et al., 2007a, Zhao et al., 2007b), core PU with good mechanical properties can moderate the deformation during crosslinking process. Similar observation was also reported by Zhao *et al.*, wherein crosslinking of Ge shell layer resulted in negligible effects on porosity of coaxial fibre membranes having semi-crystalline hydrophobic PCL core (Zhao et al., 2007b).

To sum up, the pore sizes for PU-GE core-shell fibrous membranes are mainly dependent on fibre diameter, while the pore volume was dependent on the dielectric properties of the electrospinning solution. Electrospinning duration was shown to have a decreasing effect on pore sizes and volume for the electrospinning times tested in this study.

5.5.5. Diffusion Test

The permeability of the coaxial fibre membranes 2PU10Ge and 6PU10Ge to glucose was tested using biodialysers. The effect of membrane thickness on permeability was tested using membranes electrospun for 2.5, 5 and 10 min. The thicknesses of the resulting membranes are summarised in Table 5.3.

The diffusion tests and data presentation is similar to that described in section 3.4.4 in chapter 3. The glucose diffusion followed an initial linear increase that plateaued off to a constant when the diffusion rate attained equilibrium (Figure 5.9). The slope of the linear increase typically decreased with increasing membrane thickness, which was statistically significant for 2PU10Ge-10' membrane.

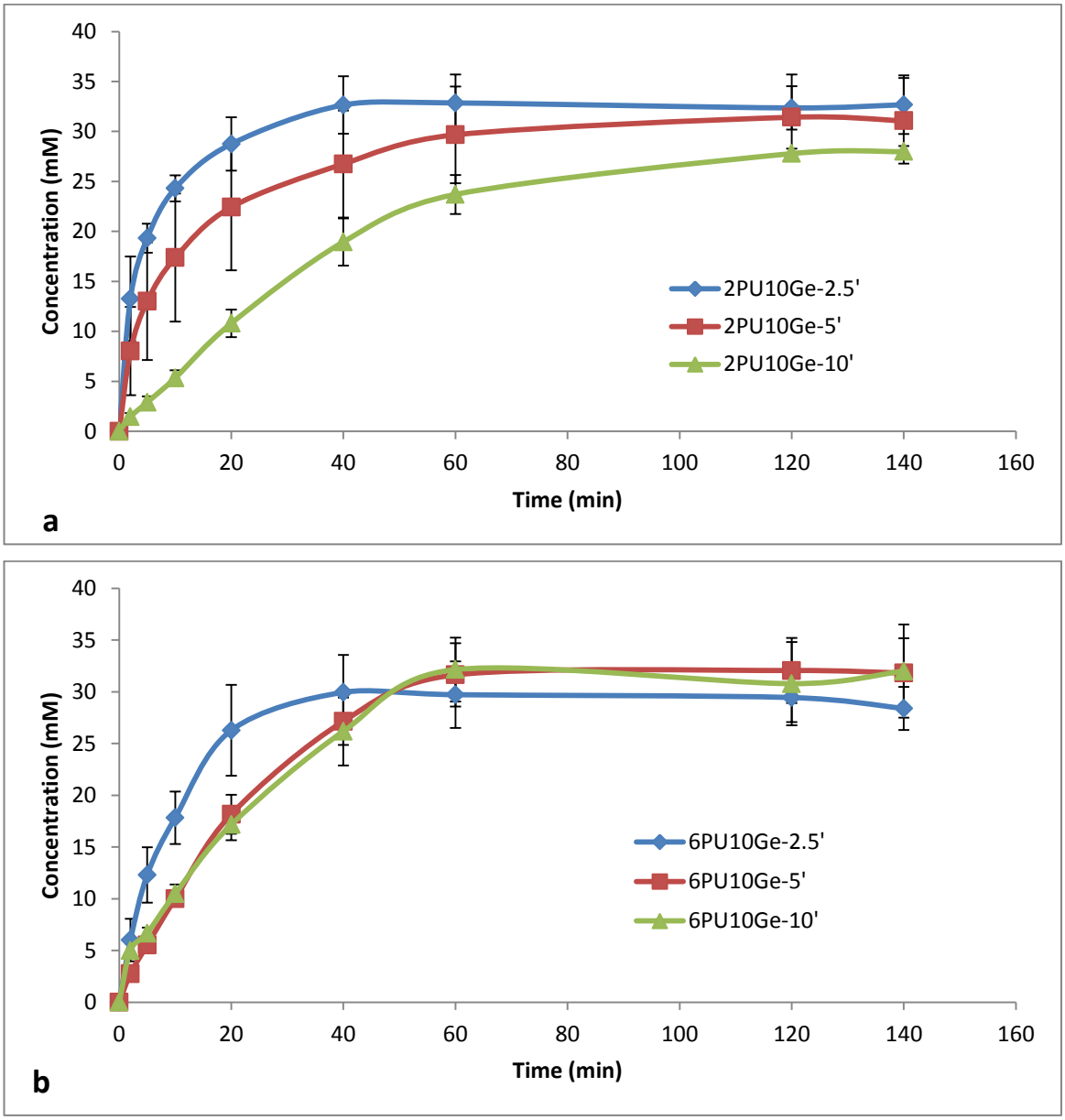

Figure 5.9 Glucose diffusion across a) 2PU10Ge and b) 6PU10Ge membranes as a function of time, and thickness (electrospinning times of 2.5, 5 and 10 min). Data is represented as Mean ± SE of mean, n=5.

Table 5.3 Thickness of coaxial fibre membranes used for diffusion tests, n=5.

Electrospinning Duration (min)	Membrane Thickness (µm)	
	2PU10GE	6PU10GE
2.5	29.6±1.8	35.5±1.5
5	32.7±2.0	44.5±2.2
10	34.9±4.3	37.5±9.7

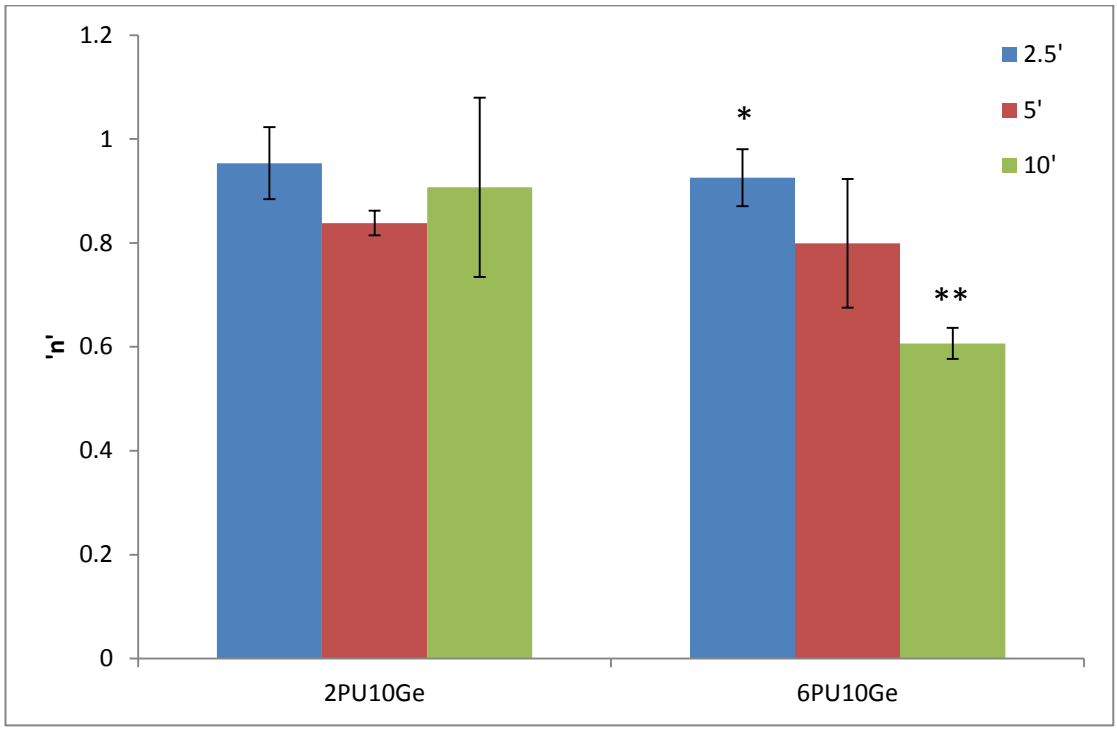

Figure 5.10 Diffusion exponent 'n' values for the different membrane configurations as a function of electrospinning time (thickness). n=5, P<0.05 between * and **.

The diffusion kinetics for the diffusion of glucose across the coaxial fibre membranes was evaluated by fitting the first 60% of the diffusion data until equilibrium was attained in equation 2.4. The resulting diffusion exponent 'n' values for the different coaxial fibre membranes are plotted in Figure 5.10. the 'n' values varied between 0.5 and 1.0 suggesting an anomalous (non-Fickian or polymer relaxation controlled diffusion). No statistical difference was observed for the diffusion exponent 'n' value for the 2PU10GE membranes electrospun for 2.5, 5 and 10 min which can be attributed to their relatively small thickness and high porosity. On the other hand, significant decrease in 'n' value for 6PU10Ge membranes was observed with increasing electrospinning time, the difference statistically significant between 6PU10Ge-2.5' and 6PU10Ge-10', which could be attributed to the decreasing pore volumes as a function of increasing electrospinning time observed as presented in Table 5.2.

5.5.6. Tensile mechanical properties of electrospun coaxial fibre membranes

The typical stress-strain curves for the electrospun coaxial fibre membranes are presented in Figure 5.11. 8PU membrane by itself and dip-coated with Ge were used as controls. All co-axial fibre membranes had their Ge shells crosslinked using GTA vapour for 3 days. On the other hand, the group of 8PU membranes dip-coated with Ge were made by dipping in 10% w/v aqueous solution of Ge, storing them overnight at 4^{o}C for gelation and then crosslinked by dipping in 1% w/v aqueous solution of GTA. All tests were done using samples wetted for overnight prior to testing.

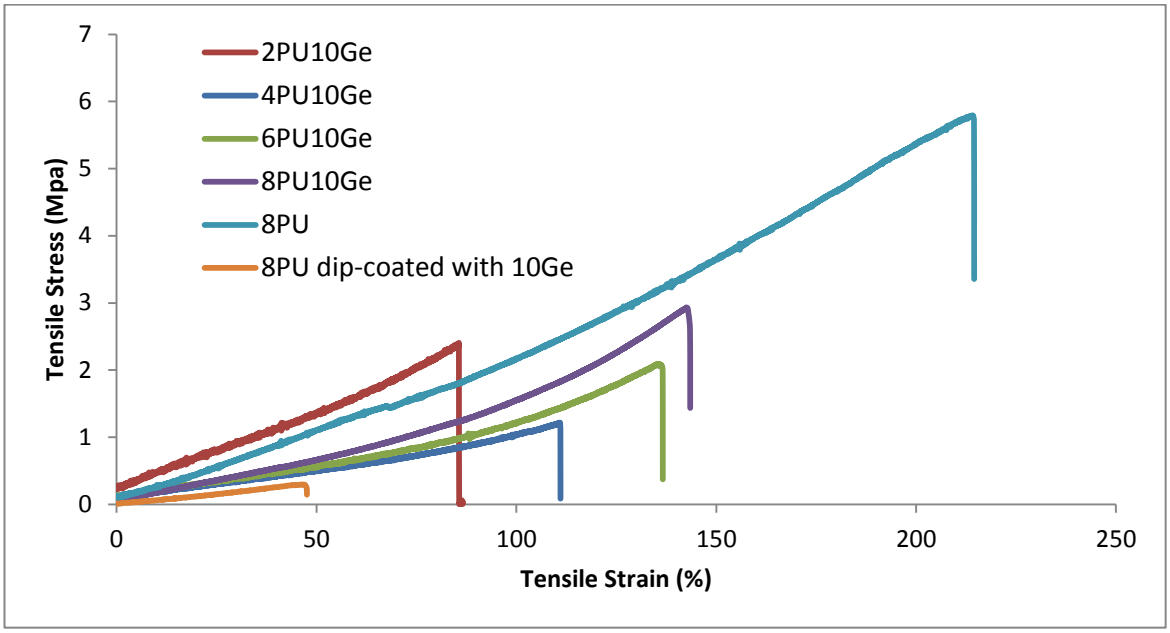

Figure 5.11 Typical stress-strain curves based on uniaxial tensile tests for the different electrospun co-axial fibre membranes compared to that of 8PU and composite membrane composed of 8PU dip-coated with Ge.

The tensile properties and structural composition for the different membranes are presented in Figure 5.12 and Table 5.4 respectively. GE-PU-composite fibrous membranes offered overwhelming advantages in mechanical properties compared to gelatin dip-coated PU membranes shown in Figure 5.11 and Figure 5.12. The substantially high mechanical properties of the co-axial fibrous membranes are a result of the exceptional uniform gelatin-PU mixing at micro- to nano-scale in form of hierarchical structure of core-shell fibrous 3D network, which is hardly achieved through conventional a wet impregnation method (e.g. dip-coating). The cross-section morphology of dip-coated 8PU membrane was observed using both SEM and optical microscope as shown in Figure 5.13. A obvious delamination fracture between Ge and PU in Figure 5.13 clearly exhibited that the gelatin solution did not penetrate into the porous structure due to its high viscosity, and the small

open pore size (~0.84μm) as well as poor compatibility between Ge and PU (e.g. opposite wetting ability proved by the contact angle measurement). Such weak interface adhesion between Ge thin film and PU fibrous membrane plus brittle nature of crosslinked GE accelerated the catastrophic failure of the sandwich structure at a low loading condition. .

Among, electrospun fibrous membranes, the tensile properties for 8PU membranes were significantly higher than that observed for all coaxial fibre membranes, with the exception of the Young's modulus for 2PU10Ge membrane, which was comparable with that of 8PU (Figure 5.11, Figure 5.12 and Table 5.4). Thus the incorporation of Ge as the coaxial-shell for PU in the coaxial fibres significantly reduced their mechanical properties when compared to pure PU fibre membranes. Among the coaxial fibre membranes, the tensile properties improved with increasing core PU content Table 5.4, with the exception of 2PU10Ge, which had significantly higher Young's modulus and lower strain at break. The higher stiffness of 2PU10Ge membranes can be attributed to the increase of fiber-fiber interconnection and the enhanced Young's modulus of individual nanofibre with a smaller diameter owing to more highly ordered chain orientation, which has been reported in a number of papers about other electrospun polymer nanofibrers. (Baji *et al.*, 2010, Wong *et al.*, 2008)

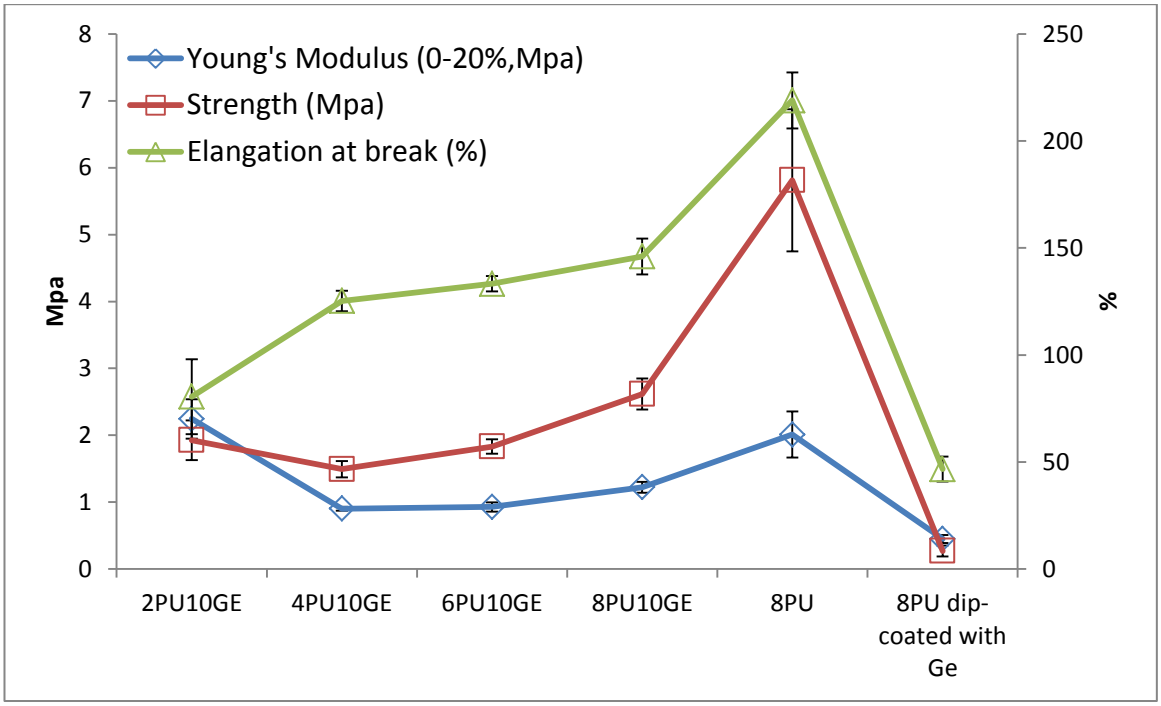

Figure 5.12 Tensile properties of the electrospun coaxial-fibre membranes, n=4. 8PU and composite membrane composed of 8PU dip-coated with Ge were used as controls. (Mean±SE)

The lower strain of 2PU10Ge membranes at break can be due to its larger content of crosslinked Ge shall (~52%), which absorbed high amount of water in wet status and became brittle (Cheng *et al.*, 2003) and the beads on string fibre structure, where in the fibres tend to break at their thinnest diameter.

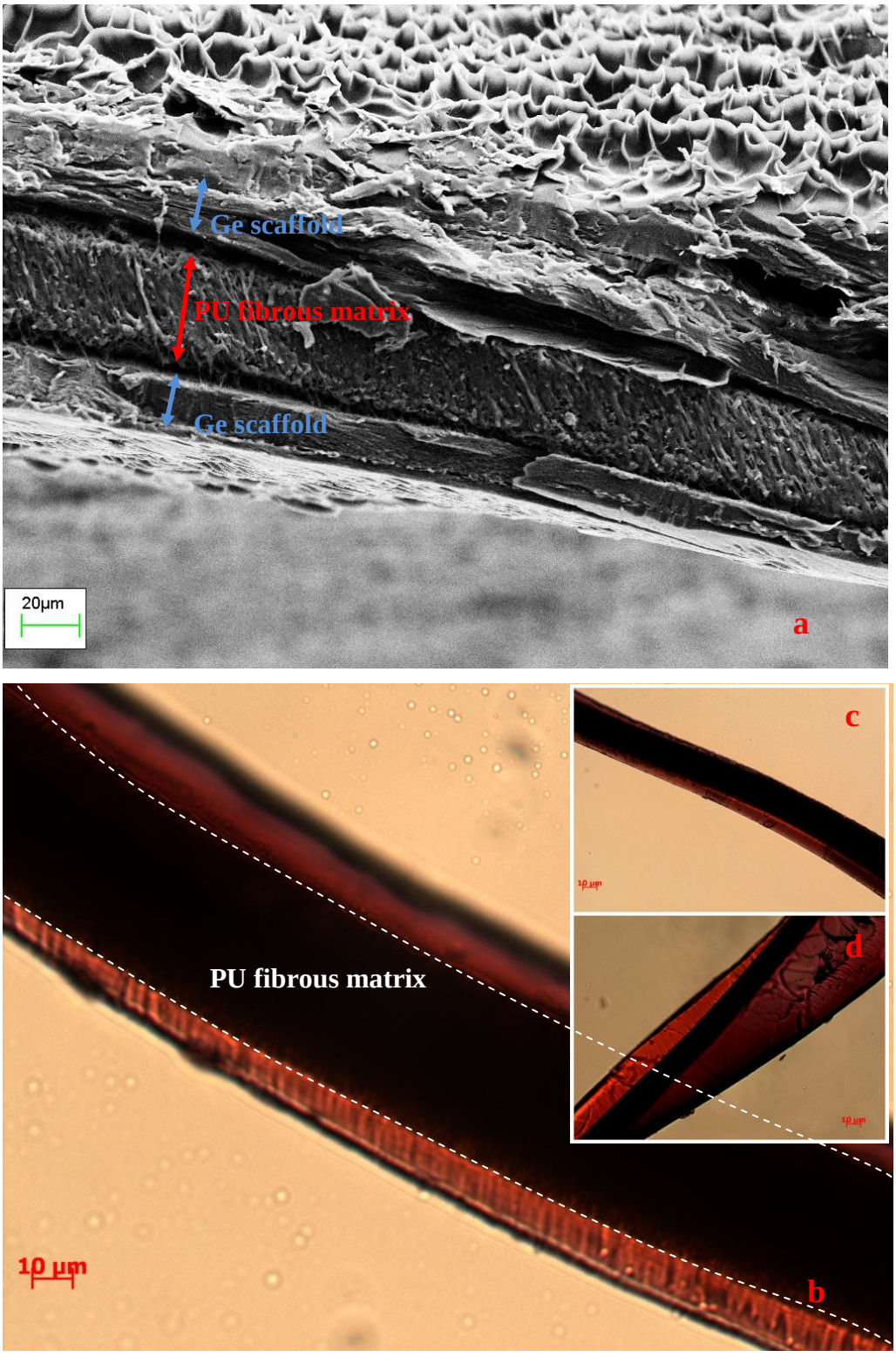

Figure 5.13 Cross-section of the 8PU membrane dip-coated with Ge a) SEM and b) optical microscope images (H&E stained)

Table 5.4 Composition of the membranes (wet) used for uniaxial tensile testing. (Mean±SD)

	8PU	2PU10Ge	4PU10Ge	6PU10 Ge	8PU10 Ge	8PU dip-coated with Ge
Total fibre diameter (nm)	347.6 ± 87.3	540.6 ± 90.8	1044.7 ± 96.5	1152.9 ±128.8	1216.4 ±112.3	-
Core (PU) diameter (nm)	-	-	610.2 ± 74.3	738.2 ± 96.9	899.6 ± 106.7	347.6 ± 87.3
Approx. PU content	100%	48.2%	58.5%	65.5%	73.4%	57.5%
Approx. Porosity	44.2 %	-	57.05±4.58	63.33± 1.34	60.60± 4.74	-
Thickness (μm)	45.0 ± 8.5	37.8 ± 3.4	44.2 ± 13.9	44.1 ± 4.0	79.1 ± 7.4	404.3 ± 117.7
Young's Modulus 0-20% (MPa)	2.3 ± 0.85	2.25±0.59	0.90±0.05	0.93± 0.14	1.22± 0.17	0.45± 0.12
Ultimate Tensile Strength (MPa)	5.8± 2.13	1.92±0.59	1.49±0.24	1.83± 0.21	2.16± 0.46	0.27± 0.16
Strain at Break (%)	191.2 ± 61.10	80.53± 35.05	125.26± 9.63	133.29 ±7.17	136.02 ±16.75	46.7± 11.71

The failure of coaxial fibres, containing Ge shell, under tensile load is said to first start with cracks in the hydrated Ge, which is then translated to the core (Kim *et al.*, 2009, Lu *et al.*, 2009, Han *et al.*, 2008). This presumption was verified by Zhao et al (Zhao *et al.*, 2007b) using SEM showing the cross section of crosslinked gelatin coated PCL fibres after fracture. Therefore, it was concluded that the mechanical properties of the core-shell fibrous membrane mainly dependent on the core synthetic polymer fibres. The increase in tensile stress and strain with increasing synthetic core polymer content was also reported by other researchers (Lu *et al.*, 2009, Heydarkhan-Hagvall *et al.*, 2008, Chen *et al.*, 2010a).

5.5.7. Contact angle

Addition of hydrophilic gelatin to the co-axial fibre structure was expected to increase the hydrophilicity of the electrospun membranes. 2PU10Ge was the only coaxial fibre configuration on which contact angle could be measured (Figure 5.14). The wetting of the coaxial fibres was too quick for contact angle measurements for 4PU10Ge,

6PU10Ge and 8PU10Ge in fact revealing their highly hydrophilic surface. As discussed in Section 3.4.5, the static contact angle measured is determined by the surface chemistry and the surface roughness of the membrane. The smooth surface of the control (GTA crosslinked) Ge solid film had a contact angle of 64^{o} showing the hydrophilicity of essentially nonporous dry Ge surface. Different from the effect of pure PU fibrous membranes on the contact angle, the hydrophilic nature of GE is the predominate parameter to determine the contact angle of the co-axial fibrous membranes with GE as shell, resulting higher hydrophilicity of most of the membranes in spite of the increased roughness of their porous surface with an exception of 2PU10Ge. In contrast, the contact angle of 2PU10Ge (101°) was significantly higher than that observed for other coaxial fibre membranes. Yet its surface was much less hydrophilic, in opposite, highly hydrophobic. This may be reminiscent of "lotus effect" in that the intrinsic hydrophobility of a surface can be enhanced by being textured with different length scale of roughness. The difference can be due to its submicron fibre diameter (~540 nm) that was less than half that of other coaxial fibre membranes and pore size (333 nm in radial) at least 4 times smaller than those micropores of the other coaxial membranes (Section 5.5.4). Such small pores (similar to pure 8PU fibre membrane) would not allow the water droplet to wet the nanostructure space between the nanofibres. This is another evidence that it is possible to achieve a transition between both hydrophobic and hydrophilic regions of a surface by fine-tuning its surface roughness. The massive nano-size pores coupled with the hydrophobic air pockets in the pores at the 2PU10Ge membrane surface can be responsible to the low hydrophilicity in spite of higher Ge content.

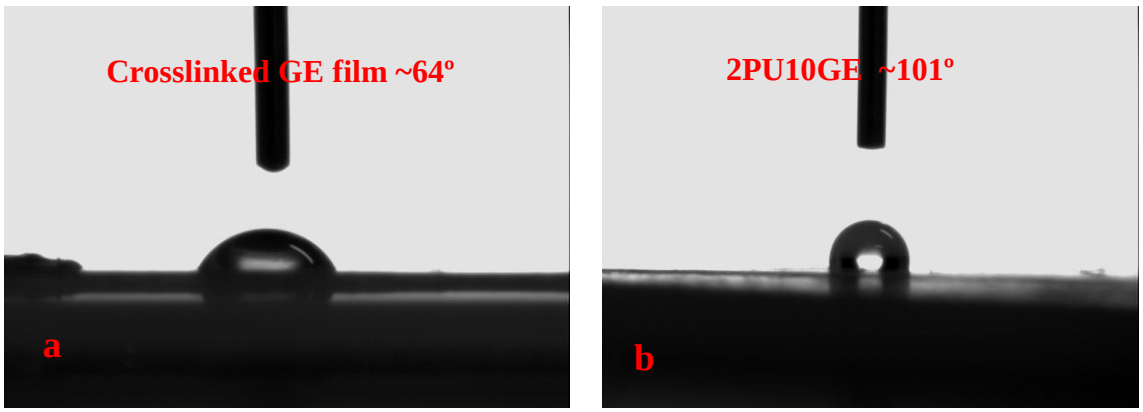

Figure 5.14 The contact angle for a) GTA crosslinked Ge film and b) 2PU10Ge coaxial fibre membrane. The surface wetting for 4PU10Ge, 6PU10Ge and 8PU10Ge membranes was too quick to take any contact angle measurements.

5.6. Efficacy of electrospun coaxial fibre membranes as coatings for implantable coil-type glucose biosensors

The membranes 2PU10Ge and 6PU10Ge were electrospun directly on glucose biosensors using the dynamic collector, wherein the biosensor was rotated at about 660 to 690 rpm in the electrospinning field (Figure 2.4). The parameters are listed in Table 2.2. Briefly, the feed rates for PU and Ge were 0.8 and 1.2 ml/h respectively and the distance between the spinneret tip to sensing element tip was kept constant at 15 cm for both the membranes. The applied voltages used for electrospinning 2PU10Ge and 6PU10Ge were 13.25 and 14 kV respectively.

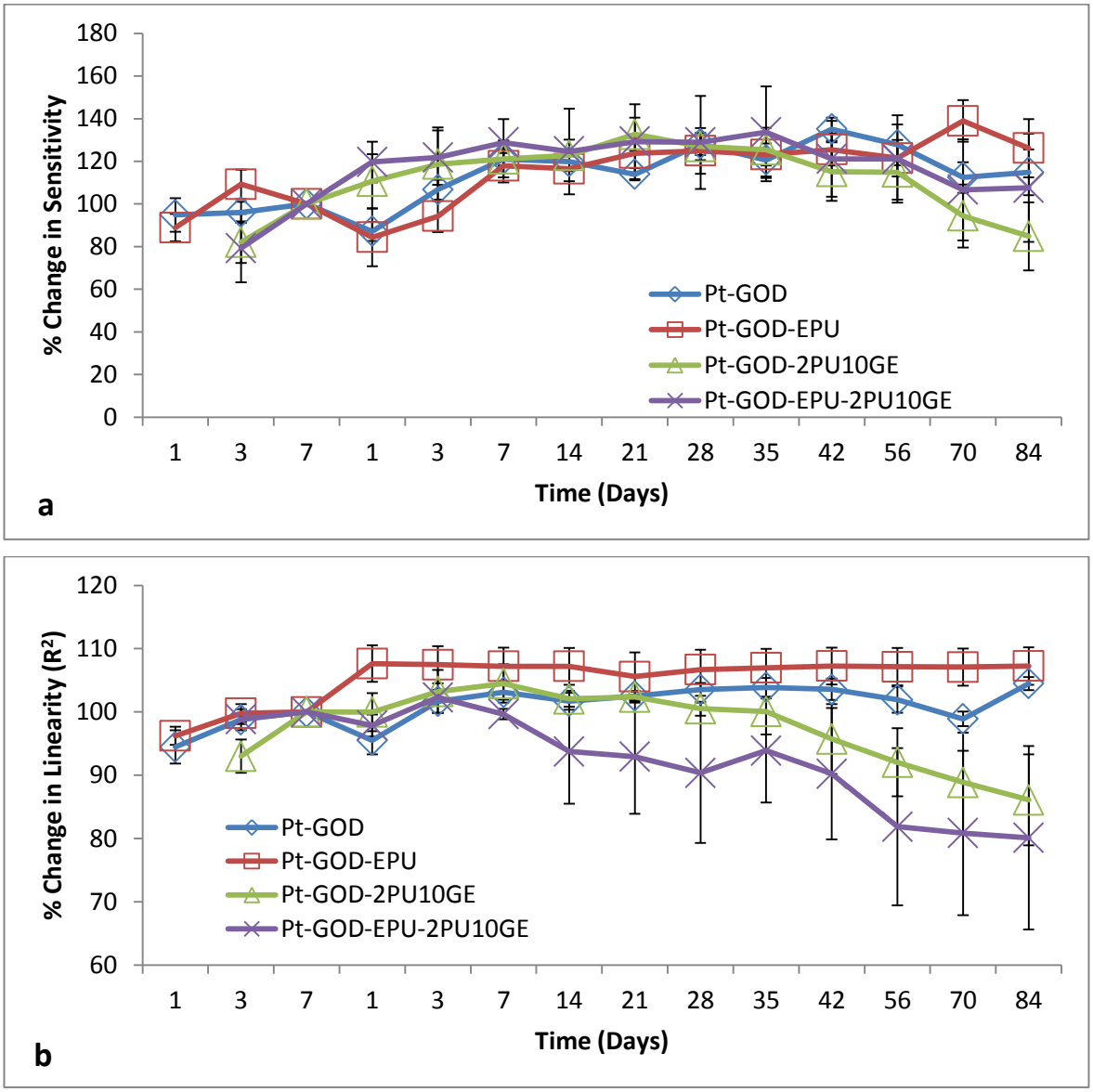

Figure 5.15 Effect of electrospun 2PU10Ge coaxial fibre membranes on the *ex vivo* function coil-type implantable glucose biosensor: a & b % change in sensitivity and linearity normalised to that at day 7 before applying coating(s) as a function of time; and c) the % change in sensitivity and linearity plotted as a function of sensor coating configurations.

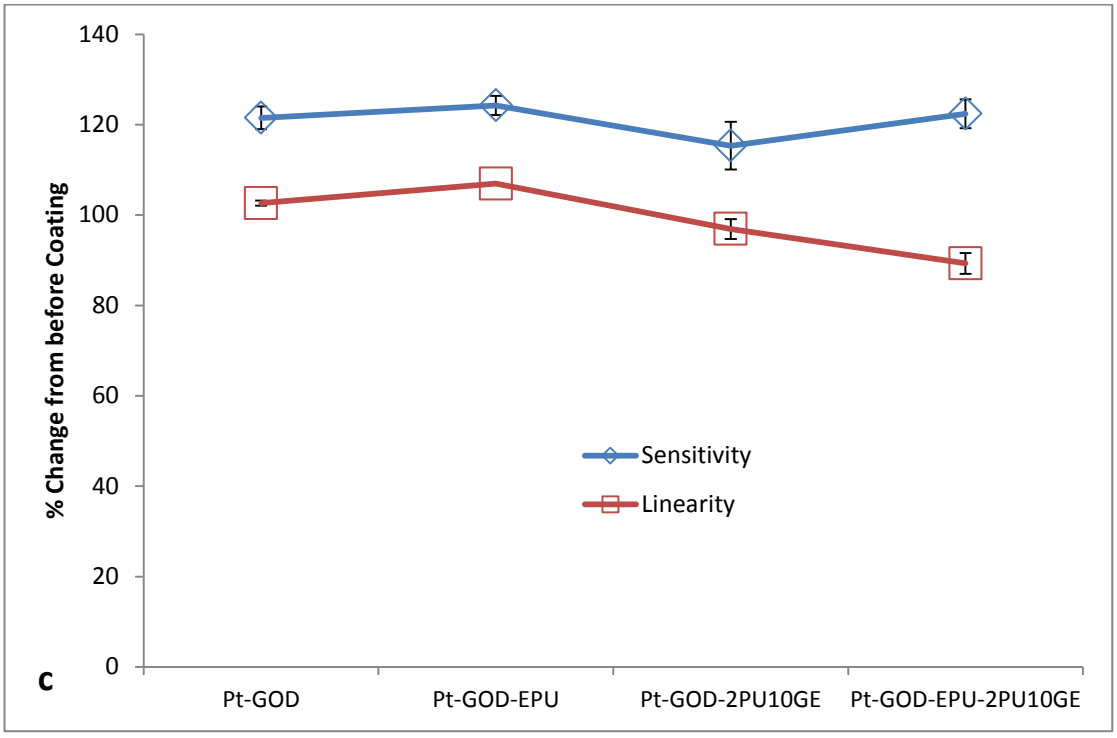

Figure 5.15 (*continued*)

Among 4PU10Ge, 6PU10Ge and 8PU10Ge, the variation in fibre diameters was narrow ranging from 1.04 to 1.22 µm. Coaxial fibre structure was not consistent for 4PU10Ge, while the pore size distribution for 8PU10Ge were broader than both 4PU10Ge and 6PU10Ge. Hence, the 6PU10Ge membrane, having consistent coaxial fibre structure and pore size, was chosen as coating for glucose biosensors. However, for studying the effects of fibre diameter of coaxial fibre membranes on sensor function, 2PU10Ge membrane that has about half the average fibre diameter observed for 6PU10Ge, was also chosen. Effectively, the effects of coaxial fibre membranes on glucose biosensor function were evaluated as a function of fibre diameter and Ge content. 2PU10Ge membrane had an average fibre diameter of 540.61±90.83 and ~51.8% Ge while that for 6PU10Ge was 1152.93±128.77 and ~34.5% respectively.

Each of the coaxial fibre membranes, were tested on sensors with (Pt-GOD-EPU) and without (Pt-GOD) EPU mass-transport limiting membrane. The results were compared with that of Pt-GOD and Pt-GOD-EPU sensors. The sensor function was tested at regular intervals starting one week before applying coatings, to 84 days (12 weeks) after coating. The sensitivity and linearity results at each tested time point were normalized to that at day 7, before applying coatings.

The effect of 2PU10Ge coatings on glucose biosensor function is illustrated in Figure 5.15. The sensitivity profiles for all sensors before and after coating with membranes were similar to that shown by Pt-GOD sensors indicating no obvious effects of either EPU or 2PU10Ge membranes on sensor sensitivity (Figure 5.15a). However, the

linearity (R^2) for the detection range of 2 to 30 mM glucose was only improved EPU membrane, indicating that the 2PU10Ge membranes did not function as a mass transport limiting membrane (Figure 5.15b). Thus, as summarised in Figure 5.15c, 2PU10Ge did not affect sensor sensitivity, but also did not function as mass-transport limiting membrane.

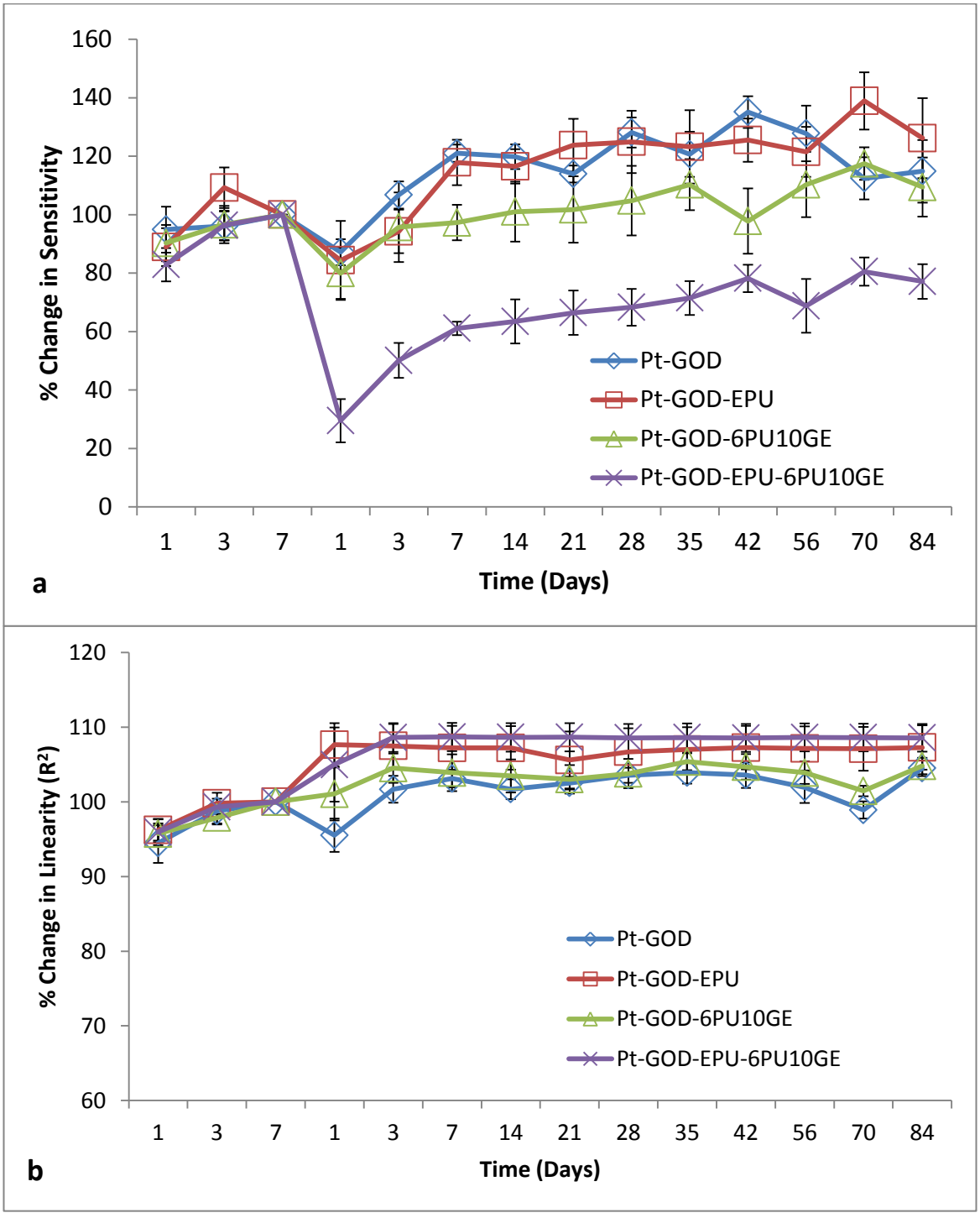

Figure 5.16 Effect of electrospun 6PU10Ge coaxial fibre membranes on the *ex vivo* function coil-type implantable glucose biosensor: a & b % change in sensitivity and linearity normalised to that at day 7 before applying coating(s) as a function of time; and c) the % change in sensitivity and linearity plotted as a function of sensor coating configurations. Each of * and ** indicate statistical difference from all other groups.

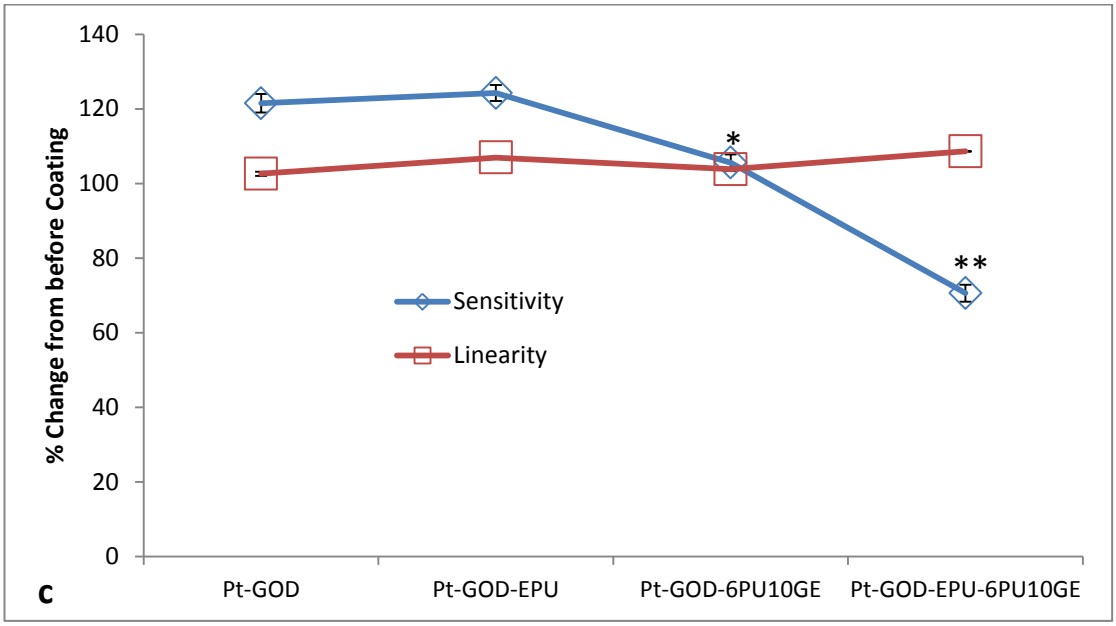

Figure 5.16 (*continued*)

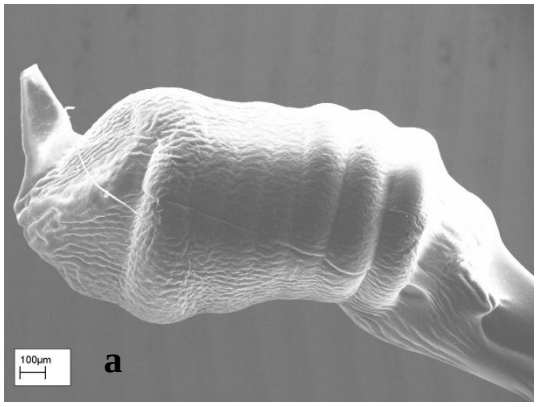

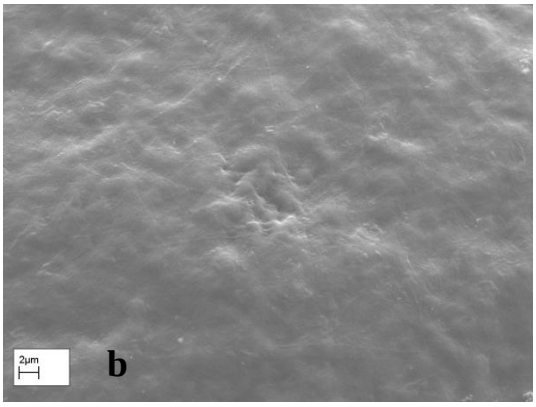

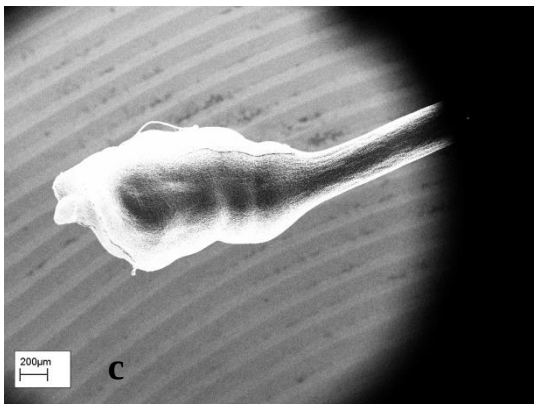

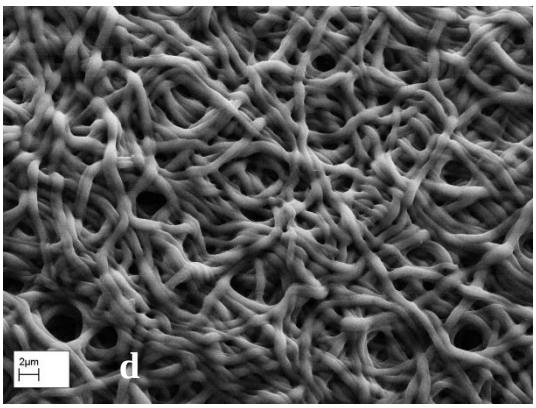

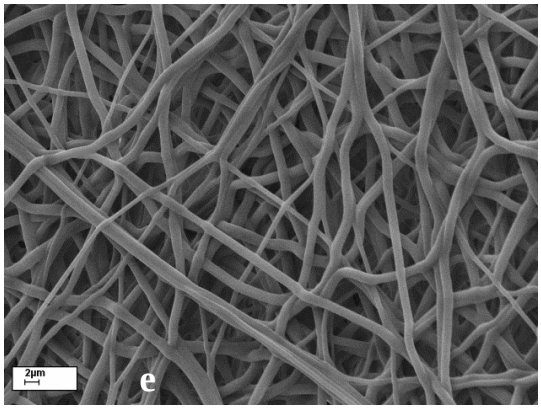

Figure 5.17 The morphology of coaxial fibre membranes after 12 weeks of immersion in PBS 7.4 and intermittent sensor function tests of 2PU10Ge (a&b) and 6PU10Ge (c&d) and 6PU10Ge before testing (e).

Contrary to 2PU10Ge coatings, 6PU10Ge caused a reduction in sensor sensitivity, but extended the linear detection range for glucose biosensors (Figure 5.16). The sensitivity profiles for sensors coated with 6PU10Ge were significantly lower than that of Pt-GOD and Pt-GOD-EPU sensors (Figure 5.16a). However, both EPU and 6PU10Ge membranes extended the linear detection range for Pt-GOD to cove the physiologically relevant detection range of 2 to 30 mM glucose, demonstrating that 6PU10Ge membranes function as a mass transport limiting membrane (Figure 5.16b). The trends in % change in sensitivity and linearity as a function of sensor coating composition further reiterate the above observations (Figure 5.16c).

5.6.1. Long-term stability of sensor function for glucose biosensors coated with coaxial fibre membranes

The sensitivity of sensors coated with both 2PU10Ge and 6PU10Ge was stable until the end of study at 12 weeks. However, a decrease in linearity for 2PU10Ge coated Pt-GOD and Pt-GODEPU sensors was observed. To identify the cause for this unexpected decrease in linearity, the morphology of the sensors after completion of the study was assessed under SEM. As shown in Figure 5.17a&b, the integrity of the membrane was disrupted, and 2PU10Ge membrane has changed its structure from fine fibro-porous architecture to a more or less like fibre-reinforced composite membrane. The swelling (especially from Ge), fusion and finally agglomeration of nano fibres in the 3D-network and resulting disruption of non-uniform micro-porous structure (pore size >300 nm) to that of a diffusion controlled nano porosity, could be responsible for the decrease in linearity. On the other hand, the fibro-porous structure of 6PU10Ge membranes showed relatively less fusion and intact fibre structure even after 12 weeks of immersion in PBS at 37^{o}C and intermittent sensor-function tests (Figure 5.17c&d).

5.7. Conclusion

The solvent, solution concentration and process parameters for electrospinning PU-core and Ge-Shell coaxial fibre membranes were optimized. To make electrospinning possible, both PU and Ge were required to be dissolved in highly polar TFE solvent. Due to the low solubility of PU in TFE, solution concentrations appropriate for comparison with that used for electrospinning PU solutions in THF-DMF was not possible. Hence, for electrospinning of co-axial fibre membranes, the Ge solution concentration was kept constant while varying PU solution concentrations. It was observed that 6% PU and 10% GE solution concentrations provided the optimum coaxial fibre membranes, while having the spinneret to collector distance at 15 cm, applied voltage of 14kV and respective flow

rates for PU and Ge feed solutions of 0.8 and 1.2 respectively. With increasing feed solution concentration, an increase in the diameter of PU core, with concomitant reduction in Ge shell thickness was demonstrated. To maintain the coaxial fibre structure crosslinking of Ge shell layer was essential, which was achieved by incubating as-spun membranes in GTA vapour saturated atmosphere. The coaxial fibre structure was achieved, but the overall fibre diameter did not increase linearly with increasing core PU content.

2PU10Ge had an overall diameter of about 0.545 µm, while that of 4PU10Ge, 6PU10Ge and 8PU10Ge membranes varied from 1.04 to 1.22 µm. Mechanical properties of the coaxial fibre membranes decreased with decreasing PU core content, which is due to the increasing brittle crosslinked Ge shell content in the coaxial fibres. However, the Ge-shell of micro-scale fibres content in the membranes made their surfaces very hydrophilic, such that the surface wetting was too fast to obtain any measurements of the contact angle for a water droplet on membrane surface. On the other hand, nano-scale porous structure of 2PU10Ge membrane could transfer the membrane surface into more hydrophobic. The diffusion kinetics for glucose across 2PU10Ge membranes was near zero order, while that across 6PU10Ge was anomalous or non-Fickian, which tended to shift towards Fickian diffusion with increasing membrane thickness. The porosity was relatively low, while fibre packing densities were high for the coaxial fibre membrane for their higher fibre diameters. As coatings for coil-type implantable glucose biosensors, *ex vivo* sensor tests showed 2PU10Ge membranes having submicron fibre diameter and about 50% Ge do not cause any decrease in sensitivity. However, they did not function as mass-transport limiting membranes. In contrast, 6PU10Ge membranes reduced sensor sensitivities, but functioned as mass-transport limiting membrane. In conclusion, a method was optimised for electrospinning coaxial fibre membranes, the membranes were shown to have mechanical properties better than soft tissues, and their effects on *ex vivo* sensor function can be controlled. Overall, the PU-core and Ge-shell coaxial fibre membranes coatings can play an important role in engineering tissue responses to the implanted biosensors.

Chapter 6 Pilot Biocompatibility and *In Vivo* Sensor Function Assessments in Rat Subcutaneous Implantation Model

6.1. Introduction

Electrospun membranes mimic the natural extracellular matrix (ECM) in its fibro-porous structure and highly interconnected porosity. Irrespective of how closely they match the 3D architecture and mechanical properties of ECM, the electrospun membranes are foreign bodies when implanted. As a result, the body works towards degrading and eliminating the implant from the body. For the current application, electrospun materials were intended for use as membranes and tissue engineering scaffolds. The former use requires sub-micron porosity while that of latter requires about 3 to 10 µm interconnected pore sizes for cells to infiltrate the scaffolds. Depending on porosity and composition, the tissue responses to implants vary for different scaffolds. In this direction, the fibre diameter, porosity and composition of the electrospun membranes were varied to assess not only their effects on host tissue responses but also for sensor function when implanted as sheets or as coatings on biosensors in the body.

The objective for this chapter was the pilot evaluation of biocompatibility and *in vivo* sensor function in a rat subcutaneous implantation model for selected electrospun membrane configurations optimized in this work. The membranes 8PU, 12PU and 6PU10Ge were chosen for the biocompatibility assessment, while using solvent cast non-porous PU film was the control. They were implanted in the subcutaneous space under the dorsal skin of rats. Two time points, namely 4 and 9 weeks were chosen and the number of scaffolds implanted for each membrane configuration was 3 per time point. At the end of each time point, the rats were killed and the implant and its surrounding tissue was harvested and processed for histology. Qualitative examination of tissue responses to each of the membrane variables was carried out on the histology sections. Further, for the assessment of effects of electrospun coatings on sensor function, four different coating configurations, namely 8PU-12PU, EPU-12PU, EPU-6PU10Ge and EPU (alone as the control) were chosen. The changes in sensitivity as a function of time and in response time of the implanted sensors were evaluated.

6.2. Biocompatibility of electrospun membranes

Subcutaneous space was chosen for biocompatibility assessment because it was the target tissue site for implantation of glucose biosensors, and rats were chosen because they are one of the most commonly used mammalian model for such studies. The membranes

were implanted under the dorsal skin on either side of the dorsal midline, to prevent the rats from accessing the implant sites and disturbing the sutures.

The different electrospun membranes prepared in this work, had fibre diameters ranging between 0.2 and 1.2 μm, and pore sizes between 0.5 and 3.0 μm. They were intended for use as mass-transport limiting membranes on glucose biosensors. Since they have pore sizes <3.0 μm, host cells were not expected to infiltrate into their porous bulk. However, because they are intended for use as coatings for implantable biosensors, it was essential to assess the nature of tissue responses they induce when implanted in the body.

8PU and 12PU membranes had average fibre diameters of 0.347 and 1.102 μm respectively, while the coaxial fibre membrane, 6PU10Ge, had fibre diameter of 1.15 μm. In addition, the crosslinked Ge shell of 6PU10Ge, due to the inherent bioactivity of Ge, was expected to modify the nature of the host tissue responses. The spread of diameters and composition (single/coaxial) also ensured a wider variation in pore sizes, contact angles (hydrophilicity), surface porosity and mechanical properties (Table 6.1) as discussed in Chapters 3 and 5. The flexibility of the membranes increased with increasing PU content, such that 6PU10Ge was the stiffest (due to its crosslinked Ge shell) and non-porous PU film the most flexible membrane (Table 6.1). The physical appearance of the different scaffolds implanted in rats is shown in Figure 6.1. In addition, the degree of wetting of the scaffolds can also be visualised in Figure 6.1b, which decreased with decreasing fibre diameter among electrospun membranes (Figure 6.1b, Table 6.1) in agreement with the results of contact angle measurements discussed in Sections 3.4.6 and 5.5.7.

Table 6.1 Properties of the electrospun membranes implanted in the subcutaneous space in rats. Non-porous solvent cast PU film was used as the control.

	8PU	**12PU**	**6PU10Ge**	**PU film**
Fibre diameter (μm)	0.347 ± 0.087	1.102 ± 0.210	1.15±0.13	-
Thickness (μm)	23.5± 4.8	133.0± 28.3	44.5±2.2	71.6 ± 16.8
Pore Volume (%)	44.19± 2.54	65.40± 1.85	63.33±1.34	-
Pore Size (μm)	0.80	1.06	1.54	-
Contact angle	104.3°	122.5°	0^{o}	86^{o}
Young's Modulus (MPa)	2.3 ± 0.85	0.97 ± 0.049	0.93 ± 0.14	2.8 ± 0.43
UTS (MPa)	5.8± 2.13	3.1 ± 0.06	1.83 ± 0.22	8.1 ± 2.00
Strain at Break (%)	191.2 ± 61.10	261.0 ± 12.09	133.29 ± 7.17	849.7 ± 258.8

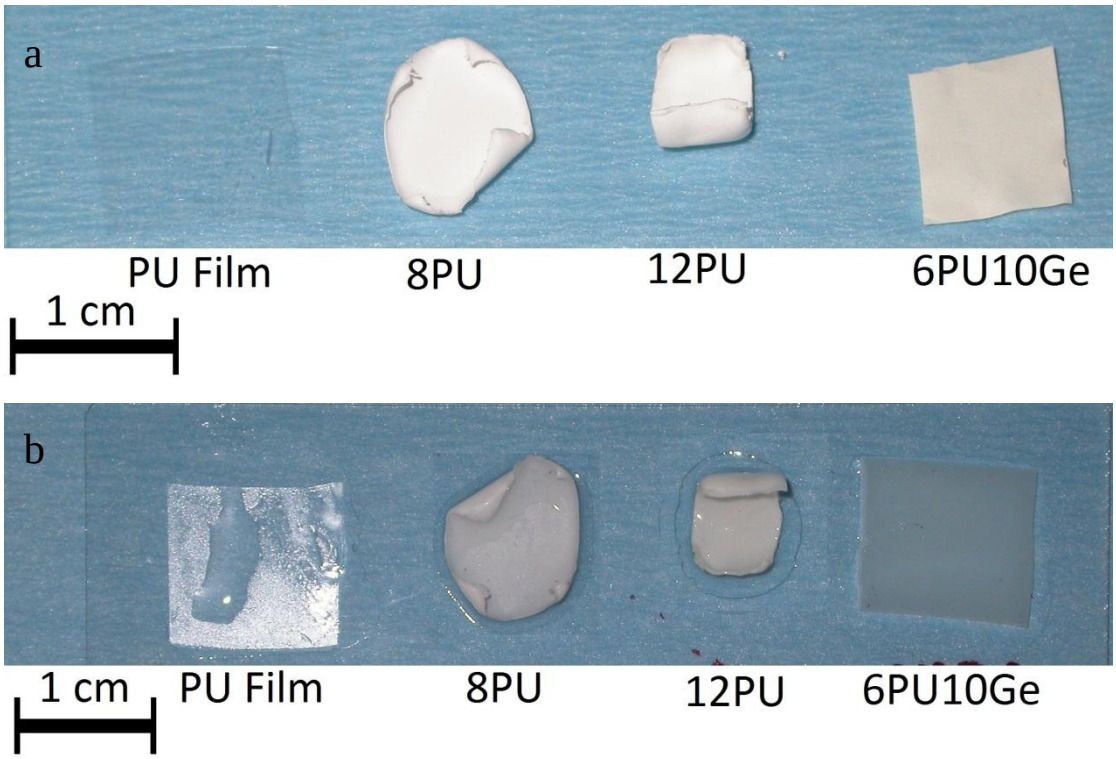

Figure 6.1 Photographs showing the physical appearance, shape (a) and wetting (b) of the different scaffolds used for implant in the subcutaneous implantation in the body.

6.2.1. Gross morphology

Following surgery, all rats recovered normally and survived the duration of the experiments. The incision and implant sites did not show any ulceration, pus, discharge or infection. No obvious swelling of the implants sites was visible. At the end of 4 and 9 week time periods, when the implant sites were accessed, all scaffolds were present and maintained their integrity.

6.2.2. Histopathology

Histologically, all the scaffolds were intact until the end of study at 9 weeks. Host cell infiltration into the bulk of the scaffold was only observed with 6PU10Ge scaffolds, while were restricted to the surface of the implants for PU film, 8PU and 12PU membranes.

The subcutaneous tissue is made of loose collagenous connective tissue, primarily containing fibroblasts and blood vessels, labelled in the Figure 6.2 to Figure 6.5 as native fibrous tissue (NF). With aging the composition of NF changes through deposition of fat cells, making it adipose connective tissue (labelled in the figures as A). When a foreign body is introduced into the subcutaneous connective tissue, it sets off a series of foreign body reactions starting with haemostasis (min) and acute inflammation (2 days), followed

by deposition of granulation tissue (1 to 2 week), which usually turn into a fibrous capsule (>2 weeks) (labelled in the figures as F).

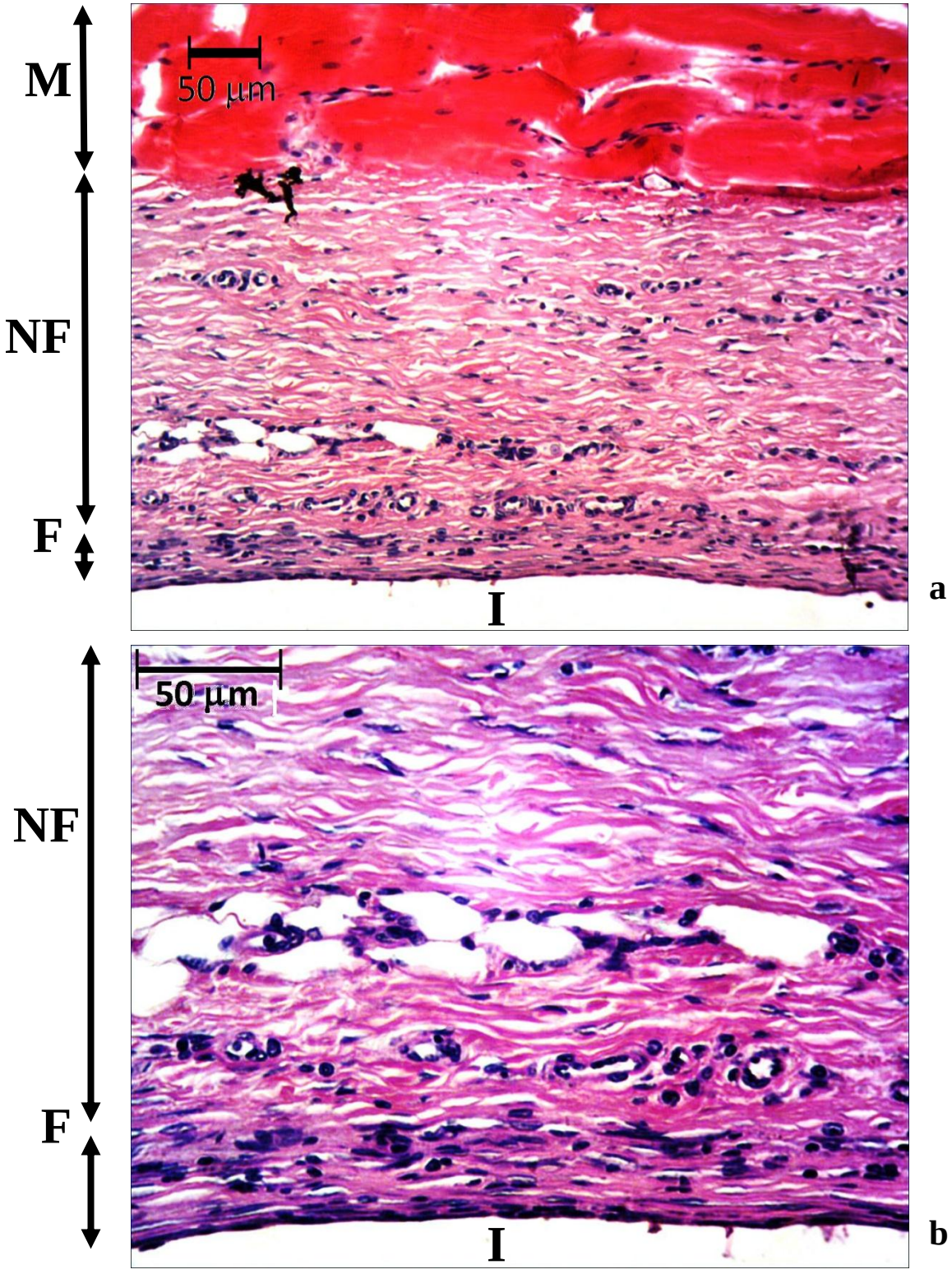

Figure 6.2 Light microscopy images showing haematoxylin and eosin (H&E) stained subcutaneous tissue above the PU film implant following 4 weeks of implantation (a) and its magnified section (b) and 9 (c), where M is subcutaneous smooth muscle, NF is native fibrous tissue, F is fibrous tissue (capsule) surrounding the implant I.

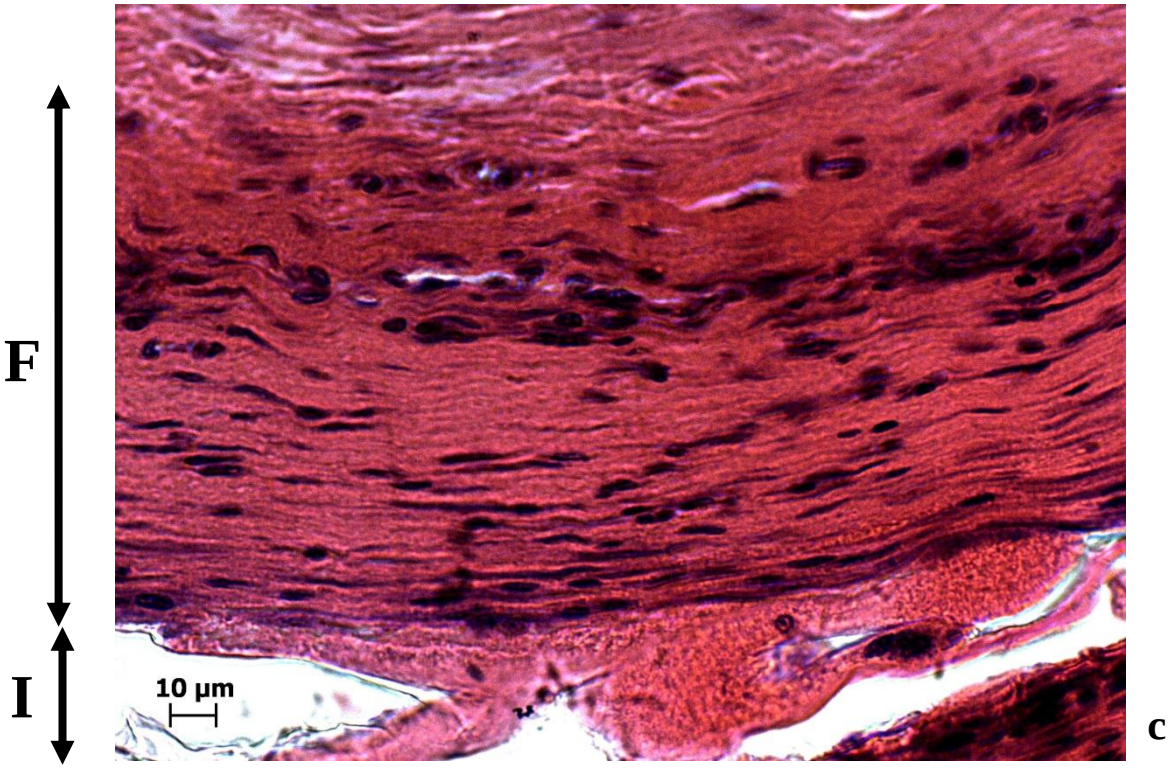

Figure 6.2 (*continued*)

Figure 6.2 shows the histology of subcutaneous tissue structure on the non-porous PU implant surface, following 4 weeks of implantation. The layered subcutaneous tissue is composed of the subcutaneous smooth muscle (M), the native fibrous tissue (NF) and the fibrous tissue surrounding the implant (F). The fibrous tissue surrounding the PU film (F) as shown in Fig 6.2 was composed of a thin inner cell layer (on immediate surface of the implant) and a thicker outer dense fibrous tissue having collagen fibres oriented parallel to the surface of the implant (I). At 4 weeks, the former for PU film implant was about 3 cells thick, while the later was between 10 and 40 µm thick. The cells in the cell layer were also compressed into spindle shaped structure similar to fibroblasts. This layer decreased to about 1 cell thick by 9 weeks after implantation. The overlying dense fibrous tissue, on the other hand, increased in thickness for up to about 100 µm. Furthermore, the cells in the fibrous tissue were primarily fibroblasts (spindle shaped cells each with a oval shaped active nucleus) at 4 weeks while that at 9 weeks was changing into fibrocytes (inactive fibroblasts, containing thin and long nucleus having inactive condensed genetic material) making this layer a mature avascular fibrous capsule. No immune cells were observed in the fibrous tissue surrounding the PU films, indicating the inert nature of the PU material.

The electrospinning introduced fibro-porous structures in the 8PU and the 12PU membranes. However, when they were implanted in the body, their pore sizes were too low (<2 µm) to allow infiltration of cells into the bulk of the membranes. As a result, the

nature of tissue response for both 8PU and 10PU was similar to that observed for non-porous PU film at both 4 and 9 weeks after implantation (Figure 6.3and Figure 6.4).

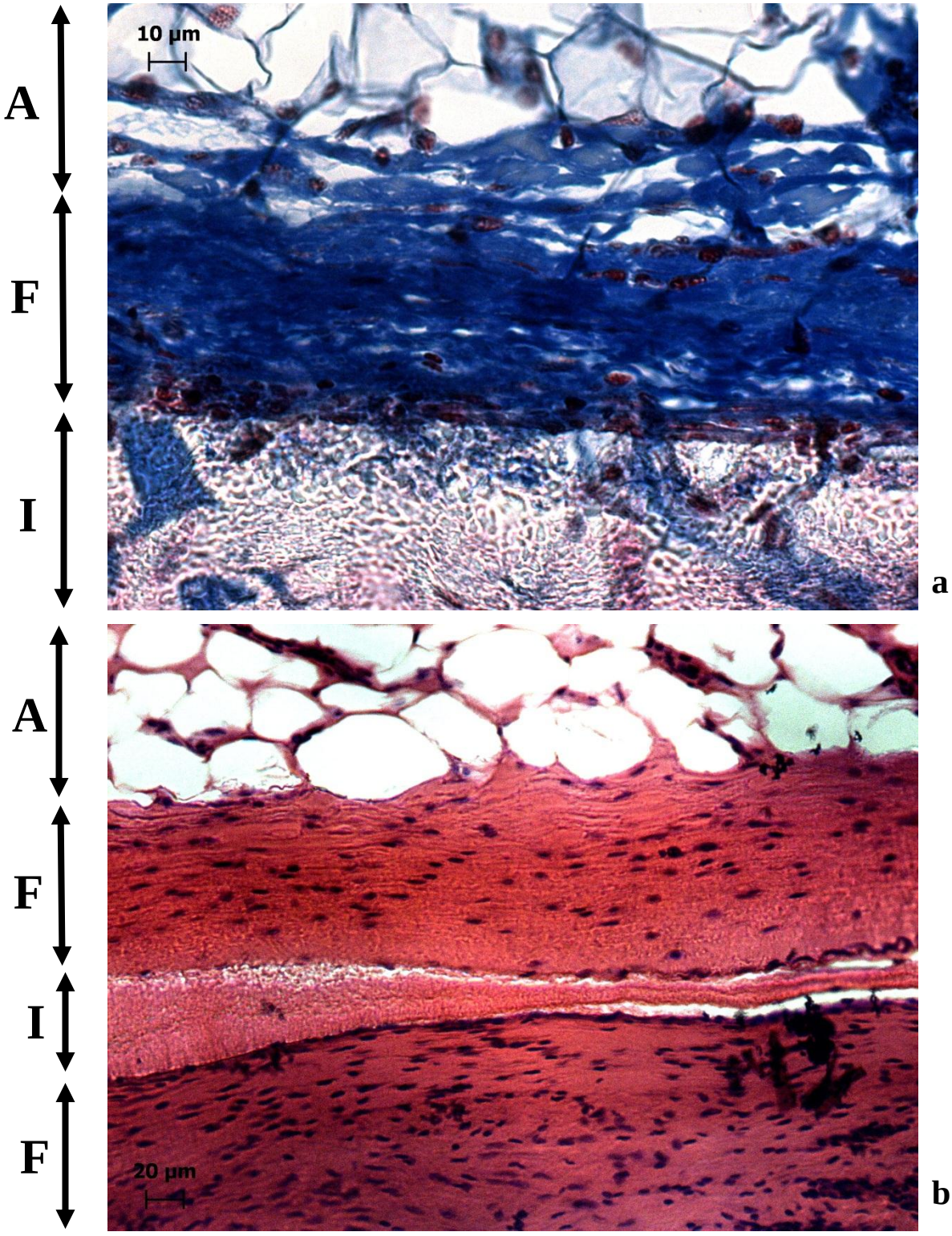

Figure 6.3 Light microscopy images showing the tissue-implant interface for 8PU membranes at a) 4 weeks (Mason's Trichrome (MT) stained) and b) 9 weeks (H&E stained) of implantation, where A is subcutaneous fat (adipose), C the cell layer, F is fibrous tissue (capsule) surrounding the implant I.

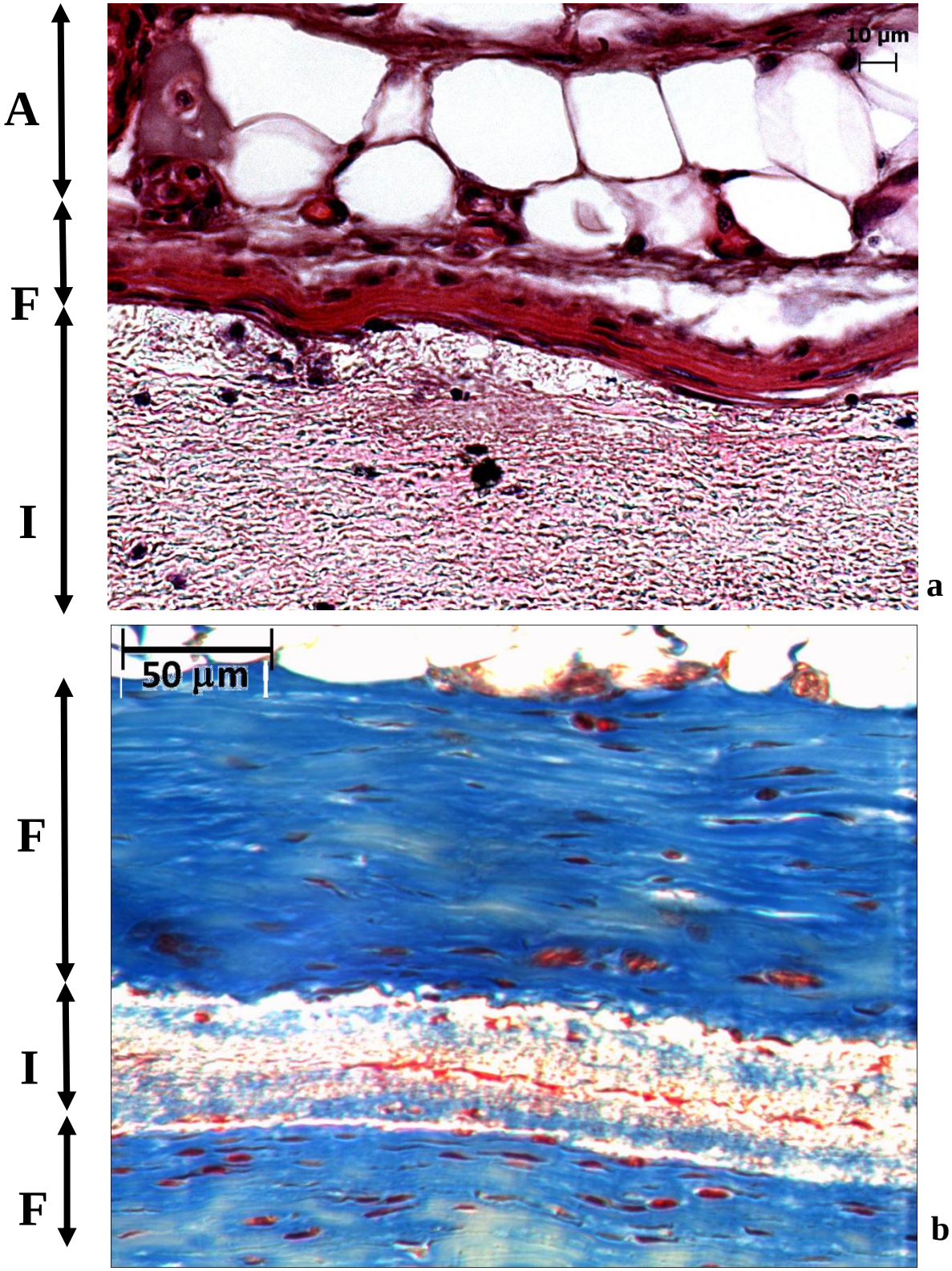

Figure 6.4 Light microscopy images showing the tissue-implant interface for 12PU membranes at a) 4 weeks (H&E stained) and b) 9 weeks (MT stained) after implantation, where A is subcutaneous fat (adipose), F is fibrous tissue (capsule) surrounding the implant I.

However, it is interesting to note that 6PU10Ge membranes, in spite of having very low pre-implantation pore sizes (<2 µm), were completely infiltrated with host cells Figure

6.5. This also ensured the prevention of dense avascular fibrous capsule on the surface of the implanted 6PU10Ge membrane. This phenomenon is clearly due the introduction of bioactive Ge in the electrospun coaxial fibre structure.

The Ge-shell of the coaxial fibres of 6PU10Ge membranes has inherent cell adhesion receptors that aid in the infiltration of the cells into the core of the membrane. Furthermore, Ge being the natural extracellular matrix derivative is susceptible to enzymatic degradation, and its resorption would make the thin PU cores discreet and flexible allowing movement of cells within the scaffold. The tiny darkly stained circular structures within the scaffold indicate cells attached to the individual electrospun fibres along the fibre axis. Such cell adhesion to fibres also indicates that the cells are fibroblasts. Occasional presence of larger cells within the scaffold was also observed indicating the infiltration of larger cells (≥10 μm) through displacement of flexible fibres.

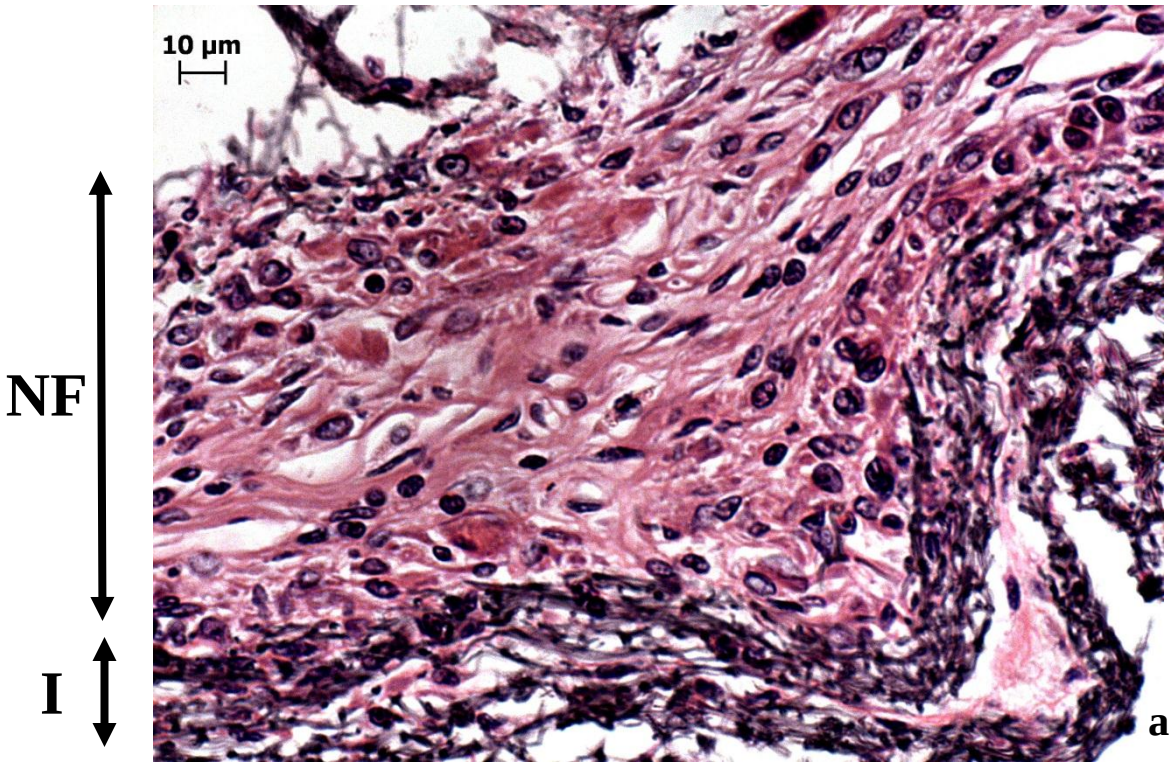

Figure 6.5 Light microscopy images showing the implant sites for 6PU10Ge a) H&E and b) MT stained sections at 4 weeks after implantation and c) MT stained section at 9 weeks after implantation, where NF is the native fibrous tissue structure, and I the implant.

The immediate surface of the host cell infiltrated 6PU10Ge membrane, unlike that of 8PU and 12PU, was not covered by dense fibrous encapsulation. It was composed of loose connective tissue similar to that of native fibrous tissue. However, the cell content in this layer is significantly higher. The cells in this layer were primarily macrophages

indicative of active resorption of Ge (Fig 6.5a). Some lymphocytes were also observed indicating mild immune response to Ge, which could further accelerate resorption of Ge.

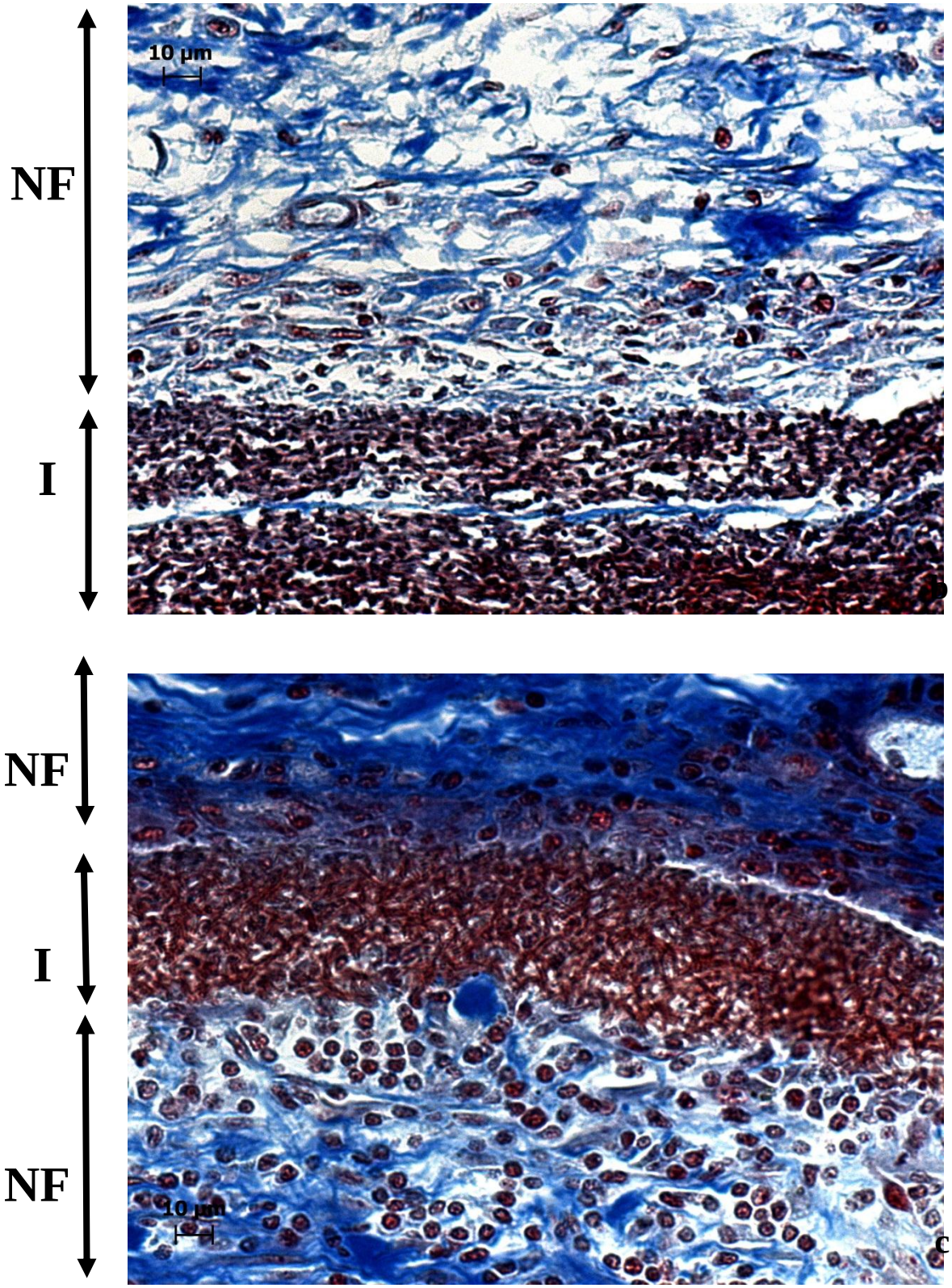

Figure 6.5 (*continued*)

The blue staining in the MT stained histology sections is collagen. At 4 weeks, hardly any blue staining was seen within the 6PU10Ge scaffold indicating minimal collagen deposition in the bulk of the scaffold. However, by 9 weeks a well organised

collagen network was seen indicating remodelled tissue integrating the electrospun membrane with the host tissue. Essentially, a composite sheet made of electrospun fibres interpenetrating with collagen was engineered, using 6PU10Ge membrane in the subcutaneous tissue of rat, which demonstrates that tissue responses to synthetic scaffolds can be engineered.

6.3. Effect of electrospun membranes on the function of implanted glucose biosensors

In a pilot study, sensor configurations Pt-GOD-8PU-12PU, Pt-GOD-EPU-12PU, Pt-GOD-EPU-6PU10Ge and Pt-GOD-EPU implanted in the rat subcutaneous tissue evaluated the effects of electrospun membranes on function of implanted glucose biosensors. *In vivo* sensor function tests were done using a glucose tolerance test and compared with their pre-implantation sensitivity. The tests were done at 1, 3 and 9 weeks after implantation. An example of a typical response current curve for an implanted sensor as a function of time is shown in Figure 6.6. The data plot also shows the corresponding change in blood glucose levels measured using a commercial glucose monitor - Freestyle Lite. The sensor response delay for the coil-type glucose biosensor implanted in the subcutaneous tissue of rat was calculated in comparison to changes of glucose level in blood as indicated in Figure 6.6.

6.3.1. Sensor Response Delay

The time taken for the glucose biosensors implanted in the subcutaneous tissue to respond to the high dose of glucose injected in the peritoneum was compared with that in blood. The effect of different coating configurations on sensor response delay plotted in Figure 6.7. At week 1 after implantation, Pt-GOD-8PU-12PU sensors showed the fastest response to glucose, which was <10 min, followed by Pt-GOD-EPU-6PU10Ge and then Pt-GOD-EPU-12PU. The control sensor Pt-GOD-EPU showed the slowest response time of about 15 min. By 3 weeks of implantation, Pt-GOD-EPU sensors showed the fastest response time, while the trend for other sensors with electrospun coatings remained the same. Moreover, the response times for all sensors coated with electrospun membranes significantly increased compared to that at week 1. The trend at week 9 was comparable with that at week 3, except that the sensor Pt-GOD-EPU-6PU10Ge showed a significant decrease in sensor response time. This decrease resulted in its sensor response time is in par with that of the control sensor Pt-GOD-EPU. The changes in response times could be indicative of the nature of changes in composition of tissue at the sensor tissue interface.

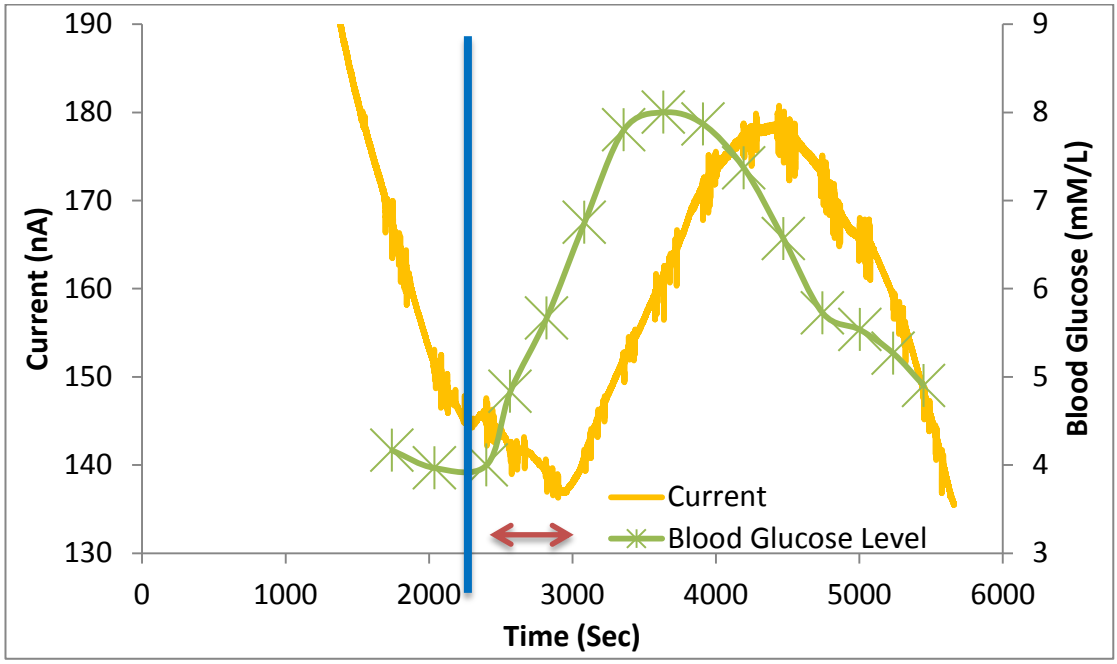

Figure 6.6 The typical sensor response current vs time plot of an implanted sensor and the corresponding change in blood glucose levels measured using a commercial blood glucose monitor. The blue line indicates time of injection of a high dose of glucose in the peritoneum. The sensor response delay for the coil-type glucose biosensor implanted in subcutaneous tissue compared to the corresponding change in blood glucose level is indicated by the double end arrow.

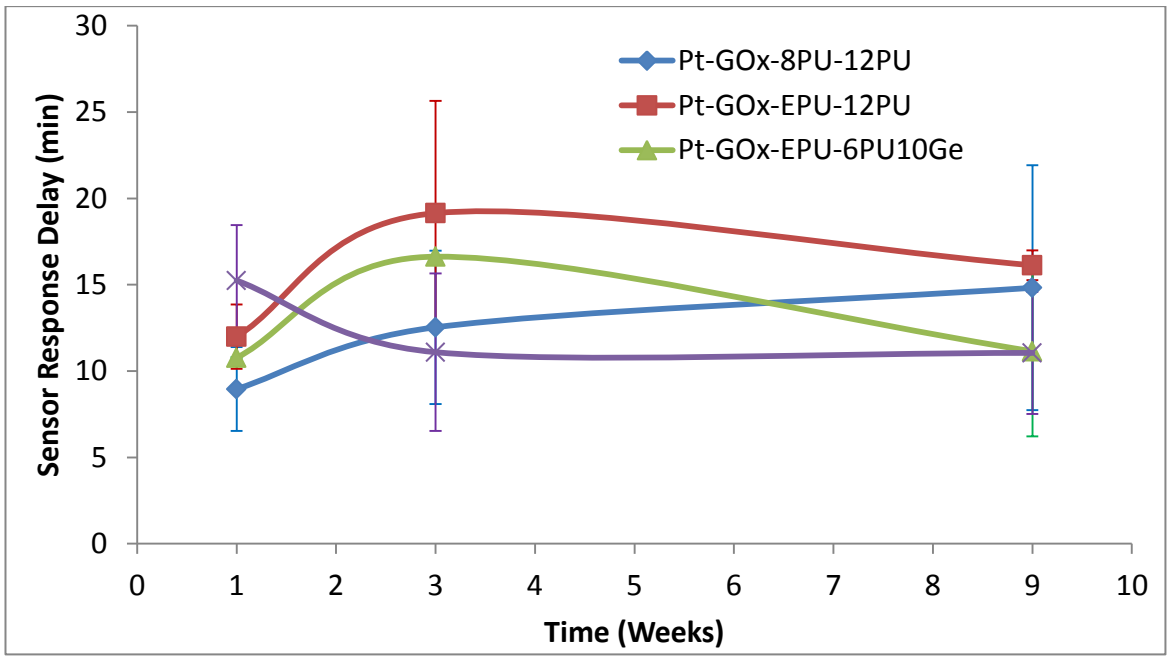

Figure 6.7 Delay in response to sensing glucose in interstitial fluid for coil-type glucose biosensors implanted in the subcutaneous tissue in relation change in blood glucose levels as a function of sensor coating configurations.

The macro-porosity of the electrospun membranes at week 1 could be responsible for their better permeability to glucose and hence faster response time. However, at week 3, the tissue build-up at their surface could be responsible for the significant increase in sensor response delay time. In contrast, the control Pt-GOD-EPU sensor showed initial slower response to glucose which could be due to poor wetting of its relatively hydrophilic surface, compare to the fluid filled pores of electrospun membranes. The wetting could have improved with deposition of snugly fit host tissue on the EPU membrane surface, thus lowering the sensor response time thereafter. The sensor response time for Pt-GOD-EPU-6PU10Ge decreasing to the level observed with Pt-GOD-EPU control sensor could be due to the resorption of Ge-shell and the establishment of stable collagenous connective tissue integrating 6PU10Ge membrane with the native subcutaneous connective tissue. This final tissue composition could be similar to that observed with that of the control sensor.

6.3.2. Sensitivity of implanted biosensor to glucose

The change in sensor response currents was directly correlated with measure blood glucose levels to determine the sensitivity (nA/mM) of the glucose biosensors implanted in the subcutaneous tissue of rats. The change in sensitivity for the different sensor configurations as function of implantation time is shown in Figure 6.8.

The sensitivity for all sensor configurations decreased with increasing implantation time (Figure 6.8). The drift in sensitivity from as soon as the sensor is implant is well known. It is interesting to note that the higher the pre-implantation sensitivity the higher was the sensitivity, as observed in the case of Pt-GOD-8PU-12PU sensors. 8PU replacing the traditional EPU mass-transport limiting membrane apparently resulted in better pre-implantation sensitivity, which translated into larger measured sensor response currents when implanted the body. Larger the measured sensor response currents, the lesser will be the signal-to-noise ratio. However, when the *in vivo* sensitivity data was normalised to the pre-implantation sensitivity, the percentage decrease in sensitivity was comparable to the other sensor configurations (Figure 6.9). The uniform percent decrease in sensitivity between Pt-GOD-8PU-12PU, Pt-GOD-EPU-12PU and Pt-GOD-EPU can be attributed to the low (<2μm) porosity, which apparently did not prevent fibrous tissue deposition on the immediate surface of the sensor. On the other hand, Pt-GOD-EPU-6PU10Ge sensors showed much slower percent decrease in sensitivity at 1 and 3 weeks compared to all other sensors. The relatively slower decrease in sensitivity for Pt-GOD-EPU-6PU10Ge sensors, as evident from Figure 6.8 and Figure 6.9, can be attributed to the prevention of dense fibrous capsule on the immediate surface of the sensor (Figure 6.5). The decrease in

sensitivity for 6PU10Ge coated sensors at 9 weeks could be due to the completion of remodelling of 6PU10Ge coating, resulting in a stable subcutaneous tissue configuration similar to that observed for EPU coated sensors.

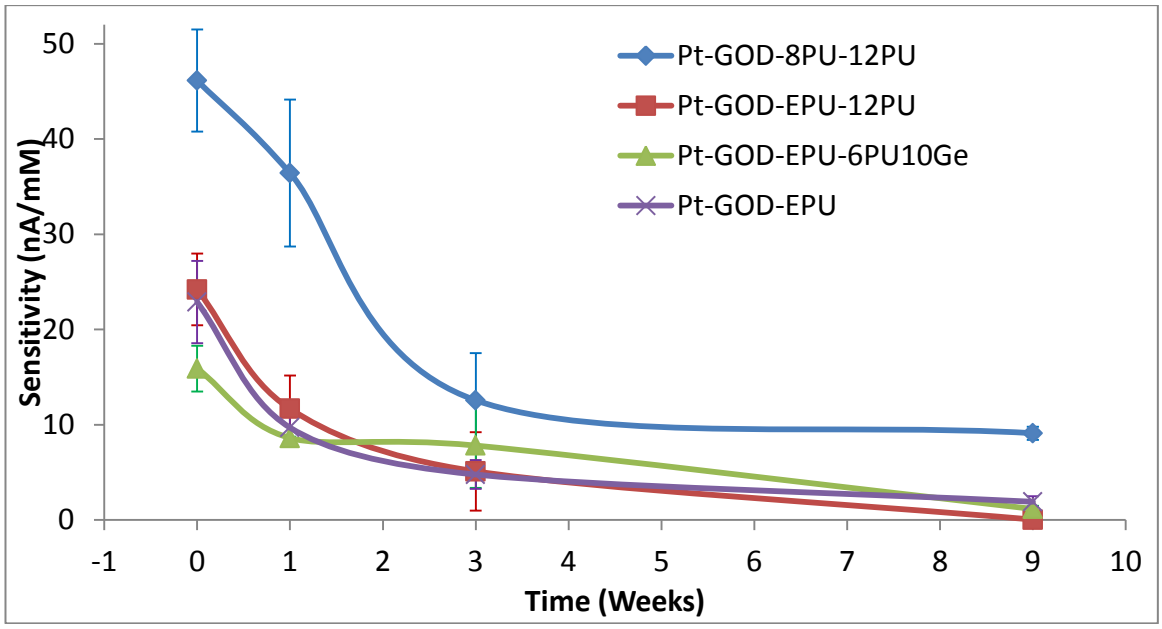

Figure 6.8 Change in sensitivity of glucose biosensors implanted in the subcutaneous tissue of rats.

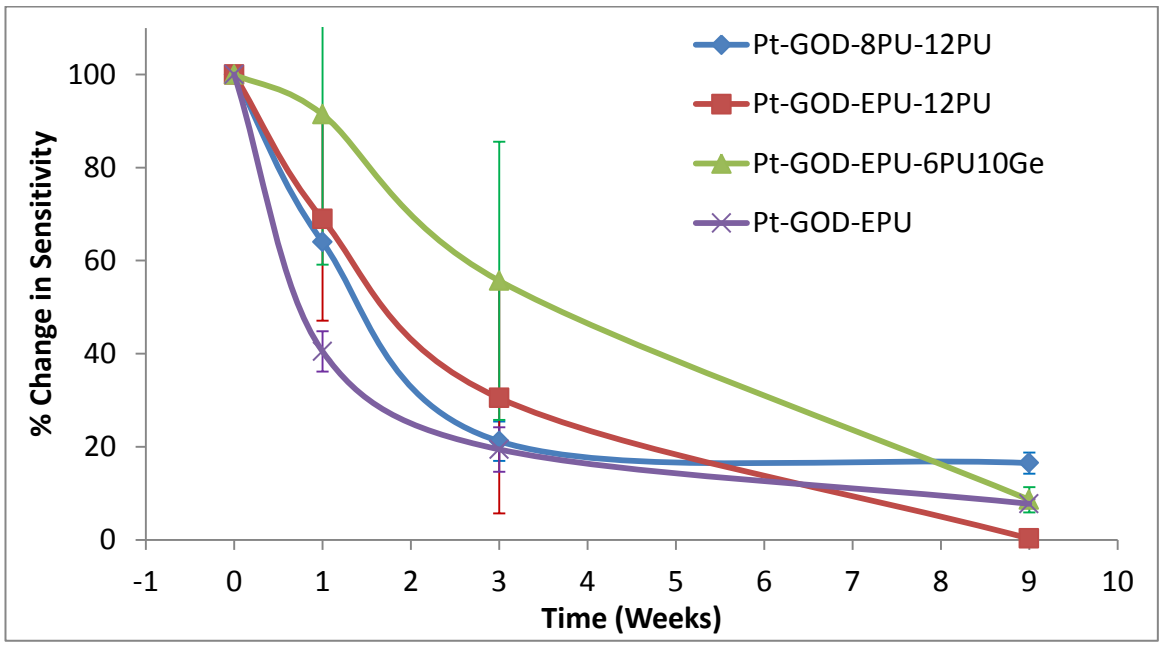

Figure 6.9 Change in sensitivity of glucose biosensors implanted in the subcutaneous tissue of rats normalised to their pre-implantation sensitivities.

In vivo studies are prone to high standard deviations. As a result, large sample sizes are needed to show statistical differences. However, the trends in this pilot study were indicative of the role of foreign body responses on sensor function. The prevention of

dense fibrous capsule on immediate surface of 6PU10Ge membranes coupled with complete infiltration of their bulk appeared to lower the decrease in sensitivity.

6.4. Chapter summary

The pilot *in vivo* biocompatibility and sensor function assessments, reported in this chapter, demonstrated that custom designed bioactive scaffolds can be used to engineer desired tissues responses. Fibro-porous structure of electrospun membranes with pore sizes <2 μm did not influence the nature of tissue responses compared to the control PU film. However, 6PU10Ge coaxial fibre membranes also have similar pore size (<2 μm) allowed host cell infiltration into its fibro-porous bulk, with the assistance of bioactive Ge shell on the core PU fibre. The Ge shell appeared to be resorbed and the pores of the resulting fibrous membrane was filled with newly deposited host collagen, thus fully integrating the electrospun coaxial fibre membrane with the surrounding subcutaneous host tissue. The resulting composite layer has a uniform host collagen interpenetrating with the electrospun PU fibres.

The nature of responses of host tissue to the subcutaneously implanted electrospun membranes appeared to correlate with the nature of their effects as coatings on glucose biosensors. The fibro-porous membranes with their high porosity formed a buffer zone between the sensor surface and the host tissue allowing free diffusion of glucose at week 1. However, the build-up of dense fibrous tissue at the membrane-tissue interface significantly decreased the sensitivity of the sensors as observed at 3 and 9 weeks after implantation. On the other hand, non-porous, smooth and relatively hydrophobic EPU membrane was not as permeable compared to when electrospun membranes were used as buffer zones, at week 1. However, deposition of granulation tissue on EPU surface by week 3 probably improved the wetting of the surface of EPU membrane, facilitating faster glucose transport and thus faster response for sensing glucose.

The slowest of decrease in sensitivity was observed for sensors coated with 6PU10Ge coaxial fibre membranes at 1 and 3 weeks. Their better sensitivity, compared to the 12PU or EPU surfaces, can be attributed to the prevention of formation of dense fibrous capsule on the immediate surface of the biosensor. However, at 9 weeks the advantage of 6PU10Ge coatings seemed to be lost when the Ge-shell was completely resorbed and replaced by the host collagen, resulting in sensor sensitivities similar to the control Pt-GOD-EPU sensors. Overall, the coaxial fibre membranes showed potential for reliably prolonging the *in vivo* sensing life-time of coil-type implantable glucose biosensors, due to their bioactive fibre surfaces compared to the relatively inert PU fibre surface.

Chapter 7 Summary and Conclusions

7.1. Introduction

Electrospinning provides the unique opportunity to prepare synthetic fibro-porous structures that mimic the natural ECM. In addition, a wide variety of synthetic and natural polymers, including the ECM components – collagen, elastin and hyaluronic acid, can be electrospun either alone or in combinations to tailor properties suiting specific applications. In this study, electrospun membranes based on pure PU and PU-Ge coaxial fibres have been prepared and tested as coatings for a model implantable glucose biosensor.

7.2. **Summary**

A versatile electrospinning setup was manufactured in our department workshop. The spinnerets and collecting systems were custom designed to spin fibres of tailorable diameters and composition. Ultra-fine elastic PU fibres having nano- and micro- scale diameters were successfully prepared using the electrospinning setup. More importantly, the solvent compositions, solution concentrations, flow rates, applied voltages, and distances to collector were identified for preparing electrospun PU membranes having desired fibre diameters. Here three membranes having statistically different average fibre diameters of 347, 738 and 1102 nm, designated as 8PU, 10PU and 12PU, were chosen to study their chemistry, morphology, porosity, solute diffusion, mechanical and hydrophilicity properties.

Analysis using FTIR spectroscopy revealed that the electrospinning process involving huge applied voltages did not affect the chemical structure of PU. In addition, FTIR spectra of electrospun membranes also confirmed the removal of any residual solvents following the drying cycles in vacuum desiccator. The duration of electrospinning had a near-linear increase in thickness for the different electrospun membranes in this study. Three electrospun membrane configurations, 8PU, 10PU and 12PU had radii for majority of their pores at about 800 (68%), 870 (36%) and 1060 (29%) μm respectively as determined using bubble point measurements. The reducing percentage of the majority of pores having uniform size is indicative of wider pore size distributions with increasing fibre diameters. As expected, gravimetry method revealed a decreasing predicted fibre packing density and increasing pore volume as a function of fibre diameters.

Slight variations in membrane thicknesses and porosities did not significantly affect the rate of transport of glucose across the electrospun PU membranes. Uniaxial tensile tests showed that the electrospun PU membranes had elasticity and tensile strengths higher than soft tissues, making them suitable candidates for implantable biomedical device

applications. The surface wetting analysis using contact angle measurements demonstrated an increase in hydrophobicity as a function of increasing fibre diameters and porosity for electrospun PU membranes. A tendency for the diffusion mechanism to shift towards anomalous (non-Fickian) diffusion was noted with increasing thickness of the membranes.

For spinning fibres directly on sensor surface, two types of collection systems namely static and dynamic collector configurations were tested. Finite element modelling was used to identify an optimum static collector configuration. Thereafter, methods were optimized for electrospinning fibres directly on the sensing element of the biosensors using both static and dynamic collector systems. Then, the effect of electrospun coatings produced with different collector configuration on biosensor function was assessed. The large volume of the fibrous membrane on sensor surface meant a significant decrease in sensor sensitivity (Figure 4.12). Further studies using the static collector system were abandoned because of the very uneven shape and thickness of the coatings. Dynamic collector was chosen for spinning uniform and snugly fitting electrospun membranes having tailorable fibre diameters, desired thickness and porosity directly on miniature biosensor surface.

The effects of thickness on sensors' *ex vivo* function were assessed, while maintaining fibre diameter by electrospinning 8PU membranes for 2.5, 5 and 10 min on Pt-GOD-EPU sensors. Thereafter, the effect of increasing fibre diameter, porosity and associated increase in thickness for 8PU, 10PU and 12PU membranes electrospun for 5 min on the function of Pt-GOD-EPU sensors was assessed. The sensors were tested for sensitivity and linearity in the glucose detection range of 2 to 30 mM, before and after coating with electrospun membranes. The electrospun coatings, irrespective of their thickness (about 22 to 100 µm) and porosity, did not cause any statistically significant decrease in sensitivity of the Pt-GOD-EPU sensors. When the 8PU-5' and 8PU-10' membranes were tested on Pt-GOD sensors, they significantly increased the linearity (Figure 4.19) for the detection range of 2 to 30 mM for glucose, proving their efficacy as mass-transport limiting membranes. A linear increase in thickness was observed for 8PU membranes on sensor as a function of electrospinning time. All sensor configurations tested after electrospun coating in this study maintained a stable sensitivity and linearity for the entire duration of the testing.

The solvent, solution concentration and process parameters for electrospinning PU-core and Ge-Shell coaxial fibre membranes were optimized. The overall fibre diameter did not increase linearly with increasing core PU content. 2PU10Ge had an overall diameter of about 0.545 µm, while that of 4PU10Ge, 6PU10Ge and 8PU10Ge membranes varied from

1.04 to 1.22 μm. Mechanical properties of the coaxial fibre membranes decreased with decreasing PU core content, which is due to the increasing brittle crosslinked Ge shell content in the coaxial fibres (wet status). However, the Ge content in the membranes made their surfaces very hydrophilic, such that the surface wetting of the membranes with micro-porous structure was too fast to obtain any measurements of the contact angle for a water droplet on membrane surface. However, nano-porous structure of 2PU10Ge membrane could transfer the membrane surface into more hydrophobic. The diffusion kinetics for glucose across 2PU10Ge membranes was near zero order, while that across 6PU10Ge was anomalous or non-Fickian, tending to shift towards Fickian diffusion with increasing membrane thickness. The porosity was comparable, while fibre packing densities were high for the coaxial fibre membrane for their higher fibre diameters. 2PU10Ge membranes having about 50% Ge do not cause any decrease in sensitivity. However, they did not function as mass-transport limiting membranes. In contrast, 6PU10Ge membranes reduced sensor sensitivities, but functioned as mass-transport limiting membrane.

Fibro-porous structure of electrospun membranes with pore sizes <2 μm did not influence the nature of tissue responses compared to the control PU film. However, 6PU10Ge coaxial fibre membranes, also having similar pore size (<2 μm), allowed host cell infiltration into its fibro-porous bulk, with the assistance of bioactive Ge shell on the core PU fibre.

When implanted in the subcutaneous tissue of rats, sensors with electrospun outer coatings showed faster response times for sensing glucose at 1 week and the trend reversed thereafter. Non-porous, smooth and relatively hydrophobic EPU membrane was not as permeable compared to when electrospun membranes were used as buffer zones at sensor tissue interface, at week 1. However, deposition of granulation tissue on EPU surface by week 3 probably improved the wetting of the EPU membrane, facilitating faster glucose transport and thus faster response to sense glucose. Electrospun pure PU fibre membranes having pore sizes less than 2 μm showed similar percentage decrease in sensitivity when compared to the control EPU membranes. The slowest of decrease for *in vivo* sensitivity was observed for sensors coated with 6PU10Ge coaxial fibre membranes at 1 and 3 weeks. However, by 9 weeks the advantage of 6PU10Ge coatings seemed to be lost when the Ge-shell was completely resorbed and replaced by the host collagen, resulting in sensor sensitivities similar to the control Pt-GOD-EPU sensors.

7.3. Conclusions

- A versatile vertical electrospinning setup was built in-house for spinning fibres using single and coaxial spinnerets, as well as static and dynamic collection systems, especially for coating miniature cylindrical devices
- Solvent systems, polymer solution concentration, feed rate, applied voltage, and distance between spinneret tip and collector were varied to tailor average fibre diameters between 200 and 1500 nm for both pure PU and PU core – Ge shell coaxial fibres.
- In conjunction with fibre diameters, the thickness and the porosity can also be precisely controlled. Owing to their fibrous mesh-like structure, irrespective of their thickness, the electrospun membranes had tensile strength and elasticity higher than that of natural soft tissues. The electrospinning process parameters, including significantly high voltages, did not have any deleterious effects on the chemical structure of the electrospun polymer(s).
- The wetting ability of PU fibre membranes decreased with increasing fibre diameters, while that for PU-Ge coaxial fibres with micro diameter was too quick to even measure contact angle for a droplet of water on the membrane surface. Furthermore, the pore sizes and volumes were significantly high than that can be achieved for conventional solvent cast membranes, which ensured zero order or closer to zero order (free) diffusion of glucose across the electrospun membranes.
- Static and dynamic collector systems were optimized for coating miniature ellipsoid sensing element of a model coil-type implantable glucose biosensor with electrospum membranes. It was the dynamic system (wherein sensor is rotated along its axis and perpendicular to the spinneret in the electrospinning field) that achieved snugly fit membranes of uniform and controllable thickness, fibre diameter and interconnected porous structure.
- It was observed that very thin electrospun membranes having thickness around 10 μm and high pore volume did not affect the sensitivity of the sensors. In addition, for membrane thicknesses of about 20 to 140 μm and pore volumes ranging between 40 and 70% tested in this study for pure PU fibres, the average % decrease in sensitivity was constant and only about 20%. They also functioned as mass-transport limiting membranes for glucose biosensors (Pt-GOD) increasing their linear detection range from about 2 to 15 mM to the desired physiological range of 2 to 30 mM for glucose detection.

- Coaxial fibre membranes having PU as core and Ge as shell in their fibre structure, depending on the total content of Ge, either did not affect sensor sensitivity (Ge content ~50% Ge) or reduced it by about 40% (Ge content ~30%).
- Biocompatibility assessments revealed that an inner 1 to 3 cell barrier layer and an outer 30 to 100 μm thick dense fibrous tissue were observed with solvent cast non-porous PU films. Introduction of surface porosity with pore radius <2 μm, did not improve the tissue responses, and similar tissue buildup as observed with PU films formed around the electrospun membranes. In contrast, coaxial fibre membranes, also having <2 μm pore sizes, were infiltrated with fibroblasts and the dense fibrous tissue did not form. In other words, the barrier tissue layer formation was prevented which is good news for implantable biosensor application.
- *In vivo* sensor function assessments revealed that higher the pre-implantation sensor sensitivity (as achieved when electrospun coating replaced tradition EPU mass-transport limiting membrane), higher was its sensitivity when implanted in the body. However, the % decrease in sensitivity for electrospun pure PU fibre membranes as a function of time was similar to that observed with control sensors having EPU membrane at the sensor-tissue interface. The sensor function test results were in agreement with biocompatibility findings. The prevention of dense fibrous tissue around the coaxial fibre membrane, translated to much lesser decrease in sensitivity for the glucose biosensors implanted in the body.
- Overall, this study proved that electrospun membranes can replace traditional mass-transport limiting membrane as well as biocompatible membranes that can significantly improve the *in vivo* sensitivity of the implantable glucose biosensors, which is a significant step forward towards achieving the goal of developing reliable long-term implantable glucose biosensors for continuous glucose monitoring without the need for patient compliance.

7.4. Future directions

The experimental results achieved in this study showed the efficacy of electrospun membranes having fibre diameters and pore sizes of <2 μm as coatings for implantable glucose biosensors. Even with such low porosities, the coaxial fibres with PU core and bioactive Ge shells allowed host cell infiltration and addressed the *in vivo* sensitivity decrease affects to some extent. Additional, extensive studies with increased number of sensor function tests in rats are needed to prove statistical significance of the improvement of *in vivo* sensitivity using coaxial fibre membranes (<2 μm) as tissue engineering coatings for implantable glucose biosensors. Future studies should also include the efficacy of

electrospun membranes with fibre diameters of 3 to 10 μm, for the engineering of tissue responses at the sensor-tissue interface.

The findings of achieving host tissue infiltration and collagen deposition in the <2 μm pore sizes of coaxial fibre membranes have potential applications in the design of artificial tissue constructs for tissue engineering and regenerative medicine.

Importantly, the key recommendation based on the results achieved in this study is the use of 'combinations of pure PU fibre membranes having submicron fibre diameter, PU-Ge coaxial fibre membranes with <2 μm pore sizes, as well as pure PU and PU-Ge coaxial fibre membranes having fibre diameter between 3 and 10 μm to support host cell infiltration, as multiple levels of defence against the deleterious host foreign body responses, while maintaining high *ex vivo* sensor sensitivities, to solve the long-awaited problem of long-term *in vivo* performance of implantable glucose biosensors'.

Bibliography

ACATAY, K., SIMSEK, E., OW-YANG, C. & MENCELOGLU, Y. Z. 2004. Tunable, superhydrophobically stable polymeric surfaces by electrospinning. *Angew. Chem. Int. Ed. Engl.,* 43**,** 5210-3.

ALLEN, D. J., JOHNSON, K. W. & NEVIN, R. S. 1994. *Hydrophilic polyurethane membranes for electrochemical glucose sensors*. US Patent 5322063.

ALTMAN, G. H., HORAN, R. L., LU, H. H., MOREAU, J., MARTIN, I., RICHMOND, J. C. & KAPLAN, D. L. 2002. Silk matrix for tissue engineered anterior cruciate ligaments. *Biomaterials,* 23**,** 4131-4141.

ANNIS, D., BORNAT, A., EDWARDS, R. O., HIGHAM, A., LOVEDAY, B. & WILSON, J. 1978. An elastomeric vascular prosthesis. *Trans. Am. Soc. Artif. Intern. Organs,* 24**,** 209-214.

ASHOK, A., NIRMALKUMAR, A. & JEYASHANTHI, N. 2010. A Novel Method for Blood Glucose Measurement by Noninvasive Technique Using Laser. *Int. J. Biolog. Med. Sci.,* 5**,** 58-64.

BADAMI, A. S., KREKE, M. R., THOMPSON, M. S., RIFFLE, J. S. & GOLDSTEIN, A. S. 2006. Effect of fiber diameter on spreading, proliferation, and differentiation of osteoblastic cells on electrospun poly(lactic acid) substrates. *Biomaterials,* 27**,** 596-606.

BAJI, A., MAI, Y. W., WONG, S. C., ABTAHI, M. & CHEN, P. 2010. Electrospinning of polymer nanofibers: Effects on oriented morphology, structures and tensile properties. *Composite Sci. Technol.,* 70**,** 703-718.

BAO, S.-J., LI, C. M., ZANG, J.-F., CUI, X.-Q., QIAO, Y. & GUO, J. 2008. New Nanostructured TiO2 for Direct Electrochemistry and Glucose Sensor Applications. *Adv. Funct. Mat.,* 18**,** 591-599.

BARBOSA, J. N., MADUREIRA, P., BARBOSA, M. A. & ÁGUAS, A. P. 2006. The influence of functional groups of self-assembled monolayers on fibrous capsule formation and cell recruitment. *J. Biomed. Mater. Res. A,* 76A**,** 737-743.

BAUMGARTEN, P. K. 1971. Electrostatic spinning of acrylic microfibers. *J. Colloid Interface. Sci.,* 36**,** 71-79.

BEDEN, B., LARGEAUD, F., KOKOH, K. B. & LAMY, C. 1996. Fourier transform infrared reflectance spectroscopic investigation of the electrocatalytic oxidation of -glucose: Identification of reactive intermediates and reaction products. *Electrochim. Acta,* 41**,** 701-709.

BHARDWAJ, N. & KUNDU, S. C. 2010. Electrospinning: a fascinating fiber fabrication technique. *Biotechnol. Adv.,* 28**,** 325-47.

BOGNITZKI, M., CZADO, W., FRESE, T., SCHAPER, A., HELLWIG, M., STEINHART, M., GREINER, A. & WENDORFF, J. H. 2001. Nanostructured Fibers via Electrospinning. *Adv. Mat.,* 13**,** 70-72.

BOO, H., PARK, S., KU, B., KIM, Y., PARK, J. H., KIM, H. C. & CHUNG, T. D. 2004. Ionic strength-controlled virtual area of mesoporous platinum electrode. *J. Am. Chem. Soc.,* 126**,** 4524-5.

BOTTOMLEY, J. M. 2010. Cases, complications, comorbidity and costs of diabetes in UK: is treatment falling wide of the mark? *Br. J. Diabetes Vascul. Disease,* 10**,** 209-215.

BRAUKER, J. H., CARR-BRENDEL, V. & TAPSAK, M. A. 2012. *Porous membranes for use with implantable devices*. US Patent 8118877.

BRAUKER, J. H., CARR-BRENDEL, V. E., MARTINSON, L. A., CRUDELE, J., JOHNSTON, W. D. & JOHNSON, R. C. 1995. Neovascularization of synthetic membranes directed by membrane microarchitecture. *J. Biomed. Mater. Res.,* 29**,** 1517-1524.

BROOKS, S. L., ASHBY, R. E., TURNER, A. P. F., CALDER, M. R. & CLARKE, D. J. 1987. Development of an On-line Glucose Sensor for Fermentation Monitoring. *Biosensors,* 3**,** 45-56.

BRUDER, S. & CAPLAN, A. 2000. Bone regeneration through cellular engineering. *In:* LANZA, R., LANGER, R. & VACANTI, J. (eds.) *Principles of tissue engineering. 2.* San Diego: Academic Press.

BUCHKO, C. J., CHEN, L. C., SHEN, Y. & MARTIN, D. C. 1999. Processing and microstructural characterization of porous biocompatible protein polymer thin films. *Polymer,* 40**,** 7397-7407.

CAMERON, B. D. & ANUMULA, H. 2006. Development of a real-time corneal birefringence compensated glucose sensing polarimeter. *Diabetes Technol. Ther.,* 8**,** 156-64.

CASPER, C. L., STEPHENS, J. S., TASSI, N. G., CHASE, D. B. & RABOLT, J. F. 2004. Controlling surface morphology of electrospun polystyrene fibers: Effect of humidity and molecular weight in the electrospinning process. *Macromolecules,* 37**,** 573-578.

CASS, A. E., DAVIS, G., FRANCIS, G. D., HILL, H. A., ASTON, W. J., HIGGINS, I. J., PLOTKIN, E. V., SCOTT, L. D. & TURNER, A. P. 1984. Ferrocene-mediated enzyme electrode for amperometric determination of glucose. *Anal. Chem.,* 56**,** 667-71.

CHANG, M. C., KO, C. C. & DOUGLAS, W. H. 2003. Conformational change of hydroxyapatite/gelatin nanocomposite by glutaraldehyde. *Biomaterials,* 24**,** 3087-94.

CHAUBEY, A. & MALHOTRA, B. D. 2002a. Mediated biosensors. *Biosens Bioelectron,* 17**,** 441-56.

CHAUBEY, A. & MALHOTRA, B. D. 2002b. Mediated biosensors. *Biosens. Bioelectron.,* 17**,** 441-56.

CHAUBEY, A., PANDE, K. K., SINGH, V. S. & MALHOTRA, B. D. 2000. Co-immobilization of lactate oxidase and lactate dehydrogenase on conducting polyaniline films. *Anal. Chim. Acta,* 407**,** 97-103.

CHEN, J., ZHANG, W.-D. & YE, J.-S. 2008. Nonenzymatic electrochemical glucose sensor based on MnO2/MWNTs nanocomposite. *Electrochem Commun,* 10**,** 1268-1271.

CHEN, R., HUANG, C., KE, Q., HE, C., WANG, H. & MO, X. 2010a. Preparation and characterization of coaxial electrospun thermoplastic polyurethane/collagen compound nanofibers for tissue engineering applications. *Colloid. Surf. B: Biointerfaces,* 79**,** 315-325.

CHEN, X. M., LIN, Z. J., CHEN, D. J., JIA, T. T., CAI, Z. M., WANG, X. R., CHEN, X., CHEN, G. N. & OYAMA, M. 2010b. Nonenzymatic amperometric sensing of glucose by using palladium nanoparticles supported on functional carbon nanotubes. *Biosens Bioelectron,* 25**,** 1803-8.

CHENG, M., DENG, J., YANG, F., GONG, Y., ZHAO, N. & ZHANG, X. 2003. Study on physical properties and nerve cell affinity of composite films from chitosan and gelatin solutions. *Biomaterials,* 24**,** 2871-2880.

CHIU, H. T., LIN, J. M., CHENG, T. H. & CHOU, S. Y. 2011. Fabrication of electrospun polyacrylonitrile ion-exchange membranes for application in lysozym. *Expr. Polym. Lett.,* 5**,** 308-317.

CHONG, E. J., LIM, C. T., PHAN, T. T., LIM, I. J. & RAMAKRISHNA, S. 2007a. *Nanofibrous mat for tissue engineering, wound dressing and dermal reconstitution.* .

CHONG, E. J., PHAN, T. T., LIM, I. J., ZHANG, Y. Z., BAY, B. H., RAMAKRISHNA, S. & LIM, C. T. 2007b. Evaluation of electrospun PCL/gelatin nanofibrous scaffold for wound healing and layered dermal reconstitution. *Acta Biomater.,* 3**,** 321-30.

CLARK, L. C. 1959. *Electrochemical device for chemical analysis.* US Patent: 2913386 Patent.

CLARK, L. C., JR. & LYONS, C. 1962. Electrode systems for continuous monitoring in cardiovascular surgery. *Ann. N. Y. Acad. Sci.,* 102**,** 29-45.

CLARKE, W. L., COX, D., GONDER-FREDERICK, L. A., CARTER, W. & POHL, S. L. 1987. Evaluating clinical accuracy of systems for self-monitoring of blood glucose. *Diabetes Care,* 10**,** 622-8.

COOLEY, J. F. 1902. *Apparatus for electrically dispersing fluids*. US Patent 0692631.

CUI, H.-F., YE, J.-S., LIU, X., ZHANG, W.-D. & SHEU, F.-S. 2006. Pt–Pb alloy nanoparticle/carbon nanotube nanocomposite: a strong electrocatalyst for glucose oxidation. *Nanotechnology,* 17**,** 2334.

CUI, W., LI, X., ZHOU, S. & WENG, J. 2008. Degradation patterns and surface wettability of electrospun fibrous mats. *Polym. Degrad. Stabil.,* 93**,** 731-738.

D'ORAZIO, P. 1996. Interference by thiocyanate on electrochemical biosensors for blood glucose. *Clin. Chem.,* 42**,** 1124-6.

DE VRIEZE, S., VAN CAMP, T., NELVIG, A., HAGSTRÖM, B., WESTBROEK, P. & DE CLERCK, K. 2009. The effect of temperature and humidity on electrospinning. *J Mat. Sci.,* 44**,** 1357-1362.

DEGANI, Y. & HELLER, A. 1987. Direct electrical communication between chemically modified enzymes and metal electrodes. I. Electron transfer from glucose oxidase to metal electrodes via electron relays, bound covalently to the enzyme. *J. Phys. Chem.,* 91**,** 1285-1289.

DEGANI, Y. & HELLER, A. 1988. Direct electrical communication between chemically modified enzymes and metal electrodes. 2. Methods for bonding electron-transfer relays to glucose oxidase and D-amino-acid oxidase. *J. Am. Chem. Soc.,* 110**,** 2615-2620.

DEITZEL, J. M., KLEINMEYER, J., HARRIS, D. & BECK TAN, N. C. 2001a. The effect of processing variables on the morphology of electrospun nanofibers and textiles. *Polymer,* 42**,** 261-272.

DEITZEL, J. M., KLEINMEYER, J. D., HIRVONEN, J. K. & BECK TAN, N. C. 2001b. Controlled deposition of electrospun poly(ethylene oxide) fibers. *Polymer,* 42**,** 8163-8170.

DEMIR, M. M. 2010. Investigation on glassy skin formation of porous polystyrene fibers electrospun from DMF. *Expr. Polym. Lett.,* 4**,** 2-8.

DEMIR, M. M., YILGOR, I., YILGOR, E. & ERMAN, B. 2002. Electrospinning of polyurethane fibers. *Polymer,* 43**,** 3303-3309.

DI GLERIA, K., GREEN, M. J., HILL, H. A. O. & MCNEIL, C. J. 1986. Homogeneous ferrocene-mediated amperometric immunoassay. *Anal. Chem.,* 58**,** 1203-1205.

DIABETES-PREVALENCE 2011. Diabetes Prevalence. *http://www.diabetes.org.uk/Professionals/Publications-reports-and-resources/Reports-statistics-and-case-studies/Reports/Diabetes-prevalence-2011-Oct-2011/*.

DIAZ, E., FERNANDEZ-NIEVES, A., BARRERO, A., MARQUEZ, M. & LOSCERTALES, G. 2008. Fabrication of structured micro and nanofibers by coaxial electrospinning. *J. Phys. Confer. Series,* 127.

DIERINGER, J. A., MCFARLAND, A. D., SHAH, N. C., STUART, D. A., WHITNEY, A. V., YONZON, C. R., YOUNG, M. A., ZHANG, X. & VAN DUYNE, R. P. 2006. Surface enhanced Raman spectroscopy: new materials, concepts, characterization tools, and applications. *Faraday Discuss,* 132**,** 9-26.

DOSHI, J. & RENEKER, D. H. 1995. Electrospinning process and applications of electrospun fibers. *J. Electrostatics,* 35**,** 151-160.

DOTTI, F., VARESANO, A., MONTARSOLO, A., ALUIGI, A., TONIN, C. & MAZZUCHETTI, G. 2007. Electrospun porous mats for high efficiency filtration. *J. Indust. Textiles,* 37**,** 151-162.

ERNST, S., HAMANN, C. H. & HEITBAUM, J. 1980. Electrooxidation of glucose in phosphate buffer solutions: Kinetics and reaction mechanism. *Ber Bunsenges Phys. Chem.,* 84**,** 50-55.

ERNST, S., HEITBAUM, J. & HAMANN, C. H. 1979. The electrooxidation of glucose in phosphate buffer solutions : Part I. Reactivity and kinetics below 350 mV/RHE. *J. Electroanal. Chem.,* 100**,** 173-183.

ESENALIEV, R. O., LARIN, K. V., LARINA, I. V. & MOTAMEDI, M. 2001. Noninvasive monitoring of glucose concentration with optical coherence tomography. *Opt. Lett.,* 26**,** 992-4.

ESPADAS-TORRE, C. & MEYERHOFF, M. E. 1995. Thrombogenic properties of untreated and poly(ethylene oxide)-modified polymeric matrices useful for preparing intraarterial ion-selective electrodes. *Anal. Chem.,* 67**,** 3108-3114.

FDA 2009. GDH-PQQ (glucose dehydrogenase pyrroloquinoline quinone) Glucose Monitoring Technology. U.S. Food and Drugs Administration, http://www.fda.gov/Safety/MedWatch/SafetyInformation/SafetyAlertsforHumanMedicalProducts/ucm177295.htm.

FILATOV, Y. N. 1977. *Electrospinning of fibrous materials [in Russian],* Moscow, Neft' i Gas Publishing House.

FISHER, A. C., DE COSSART, L., HOW, T. V. & ANNIS, D. 1985. Long term in-vivo performance of an electrostatically-spun small bore arterial prosthesis: the contribution of mechanical compliance and anti-platelet therapy. *Life Support Syst.,* 1**,** 462-465

FONG, H., CHUN, I. & RENEKER, D. H. 1999. Beaded nanofibers formed during electrospinning. *Polymer,* 40**,** 4585-4592.

FORMHALS, A. 1934. *Process and apparaturs for preparing artificial threads*. US Patent 1975504.

FORMHALS, A. 1938a. *Artificial fiber construction*. US Patent 2109333.

FORMHALS, A. 1938b. *Method and apparatus for the production of fibers*. US Patent 2116942 and 2123992.

FORMHALS, A. 1939a. *Method and apparatus for spinning*. US Patent 2160962.

FORMHALS, A. 1939b. *Method and apparatus for the production of artificial fibers*. US Patent 2158416.

FOULDS, N. C. & LOWE, C. R. 1986. Enzyme entrapment in electrically conducting polymers. Immobilisation of glucose oxidase in polypyrrole and its application in amperometric glucose sensors. *J. Chem. Soc. Faraday Trans. Phys. Chem. Condens. Phases,* 82.

FREW, J. E. & HILL, H. A. O. 1987. Electrochemical biosensors. *Anal. Chem.,* 59**,** 933A-944A.

FRIDRIKH, S. V., YU, J. H., BRENNER, M. P. & RUTLEDGE, G. C. 2003. Controlling the fiber diameter during electrospinning. *Phys. Rev. Lett.,* 90**,** 144502.

GALESKA, I., CHATTOPADHYAY, D., MOUSSY, F. & PAPADIMITRAKOPOULOS, F. 2000. Calcification-Resistant Nafion/Fe3+ Assemblies for Implantable Biosensors. *Biomacromolecules,* 1**,** 202-207.

GILBERT, W. 1628. *De Magnete, Magneticisque Corporibus, et de Magno Magnete Tellure (On the Magnet and Magnetic Bodies, and on That Great Magnet the Earth),* London, Peter Short.

GOPAL, R., KAUR, S., MA, Z., CHAN, C., RAMAKRISHNA, S. & MATSUURA, T. 2006. Electrospun nanofibrous filtration membrane. *J. Membr. Sci.,* 281**,** 581-586.

GOUGH, D. A., KUMOSA, L. S., ROUTH, T. L., LIN, J. T. & LUCISANO, J. Y. 2010. Function of an implanted tissue glucose sensor for more than 1 year in animals. *Sci. Transl. Med.,* 2**,** 42ra53.

GOUGH, D. A., LUCISANO, J. Y. & TSE, P. H. S. 1985. Two-Dimensional Enzyme Electrode Sensor for Glucose. *Anal. Chem.,* 57**,** 2351-2357.

GREGG, B. A. & HELLER, A. 1990. Cross-linked redox gels containing glucose oxidase for amperometric biosensor applications. *Anal. Chem.,* 62**,** 258-263.

GRIFFIN, J., DELGADO-RIVERA, R., MEINERS, S. & UHRICH, K. E. 2011. Salicylic acid-derived poly(anhydride-ester) electrospun fibers designed for regenerating the peripheral nervous system. *J. Biomed. Mater. Res. A,* 97A**,** 230-242.

GROOM, C. A., LUONG, J. H. T. & THATIPALMALA, R. 1995. Dual functionalities of 4-aminodiphenylamine in enzymatic assay and mediated biosensor construction. *Anal. Biochem.,* 231**,** 393-399.

HAN, D., BOYCE, S. T. & STECKL, A. J. Versatile core-sheath biofibers using coaxial electrospinning. Mater. Res. Soc. Symp. Proc., 2008. 33-38.

HAN, D. & STECKL, A. J. 2009. Superhydrophobic and oleophobic fibers by coaxial electrospinning. *Langmuir,* 25**,** 9454-9462.

HARTMAN, O., ZHANG, C., ADAMS, E. L., FARACH-CARSON, M. C., PETRELLI, N. J., CHASE, B. D. & RABOLT, J. F. 2009. Microfabricated Electrospun Collagen Membranes for 3-D Cancer Models and Drug Screening Applications. *Biomacromolecules,* 10**,** 2019-2032.

HE, W., MA, Z., YONG, T., TEO, W. E. & RAMAKRISHNA, S. 2005. Fabrication of collagen-coated biodegradable polymer nanofiber mesh and its potential for endothelial cells growth. *Biomaterials,* 26**,** 7606-7615.

HECHT, H. J., KALISZ, H. M., HENDLE, J., SCHMID, R. D. & SCHOMBURG, D. 1993. Crystal-Structure of Glucose-Oxidase from Aspergillus-Niger Refined at 2 .3 Angstrom Resolution. *J. Mol. Biol.,* 229**,** 153-172.

HELLER, A. 1990. Electrical wiring of redox enzymes. *Accounts Chem. Res.,* 23**,** 128-134.

HELLER, A. 1992. Electrical connection of enzyme redox centers to electrodes. *J. Phys. Chem.,* 96**,** 3579-3587.

HELLER, A. & FELDMAN, B. 2008. Electrochemical glucose sensors and their applications in diabetes management. *Chem. Rev.,* 108**,** 2482-505.

HELLER, A. & FELDMAN, B. 2010. Electrochemistry in Diabetes Management. *Accounts Chem. Res.,* 43**,** 963-973.

HENNING, T. 2010. Commercially available continous glucose monitoring systems. *In:* CUNNINGHAM, D. D. & STENKEN, J. A. (eds.) *In vivo glucose sensing.* Hoboken, New Jersey: John Wiley & Sons, Inc.

HENRY, C. 1998. Getting under the skin: Implantable Glucose Sensors. *Anal. Chem.,* 70**,** 594A-598A.

HEYDARKHAN-HAGVALL, S., SCHENKE-LAYLAND, K., DHANASOPON, A. P., ROFAIL, F., SMITH, H., WU, B. M., SHEMIN, R., BEYGUI, R. E. & MACLELLAN, W. R. 2008. Three-dimensional electrospun ECM-based hybrid scaffolds for cardiovascular tissue engineering. *Biomaterials,* 29**,** 2907-2914.

HIGSON, S. P. J. & VADGAMA, P. M. 1995. Diamond like carbon coated films for enzyme electrodes; characterization of biocompatibility and substrate diffusion limiting properties. *Anal. Chim. Acta,* 300**,** 77-83.

HILDITCH, P. I. & GREEN, M. J. 1991. Disposable electrochemical biosensors. *Analyst,* 116**,** 1217-1220.

HOHMAN, M. M., SHIN, Y. M., RUTLEDGE, G. & BRENNER, M. P. 2001a. Electrospinning and Electrically Forced Jets: I. Stability Theory. *Phys. Fluids,* 13**,** 2201-2220.

HOHMAN, M. M., SHIN, Y. M., RUTLEDGE, G. & BRENNER, M. P. 2001b. Electrospinning and Electrically Forced Jets: II. Application. *Phys. Fluids,* 13**,** 2221-2240.

HRAPOVIC, S., LIU, Y. L., MALE, K. B. & LUONG, J. H. T. 2004. Electrochemical biosensing platforms using platinum nanoparticles and carbon nanotubes. *Anal. Chem.,* 76**,** 1083-1088.

HSU, C.-M. & SHIVKUMAR, S. 2004. N,N-Dimethylformamide Additions to the Solution for the Electrospinning of Poly(ε-caprolactone) Nanofibers. *Macromol. Mater. Eng.,* 289**,** 334-340.

HTTP://EN.WIKIPEDIA.ORG/WIKI/ELECTROSPINNING 2012. Electrospinning.

HUANG, Z.-M., ZHANG, Y. Z., RAMAKRISHNA, S. & LIM, C. T. 2004. Electrospinning and mechanical characterization of gelatin nanofibers. *Polymer,* 45**,** 5361-5368.

HUANG, Z. M., ZHANG, Y. & RAMAKRISHNA, S. 2005. Double-layered composite nanofibers and their mechanical performance. *J. Polym. Sci. B Polym. Phys.,* 43**,** 2852-2861.

HUANG, Z. M., ZHANG, Y. Z., KOTAKI, M. & RAMAKRISHNA, S. 2003. A review on polymer nanofibers by electrospinning and their applications in nanocomposites. *Comp. Sci. Technol.,* 63**,** 2223-2253.

HUTMACHER, D. W. 2000. Scaffolds in tissue engineering bone and cartilage. *Biomaterials,* 21**,** 2529-2543.

IATRIDIS, J. C., WU, J., YANDOW, J. A. & LANGEVIN, H. M. 2003. Subcutaneous tissue mechanical behavior is linear and viscoelastic under uniaxial tension. *Connective tissue research,* 44**,** 208-17.

JAMES, N. R., PHILIP, J. & JAYAKRISHNAN, A. 2006. Polyurethanes with radiopaque properties. *Biomaterials,* 27**,** 160-166.

JARUSUWANNAPOOM, T., HONGROJJANAWIWAT, W., JITJAICHAM, S., WANNATONG, L., NITHITANAKUL, M., PATTAMAPROM, C., KOOMBHONGSE, P., RANGKUPAN, R. & SUPAPHOL, P. 2005. Effect of solvents on electro-spinnability of polystyrene solutions and morphological appearance of resulting electrospun polystyrene fibers. *European Polymer Journal,* 41**,** 409-421.

JIANG, L. C. & ZHANG, W. D. 2010. A highly sensitive nonenzymatic glucose sensor based on CuO nanoparticles-modified carbon nanotube electrode. *Biosens Bioelectron,* 25**,** 1402-7.

JIANG, Z., YUAN, K. J., LI, S. F. & CHOW, W. K. 2006. Study of FTIR spectra and thermal analysis of polyurethane (in Chinese). *Spectrosc. Spectr. Anal.,* 26**,** 624-628.

JIANXIONG, W., XIAOWEI, S., XIANPENG, C., YU, L., LI, S. & SHISHENG, X. 2007. Nonenzymatic Glucose Sensor Using Freestanding Single-Wall Carbon Nanotube Films. *Electrochem Solid State Lett,* 10**,** J58-J60.

JIN, X. & HSIEH, Y.-L. 2005. pH-responsive swelling behavior of poly(vinyl alcohol)/poly(acrylic acid) bi-component fibrous hydrogel membranes. *Polymer,* 46**,** 5149-5160.

JIRSAK, O., SANETRINIK, F., LUKAS, D., KOTEK, V., MARTINOVA, L. & CHALOUPEK, J. 2005. A method of nanofibers production from a polymer solution using electrostatic spinning and a device for carrying out the method. *World Patent,* WO2005024101.

JOSE, S. 2008. Market for Biosensors to Reach $6.1 Billion by 2012, According to New Report by Global Industry Analysts, Inc. . CA: Global Industry Analysts, Inc.

KANG, X., MAI, Z., ZOU, X., CAI, P. & MO, J. 2007. A sensitive nonenzymatic glucose sensor in alkaline media with a copper nanocluster/multiwall carbon nanotube-modified glassy carbon electrode. *Anal Biochem,* 363**,** 143-50.

KESSICK, R., FENN, J. & TEPPER, G. 2004. The use of AC potentials in electrospraying and electrospinning processes. *Polymer,* 45**,** 2981-2984.

KHAN, G. F., OHWA, M. & WERNET, W. 1996. Design of a Stable Charge Transfer Complex Electrode for a Third-Generation Amperometric Glucose Sensor. *Analytical Chemistry,* 68**,** 2939-2945.

KHIL, M.-S., CHA, D.-I., KIM, H.-Y., KIM, I.-S. & BHATTARAI, N. 2003. Electrospun nanofibrous polyurethane membrane as wound dressing. *Journal of Biomedical Materials Research Part B: Applied Biomaterials,* 67B**,** 675-679.

KIM, H.-W., YU, H.-S. & LEE, H.-H. 2008a. Nanofibrous matrices of poly(lactic acid) and gelatin polymeric blends for the improvement of cellular responses. *Journal of Biomedical Materials Research Part A,* 87A**,** 25-32.

KIM, K., LEE, K., KHIL, M., HO, Y. & KIM, H. 2004. The effect of molecular weight and the linear velocity of drum surface on the properties of electrospun poly(ethylene terephthalate) nonwovens. *Fibers and Polymers,* 5**,** 122-127.

KIM, M., KIM, J.-H., YI, G., LIM, S.-H., HONG, Y. & CHUNG, D. 2008b. In vitro and in vivo application of PLGA nanofiber for artificial blood vessel. *Macromolecular Research,* 16**,** 345-352.

KIM, S. E., HEO, D. N., LEE, J. B., KIM, J. R., PARK, S. H., JEON, S. H. & KWON, I. K. 2009. Electrospun gelatin/polyurethane blended nanofibers for wound healing. *Biomed Mater,* 4**,** 044106.

KIMURA, H., TAKEYAMA, H., KOMORI, K., YAMAMOTO, T., SAKAI, Y. & FUJII, T. 2010. Microfluidic Device with Integrated Glucose Sensor for Cell-Based Assay in Toxicology. *J Robotics Mechatronics,* 22**,** 594-600.

KOIDE, S. & YOKOYAMA, K. 1999. Electrochemical characterization of an enzyme electrode based on a ferrocene-containing redox polymer. *Journal of Electroanalytical Chemistry,* 468**,** 193-201.

KOKKINIDIS, G. & XONOGLOU, N. 1985. Comparative study of the electrocatalytic influence of underpotential heavy metal adatoms on the anodic oxidation of monosaccharides on Pt in acid solutions. *Bioelectrochemistry and Bioenergetics,* 14**,** 375-387.

KONDEPATI, V. R. & HEISE, H. M. 2007. Recent progress in analytical instrumentation for glycemic control in diabetic and critically ill patients. *Anal Bioanal Chem,* 388**,** 545-63.

KOOPAL, C. G. J., FEITERS, M. C., NOLTE, R. J. M., DE RUITER, B. & SCHASFOORT, R. B. M. 1992. Third-generation amperometric biosensor for glucose. Polypyrrole deposited within a matrix of uniform latex particles as mediator. *Bioelectrochem. Bioenerg.,* 29**,** 159-175.

KORSMEYER, R. W., GURNY, R., DOELKER, E., BURI, P. & PEPPAS, N. A. 1983. Mechanisms of solute release from porous hydrophilic polymers. *Int. J. Pharm.,* 15**,** 25-35.

KOSCHWANEZ, H. E., YAP, F. Y., KLITZMAN, B. & REICHERT, W. M. 2008. In vitro and in vivo characterization of porous poly-L-lactic acid coatings for subcutaneously implanted glucose sensors. *J Biomed Mater Res,* 87**,** 792-807.

KRISHNAN, S., WEINMAN, C. J. & OBER, C. K. 2008. Advances in polymers for anti-biofouling surfaces. *J Mater Chem,* 18**,** 3405-3413.

KULYS, J., HANSEN, H. E., BUCH-RASMUSSEN, T., WANG, J. & OZSOZ, M. 1994. Glucose biosensor based on the incorporation of Meldola Blue. *Analytica Chimica Acta,* 288**,** 193-196.

KULYS, J. J., SAMALIUS, A. S. & SVIRMICKAS, G. J. S. 1980. Electron exchange between the enzyme active center and organic metal. *FEBS Letters,* 114**,** 7-10.

KURAMOTO, N. & SHISHIDO, Y. 1998. Property of thermo-sensitive and redox-active poly(N-cyclopropylacrylamide-co-vinylferrocene) and poly(N-isopropylacrylamide-co-vinylferrocene). *Polymer,* 39**,** 669-673.

LANDAU, L. D. & LIFSHITZ, E. M. 1984. *Electrodynamics of continuous media,* Oxford, Butterworth-Heinemann.

LARMOR, J. 1898. Note on the complete scheme of electrodynamic equations of a moving material medium, and on electrostriction. *Proc. R. Soc.,* 63**,** 365.

LEE, D., LEE, J., KIM, J., KIM, J., NA, H. B., KIM, B., SHIN, C. H., KWAK, J. H., DOHNALKOVA, A., GRATE, J. W., HYEON, T. & KIM, H. S. 2005. Simple Fabrication of a Highly Sensitive and Fast Glucose Biosensor Using Enzymes Immobilized in Mesocellular Carbon Foam. *Advanced Materials,* 17**,** 2828-2833.

LEE, J. H., KOPECEK, J. & ANDRADE, J. D. 1989. Protein-resistant surfaces prepared by PEO-containing block copolymer surfactants. *J Biomed Mater Res,* 23**,** 351-68.

LEE, J. S., CHOI, K. H., GHIM, H. D., KIM, S. S., CHUN, D. H., KIM, H. Y. & LYOO, W. S. 2004a. Role of molecular weight of atactic poly(vinyl alcohol) (PVA) in the structure and properties of PVA nanofabric prepared by electrospinning. *Journal of Applied Polymer Science,* 93**,** 1638-1646.

LEE, K. H., KIM, H. Y., BANG, H. J., JUNG, Y. H. & LEE, S. G. 2003. The change of bead morphology formed on electrospun polystyrene fibers. *Polymer,* 44**,** 4029-4034.

LEE, K. H., LA YM,LEE DR, SUNG NH, 2002. Influence of a Mixing Solvent with Tetrahydrofuran and N,N-Dimethylformamide on Electrospun Poly(vinyl chloride) Nonwoven Mats. *J. Polym. Sci. B Polym. Phys.,* 40**,** 2259–2268.

LEE, M.-C., KABILAN, S., HUSSAIN, A., YANG, X., BLYTH, J. & LOWE, C. R. 2004b. Glucose-Sensitive Holographic Sensors for Monitoring Bacterial Growth. *Anal Chem,* 76**,** 5748-5755.

LI, C. M., DONG, H., CAO, X., LUONG, J. H. & ZHANG, X. 2007. Implantable electrochemical sensors for biomedical and clinical applications: progress, problems, and future possibilities. *Curr Med Chem,* 14**,** 937-51.

LI, D. & XIA, Y. 2004. Electrospinning of Nanofibers: Reinventing the Wheel? *Advanced Materials,* 16**,** 1151-1170.

LI, Q.-S., YE, B.-C., LIU, B.-X. & ZHONG, J.-J. 1999. Improvement of the performance of H2O2 oxidation at low working potential by incorporating TTF-TCNQ into a platinum wire electrode for glucose determination. *Biosensors and Bioelectronics,* 14**,** 327-334.

LI, W.-J., DANIELSON, K. G., ALEXANDER, P. G. & TUAN, R. S. 2003. Biological response of chondrocytes cultured in three-dimensional nanofibrous poly(ϵ-caprolactone) scaffolds. *Journal of Biomedical Materials Research Part A,* 67A**,** 1105-1114.

LI, W.-J., TULI, R., OKAFOR, C., DERFOUL, A., DANIELSON, K. G., HALL, D. J. & TUAN, R. S. 2005. A three-dimensional nanofibrous scaffold for cartilage tissue engineering using human mesenchymal stem cells. *Biomaterials,* 26**,** 599-609.

LINDNER, E., COSOFRET, V. V., UFER, S., BUCK, R. P., KAO, W. J., NEUMAN, M. R. & ANDERSON, J. M. 1994. Ion-selective membranes with low plasticizer content: Electroanalytical characterization and biocompatibility studies. *Journal of Biomedical Materials Research,* 28**,** 591-601.

LIU, D., LUO, Q. & ZHOU, F. 2010. Nonenzymatic glucose sensor based on gold-copper alloy nanoparticles on defect sites of carbon nanotubes by spontaneous reduction. *Synthetic Met,* 160**,** 1745-1748.

LIU, J. & WANG, J. 2001. A Novel Improved Design for the First-generation Glucose Biosensor. *Food Technol. Biotechnol.,* 39**,** 55-58.

LIU, Y., WU, N., WEI, Q., CAI, Y. & WEI, A. 2008. Wetting behavior of electrospun poly(L-lactic acid)/poly(vinyl alcohol) composite nonwovens. *J. Appl. Polym. Sci.,* 110**,** 3172-3177.

LU, Y., JIANG, H., TU, K. & WANG, L. 2009. Mild immobilization of diverse macromolecular bioactive agents onto multifunctional fibrous membranes prepared by coaxial electrospinning. *Acta Biomaterialia,* 5**,** 1562-1574.

LUKAS, D., SARKAR, A., MARTINOVA, L., VODSED'ALKOVA, K., LUBASOVA, D., CHALOUPEK, J., POKORNY, P., MIKES, P., CHVOJKA, J. & KOMAREK, M. 2009. Physical principles of electrospinning (Electrospinning as a nano-scale technology of the twenty-first century). *Textile Progress,* 41**,** 59-140.

LUNDBORG, G., DAHLIN, L., DOHI, D., KANJE, M. & TERADA, N. 1997. A new type of "bioartificial" nerve graft for bridging extended defects in nerves. *J Hand Surg Br,* 22**,** 299-303.

MA, M., MAO, Y., GUPTA, M., GLEASON, K. K. & RUTLEDGE, G. C. 2005. Superhydrophobic Fabrics Produced by Electrospinning and Chemical Vapor Deposition. *Macromolecules,* 38**,** 9742-9748.

MAINES, A., ASHWORTH, D. & VADGAMA, P. 1996. Diffusion restricting outer membranes for greatly extended linearity measurements with glucose oxidase enzyme electrodes. *Analytica Chimica Acta,* 333**,** 223-231.

MALITESTA, C., PALMISANO, F., TORSI, L. & ZAMBONIN, P. G. 1990. Glucose Fast-Response Amperometric Sensor Based on Glucose-Oxidase Immobilized in an Electropolymerized Poly(Ortho-Phenylenediamine) Film. *Anal Chem,* 62**,** 2735-2740.

MANESH, K. M., KIM, H. T., SANTHOSH, P., GOPALAN, A. I. & LEE, K.-P. 2008. A novel glucose biosensor based on immobilization of glucose oxidase into multiwall carbon nanotubes 鈥 olyelectrolyte-loaded electrospun nanofibrous membrane. *Biosensors and Bioelectronics,* 23**,** 771-779.

MARGULES, G., HUNTER, C. & MACGREGOR, D. 1983. Hydrogel based in vivo reference electrode catheter. *Medical and Biological Engineering and Computing,* 21**,** 1-8.

MARMUR, A. 2003. Wetting on Hydrophobic Rough Surfaces:鈥?To Be Heterogeneous or Not To Be? *Langmuir,* 19**,** 8343-8348.

MATSUDA, T., IHARA, M., INOGUCHI, H., KWON, I. K., TAKAMIZAWA, K. & KIDOAKI, S. 2005. Mechano-active scaffold design of small-diameter artificial graft made of electrospun segmented polyurethane fabrics. *Journal of Biomedical Materials Research Part A,* 73A**,** 125-131.

MATTHEWS, D. R., BOWN, E., WATSON, A., HOLMAN, R. R., STEEMSON, J., HUGHES, S. & SCOTT, D. 1987. PEN-SIZED DIGITAL 30-SECOND BLOOD GLUCOSE METER. *The Lancet,* 329**,** 778-779.

MATTHEWS, J. A., WNEK, G. E., SIMPSON, D. G. & BOWLIN, G. L. 2002. Electrospinning of Collagen Nanofibers. *Biomacromolecules,* 3**,** 232-238.

MATTHEWS, J. B. 1967. Mass Loss and Distortion of Freely Falling Water Drops in an Electric Field. *J. Geophys. Res.,* 72**,** 3007-3013.

MCKINLEY, B. A., WONG, K. C., JANATA, J., JORDAN, W. S. & WESTENSKOW, D. R. 1981. In vivo continuous monitoring of ionized calcium in dogs using ion sensitive field effect transistors. *Crit Care Med,* 9**,** 333-9.

MEGELSKI, S., STEPHENS, J. S., CHASE, D. B. & RABOLT, J. F. 2002. Micro- and Nanostructured Surface Morphology on Electrospun Polymer Fibers. *Macromolecules,* 35**,** 8456-8466.

MERCADO, R. C. & MOUSSY, F. 1998. In vitro and in vivo mineralization of Nafion membrane used for implantable glucose sensors. *Biosens Bioelectron,* 13**,** 133-145.

MIT-UPPATHAM, C., NITHITANAKUL, M. & SUPAPHOL, P. 2004. Ultrafine Electrospun Polyamide-6 Fibers: Effect of Solution Conditions on Morphology and Average Fiber Diameter. *Macromolecular Chemistry and Physics,* 205**,** 2327-2338.

MORAIS, J., PAPADIMITRAKOPOULOS, F. & BURGESS, D. 2010. Biomaterials/Tissue Interactions: Possible Solutions to Overcome Foreign Body Response. *The AAPS Journal,* 12**,** 188-196.

MORTON, W. J. 1902. *Method of dispersing fluids*. US Patent 0705691.

MOUSSY, F., HARRISON, D. J. & RAJOTTE, R. V. 1994. A miniaturized Nafion-based glucose sensor: in vitro and in vivo evaluation in dogs. *Int J Artif Organs,* 17**,** 88-94.

MULCHANDANI, A. & PAN, S. 1999. Ferrocene-Conjugated m-Phenylenediamine Conducting Polymer-Incorporated Peroxidase Biosensors. *Analytical Biochemistry,* 267**,** 141-147.

MURRAY, R. W., EWING, A. G. & DURST, R. A. 1987. Chemically modified electrodes. Molecular design for electroanalysis. *Anal Chem,* 59**,** 379A-390A.

MWANGI, J. W. & OFNER III, C. M. 2004. Crosslinked gelatin matrices: release of a random coil macromolecular solute. *Int. J. Pharm.,* 278**,** 319-327.

NEFF, J. & CALDWELL, K. D. 1999. *Surface Modification of Biomaterials,* Philadelphia Taylor & Francis.

NELSON, L. A., MCCANN, J. C., LOEPKE, A. W., WU, J., BEN DOR, B. & KURTH, C. D. 2006. Development and validation of a multiwavelength spatial domain near-infrared oximeter to detect cerebral hypoxia-ischemia. *J Biomed Opt,* 11**,** 064022.

NEWMAN, J. D. & TURNER, A. P. F. 2005. Home blood glucose biosensors: a commercial perspective. *Biosensors and Bioelectronics,* 20**,** 2435-2453.

NEWMAN, J. D., WHITE, S. F., TOTHILL, I. E. & TURNER, A. P. F. 1995. Catalytic Materials, Membranes, and Fabrication Technologies Suitable for the Construction of Amperometric Biosensors. *Analytical Chemistry,* 67**,** 4594-4599.

NOLLET, A. 1749. *Recherches Sur les Causes Particulieres des Phenomenes Electrigues,* Paris, les Freres Guerin.

NORTON, C. L. 1936. *Method of and apparatus for producing fibrous or filamentary material*. US Patent 2048651.

OHARA, T. J., VREEKE, M. S., BATTAGLINI, F. & HELLER, A. 1993. Bienzyme Sensors Based on Electrically Wired Peroxidase. *Electroanal,* 5**,** 825-831.

OLIVER, N. S., TOUMAZOU, C., CASS, A. E. & JOHNSTON, D. G. 2009. Glucose sensors: a review of current and emerging technology. *Diabetes Med,* 26**,** 197-210.

PALMISANO, F., ZAMBONIN, P. G., CENTONZE, D. & QUINTO, M. 2002. A Disposable, Reagentless, Third-Generation Glucose Biosensor Based on Overoxidized Poly(pyrrole)/Tetrathiafulvalene 鉴 ?Tetracyanoquinodimethane Composite. *Anal. Chem.,* 74**,** 5913-5918.

PARK, S., BOO, H. & CHUNG, T. D. 2006. Electrochemical non-enzymatic glucose sensors. *Anal Chim Acta,* 556**,** 46-57.

PARK, S., CHUNG, T. D. & KIM, H. C. 2003. Nonenzymatic glucose detection using mesoporous platinum. *Anal Chem,* 75**,** 3046-9.

PEDICINI, A. & FARRIS, R. J. 2003. Mechanical behavior of electrospun polyurethane. *Polymer,* 44**,** 6857-6862.

PFUTZNER, A., CADUFF, A., LARBIG, M., SCHREPFER, T. & FORST, T. 2004. Impact of posture and fixation technique on impedance spectroscopy used for continuous and noninvasive glucose monitoring. *Diabetes Technol Ther,* 6**,** 435-41.

PICKUP, J. C., HUSSAIN, F., EVANS, N. D., ROLINSKI, O. J. & BIRCH, D. J. S. 2005. Fluorescence-based glucose sensors. *Biosensors and Bioelectronics,* 20**,** 2555-2565.

PRABHAKARAN, M. P., VENUGOPAL, J. & RAMAKRISHNA, S. 2009. Electrospun nanostructured scaffolds for bone tissue engineering. *Acta Biomaterialia,* 5**,** 2884-2893.

QUEINNEC, I., DESTRUHAUT, C., POURCIEL, J. B. & GOMA, G. 1992. An effective automated glucose sensor for fermentation monitoring and control. *W J Microbiol Biotechnol,* 8**,** 7-13.

RAMAKRISHNA, S., FUJIHARA, K., TEO, W. & TC, L. 2005a. Chapter 3 Electrospinning Process. *An introduction to eletrospinning and nanofibers.* World Scientific Publishing Co. Pvt. Ltd.

RAMAKRISHNA, S., FUJIHARA, K., TEO, W. & TC, L. 2005b. An introduction to eletrospinning and nanofibers. World Scientific Publishing Co. Pvt. Ltd.

RANGAPPA, N., ROMERO, A., NELSON, K. D., EBERHART, R. C. & SMITH, G. M. 2000. Laminin-coated poly(L-lactide) filaments induce robust neurite growth while providing directional orientation. *Journal of Biomedical Materials Research,* 51**,** 625-634.

RAYLEIGH, L. 1882. On the equilibrium of liquid conducting masses charged with electricity. *Phil. Mag.,* 14**,** 184-186.

REDDY, S. & VADGAMA, P. 1997a. Membranes to improve amperometric sensor characteristics *In:* E, K.-R. (ed.) *Handbook of biosensors and electronic noses: medicine, food, and the environment* CRC Press.

REDDY, S. M. & VADGAMA, P. 2002. Entrapment of glucose oxidase in non-porous poly(vinyl chloride). *Analytica Chimica Acta,* 461**,** 57-64.

REDDY, S. M. & VADGAMA, P. M. 1997b. Surfactant-modified poly(vinyl chloride) membranes as biocompatible interfaces for amperometric enzyme electrodes. *Analytica Chimica Acta,* 350**,** 77-89.

REICHERT, W. M. & SHARKAWY, A. A. 1999. Biosensors. *In:* VON RECUM, A. (ed.) *Handbook of Biomaterials Evaluation: Scientific, Technical, and Clinical Testing of Implant Materials.* Philadelphia: Taylor & Francis.

REN, G., XU, X., LIU, Q., CHENG, J., YUAN, X., WU, L. & WAN, Y. 2006. Electrospun poly(vinyl alcohol)/glucose oxidase biocomposite membranes for biosensor applications. *Reactive and Functional Polymers,* 66**,** 1559-1564.

RENEKER, D. H. & CHUN, L. 1996. Nanometre diameters of polymer, produced by electrospinning. *Nanotechnology* 7**,** 216-223.

RENEKER, D. H., YARIN, A. L., FONG, H. & KOOMBHONGSE, S. 2000. Bending instability of electrically charged liquid jets of polymer solutions in electrospinning. *Journal of Applied Physics,* 87**,** 4531-4547.

RIBOLDI, S. A., SAMPAOLESI, M., NEUENSCHWANDER, P., COSSU, G. & MANTERO, S. 2005. Electrospun degradable polyesterurethane membranes: potential scaffolds for skeletal muscle tissue engineering. *Biomaterials,* 26**,** 4606-4615.

RITGER, P. L. & PEPPAS, N. A. 1987a. A simple equation for description of solute release I. Fickian and non-fickian release from non-swellable devices in the form of slabs, spheres, cylinders or discs. *J Control Release,* 5**,** 23-36.

RITGER, P. L. & PEPPAS, N. A. 1987b. A simple equation for description of solute release II. Fickian and anomalous release from swellable devices. *J Control Release,* 5**,** 37-42.

RONG, L.-Q., YANG, C., QIAN, Q.-Y. & XIA, X.-H. 2007. Study of the nonenzymatic glucose sensor based on highly dispersed Pt nanoparticles supported on carbon nanotubes. *Talanta,* 72**,** 819-824.

RUCKENSTEIN, E. & LI, Z. F. 2005. Surface modification and functionalization through the self-assembled monolayer and graft polymerization. *Advances in Colloid and Interface Science,* 113**,** 43-63.

RUTLEDGE, G. C., LI, Y., FRIDRIKH, S., WARNER, S. B., KALAYCI, V. E. & PATRA, P. 2001. Electrostatic Spinning and Properties of Ultrafine Fibers, National Textile Center, Annual Report (M98-D01). National Textile Centre.

RUTLEDGE, G. C., LI, Y., FRIDRIKH, S., WARNER, S. B., KALAYCI, V. E. & PATRA, P. 2001 Electrostatic Spinning and Properties of Ultrafine Fiber. *National Textile Center Annual Report: 2001 (M01-D22).* National Textile Centre.

SAITO, T. & WATANABE, M. 1998. Characterization of poly(vinylferrocene-co-2-hydroxyethyl methacrylate) for use as electron mediator in enzymatic glucose sensor. *Reactive and Functional Polymers,* 37**,** 263-269.

SAKAMOTO, M. & TAKAMURA, K. 1982. Catalytic oxidation of biological components on platinum electrodes modified by adsorbed metals: Anodic oxidation of glucose. *Bioelectrochem Bioenerg,* 9**,** 571-582.

SANDERS, J. E. 2011. *Medical devices comprising small fiber biomaterials, and methods of use*. US Patent 7947069.

SANDERS, J. E., CASSISI, D. V., NEUMANN, T., GOLLEDGE, S. L., ZACHARIAH, S. G., RATNER, B. D. & BALE, S. D. 2003. Relative influence of polymer fiber diameter and surface charge on fibrous capsule thickness and vessel density for single-fiber implants. *J Biomed Mater Res,* 65A**,** 462-467.

SASSO, S. V., PIERCE, R. J., WALLA, R. & YACYNYCH, A. M. 1990. Electropolymerized 1,2-Diaminobenzene as a Means to Prevent Interferences and Fouling and to Stabilize Immobilized Enzyme in Electrochemical Biosensors. *Anal Chem,* 62**,** 1111-1117.

SCHMIDTKE, D. W., FREELAND, A. C., HELLER, A. & BONNECAZE, R. T. 1998. Measurement and modeling of the transient difference between blood and subcutaneous glucose concentrations in the rat after injection of insulin. *Proceedings of the National Academy of Sciences,* 95**,** 294-299.

SCHUHMANN, W. 1993. Non-leaking amperometric biosensors based on high-molecular ferrocene derivatives. *Biosensors and Bioelectronics,* 8**,** 191-196.

SCHUHMANN, W. 1995. Electro-transfer pathways in in ampermatric biosensor. Ferrocene-modified enzymes entrapped in conducting-polymer layers. *Biosens. Bioelectron.,* 10**,** 181-193.

SHARKAWY, A., NEUMAN, M. & REICHERT, W. M. 1997a. Design considerations for biosensor based drug delivery systems. . *In:* PARK, K. (ed.) *Controlled Drug Delivery: The Next Generation.* Washington, DC: ACS.

SHARKAWY, A. A., KLITZMAN, B., TRUSKEY, G. A. & REICHERT, W. M. 1997b. Engineering the tissue which encapsulates subcutaneous implants. I. Diffusion properties. *J Biomed Mater Res,* 37**,** 401-12.

SHARKAWY, A. A., KLITZMAN, B., TRUSKEY, G. A. & REICHERT, W. M. 1998a. Engineering the tissue which encapsulates subcutaneous implants. II. Plasma-tissue exchange properties. *J Biomed Mater Res,* 40**,** 586-97.

SHARKAWY, A. A., KLITZMAN, B., TRUSKEY, G. A. & REICHERT, W. M. 1998b. Engineering the tissue which encapsulates subcutaneous implants. III. Effective tissue response times. *J Biomed Mater Res,* 40**,** 598-605.

SHAW, J. E., SICREE, R. A. & ZIMMET, P. Z. 2010. Global estimates of the prevalence of diabetes for 2010 and 2030. *Diabetes Research and Clinical Practice,* 87**,** 4-14.

SHEN, Y. C., DAVIES, A. G., LINFLELD, E. H., ELSEY, T. S., TADAY, P. F. & ARNONE, D. D. 2003. The use of Fourier-transform infrared spectroscopy for the quantitative determination of glucose concentration in whole blood. *Phys Med Biol,* 48**,** 2023-32.

SHENOY, S. L., BATES, W. D., FRISCH, H. L. & WNEK, G. E. 2005. Role of chain entanglements on fiber formation during electrospinning of polymer solutions: good solvent, non-specific polymer 鈥損 olymer interaction limit. *Polymer,* 46**,** 3372-3384.

SHICHIRI, M., KAWAMORI, R., YAMASAKI, Y., HAKUI, N. & ABE, H. 1982. Wearable artificial endocrine pancrease with needle-type glucose sensor. *Lancet,* 2**,** 1129-31.

SHIMADA, K., YANO, M., SHIBATANI, K., KOMOTO, Y., ESASHI, M. & MATSUO, T. 1980. Application of catheter-tip i.s.f.e.t. for continuous in vivo measurement. *Med Biol Eng Comput,* 18**,** 741-5.

SHIN, Y. M., HOHMAN, M. M., BRENNER, M. P. & RUTLEDGE, G. C. 2001. Experimental characterization of electrospinning: the electrically forced jet and instabilities. *Polymer,* 42**,** 09955-09967.

SHULTS, M. C., UPDIKE, S. J., RHODES, R. K., GILLIGAN, B. J. & TAPSAK, M. A. 2010. *Device and method for determining analyte levels*. US Patent: 6862465 Patent.

SMEAL, R., RABBITT, R., BIRAN, R. & TRESCO, P. 2005. Substrate Curvature Influences the Direction of Nerve Outgrowth. *Annals of Biomedical Engineering,* 33**,** 376-382.

SMITH, D. J., RENEKER, D. H., MCMANUS, A. T., SCHREUDER-GIBSON, H. L., MELLO, C. & SENNETT, M. S. 2004. *Electrospun fibers and an apparatus therefor*. US Patent 6753454.

SOLIMAN, S., SANT, S., NICHOL, J. W., KHABIRY, M., TRAVERSA, E. & KHADEMHOSSEINI, A. 2011. Controlling the porosity of fibrous scaffolds by modulating the fiber diameter and packing density. *Journal of Biomedical Materials Research Part A,* 96A**,** 566-574.

SON, W. K., YOUK, J. H., LEE, T. S. & PARK, W. H. 2004. Electrospinning of ultrafine cellulose acetate fibers: Studies of a new solvent system and deacetylation of ultrafine cellulose acetate fibers. *Journal of Polymer Science Part B: Polymer Physics,* 42**,** 5-11.

SRIVASTAVA, Y., MARQUEZ, M. & THORSEN, T. 2007. Multijet electrospinning of conducting nanofibers from microfluidic manifolds. *Journal of Applied Polymer Science,* 106**,** 3171-3178.

STEUER, H., FADALE, R., M 眉 LLER, E., M 眉 LLER, H.-W., PLANCK, H. & SCHLOSSHAUER, B. 1999. Biohybride nerve guide for regeneration: degradable polylactide fibers coated with rat Schwann cells. *Neuroscience Letters,* 277**,** 165-168.

STITZEL, J., LIU, J., LEE, S. J., KOMURA, M., BERRY, J., SOKER, S., LIM, G., VAN DYKE, M., CZERW, R., YOO, J. J. & ATALA, A. 2006. Controlled fabrication of a biological vascular substitute. *Biomaterials,* 27**,** 1088-1094.

SUN, Y., BUCK, H. & MALLOUK, T. E. 2001. Combinatorial discovery of alloy electrocatalysts for amperometric glucose sensors. *Anal Chem,* 73**,** 1599-604.

ŠVANCARA, I., VYTŘAS, K., KALCHER, K., WALCARIUS, A. & WANG, J. 2009. Carbon Paste Electrodes in Facts, Numbers, and Notes: A Review on the Occasion of the 50-Years Jubilee of Carbon Paste in Electrochemistry and Electroanalysis. *Electroanal,* 21**,** 7-28.

TAN, C. K., LOH, K. P. & JOHN, T. T. L. 2008. Direct amperometric detection of glucose on a multiple-branching carbon nanotube forest. *Analyst,* 133**,** 448-451.

TAN, S. H., INAI, R., KOTAKI, M. & RAMAKRISHNA, S. 2005. Systematic parameter study for ultra-fine fiber fabrication via electrospinning process. *Polymer,* 46**,** 6128-6134.

TANG, L., WU, Y. & TIMMONS, R. B. 1998. Fibrinogen adsorption and host tissue responses to plasma functionalized surfaces. *J Biomed Mater Res,* 42**,** 156-163.

TAYLOR, G. 1964. Disintegration of water drops in an electri field. *Proc. R. Soc. A,* 280**,** 383.

TAYLOR, G. 1966. Studies in electrodynamics: I. The circulation produced in a drop by electrical field. *Proc. R. Soc. A,* 291**,** 145.

TAYLOR, G. 1969. Electrically Driven Jets. *Proc. R. Soc. A,* 313**,** 453-475.

TEO, W. E. & RAMAKRISHNA, S. 2006. A review on electrospinning design and nanofibre assemblies. *Nanotechnology,* 17**,** R89.

THERON, S. A., ZUSSMAN, E. & YARIN, A. L. 2004. Experimental investigation of the governing parameters in the electrospinning of polymer solutions. *Polymer,* 45**,** 2017-2030.

TOGHILL, K. E. & COMPTON, R. G. 2010. Electrochemical Non-enzymatic Glucose Sensors: A Perspective and an Evaluation. *Int. J. Electrochem. Sci.,* 5**,** 1246-1301.

TONYUSHKINA, K. & NICHOLS, J. H. 2009. Glucose meters: a review of technical challenges to obtaining accurate results. *J Diabetes Sci Technol,* 3**,** 971-80.

TOTHILL, I. E., NEWMAN, J. D., WHITE, S. F. & TURNER, A. P. F. 1997. Monitoring of the glucose concentration during microbial fermentation using a novel mass-producible biosensor suitable for on-line use. *Enzyme and Microbial Technology,* 20**,** 590-596.

TRELOAR, P. H., CHRISTIE, I. M. & VADGAMA, P. M. 1995. Engineering the right membranes for electrodes at the biological interface; solvent cast and electropolymerised. *Biosens Bioelectron,* 10**,** 195-201.

TRZEBINSKI, J., MONIZ, A. R.-B., SHARMA, S., BURUGAPALLI, K., MOUSSY, F. & CASS, A. E. G. 2011. Hydrogel membrane improves batch-to-batch reproducibility of an enzymatic glucose biosensor. *Electroanalysis,* 23**,** 2789-2795.

TSUJIMURA, S., KOJIMA, S., KANO, K., IKEDA, T., SATO, M., SANADA, H. & OMURA, H. 2006. Novel FAD-dependent glucose dehydrogenase for a dioxygen-insensitive glucose biosensor. *Biosci Biotechnol Biochem,* 70**,** 654-9.

VALDES, T. I. & MOUSSY, F. 2000. In vitro and in vivo degradation of glucose oxidase enzyme used for an implantable glucose biosensor. *Diabetes Technol Ther,* 2**,** 367-76.

VASSILYEV, Y. B., KHAZOVA, O. A. & NIKOLAEVA, N. N. 1985. Kinetics and mechanism of glucose electrooxidation on different electrode-catalysts: Part I. Adsorption and oxidation on platinum. *Journal of Electroanalytical Chemistry and Interfacial Electrochemistry,* 196**,** 105-125.

WANG, J. 2008. Electrochemical glucose biosensors. *Chem Rev,* 108**,** 814-25.

WANG, J., LIU, J., CHEN, L. & LU, F. 1994. Highly Selective Membrane-Free, Mediator-Free Glucose Biosensor. *Anal Chem,* 66**,** 3600-3603.

WANG, J. & LU, F. 1998. Oxygen-Rich Oxidase Enzyme Electrodes for Operation in Oxygen-Free Solutions. *Journal of the American Chemical Society,* 120**,** 1048-1050.

WANG, J., NASER, N., ANGNES, L., WU, H. & CHEN, L. 1992. Metal-Dispersed Carbon Paste Electrodes. *Anal Chem,* 64**,** 1285-1288.

WANG, X., UM, I. C., FANG, D., OKAMOTO, A., HSIAO, B. S. & CHU, B. 2005. Formation of water-resistant hyaluronic acid nanofibers by blowing-assisted electro-spinning and non-toxic post treatments. *Polymer,* 46**,** 4853-4867.

WANG, Y., ZHANG, D., ZHANG, W., GAO, F. & WANG, L. 2009a. A facile strategy for nonenzymatic glucose detection. *Anal Biochem,* 385**,** 184-186.

WANG, Z. G., WANO, Y., XU, H., LI, G. & XU, Z. K. 2009b. Carbon Nanotube-Filled Nanofibrous Membranes Electrospun from Poly(acrylonitrile-co-acrylic acid) for Glucose Biosensor. *Journal of Physical Chemistry C,* 113**,** 2955-2960.

WEISS, R., YEGORCHIKOV, Y., SHUSTERMAN, A. & RAZ, I. 2007. Noninvasive continuous glucose monitoring using photoacoustic technology-results from the first 62 subjects. *Diabetes Technol Ther,* 9**,** 68-74.

WEN, X. & TRESCO, P. A. 2006. Effect of filament diameter and extracellular matrix molecule precoating on neurite outgrowth and Schwann cell behavior on multifilament entubulation bridging device in vitro. *Journal of Biomedical Materials Research Part A,* 76A**,** 626-637.

WILSON, R. & TURNER, A. P. F. 1992. Glucose oxidase: an ideal enzyme. *Biosensors and Bioelectronics,* 7**,** 165-185.

WISNIEWSKI, N., KLITZMAN, B., MILLER, B. & REICHERT, W. M. 2001. Decreased analyte transport through implanted membranes: Differentiation of biofouling from tissue effects. *J Biomed Mater Res,* 57**,** 513-521.

WISNIEWSKI, N., MOUSSY, F. & REICHERT, W. M. 2000. Characterization of implantable biosensor membrane biofouling. *Fresenius J Anal Chem,* 366**,** 611-21.

WISNIEWSKI, N. & REICHERT, M. 2000. Methods for reducing biosensor membrane biofouling. *Colloid Surface B,* 18**,** 197-219.

WITTSTOCK, G., STRUBING, A., SZARGAN, R. & WERNER, G. 1998. Glucose oxidation at bismuth-modified platinum electrodes. *J. Electroanal. Chem.,* 444**,** 61-73.

WONG, S.-C., BAJI, A. & LENG, S. 2008. Effect of fiber diameter on tensile properties of electrospun poly(-caprolactone). *Polymer,* 49**,** 4713-4722.

XU, C. Y., INAI, R., KOTAKI, M. & RAMAKRISHNA, S. 2004. Aligned biodegradable nanofibrous structure: a potential scaffold for blood vessel engineering. *Biomaterials,* 25**,** 877-886.

XU, X., TIAN, B. Z., KONG, J. L., ZHANG, S., LIU, B. H. & ZHAO, D. Y. 2003. Ordered Mesoporous Niobium Oxide Film: A Novel Matrix for Assembling Functional Proteins for Bioelectrochemical Applications. *Advanced Materials,* 15**,** 1932-1936.

YANG, F., MURUGAN, R., WANG, S. & RAMAKRISHNA, S. 2005. Electrospinning of nano/micro scale poly(l-lactic acid) aligned fibers and their potential in neural tissue engineering. *Biomaterials,* 26**,** 2603-2610.

YANG, F., XU, C. Y., KOTAKI, M., WANG, S. & RAMAKRISHNA, S. 2004a. Characterization of neural stem cells on electrospun poly(L-lactic acid) nanofibrous scaffold. *J Biomater Sci Polym Ed,* 15**,** 1483-97.

YANG, J., JIANG, L. C., ZHANG, W. D. & GUNASEKARAN, S. 2010. A highly sensitive non-enzymatic glucose sensor based on a simple two-step electrodeposition of cupric oxide (CuO) nanoparticles onto multi-walled carbon nanotube arrays. *Talanta,* 82**,** 25-33.

YANG, P., ZHAO, D., MARGOLESE, D. I., CHMELKA, B. F. & STUCKY, G. D. 1998. Generalized syntheses of large-pore mesoporous metal oxides with semicrystalline frameworks. *Nature,* 396**,** 152-155.

YANG, Q., LI, Z., HONG, Y., ZHAO, Y., QIU, S., WANG, C. & WEI, Y. 2004b. Influence of solvents on the formation of ultrathin uniform poly(vinyl pyrrolidone) nanofibers with electrospinning. *Journal of Polymer Science Part B: Polymer Physics,* 42**,** 3721-3726.

YANG, Y., JIA, Z., LIU, J., LI, Q., HOU, L., WANG, L. & GUAN, Z. 2008. Effect of electric field distribution uniformity on electrospinning. *Journal of Applied Physics,* 103**,** 104307-11.

YAO, L., HAAS, T. W., GUISEPPI-ELIE, A., BOWLIN, G. L., SIMPSON, D. G. & WNEK, G. E. 2003. Electrospinning and Stabilization of Fully Hydrolyzed Poly(Vinyl Alcohol) Fibers. *Chemistry of Materials,* 15**,** 1860-1864.

YATES, E. W., RUPANI, A., FOLEY, G. T., KHAN, W. S., CARTMELL, S. & ANAND, S. J. 2012. Ligament Tissue Engineering and Its Potential Role in Anterior Cruciate Ligament Reconstruction. *Stem Cells International,* 2012**,** Article ID 438125, 6 pages.

YE, J.-S., WEN, Y., DE ZHANG, W., MING GAN, L., XU, G. Q. & SHEU, F.-S. 2004. Nonenzymatic glucose detection using multi-walled carbon nanotube electrodes. *Electrochem Commun,* 6**,** 66-70.

YEHEZKELI, O., OVITS, O., TEL-VERED, R., RAICHLIN, S. & WILLNER, I. 2010. Reconstituted Enzymes on Electropolymerizable FAD-Modified Metallic Nanoparticles: Functional Units for the Assembly of Effectively "Wired" Enzyme Electrodes. *Electroanal,* 22**,** 1817-1823.

YEHEZKELI, O., YAN, Y. M., BARAVIK, I., TEL-VERED, R. & WILLNER, I. 2009. Integrated oligoaniline-cross-linked composites of Au nanoparticles/glucose oxidase

electrodes: a generic paradigm for electrically contacted enzyme systems. *Chem. Eur. J.,* 15**,** 2674-9.

YEO, I.-H. & JOHNSON, D. C. 2000. Anodic response of glucose at copper-based alloy electrodes. *Journal of Electroanalytical Chemistry,* 484**,** 157-163.

YOO, E. H. & LEE, S. Y. 2010. Glucose biosensors: An overview of use in clinical practice. *Sensors,* 10**,** 4558-4576.

YOON, K., KIM, K., WANG, X., FANG, D., HSIAO, B. S. & CHU, B. 2006. High flux ultrafiltration membranes based on electrospun nanofibrous PAN scaffolds and chitosan coating. *Polymer,* 47**,** 2434-2441.

YOU, T., NIWA, O., TOMITA, M. & HIRONO, S. 2003. Characterization of platinum nanoparticle-embedded carbon film electrode and its detection of hydrogen peroxide. *Anal Chem,* 75**,** 2080-5.

YU, B., JU, Y., WEST, L., MOUSSY, Y. & MOUSSY, F. 2007. An investigation of long-term performance of minimally invasive glucose biosensors. *Diabetes Technol Ther,* 9**,** 265-75.

YU, B., LONG, N., MOUSSY, Y. & MOUSSY, F. 2006. A long-term flexible minimally-invasive implantable glucose biosensor based on an epoxy-enhanced polyurethane membrane. *Biosens. Bioelectron.,* 21**,** 2275-2282.

YU, B., MOUSSY, Y. & MOUSSY, F. 2005a. Coil-type implantable glucose biosensor with excess enzyme loading. *Front. Biosci.,* 10**,** 512-20.

YU, B., MOUSSY, Y. & MOUSSY, F. 2005b. Lifetime Improvement of Glucose Biosensor by Epoxy-Enhanced PVC Membrane. *Electroanal,* 17**,** 1771-1779.

YU, B., WANG, C., JU, Y. M., WEST, L., HARMON, J., MOUSSY, Y. & MOUSSY, F. 2008a. Use of hydrogel coating to improve the performance of implanted glucose sensors. *Biosens Bioelectron,* 23**,** 1278-84.

YU, J., YU, D., ZHAO, T. & ZENG, B. 2008b. Development of amperometric glucose biosensor through immobilizing enzyme in a Pt nanoparticles/mesoporous carbon matrix. *Talanta,* 74**,** 1586-1591.

YU, J. H., FRIDRIKH, S. V. & RUTLEDGE, G. C. 2004. Production of Submicrometer Diameter Fibers by Two-Fluid Electrospinning. *Advanced Materials,* 16**,** 1562-1566.

ZELENY, J. 1914. The Electrical Discharge from Liquid Points, and A Hydrostatic Method of Measuring the Electric Intensity at their Surfaces. *Phys. Rev.,* 3**,** 69-91.

ZENG, J., XU, X., CHEN, X., LIANG, Q., BIAN, X., YANG, L. & JING, X. 2003. Biodegradable electrospun fibers for drug delivery. *Journal of Controlled Release,* 92**,** 227-231.

ZHANG, C., YUAN, X., WU, L., HAN, Y. & SHENG, J. 2005. Study on morphology of electrospun poly(vinyl alcohol) mats. *European Polymer Journal,* 41**,** 423-432.

ZHANG, D. & CHANG, J. 2007. Patterning of Electrospun Fibers Using Electroconductive Templates. *Advanced Materials,* 19**,** 3664-3667.

ZHANG, D., KARKI, A. B., RUTMAN, D., YOUNG, D. P., WANG, A., COCKE, D., HO, T. H. & GUO, Z. 2009. Electrospun polyacrylonitrile nanocomposite fibers reinforced with Fe3O4 nanoparticles: Fabrication and property analysis. *Polymer,* 50**,** 4189-4198.

ZHANG, X., CHAN, K.-Y., YOU, J.-K., LIN, Z.-G. & TSEUNG, A. C. C. 1997. Partial oxidation of glucose by a Pt|WO3 electrode. *Journal of Electroanalytical Chemistry,* 430**,** 147-153.

ZHANG, Y., HUANG, Z.-M., XU, X., LIM, C. T. & RAMAKRISHNA, S. 2004a. Preparation of Core-shell Structured PCL-r-Gelatin Bi-Component Nanofibers by Coaxial Electrospinning. *Chemistry of Materials,* 16**,** 3406-3409.

ZHANG, Y., HUANG, Z. M., XU, X., LIM, C. T. & RAMAKRISHNA, S. 2004b. Preparation of core-shell structured PCL-r-gelatin bi-component nanofibers by coaxial electrospinning. *Chemistry of Materials,* 16**,** 3406-3409.

ZHAO, M., GANG, S., DENG, X. L., LU, J. G., RYU, S. K. & YANG, X. P. 2006. PLLA/HA electrospin hybrid nanofiber scaffolds: morphology, in vitro degradation and cell culture potential. *Adv Mat Res,* 11–12**,** 243–246.

ZHAO, P., JIANG, H., PAN, H., ZHU, K. & CHEN, W. 2007a. Biodegradable fibrous scaffolds composed of gelatin coated poly(ϵ-caprolactone) prepared by coaxial electrospinning. *Journal of Biomedical Materials Research Part A,* 83A**,** 372-382.

ZHAO, P., JIANG, H., PAN, H., ZHU, K. & CHEN, W. 2007b. Biodegradable fibrous scaffolds composed of gelatin coated poly(ε-caprolactone) prepared by coaxial electrospinning. *Journal of Biomedical Materials Research Part A,* 83A**,** 372-382.

ZHAO, S., WU, X., WANG, L. & HUANG, Y. 2004. Electrospinning of ethyl–cyanoethyl cellulose/tetrahydrofuran solutions. *Journal of Applied Polymer Science,* 91**,** 242-246.

ZHOU, M., SHANG, L., LI, B., HUANG, L. & DONG, S. 2008. Highly ordered mesoporous carbons as electrode material for the construction of electrochemical dehydrogenase- and oxidase-based biosensors. *Biosensors and Bioelectronics,* 24**,** 442-447.

ZHU, H., LU, X., LI, M., SHAO, Y. & ZHU, Z. 2009. Nonenzymatic glucose voltammetric sensor based on gold nanoparticles/carbon nanotubes/ionic liquid nanocomposite. *Talanta,* 79**,** 1446-1453.

ZHU, H., STEIN, E. W., LU, Z., LVOV, Y. M. & MCSHANE, M. J. 2005. Synthesis of Size-Controlled Monodisperse Manganese Carbonate Microparticles as Templates for Uniform Polyelectrolyte Microcapsule Formation. *Chemistry of Materials,* 17**,** 2323-2328.

ZHU, L., TIAN, C., ZHU, D. & YANG, R. 2008. Ordered Mesoporous Carbon Paste Electrodes for Electrochemical Sensing and Biosensing. *Electroanalysis,* 20**,** 1128-1134.

ZONG, X., KIM, K., FANG, D., RAN, S., HSIAO, B. S. & CHU, B. 2002. Structure and process relationship of electrospun bioabsorbable nanofiber membranes. *Polymer,* 43**,** 4403-4412.

ZOU, D. J., ZHAO, H., QI, M. & YANG, D. Z. 2007. The effect of solvent to electrospinning polyurethane bionic coating. *J. FUNCT. MAT,* 38**,** 1176-1181.